The effects of substituents and coverage on the bonding of thiophene to Cu(111).

By Peter K. Milligan

A thesis presented in partial fulfilment for the degree of Doctor of Philosophy in the Faculty of Science of the University of Glasgow.

Chemistry Department

September 2000

Some people work very hard,
but still they never get it right.
Well, I'm beginning to see the light

Lou Reed

Acknowledgements

I would like to thank my supervisor, Dr. Malcolm Kadodwala, for all of his help in the completion of this project. As this project involved building a Surface Science machine at Glasgow and simultaneously doing synchrotron experiments at Daresbury, I was fortunate enough to come into contact with many people who helped me in many ways throughout the course of the project.

At Daresbury, I was tutored in the ways of Station 6.3, by Dr. Bruce Cowie and Bridget Murphy. In Glasgow, I greatly benefited from working with other students in the lab, who are, in chronological order, Kevin Campbell, Andreas Sotiropoulos, Shona Johnston and Gilles Rousseau.

I am indebted to the mechanical workshop (Tony Osborne, John Gillan and Neil M^{C}Lachlan), the electronic workshop (Jarnail Bhumbra) and the glass-blowing workshop (Willie M^{C}Cormack and Arlene Douglas) whose expertise kept my project going along when my equipment started to go wrong/break down.

Also, I would like to thank the members of staff who popped into the lab to find out how I was getting on, to lend some helpful advice and to whom I would consult on matters chemical, namely, Dr. Kelvin Tyler, Dr. David Lennon and Dr. Dave Morris. At the Daresbury laboratory, we always seemed to be there at the same time as the Leicester Surface Physics group of Dr. Chris Binns. I'd like to thank Chris, Steve and Kevin for their hospitality, especially in that never-ending four week period I spent at Station 6.3 in the summer of 1997.

As a Ph.D student in the Chemistry Department at Glasgow it's never all work and no play. I am indebted to the many friends and colleagues I've had the privilege to know in my time at Glasgow. Especially Graeme, Russell, Simon, Bernie, Phil, John, Alwin, Josie, Heather, Chris, Ed, the people I shared offices with in both the EM and Fluorine offices, and countless other people I've probably forgotten to mention.

Thanks to the guys in the band, John, Dan, Chris and Paul. During my writing-up period, which seemed to take forever (I think most people noticed that!), it was good to be in the band and I suppose I've no excuse for not writing more songs now that I'm not writing my thesis any more.

Thanks to my long-suffering family, Mum, Dad and Kerry, whose support, both emotionally and financially has seen me through some difficult times over the past few years, especially during the writing of this thesis. Finally, thanks to my girlfriend Emma, for her support during my writing-up period.

Acronyms and abbreviations used in this thesis

AES	Auger Electron Spectroscopy
AO	Atomic Orbital
ARUPS	Angle Resolved Ultra Violet Photoemission Spectroscopy
CHA	Concentric Hemispherical Analyser
HREELS	High Resolution Electron Energy Spectroscopy
LCAO	Linear Combination of Atomic Orbitals
LEED	Low Energy Electron Diffraction
ML	Monolayer
NEXAFS	Near Edge X-ray Absorption Fine Structure
NIXSW	Normal Incidence X-ray Standing Wavefield
PhD	Photoelectron Diffraction
QMS	Quadropole Mass Spectrometer
RAIRS	Reflectance Absorbance Infra Red Spectroscopy
RFA	Retarding Field Analyser
SEXAFS	Surface Extended X-ray Absorption Fine Structure
SHG	Second Harmonic Generation
STM	Scanning Tunnelling Microscopy
TPD	Temperature Programmed Desorption
TSP	Titanium Sublimation Pump
2PPE	Two Photon Photoemission
UPS	Ultraviolet Photoelectron Spectroscopy
UHV	Ultra High Vacuum
XPS	X-ray Photoelectron Spectroscopy
XSW	X-ray Standing Wavefield

Abstract

The purpose of this project was to study the effects of substituent groups and coverage on the bonding of thiophene to Cu(111). The substituent groups that were studied were chloro- (3-chlorothiophene), methyl- (3-methylthiophene) and methoxy- (3-methoxythiophene). In each case the substitution was at the 3-position of the thiophene ring.

This was a two-fold project in that the characterisation of the adsorption was performed in Glasgow by using TPD, AES and LEED and further structural information was obtained by using the synchrotron-based techniques NIXSW and NEXAFS, at the Daresbury Laboratory.

The characterisation experiments indicated that the adsorption of thiophene on Cu(111) is molecular and reversible. From TPD data, four adsorption states could be identified. These were desorption from multilayers, two monolayer states α- and β- and defect sites. NIXSW and NEXAFS experiments were then performed in order to determine the structure of thiophene at α-state and β-state coverage. It was found that the adsorption site of thiophene at both α-state and β-state coverage was displaced atop but the orientations were significantly different. At α-state coverage, the molecules are oriented in an almost flat lying, π-bonded orientation but at β-state coverage, the molecules are oriented in a much more inclined geometry. This coverage dependent phase transition is a result of the dual bonding modes of thiophene in that the molecule can bond either in a π-bonded manner or *via* the S lone pairs.

The object therefore of adding a substituent group at the 3-position of the thiophene ring was to try and influence the bonding mode of the molecule. TPD studies of 3-chlorothiophene, 3-methoxythiophene and 3-methylthiophene all show that there is no β-like adsorption state. Therefore there is no evidence of any coverage dependent phase transition on Cu(111) for these molecules. As in the case of thiophene, NIXSW studies show that at monolayer coverage, which corresponds to the thiophene α-state coverage, the adsorption site is displaced atop and the Cu-S bond length for all four molecules studied is identical within experimental error. NEXAFS studies show that at monolayer coverage, 3-chlorothiophene, 3-methylthiophene and 3-methoxythiophene are

all bonded to the surface in roughly flat orientations with the same angle of inclination as thiophene at α-state coverage, within experimental error.

The adsorption of 3-methylthiophene was found to be molecular and reversible. There is a small amount of dissociation in the adsorption of 3-chlorothiophene and 3-methoxythiophene. This is probably due to the molecules bonding strongly to defect sites. The chloro- and methoxy- groups are found to have a subtle effect on the bonding of thiophene to Cu(111) because they interact, albeit weakly, with the surface *via* lone pair-surface interactions.

Contents

Chapter 1. Introduction and Literature Review

1.1 Introduction

The purpose of this project was to study the effect of adding a substituent group to the 3-position of thiophene in terms of the bonding and orientation of the molecule to Cu(111). Previous work concerned with the adsorption of aromatic molecules such as pyridine on Ag(111)[1] and thiophene on Ag(111)[2] shows that heterocyclic molecules are capable of undergoing a phase transition from a flat to an upright geometry with increasing coverage. This is possible due to the dual bonding modes of heterocyclic molecules in that they can bond to the surface *via* the aromatic ring in a flat π-bonded orientation, or *via* the lone pair(s) on the hetero-atom in a more upright orientation.

It was proposed that by adding electron-withdrawing or electron-donating groups at the 3-position[3] of the thiophene ring it may be possible to influence the orientation of thiophene on Cu(111). The substituent groups chosen had to be small enough to ensure that there were no large steric effects influencing the bonding and for this reason, it was decided to study the effect of substitution at the 3-position and not the 2-position.

The substituent groups that were chosen are chloro- (electron-withdrawing), methyl- and methoxy- (electron donating). It was hoped that in each case the bonding of the molecules would be either *via* the aromatic ring or the hetero-atom and not exclusively *via* the substituent group.

The purpose of the study therefore was to probe the influence of a substituent on the bonding of thiophene to Cu(111). It was proposed that by adding and electron-withdrawing group (chloro-) to the 3-position, sufficient electron density would be withdrawn from the aromatic ring to force the molecule to bond to the surface in a more upright geometry, *via* the S lone pairs. Conversely, the addition of an electron-donating group (methyl, methoxy) might push electron density onto the aromatic ring thereby favouring a π-bonded geometry.

In order to study the adsorption structure of these molecules and subsequently probe the effects of the substituent groups, it was necessary to choose a single crystal metal substrate that did not support the decomposition of the molecule. The vast

majority of previous work concerning the surface structure of intact aromatic compounds on single crystal metal surfaces has been concerned with the noble metals silver and copper, which will be reviewed later in this section. For this reason, it was decided to use a copper crystal and the (111) surface, the least reactive of the common single crystal surfaces.

The first systematic study of the effects of different substituent groups on the bonding of aromatic compounds to metal surfaces was made by Somorjai and Nakazawa[4]. This study concluded that when an electron-withdrawing group was attached to a benzene ring, the bonding to a polycrystalline gold surface was *via* the substituent group and when an electron-donating group was present the bonding was *via* the aromatic ring. This is not surprising as electron-withdrawing groups such as NO_2, COOH and SO_3 have lots of lone pairs and the possibility of bidentate bonding with the surface. This is precisely the scenario that was hoped to be avoided in the current work. It was hoped that in choosing the three substituent groups described previously, a more subtle, electronic effect could be achieved in the bonding of the corresponding molecules to the surface.

Systematic studies of substituent effects have also been studied in the work of Andrew Gellman[5]. However, the impetus in these studies has mostly been the step-wise introduction of a substituent group (fluoro) into the methyl groups of adsorbed organic species in order to probe the reaction kinetics involved in the transition states of important surface reactions.

The current work therefore represents the first systematic structural study of the effect of substitution of an aromatic compound on a single crystal metal surface. What follows is a literature review of previous related studies of thiophene, benzene, pyridine and related compounds, on mostly single crystal Ag and Cu surfaces. In order to study the effects of substituent groups in the current work, it is important to analyse the previous studies of related molecules, and the very few studies that have used similar substituent groups as the ones chosen here.

1.2. Literature Review

The following review is a summary of previous work concerning the adsorption of thiophene, benzene and pyridine on single crystal copper and silver surfaces. In each study referred to, the adsorption of the aromatic adsorbate was found to be molecular and reversible, thus allowing the structure of the intact molecule to be probed. At the end of this section there is a short summary on previous work concerning methyl and chloro-substituted aromatic molecules on a variety of substrates. The reason for reviewing previous work on substrates other than copper and silver is that there are very few studies in this area with which to compare the results of the current study.

1.2.1. Thiophene adsorption on single crystal copper and silver surfaces.

The first study of thiophene on Cu(111) was made by Richardson and Campuzano[6]. In this study, the adsorption of thiophene at room temperature was probed by ARUPS. Polarisation dependence of the adsorbate-induced features in the spectra suggested that the molecule was oriented in a flat, weakly π- bonded orientation on the surface.

A TPD and HREELS study of pyrrole, furan and thiophene on Cu(100) was made by Sexton[7] in which TPD data showed the presence of multilayer, bilayer and monolayer states for pyrrole and furan, but multilayer and a broader monolayer state for thiophene. Screening of the in-plane vibrations was observed in the HREELS data for all three molecules at monolayer coverage indicating, via the surface dipole selection rule, that the molecules are weakly π-bonded, oriented in flat orientations on the surface. At bilayer coverage, for pyrrole and furan, strong in-plane vibrations were observed indicating that the second layer in each case is oriented in an upright geometry. The presence of a bilayer was ruled out in the thiophene study due to the lack of any distinct peak in the TPD data. However, similar HREELS data to the other two molecules was found at slightly higher monolayer coverages by annealing the surface to the lower temperature part of the broad monolayer peak. At this coverage, the author assigns the structure to a "compression" in which there are both

upright and flat lying molecules on the surface. The author suggest that the difference between the "compression" model and the bilayer model is that the upright molecules in the bilayer model are above the flat monolayer molecules but the upright molecules in the "compression" model are bonded directly to the surface, *via* the S lone pairs. These two models are very similar and in the case of pyrrole and furan, the author justifies the assignments on the basis of the distinct changes in in-plane vibrations at bilayer coverage. In the case of thiophene, the author states that the gradual decrease in in-plane vibrations as the coverage is decreased over the broad monolayer state signifies that the more upright molecules, that are more weakly bound to the surface, desorb to leave flat lying molecules.

A TPD and XPS study of thiophene on Ag(111) by Umbach[8] *et al.* shows TPD data that resembles that of pyrrole and furan in the Sexton study, that of two sub-multilayer coverage states, in addition to multilayers. The authors conclude that the monolayer is physisorbed in a flat orientation due to the low desorption temperature (204 K) and the similarity of the monolayer XPS data with that of the multilayer data, signifying that there is no significant chemical change on adsorption. As there is a three times higher intensity of the XPS peak at the higher lower temperature state coverage, the authors conclude that the second peak evident in their TPD data is due to molecules oriented in a more upright geometry above the monolayer. This is a different model to that proposed by Sexton (bilayer) in that it involves a phase transition from flat oriented molecules to more upright molecules with increasing coverage. The authors come to this conclusion because there would be no other way of stacking so many molecules. The authors compare the difference between their conclusion and that of Sexton's thiophene work and state that the differing heating rates could account for the fact that they see a distinct second peak and Sexton does not. A later TPD and NEXAFS study by Fink[2] *et al.* of thiophene on Ag(111) shows similar TPD data, in that there are two sub-multilayer coverage peaks. These peaks are assigned to two distinct adsorption states, one of which is a flat monolayer state and the other is a more upright state which has undergone a phase transition. Polarisation dependence of C K-edge and S $L_{2,3}$-edge NEXAFS spectra along with Xα scattered-wave calculations, show that the monolayer is flat and that the increased coverage layer is oriented with an angle of 40-45 °

Information on both the orientation and S-Cu surface distance was obtained in two separate studies by Ohta *et al.,* who studied the adsorption of thiophene on Cu(100)[9] and Cu(111)[10] using S K-edge NEXAFS and SEXAFS. In each study, thiophene surfaces were prepared with sub-monolayer coverages. In each case, S K-edge NEXAFS shows that the molecules are oriented in flat π-bonded orientations on the surface. For thiophene bonded to the Cu(100) surface at the same coverage as the NEXAFS experiment, S K-edge SEXAFS shows that the S atom of the thiophene ring is bonded to a bridge site with a S-Cu surface distance of 2.43±0.03 Å. For thiophene bonded to the Cu(111) surface, the authors state that they could not assign the adsorption site but they could state a S-Cu surface distance of 2.50±0.02 Å which is significantly longer than their previous study concerning Cu(100). The authors conclude that the difference in S-Cu surface distances between the two surfaces is due to the dissimilar atomic densities resulting in more charge transfer from the (100) surface to the adsorbate than from the (111) surface to the adsorbate. From NEXAFS data, the authors suggest that the amount of charge transfer in the Cu(100) study is double that of the Cu(111) study.

STM studies of thiophene on Ag(111) by Hamers *et al.* show that at low coverages and at low temperatures the molecules preferentially bond to step edges[11]. The interaction at the step edges appears to be sufficient to allow the molecules to be oriented in the same direction. Further studies[12] show that the upper step edges are more favourable for initial bonding to the surface than the lower step edges. The authors postulate that the reason for the molecules bonding to the upper step edge is due to charge transfer between the molecule and substrate dominating over purely electrostatic interactions. A purely electrostatic interaction would involve the thiophene molecule simply bonding across the step, thereby maximising the adsorbate/surface interaction. In their study, they quote the Smoluchowski effect,[13] in which electrons spill over step edges leaving the upper step edge depleted of electrons and the lower step edge enriched of electrons. The result of this is an in-plane surface dipole with its positive end on the upper terrace and its negative end on the lower terrace. The authors then state that this model helps to explain why the molecules align themselves along the top of the step edge. At higher coverages, they note that the molecules may be tilted slightly.

1.2.2. Benzene adsorption on single crystal copper and silver surfaces.

The adsorption of benzene on Cu(111) was studied using the techniques of TPD, HREELS and NEXAFS by Bent[14] *et al.* TPD data shows the presence of two sub-multilayer states as noted in Sexton's study of pyrrole and furan on Cu(111) and Umbach's study of thiophene on Ag(111). One state is a broad feature at 225 K and the other one is at 157 K. As described before, the presence of this second peak was assigned to bilayer formation by Sexton and a phase transition by Umbach. Using the HREELS data and similar arguments to that of Sexton, the authors assign the higher temperature peak to that of a monolayer in a flat orientation. By analysing the polarisation dependence of C K-edge NEXAFS spectra, the flat orientation of the monolayer was re-inforced. However, NEXAFS and HREELS data for the 157 K adsorption state indicate that the molecules are bonded in a more upright orientation. The authors conclude, by calculating the Van der Waal's size of benzene on the surface, by careful analysis of their NEXAFS data, and by comparison with the T-shaped crystal structure of solid benzene, that the peak at 157 K in the TPD data is due to bilayer formation in which the second layer is oriented almost perpendicular to the surface.

Work function measurements in a 2PPE study of benzene on Cu(111) by Ertl[15] *et al.* do re-inforce the bilayer model in that a plot of work function versus coverage shows a smooth curve with three distinct portions signifying the monolayer, bilayer and multilayer states. If the TPD data in the work of Bent *et al.* signified a phase transition, there would be a much more drastic change in work function at the coverage where the molecules change orientation.

Another feature of note in the study of Bent *et al.* is the broadening to lower desorption temperatures of the monolayer peak with increasing coverage. The authors attribute this broadening to repulsive lateral interactions within the monolayer. However, an STM study by Weiss[16] *et al.* shows, that as in the STM study of thiophene on Ag(111)[11], benzene also aligns along step edges. This is then extended to the idea that the adsorbed molecules on step edges then perturb the sites adjacent to them on the terrace and supports the formation of islands of benzene molecules[17, 18]. Benzene islands therefore have attractive lateral interactions, in contrast with the

conclusion arrived at by Bent *et al.* above. Weiss explains the broadening to lower desorption temperatures as desorption of islands of benzene of different sizes.

Broadening to lower desorption temperatures of the monolayer peak was also observed in a TPD study of benzene on Cu(110) by Lambert[19] *et al.* In a later HREELS and NEXAFS study of the same system[20], the authors do not rule out the possibility of either repulsive lateral adsorbate-adsorbate interactions or a continual change in orientation within the monolayer to account for this. They do point out that the adsorbed molecules are tilted at all coverages, presumably fitting into the troughs present on the (110) surface, but they do not say what the angles of orientation are, so it is unclear as to whether they are changing or not.

The orientation of benzene on Ag(110)[21, 22] and Ag(111)[23] has also been determined by NEXAFS. In the case of Ag(110) at sub-monolayer coverage, the molecule was found to be bonded to the surface in a flat orientation, which is also the result of the benzene on Ag(111) study at monolayer coverage.

1.2.3. Pyridine adsorption on single crystal copper and silver surfaces.

The dual bonding modes of pyridine were evidenced in a study by Sanda[1] *et al.* who used both HREELS and UPS to study a compressional phase transition of pyridine on Ag(111). They found that at low coverages, the molecules bonded to the surface *via* the aromatic ring. However, as the coverage was increased, the molecules started to tilt with an estimated 67 % more molecules bonded in the inclined N lone-pair bonded mode. They also found that the phase transition was reversible and by heating the upright layer to desorb some of the molecules, they found that the molecules reverted to a flat-lying orientation.

A NEXAFS study of pyridine on Ag(111) by Otto[24] *et al.* also shows evidence of a phase transition, but in this study the authors suggest that the molecules are not in a flat orientation at low coverages. Analysis of their NEXAFS spectra indicated that the molecules were oriented at an angle of 45±5 ° at low coverage, which changed to an almost perpendicular 70±5 ° at higher coverage. A coverage dependent phase transition was also found in a SHG study of pyridine on Ag(110) by Dai[25] *et al.*

A TPD study of pyridine on Ag(111) by Grassian[26] *et al.* shows evidence for monolayer and multilayer desorption. There is no other sub-multilayer peak, as in the thiophene TPD study of Umbach[8] *et al.* but the monolayer peak is quite broad. The observed phase transition described previously could explain the presence of the broad monolayer peak. The heating rates in each case are similar (1 Ks^{-1} (Umbach) and 1.5 Ks^{-1} (Grassian)), so the lack of an extra peak in the Grassian study must be due to the different properties of the adsorbates and the corresponding energy differences between flat and upright molecules for each study.

An XPS and HREELS study of pyridine adsorption on Cu(111) by Davies and Shukla[27] concludes that pyridine is reversibly adsorbed on the surface in a flat orientation at 190 K. A RAIRS study of pyridine adsorption on Cu(110) by Haq and King[28] shows that the orientation of pyridine is perpendicular to the surface at all coverages. They do not find any evidence for π-bonding to the surface, and conclude that the main source of adsorbate-substrate bonding is *via* the N lone pair. A PhD study of the same system by Woodruff[29] *et al.* states that the molecule is tilted by 20 ° to the surface normal and that the N sits nearly atop a Cu atom in the close-packed rows. In either study, there is no evidence of bonding from any other part of the pyridine molecule than the N lone pairs.

1.2.4. A review of relevant studies of methyl- and chloro- substituted aromatic molecules on single crystal surfaces.

There are very few studies of methyl- and chloro- substituted aromatic molecules on silver and copper substrates. There are no previously reported studies of methoxy-substituted aromatic molecules on any substrate. The following review presents a brief summary of the effects of these substituent groups, albeit on a variety of substrates, some of which support the decomposition of the adsorbates and some of which do not.

The aforementioned STM study by Hamers[11,12] *et al.* concerning thiophene on Ag(111) also studied 2,5-dimethylthiophene. In this study it was found that 2,5-dimethylthiophene also aligned itself on the top of step edges and supported the formation of islands, in an identical manner to that of thiophene. The adsorption of thiophene, 3-methylthiophene and 2,5-dimethylthiophene on Ni(111) has been studied

using HREELS, XPS and TPD by Huntley[30] *et al.* This study was primarily concerned with looking at the decomposition of these compounds on Ni(111). All of the compounds do decompose and 2,5-dimethylthiophene was found to decompose more readily than 3-methylthiophene, due to what the authors claim is the increased activity of the 2 and 5 positions of the thiophene ring during η^5 co-ordination. The authors claim that substitution of the thiophene ring by a methyl-group at the 3-position therefore does not interfere very much with the bonding of the molecule to the surface.

TPD data of toluene on Cu (110) has been reported by Bent[31] *et al.* in which the data looks very similar to that of benzene on Cu(110) by Lambert[19] *et al.* No structural studies were made of toluene on Cu(110) but the similar TPD spectra to benzene does imply that the methyl-group is not having a major effect on the adsorption. Other studies of toluene on single crystal metal (111) surfaces show differing behaviour with respect to the methyl-group. Raval[32] *et al.* who studied toluene on Ni(111) and Tardy[33] *et al.* who studied toluene on Pt(111) both conclude that the methyl group is strengthening the bond between the molecule, in comparison with benzene studies on the same corresponding surfaces. However, Muetterties and Grassian[34] who studied both benzene and toluene on Pd(111) at 180 K show that the methyl group makes no difference to the bonding of the aromatic ring to the surface.

A PhD study of 2-methylpyridine on Cu(110) by Woodruff[35] *et al.* shows that, as in the pyridine study[29], the molecule bonds in an almost perpendicular orientation to an almost atop-site on the surface. The methyl group causes a twist of the molecule so that the methyl group is pointed away from the surface.

TPD data of chlorobenzene on Ag(111) by Zhou and White[36] shows that the adsorption is molecular and reversible. The T_{max} of chlorobenzene was found to be 20 K higher than that of benzene on Ag(111). The authors point to a possible interaction of the Cl-group with the surface to explain this. The T_{max} of chlorobenzene on Si(111)7x7, as studied by Xu[37] *et al.* is also 20 K higher than that of benzene on Si(111)7x7 and the authors suggest the same reason as Zhou and White to explain this. A NEXAFS study of chlorobenzene on Cu(111) by White[38] *et al.* states that the angle of orientation of a sub-monolayer coverage of chlorobenzene is 46±5 °. An HREELS study of chlorobenzene on Ag(111), also by White[39] *et al.*

suggests that the molecules are bonded in a flat geometry on the surface. The authors do not suggest any reasons for this difference.

A TPD[26] and RAIRS[40] study of 3-chloropyridine by Grassian *et al.* shows that 3-chloropyridine desorbs molecularly from Ag(111) and at high coverages is oriented in a tilted geometry, similar to pyridine on Ag(111)[1,24]. Also studied was chlorobenzene[40] which was found to also desorb molecularly from Ag(111), with RAIRS showing that the molecule was oriented in a flat geometry on the surface, agreeing with the work by Zhou and White[36].

There are no surface science studies of methoxy-substituted aromatic compounds on any substrate. A theoretical study by Hay and Nicholas[41], which looked at the interaction between alkali metal ions and anisole (methoxybenzene), concluded that, for small alkali metal ions, there is an equal interaction between the ion and the aromatic ring and the ion and oxygen. For larger metal ions, the interaction between the ion and the oxygen was greater than that of the ion and the aromatic ring. Obviously, great care must be taken in comparing the present work concerning 3-methoxythiophene and Cu(111) with this theoretical study.

1.3 References

1. J.E. Demuth, J. Christmann and P.N. Sanda, *Chemical Physics Letters,* 1980, **76 (2)** 201-206.
2. P. Väterlein, M. Schmelzer, J. Taborski, T. Krause, F. Viczian, M. Bäßler, R. Fink, E. Umbach and W.Wurth, *Surface Science,* 2000, **452**, 20-32.
3. L. J. Sæthre and T.D. Thomas, *Journal of Organic Chemistry,* 1991, **56**, 3935-3942.
4. M. Nakazawa and G.A. Somorjai, *Applied Surface Science,* 1993, **68 (4)**, 517-537.
5. A.J. Gellman, *Accounts of Chemical Research,* 2000, **33 (1)**, 19-26.
6. N.V. Richardson and J.C. Campuzano, *Vacuum*, 1981, **31 (10-12)**, 449-451.
7. B.A. Sexton, *Surface Science,* 1985, **163**, 99-113.
8. K. M. Baumgärtner, M. Volmer-Uebing, J. Taborski, P Bäuerle and E. Umbach, *Berichte der Bunsengellshaft fur Physikalische Chemie,* 1991, **95**, 1488-1495.
9. A. Imanishi, S. Yagi, T. Yokoyama, Y. Kitajima and T. Ohta, *Journal of Electron Spectroscopy and Related Phenomena,* 1996, **80**, 151-154.
10. A. Imanishi, T. Yokoyama, Y. Kitajima and T. Ohta, *Bulletin of the Chemical Society of Japan,* 1998, **71**, 831-835.
11. E.R. Frank, X.X. Chen and R.J. Hamers, *Surface Science,* 1995, **334**, L709-L714.
12. X.Chen, E.R. Frank and R.J. Hamers, *Journal of Vacuum Science and Technology B,* 1996, **14 (2)**, 1136-1140.
13. R. Smoluchowski, *Physical Review,* 1941, **60**, 661.
14. M. Xi, M.X. Yang, S.K. Jo, B.E. Bent and P. Stevens, *Journal of Chemical Physics,* 1994, **101 (10)**, 9122-9131.
15. D. Velic, A. Hotzel, M. Wolf and G Ertl, *Journal of Chemical Physics,* 1998, **109 (20)**, 9155-9165.
16. S.J. Stranick, M.M. Kamma and P.S. Weiss, *Surface Science,* 1995, **338**, 41-59.
17. S.J. Stranick, M.M. Kamma and P.S. Weiss, *Nanotechnology,* 1996, **7**, 443-446.
18. S.J. Stranick, M.M. Kamma and P.S. Weiss, *Science,* 1996, **274**, 118-119.
19. J.R. Lomas, C.J. Baddely, M.S. Tikhov and R.M. Lambert, *Langmuir,* 1995, **11**, 3048-3053.
20. J.R. Lomas, C.J. Baddeley, M.S. Tikhov and R.M. Lambert, *Chemical Physics Letters,* 1996, **263**, 591-596.

21. A.C. Liu, J Stöhr, C.M. Friend and R.J. Madix, *Surface Science,* 1990, **235**, 107-115.

22. J.L. Solomon, R.J. Madix and J Stöhr, *Surface Science,* 1991, **255**, 12-30.

23. P. Yannoulis, R. Dudde, K.H. Frank and E.E. Koch, *Surface Science,* 1987, **189/190**, 519-528.

24. M. Bader, J. Haase, K.-H. Frank, A. Puschmann and A. Otto, *Physical Review Letters,* 1986, **56 (18)**, 1921-1924.

25. D. Heskett, K.J. Song, A. Burns, E.W. Plummer and H.L. Dai, *Journal of Chemical Physics,* 1986, **85 (12)**, 7490-7492.

26. K.B. Myli and V.H. Grassian, *Journal of Physical Chemistry,* 1994, **98 (25)**, 6237-6240.

27. P.R. Davies and N. Shukla, *Surface Science,* 1995, **322**, 8-20.

28. S. Haq and D.A. King, *Journal of Physical Chemistry,* 1996, **100**, 16957-16965.

29. T. Gießel, O. Schaff, R.Lindsay, P. Baumgärtel, M. Polcik, A.M. Bradshaw, A. Koebbel, T. McCabe, M. Bridge, D.R. Lloyd and D.P. Woodruff, *Journal of Chemical Physics,* 1999, **110 (19)**, 9666-9672.

30. D. R. Huntley, D.R. Mullins and M.P. Wingeier, *Journal of Physical Chemistry,* 1996, **100**, 19620-19627.

31. P.W. Kash, D.-H. Sun, M. Xi, G.W. Flynn and B.E. Bent, *Journal of Physical Chemistry,* 1996, **100**, 16621-16628.

32. A.M. Coats, E. Cooper and R. Raval, *Surface Science,* 1994, **307-309**, 89-94.

33. M. Abon, J.C. Bertolini, J. Billy, J. Massardier and B. Tardy, *Surface Science,* 1985, **162**, 395-401.

34. V.H. Grassian and E.L. Muetterties, *Journal of Physical Chemistry,* 1987, **91**, 389-396.

35. R. Terborg, M. Polcik, J.-T. Hoeft, M. Kittel, M. Pascal, J.H. Kang, C.L.A. Lamont, A.M. Bradshaw and D.P. Woodruff, *Surface Science,* 2000, **457**, 1-10.

36. X.-L. Zhou and J.M. White, *Journal of Chemical Physics,* 1990, **92 (9)**, 5612-5621.

37. Y. Cao, J.F. Deng and G.Q. Xu, *Journal of Chemical Physics,* 2000, **112 (10)**, 4759-4767.

38. M.X. Yang, M.Xi, H. Yuan, B.E. Bent, P. Stevens and J.M. White, *Surface Science,* 1995, **341**, 9-18.

39. Y. Song, P. Gardner, H. Conrad, A.M. Bradshaw and J.M. White, *Surface Science,* 1991, **248**, L279-L284.

40. K.B. Myli, S.R. Coon and V.H. Grassian, *Journal of Physical Chemistry,* 1995, **99**, 16407-16415.

41. J.B. Nicholas and B.P. Hay, *Journal of Physical Chemistry A,* 1999, **103**, 9815-9820.

Chapter 2. Theory

2.1. Introduction

This section deals with the six techniques that were used in the current work. These are TPD, AES, LEED, XPS, NEXAFS and NIXSW. As these are established techniques, more extensive reviews than what will be presented here can be found for TPD, AES, LEED and XPS in a text by Woodruff and Delchar[1], for NEXAFS in a text by Stöhr[2] and for NIXSW in a review by Woodruff[3].

2.2 Theory

2.2.1. TPD

In a TPD experiment, a constant heating ramp is applied to an adsorbate-covered sample. Desorption from the sample is monitored by a QMS placed directly in front of the sample. If the pumping speed of the chamber is very large compared to the rate of desorption, the pressure rise in the chamber caused by the desorption process is proportional to the desorption rate and peaks present in the corresponding pressure-temperature curve represent different adsorption states. The temperature at which maximum desorption occurs, T_{max}, on the pressure-temperature curve corresponds to the maximum desorption rate.

The main information of interest that can be gained from a TPD experiment are the activation energy of desorption, E_d, the order of desorption, n=0,1,2..., and the rate constant for desorption, k_d. However, in the current work, TPD was used to identify adsorption states and calculate relative coverages, owing to the fact that the area under a TPD spectrum is proportional to coverage.

Desorption from a single crystal surface under UHV conditions can be represented by the following Arrhenius-type relationship

$$k_d = A\exp\frac{-E_d}{RT} \qquad (1)$$

where k_d is the rate constant for desorption, A is the pre-exponential factor ($\approx 10^{13}$ s^{-1}), E_d is the activation energy for desorption, R is the gas constant and T is the temperature. Equation (1) implies that the rate of desorption should increase exponentially. The reason a maximum is observed in the pressure-temperature curve is because as k_d increases, the surface coverage decreases. Hence, desorption can also be described by the following equation:

$$-\frac{d\theta}{dt} = k_d \theta^n \qquad (2)$$

where θ is the number of adsorbed molecules and n is the order of the reaction.
Re-arranging

$$\frac{d\theta}{dt} = \frac{d\theta}{dT} x \frac{dT}{dt} = \frac{d\theta}{dT}\beta \qquad (3)$$

where $\beta = \frac{dT}{dt}$, which corresponds to the heating rate. By exchanging $\frac{d\theta}{dt}$ for $\frac{d\theta}{dT}\beta$ and substituting into (1)

$$-\frac{d\theta}{dT} = \theta^n \frac{A}{\beta} \exp(\frac{-E_d}{RT}) \qquad (4)$$

At T_{max}, $\frac{d^2\theta}{dT^2}$ = 0, as the rate of desorption is at a maximum, so differentiating equation (4) with respect to T, gives the general expression

$$\frac{E_d}{RT_{max}^2} = \frac{A}{\beta} n\theta^{n-1} \exp(\frac{-E_d}{RT_{max}}) \qquad (5)$$

So for 1st order desorption

$$\frac{E_d}{RT_{max}^2} = \frac{A}{\beta} \exp(\frac{-E_d}{RT_{max}}) \qquad (6)$$

and for 2nd order desorption

$$\frac{E_d}{RT_{max}^2} = \frac{2A\theta}{\beta}\exp(\frac{-E_d}{RT_{max}}) \qquad (7)$$

As is obvious from equations (6) and (7), second order desorption processes are coverage dependent due to the θ term in equation (7). A "rule of thumb" in assigning the reaction kinetics of a desorption experiment from the spectra is that 1st order desorption spectra are asymmetric about T_{max} and 2nd order desorption spectra are symmetric about T_{max}. Also, as 1st order desorption processes are independent of coverage, if the desorption temperature, T_{max}, shifts with changing coverage, then the process being studied follows 2nd order kinetics.

Great care must be taken however in using these rules. Adsorbate-adsorbate interactions can invalidate the simple assigning of 1st and 2nd order kinetics. First order desorption processes with variable activation energies might also give symmetric desorption peaks. If E_d varies with coverage, then T_{max} becomes coverage dependent. However, a plot of ln (θT_{max}) versus $1/T_{max}$ gives a straight line for 2nd order desorption with a fixed E_d.

2.2.2 AES

A schematic representation of a $KL_1L_{2,3}$ Auger process is shown in figure 1. For low atomic number, Z, Auger processes predominate after the formation of the core hole, but at higher Z, the Auger electron is not emitted and energy is emitted instead in the form of X-ray fluorescence.

The kinetic energy of the Auger electron represented in figure 1 is

$$E_{kin} = E_K - E_{L1} - E_{L2,3} - \phi \qquad (8)$$

Where φ is the work function of the material being studied. The kinetic energy of an Auger electron is independent of the kinetic energy of the incident radiation. Auger electrons are characteristic of elemental species because their energies are dependent on the energy levels within the atom. Therefore, AES can be used to identify atomic

species. It is also quantitative as the AES signal is proportional to the surface coverage up to saturated monolayer coverage. Above this coverage, inelastic energy losses by Auger electrons from the monolayer by subsequent layers leads to inaccurate (smaller) calculated coverages.

Figure 1: *Schematic representation of a $KL_1L_{2,3}$ Auger process. The energy levels in this diagram are not drawn to scale.*

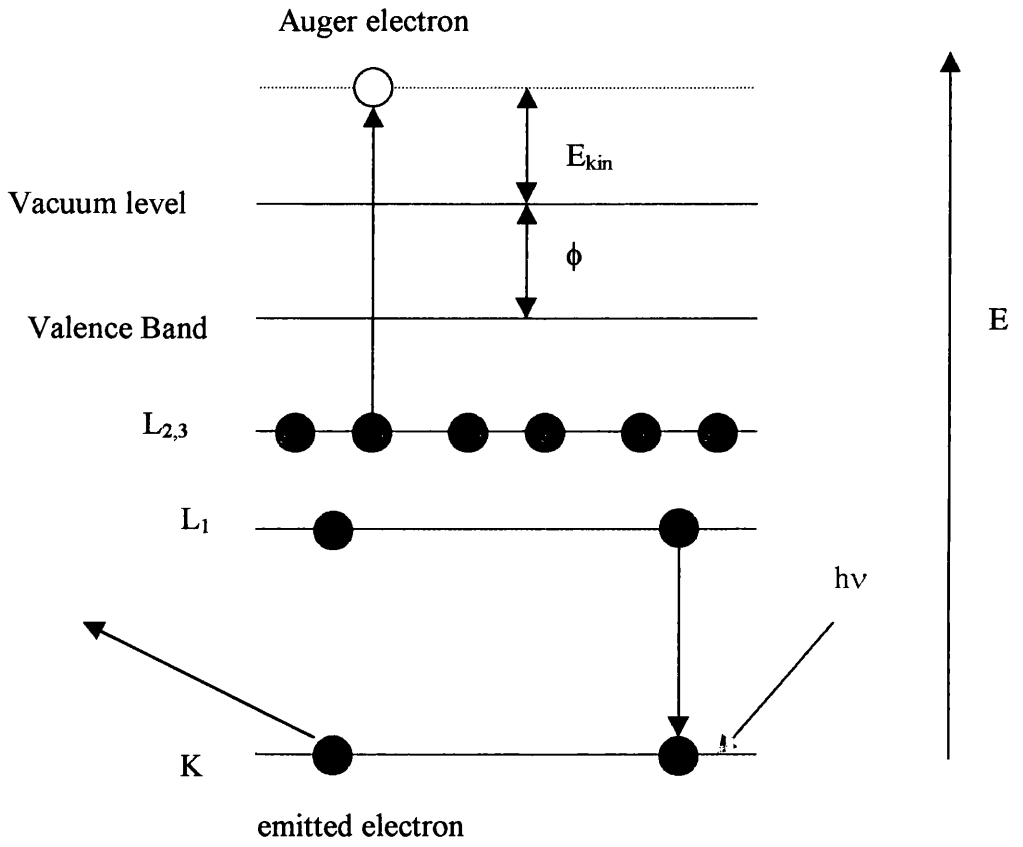

2.2.3. LEED

In a LEED experiment, electrons with kinetic energies ranging from 20-1000 eV are elastically scattered from a surface. Electrons in this energy range possess inelastic mean free paths of between 5-20 Å and are therefore ideal for surface studies. Using this energy range, the electrons have de Broglie wavelengths similar to interatomic spacings and are therefore diffracted to give characteristic patterns due to the long-range order present on a single crystal surface.

Figure 2: *Schematic diagram of diffraction of a beam of electrons from a hypothetical 1-dimensional array of point scatterers of equal spacing, a. From "Surfaces", by Attard and Barnes, Oxford University Press, Oxford, 1998*[4].

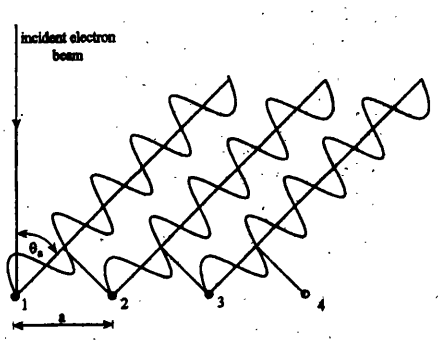

From figure 2, for constructive interference of the scattered waves

$$n\lambda = a\sin\theta_a \qquad (9)$$

where n = 0, ±1, ±2, ±3... and the wavelength is

$$\lambda = \frac{h}{mv} \qquad (10)$$

where h is Planck's constant, m is mass and v is velocity.

The magnitude of the incident wave-vector, $\mathbf{k}_0$, is defined as

$$|\mathbf{k}_0| = \frac{2\pi}{\lambda} \qquad (11)$$

Combining (10) and (11) and substituting into (9) gives

$$|\mathbf{k}_0|\sin\theta_a = \left(\frac{2\pi}{a}\right)n \qquad (12)$$

Figure 3 shows that $|\mathbf{k}_0|\sin\theta_a$ is in fact the component of momentum parallel to the surface, $\mathbf{k}_{\|}$, of the incident electron.

Figure 3: *This diagram shows the components of* $\mathbf{k}_0$ *and from this diagram,* $|\mathbf{k}_{\parallel}| = |\mathbf{k}_0| \sin\theta$ and $\mathbf{k}_{\perp}| = |\mathbf{k}_0| \cos\theta$.

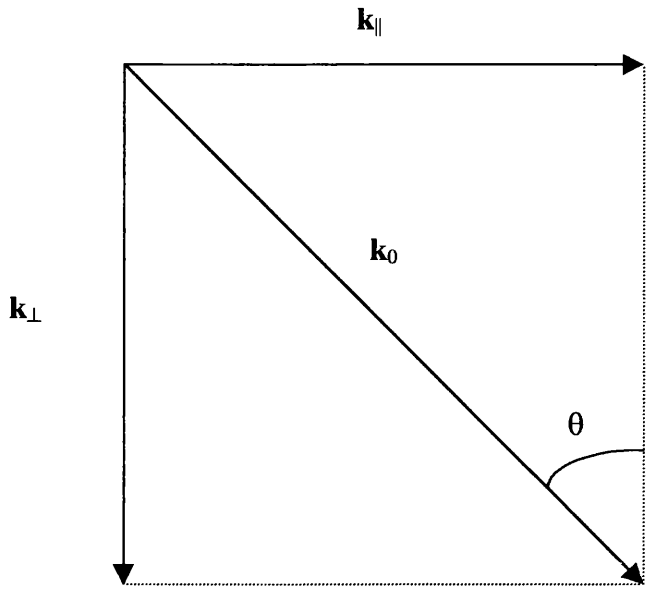

As n can only take values of 0, ±1, ±2, ±3..., parallel momentum can only be exchanged with the surface in quantized units of $\frac{2\pi}{a}$ (equation (12)). Hence, $\left\{\frac{2\pi}{a}\right\}$ is the magnitude of the one-dimensional reciprocal lattice vector associated with the diffraction of the electron beam. Conservation of momentum in the scattering process means that in order for the electrons to change direction, they must exchange momentum with the one-dimensional lattice. Hence

$$\Delta \mathbf{k}_{\parallel} = |\mathbf{k}_0| \sin\theta_a = \frac{2\pi}{a} n \qquad (13)$$

Introducing a second orthogonal array of scatterers with a lattice spacing b means that the following equation can be derived in an identical manner

$$\Delta \mathbf{k}_{\parallel} = |\mathbf{k}_0| \sin\theta_b = \frac{2\pi}{b} m \qquad (14)$$

Where m is analogous to n and can take values from 0, ±1, ±2, ±3...

For diffraction to occur from a 2-dimensional array, equations (13) and (14) must be satisfied simultaneously. In this case, the exchange of parallel momentum is restricted to a 2-dimensional reciprocal lattice vector, **G**.

$$\mathbf{G} = \Delta \mathbf{k}_{\|} = n\frac{2\pi}{a} + m\frac{2\pi}{b} \qquad (15)$$

The 2-dimensional array generates a reciprocal lattice upon diffraction according to

$$\mathbf{G} = n\mathbf{a}^* + m\mathbf{b}^* \qquad (16)$$

where

$$|\mathbf{a}^*| = \frac{2\pi}{|a|} \qquad (17)$$

$$|\mathbf{b}^*| = \frac{2\pi}{|b|} \qquad (18)$$

$$\mathbf{a}\cdot\mathbf{b}^* = \mathbf{a}^*\cdot\mathbf{b} = 0 \qquad (19)$$

Where **a,b** are the vectors of the surface 2-dimensional array and **a*,b*** are the vectors of the corresponding reciprocal lattice. Thus

$$\mathbf{k}_0^{\|} = \mathbf{k}_s^{\|} + \mathbf{G} \qquad (20)$$

therefore becomes the condition for diffraction, where $\mathbf{k}_s^{\|}$ is the parallel component of the scattered electron.

Ewald Sphere Construction

An alternative way of explaining electron diffraction is by constructing an Ewald sphere. The Ewald sphere consists of a circle, in 2-dimensions, of radius $|\mathbf{k}_0|$. Diffraction occurs each time the sphere cuts a reciprocal lattice rod (figure 4).

Figure 4: *Ewald sphere construction. From "Surfaces", by Attard and Barnes, Oxford University Press, Oxford, 1998*[4].

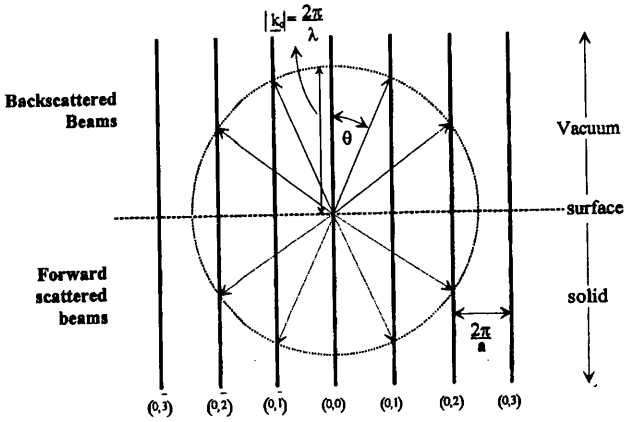

2.2.4. XPS

In XPS, an electron is emitted from an energy level by an X-ray beam, figure 5. The energy of the emitted photoelectron shown in figure 5 is given by

$$E_k = h\nu - E_B + \phi \qquad (21)$$

Hence, unlike Auger electrons, the kinetic energy of photoelectrons is dependent on the kinetic energy of the incident X-rays. However, equation (21) is only valid if the electronic states of the system are the same after the ionisation of the electron as they were before. This is known as Koopman's theorem.

Figure 5: *Schematic diagram showing an XPS process. The energy levels in this diagram are not drawn to scale. From "Surfaces", by Attard and Barnes, Oxford University Press, Oxford, 1998*[4].

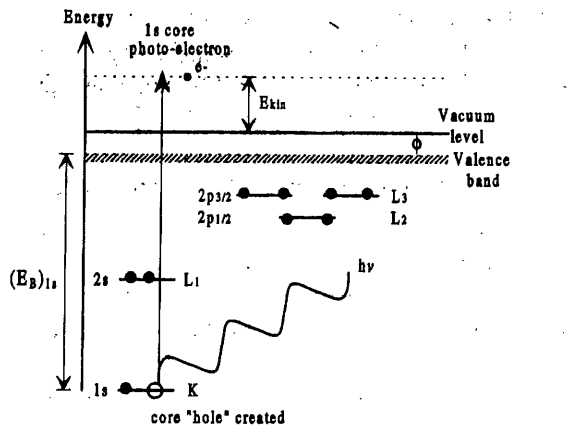

Breakdown of Koopman's theorem

In a real system, the electronic states after ionisation are different to those before the ionisation event. The remaining electrons relax to a different energy state after the ionisation event in order to screen the core hole that has been created, a so-called "final-state shift". This gives the emitted photoelectron slightly more energy and so its kinetic energy can be re-stated as

$$E_k = h\nu - E_B + \phi + E_R \qquad (22)$$

Where E_R is the final-state shift energy and is of the order of a few eV.

XPS is often used as a probe of the chemical environment of elemental species. This is because atoms with partial positive charges have higher binding energies associated with increased Coulombic attraction between the core electrons and the nucleus. Conversely, atoms with partial negative charges have lower binding energies associated with decreased Coulombic attraction between core electrons and the nucleus. Therefore atoms in a high formal oxidation state will yield XPS peaks at higher binding energies relative to the same atom in a low oxidation state.

2.2.5. NEXAFS

In a NEXAFS experiment, a surface atom is selected by one of its characteristic absorption edges. In the current work, all of the NEXAFS experiments performed on each adsorbate studied were S K-edge NEXAFS experiments.

The X-ray absorption cross-section of an atom or molecule is defined as the number of electrons excited per unit time divided by the number of incident photons per unit time per unit area. The cross–section can be calculated from Fermi's "Golden rule" for the transition probability per unit time from a state $|i\rangle$ to a state $|f\rangle$, and is given by

$$\sigma_x = \frac{4\pi^2\hbar^2}{m^2}\frac{e^2}{\hbar c}\frac{1}{\hbar\omega}\left|\langle f|\mathbf{e}\cdot\mathbf{p}|i\rangle\right|^2 \rho_f(E) \qquad (23)$$

where ω is frequency, $\mathbf{e}$ is the unit vector of electromagnetic wave, $\mathbf{p} = \Sigma\mathbf{p}_i$, the sum of the linear momentum operators of the electrons and $\rho_f(E)$ is the energy density of final states.

The important resonant transitions in NEXAFS work are transitions from the K-edge (s-type) level to π^* or σ^* final states. The polarization dependence of the intensity of a particular orbital can be obtained from the dipole matrix element in (23) and therefore the transition intensity, I_{if}, can be written as

$$I_{if} \propto \left|\langle f|\mathbf{e}\cdot\mathbf{r}|i\rangle\right|^2 \propto \left|\ \mathbf{e}\cdot\langle f|\mathbf{r}|i\rangle\ \right|^2 \qquad (24)$$

assuming that the X-rays are linearly polarised in the direction of the unit vector, $\mathbf{e}$. $\mathbf{r}$ is the position vector and can be expressed in spherical co-ordinates as

$$\mathbf{r} = r(\sin\theta\cos\phi\,\mathbf{e}_x + \sin\theta\sin\phi\,\mathbf{e}_y + \cos\theta\,\mathbf{e}_z) \qquad (25)$$

The initial 1s state, $|i\rangle = R_{1s}(r)$ is spherically symmetric and to a good approximation can be represented by the atomic 1s wavefunction of the excited atom in the molecule. The 1s initial state is localised and hence it is the atomic valence components of the

excited atom that dominate in the evaluation of the dipole matrix element. So, for sulfur, only the 2s and 2p terms need be considered in the final state wave function and a LCAO representation of this is shown in equation (26).

$$\begin{aligned} |f\rangle &= a|2s\rangle + b|2p_x\rangle + c|2p_y\rangle + d|2p_z\rangle \\ &= aR_{2s}(r) + R_{2p}(r)(b\sin\theta\cos\phi + c\sin\theta\cos\phi + d\cos\theta) \\ &= aR_{2s}(r) + R_{2p}(r)(b\sin\theta\cos\phi + c\sin\theta\cos\phi + d\cos\theta) \end{aligned} \qquad (26)$$

where a, b, c, d, give the weights of the AOs in the LCAO expansion and R_{2s} (r) and R_{2p} (r) are the radial atomic wavefunctions. From (26), the maximum amplitude of the final state orbital is in the direction **O**, where $\mathbf{O} = b\mathbf{e}_x + c\mathbf{e}_y + d\mathbf{e}_z$. **O** is simply the superposition of the three p-orbitals and $\mathbf{e}_I$ are unit vectors.

Combining (25) and (26) and integrating

$$\langle f|\mathbf{r}|i\rangle = R\frac{4}{\pi}(b\mathbf{e}_x + c\mathbf{e}_y + d\mathbf{e}_z) \qquad (27)$$

where

$$R = \int R_{2s}(r)R_{2p}(r)r^3 dr \qquad (28)$$

So, according to (27), for K-shell excitation, the vector matrix element points in the same direction as the p-component in the final state orbital on the excited atom.

This conclusion forms the basis of the selection rules in NEXAFS for calculating the orientation of molecules adsorbed on surfaces. The next section extends this idea to the real case of thiophenic molecules.

NEXAFS spectroscopy of adsorbed thiophene

It is usual in NEXAFS methodology, whilst discussing the polarisation of K-shell excitation, to classify molecules into groups[5]. This is due to the fact that π^* and σ^* orbitals in organic molecules describe the nature of the bonding in the molecules. Hence, by using polarised X-rays, the presence, or absence, of π^* and σ^* orbitals can provide information on the geometry of the adsorbed species.

It is convenient to describe the MOs of thiophene as consisting of "vectors" and "planes". In thiophene, the atoms in the ring are σ-bonded to one another. Hence, this can be viewed as a planar arrangement of σ* orbitals in the plane of the ring. The π* orbitals are perpendicular to the ring and can be viewed as a set of vectors, figure 6.

Figure 6: *Diagram showing how the σ-bonds in thiophene can be represented by a plane of bonds in the plane of the ring and the π-bonds can be represented as vectors perpendicular to the ring.*

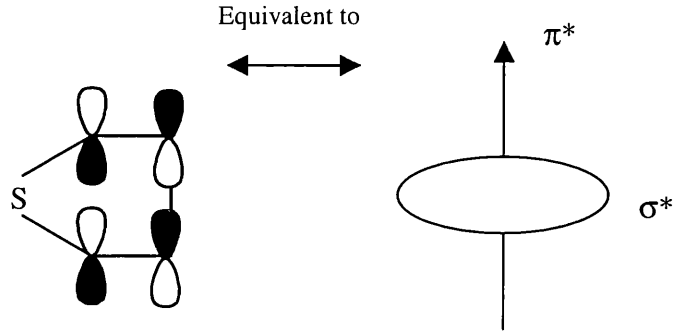

The transitions of main in interest in NEXAFS are that from an s-initial state (K-level) to the p-component of a of π* or σ* final states. Figure 7 shows thiophene drawn with a co-ordinate system.

Figure 7: *Thiophene drawn with an accompanying co-ordinate system.*

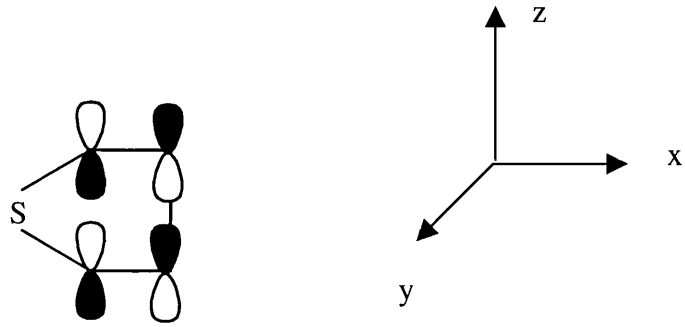

The incoming X-radiation can be defined by an electric field vector **e** with spherical angles θ' and ϕ'. The polarisation intensity of the π^* resonance can be shown to be[5]

$$I_{if}(\pi) \propto \left| \mathbf{e} \cdot \mathbf{e}_z \right|^2 \propto \cos^2 \theta' \qquad (29)$$

and of the σ^* resonance

$$I_{if}(\sigma) \propto \left| \mathbf{e} \cdot \mathbf{e}_x \right|^2 + \left| \mathbf{e} \cdot \mathbf{e}_y \right|^2 \propto \sin^2 \theta' \cos^2 \phi' + \sin^2 \theta' \sin^2 \theta' \propto \sin^2 \theta' \qquad (30)$$

Therefore, the resonances associated with π^* and σ^* final states have strong and opposite polarisation dependence.

In simple terms, when the molecule is oriented in a flat orientation in the xy-plane, there is maximum overlap between the π^* orbitals and the polarisation of the incoming X-ray beam when the beam is at grazing incidence. When the incoming X-radiation is at normal incidence, there is maximum overlap between the σ^* orbitals and the polarisation of the beam, if the molecule is oriented in a flat orientation. Conversely, if the molecule is oriented in an upright orientation, there is maximum overlap between the σ^* orbitals and the polarisation of the beam at grazing incidence and maximum overlap between the π^* orbitals and the polarisation of the beam at normal incidence, figure 8.

Figure 8 shows the basic selection rules that can be used in assigning the orientation of thiophenic molecules on surfaces. However, the actual angle can be calculated by analysis of the relative areas of the π^* and σ^* resonances in NEXAFS spectra. It can be shown[5] that, by using the π^* resonances, the angle of orientation can be calculated from:

$$I(\theta) \propto \frac{1}{3} P \left[1 + \frac{1}{2} \left(3\cos^2 \theta - 1 \right) \left(3\cos^2 \alpha - 1 \right) \right] \qquad (31)$$

and by using the σ^* resonances, the angle of orientation can be calculated from:

$$I(\theta)=\frac{2}{3}\left[1-\frac{1}{4}\left(3\cos^2\theta-1\right)\left(3\cos^2\gamma-1\right)\right] \qquad (32)$$

where P is the degree of polarisation of the X-ray beam (0.85)[6], θ is the angle of X-ray incidence (19.5 ° for grazing and 90 ° for normal), and α and γ represent the angle that the molecules makes with the surface.

Figure 8: *Hypothetical thiophene molecules in flat (a) and upright (b) orientations and how the orbitals overlap with the polarisation vector of the incoming X-ray (red). The black arrows indicate the incoming X-ray.*

(a)

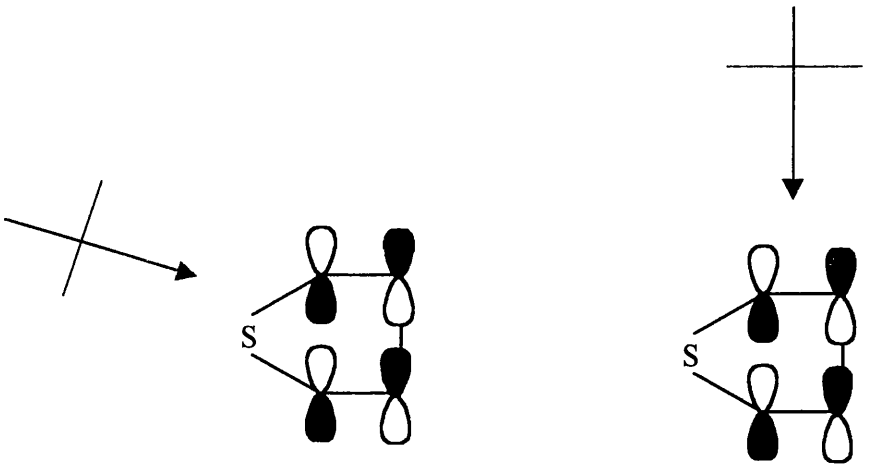

(b)

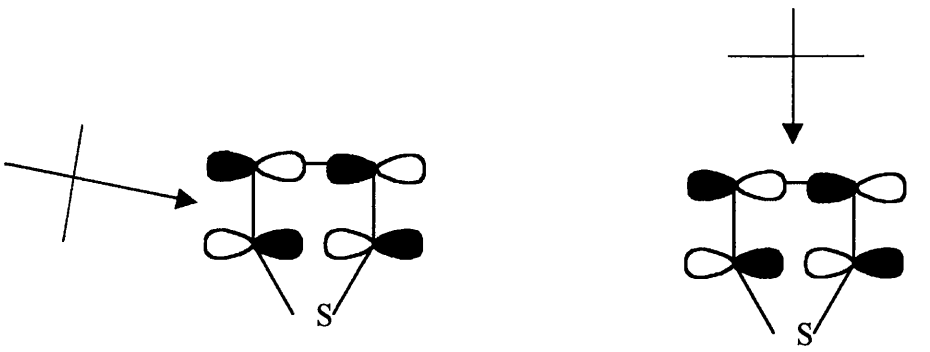

2.2.6. NIXSW

In a NIXSW experiment, a Bragg condition is established in a crystal by X-radiation of the required energy at normal incidence. The incident and back-scattered X-ray waves combine to form an X-ray standing wave (XSW) which has an intensity periodicity equal to the spacings of the scatterer plane.

The XSW can penetrate up to a μm into the surface of the crystal and extends as a coherent XSW outside the crystal over a distance comparable to the distance of a typical bonded adsorbate. As the nodes of the XSW are related to the scatterer plane distance, the XSW can be viewed as creating hypothetical lattice planes above the surface from which the position of an adsorbate can be determined. In practice this is achieved by monitoring either adsorbate Auger electron emission, photoemission or X-ray fluorescence. In the current work, only Auger electron and photoemission were monitored in NIXSW experiments.

The intensity of an XSW in a crystal can be represented as

$$I = \left| 1 + \left(\frac{E_H}{E_O} \right) \left(\exp\left(-2\pi i z / d_H \right) \right) \right|^2 \qquad (33)$$

where E_H and E_O are the amplitudes of the reflected and incident X-rays respectively, z, is the perpendicular distance of the adsorber atom from the surface and d_H is the scattering plane distance. The amplitude of the scattered wave relative to the incident wave is the square root of the reflectivity, R, multiplied by a phase factor

$$\frac{E_H}{E_O} = \sqrt{R} \exp(i\varphi) \qquad (34)$$

which means that

$$I = 1 + R + 2\sqrt{R} \cos\left(\varphi - 2\pi z / d_H \right) \qquad (35)$$

This analysis is only strictly true for a single adsorbate position on a rigid lattice. In reality, there may be a distribution of adsorption sites due to vibrational or static disorder. This can be represented by a distribution of z-values such that

$$\int_0^{d_H} f(z)dz = 1 \qquad (36)$$

In this case, the absorption profile is given by

$$I = 1 = R + 2\sqrt{R}\int_0^{d_H} f(z)\cos(\varphi - 2\pi z / d_H)d_z \qquad (37)$$

which can also be written as

$$I = 1 + R + 2f_{co}\sqrt{R}\cos(\varphi - 2\pi D(hkl)/d_H) \qquad (38)$$

in terms of two parameters, the coherent fraction, f_{co} and the coherent position, D(hkl). The coherent fraction is a measure of how well-defined the adsorption site is and is expressed as a number between 0-1. The coherent position is the perpendicular distance from the nearest scattering plane to the adsorbate in Å. This scattering plane may or may not go through the surface and the coherent position extracted from analysis of NIXSW profiles may be with respect to the hypothetical lattice planes that are formed in the formation of an XSW.

It is convenient to re-write equation (38) in the form:

$$I = f_{co}\left(1 + R + 2\sqrt{R}\cos(\varphi - (2\pi D(hkl)/d_H))\right) + (1 - f_{co})(1 + R) \qquad (39)$$

The first half of this equation is now the right hand-side of equation (35) multiplied by f_{co} while the second term is (1- f_{co}) (the incoherent fraction) multiplied by (1+R), the wavefield intensity sum of the incident and reflected waves in the absence of coherent interference. A simpler way of relating the coherent fraction and coherent position is:

$$f_{co}\exp(2\pi iD(hkl)/d_H)=\int_0^{d_H} f(z)\exp(2\pi iz/d_H)dz \qquad (40)$$

This final equation allows the construction of an Argand diagram to show how the quantities f_{co} and D(hkl) relate to the integral in (40) over a real spatial distribution function.

In the Argand diagram, each vector is defined by its length, f_{co} and angle, $2\pi D(hkl)/d_H$, figure 9.

Figure 9: *Argand diagram representation of coherent fraction, f_{co}, and coherent position, D(hkl). The axes are labelled I for imaginary and R for real.*

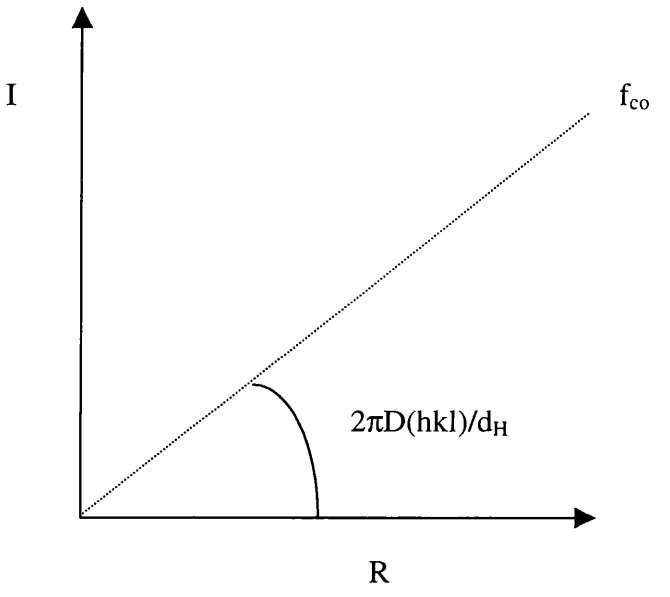

Adsorption Site Occupation

The four principal adsorption sites on a (111) surface are atop, bridge, f.c.c. and h.c.p., figure 10. In order to unambiguously assign an adsorption site, NIXSW experiments are performed with respect to the (111) and ($\bar{1}11$) planes. This results in two sets of coherent fractions and coherent positions for the same adsorbate. Using a process of real space triangulation of the coherent positions using the following equations it is possible to assign the adsorption site. In effect, these equations allow the calculation of D($\bar{1}11$) for each of the four sites mentioned and it is then a case of

matching the experimental D($\bar{1}11$) value from the ($\bar{1}11$) NIXSW experiment to assign the adsorption site.

Figure 10: *Diagram showing the four principal adsorption sites on a (111) surface and the two different planes, (111) and ($\bar{1}11$) that are used in NIXSW experiments. The values noted in Å are not related to the current work and are top be ignored. From reference 3.*

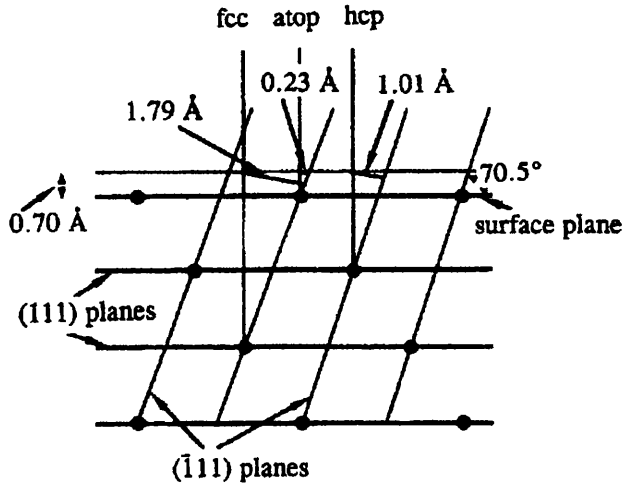

$$\text{Atop: } D(\bar{1}11) = D(111)/3 \qquad (41)$$

$$\text{Bridge: } D(\bar{1}11) = D(111)/3 + d(111)/2 \qquad (42)$$

$$\text{F.C.C.: } D(\bar{1}11) = (D(111) + 2d(111))/3 \qquad (43)$$

$$\text{H.C.P.: } D(\bar{1}11) = (D(111) + d(111))/3 \qquad (44)$$

This procedure works perfectly well with high coherent fraction and single adsorption sites. With lower coherent fractions, there is the possibility of multiple site occupation and in this case, Argand diagrams have to be used to derive the adsorption site(s). A vector is drawn on the diagram which represents the experimental D($\bar{1}11$) result and four other vectors representing the four sites mentioned are drawn derived

from the (111) data. The lengths and angles of the four other vectors can be directly derived from the (111) data however, the length of the bridging vector is 1/3 of the other vectors, because there are two inequivalent ($\bar{1}11$) layer spacings for this site with weightings of 1/3 and 2/3 respectively. On any Argand diagram, these vectors are π radians apart, and hence the resultant vector has a weighting of 1/3 and is therefore a third of the length of the atop, h.c.p. and f.c.c. vectors. By manipulation of the derived vectors it is usually possible to derive the possible adsorption site(s) from Argand diagrams.

Non-dipole effects in photoemission NIXSW studies

In using photoemission as a monitor of X-ray absorption in NIXSW experiments, it is important that the measured photoemission signal provides an accurate description of the intensity of the X-ray standing wave at the absorber. As electron spectrometers are angle-resolving, this may not be the case. Naturally in a NIXSW experiment, the photoelectrons are detected in a "backwards" direction with respect to the incident X-rays. However, the detector is in the "forward" direction with respect to the reflected beam. Therefore, any backward/forward asymmetry in the photoemission due to non-dipole excitation results in differing efficiency in the measurement of the incident and reflected components of the XSW. This results in a XSW profile which differs from a purely dipole absorption profile.

The net effect of this is that the analysis of photoemission XSW profiles leads to coherent fractions that are too high, sometimes >1. Recent NIXSW studies have rectified this problem by introducing a "Q-factor" into the analysis to account for this anomaly and therefore, correctly fit NIXSW data[7]. S 1s NIXSW profiles from thiophene studies are shown, together with S KLL Auger NIXSW profiles, in Chapter 4 where the absence of non-dipole effects in S 1s NIXSW experiments is shown.

2.3 References

1. D.P. Woodruff and T.A. Delchar, *Modern Techniques in Surface Science – Second Edition,* Cambridge University Press, Cambridge, 1994.
2. J. Stöhr, *NEXAFS Spectroscopy,* Springer-Verlag, New York, 1996.
3. D.P. Woodruff, *Progress in Surface Science*, 1998, **57** (1), 1-60.
4. G. Attard and C. Barnes, *Surfaces*, Oxford University Press, Oxford, 1998.
5. This is detailed in Chapter 9 in reference 2.
6. A.A. M^{c}Dowell, D. Norman, J.B. West, J.C. Campuzano and R.G. Jones, *Nuclear Instrumental Methods A,* 1986, **246**, 131.
7. C.J. Fisher, R. Ithin, R.G. Jones, G.J. Jackson, D.P. Woodruff and B.C.C. Cowie, *Journal of Physics: Condensed Matter,* 1998, **10**, L629.

Chapter 3. Experimental

3.1 Introduction

This chapter presents an outline of the UHV chamber that was constructed in the Chemistry department at Glasgow. The chamber was equipped with TPD, AES and LEED capabilities and the experimental procedures involved in performing experiments using these techniques is also described. Other experiments described in the current work were performed at Station 6.3 of the Daresbury Laboratory and the description of this chamber and beamline can be found in reference 1.

3.2 Experimental (Glasgow)

3.2.1 Obtaining UHV conditions

Figure 1 shows a schematic diagram of the Glasgow UHV system. Figure 2 shows a simplified version of the chamber showing a schematic diagram of the pumping arrangement. Four pumps are used to reduce the pressure in the chamber from atmospheric pressure to $1x10^{-10}$ mbar. Firstly, the rotary pump (Edwards) is used to acquire a pressure of $1x10^{-2}$ mbar. At this pressure, the turbomolecular pump (Varian V-250) is then used to reach pressures of $1x10^{-7}$ mbar. By then using the ion pump (Varian Vac-Ion Plus 300 Triode) it is possible to obtain pressures of $1x10^{-8}$ mbar.

In order to obtain UHV pressures, that is of the order of $1x10^{-10}$ mbar, it is necessary to bake the entire chamber. This is achieved by placing ceramic heaters on the table, figure 1, and encasing the upper part of the chamber with cladded steel covers. The part of the chamber underneath the table is covered with separate heating straps and all bare metal parts of the chamber are covered in aluminium foil. There is a separate heater for the ion pump. During the bake-out procedure, which usually lasts for 16 hours, the turbomolecular pump is continuously cooled with water. Once the bakeout has been in operation for 3-4 hours the ion pump is switched on, providing the pressure in the chamber is at least as low as $1x10^{-6}$ mbar. Once the

pressure reaches $1.5x10^{-7}$ mbar, which usually takes 16 hours, the bakeout is switched off.

During bakeout, the TSP (Varian 916-0017) is left on at a current of 25 A. and after bake-out, the TSP is fired once every ten minutes at a working current of 45-50 A during the first post-bakeout hour and subsequently once every three hours. A UHV base pressure of $1x10^{-10}$ mbar is obtained on de-gassing of the sample, ion gun (PSP Vacuum Technology), QMS (RC RGA Hiden Analytical), LEED/AES electron gun (RVL, VG Microtech) and ion gauge.

3.2.2 Sample Preparation

The Cu(111) crystal was mounted onto a sample re-entrant, as shown in figure 4, by spot-welding a strip of tantalum to the two tungsten rods at the bottom of the device. Tantalum was used because it is non-magnetic and the sample holder had to be capable of supporting the use of the HREELS spectrometer, which uses a low energy electron beam, however, HREELS experiments were not performed in this project.

The principle problems with the design of the sample holder were related to both the cooling and heating of the sample. Cooling of the sample to 122 K was achieved by filling the glass re-entrant with liquid nitrogen. Sufficient thermal contact had to be made between the strip of tantalum and the crystal to allow for cooling. Figure 3 shows a more detailed drawing of the sample holder.

The crystal temperature was measured by means of a chromel/alumel thermocouple in which two wires, one chromel and one alumel, were twisted together and inserted into a hole at the top of the crystal. The two wires were then separated and covered in ceramic pipes close to the crystal and a plastic sheathing further up the sample holder. The two wires were connected to corresponding chromel/alumel connections at the top of the sample holder and this was then connected to a Eurotherm box.

A dedicated power supply (Thurlby TSX) was used to provide a constant current supply in order to anneal the crystal. A clean Cu(111) crystal surface was prepared by firstly bombarding the sample with Ar^+ ions using an ion gun. The target

Figure 1: *Schematic diagram of Glasgow UHV system. Certain parts of the system concerned with pumping have been omitted for clarity but are shown in figure 2.*

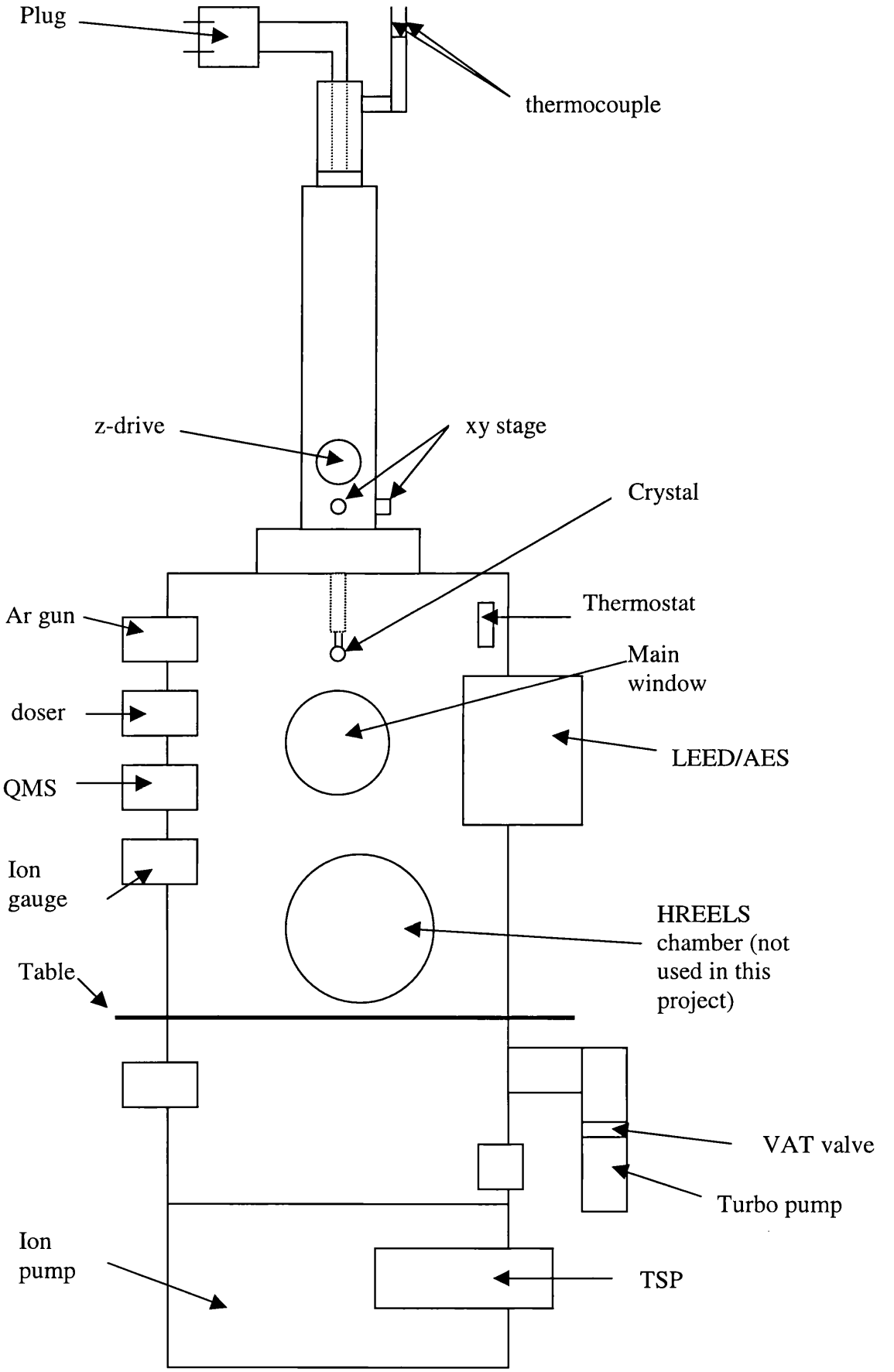

Figure 2: *Schematic diagram of the pumping arrangement of the Glasgow UHV system.*

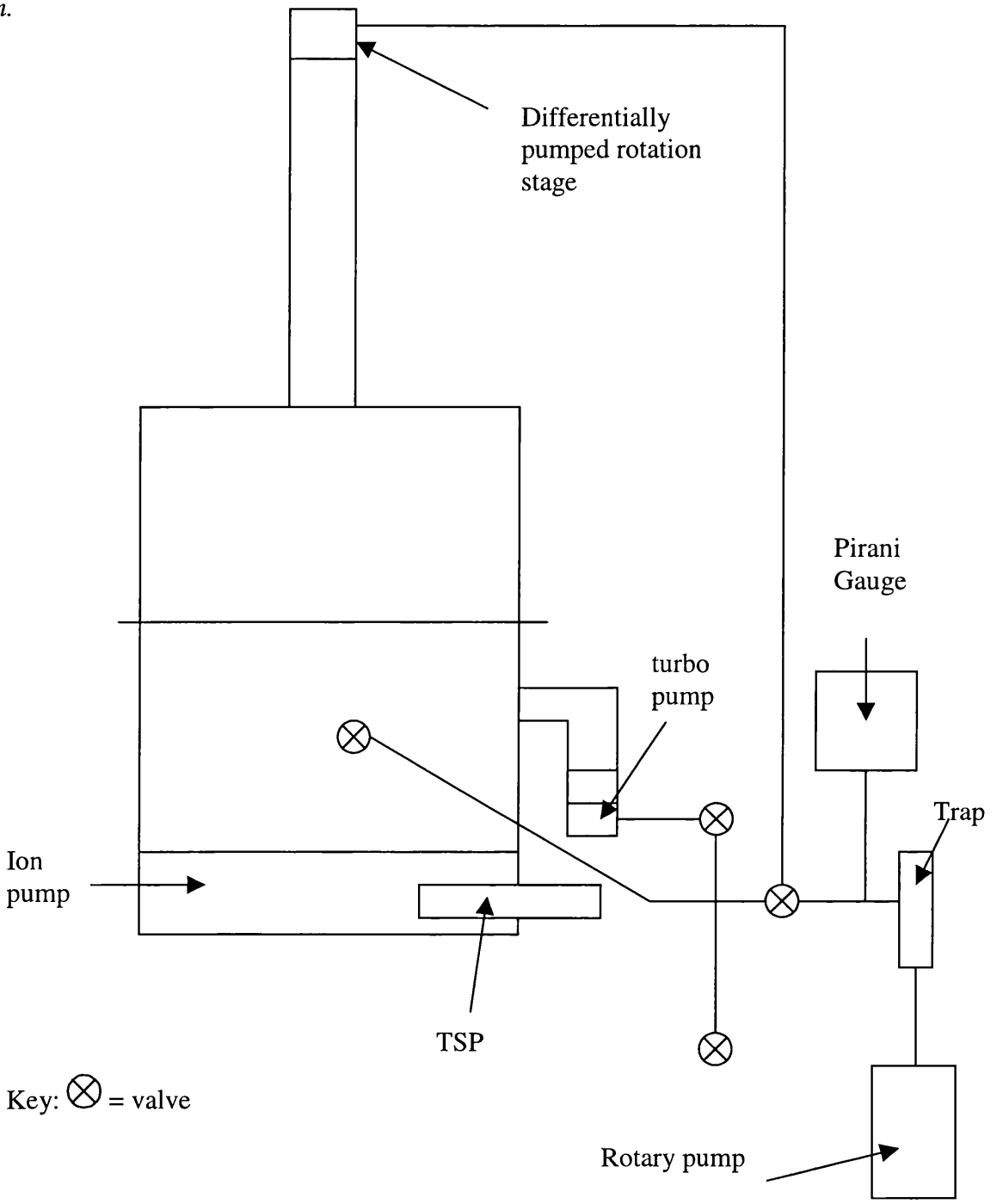

Figure 3: *The sample holder.*

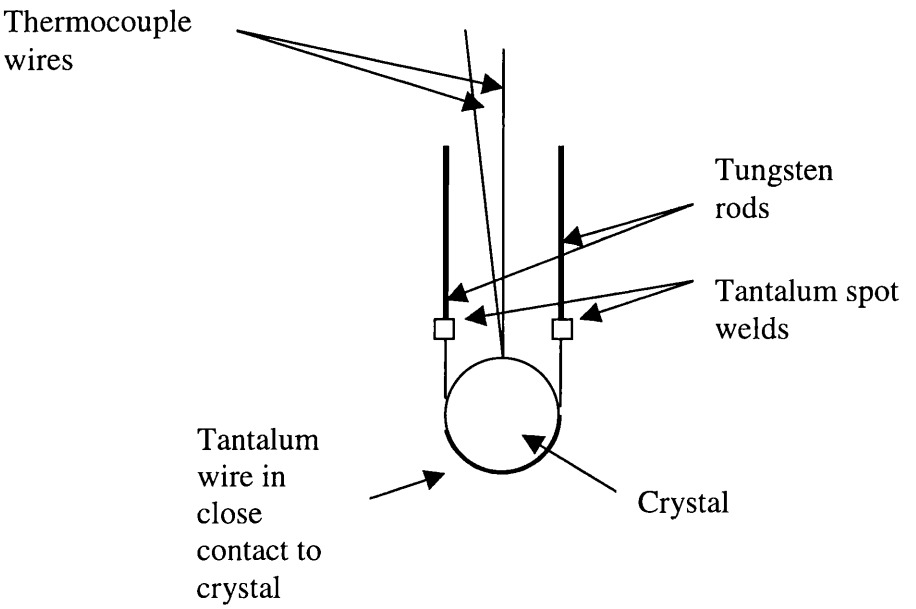

current obtained was 10 μA and the bombarding procedure was performed for 20 minutes. The crystal would then be annealed to 823 K for a further 30 minutes. AES and LEED were then used to check for both surface cleanliness and crystallographic order.

The sample holder therefore had to withstand temperatures ranging from 122 – 823 K. It was found that the spot welds on the sample holder would eventually break, due to repeated heating and cooling cycles and the equipment would have to be re-made. This usually meant starting all over from scratch as the tungsten rods did not support the re-welding of a new crystal holder. Also, the entire re-entrant was made of glass and as the main supporting manipulator (MDC Vacuum products) is very heavy, the re-entrant would often break when attempting to add the manipulator to the top of the chamber. It was then decided to use a re-entrant that was made of glass at the bottom and metal at the top. This meant that a glass-metal flange was needed to connect the two pieces together but a much smaller part of the re-entrant was made of glass and hence a much smaller piece of glass would be required if the re-entrant had to be re-made. A complete picture of the sample manipulator with the crystal included is shown in figure 5.

Figure 4: *The sample re-entrant.*

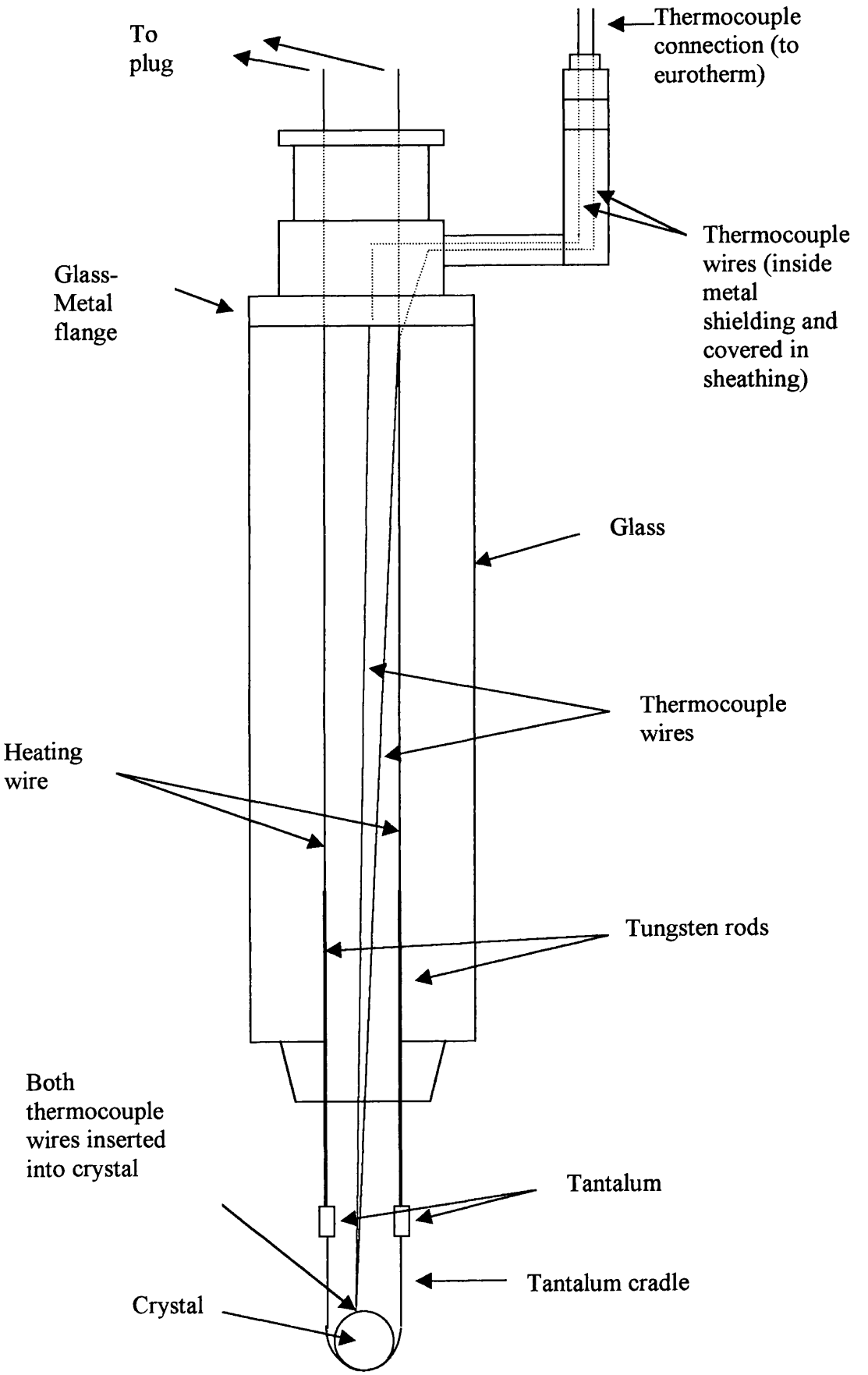

Figure 5: *The sample manipulator*

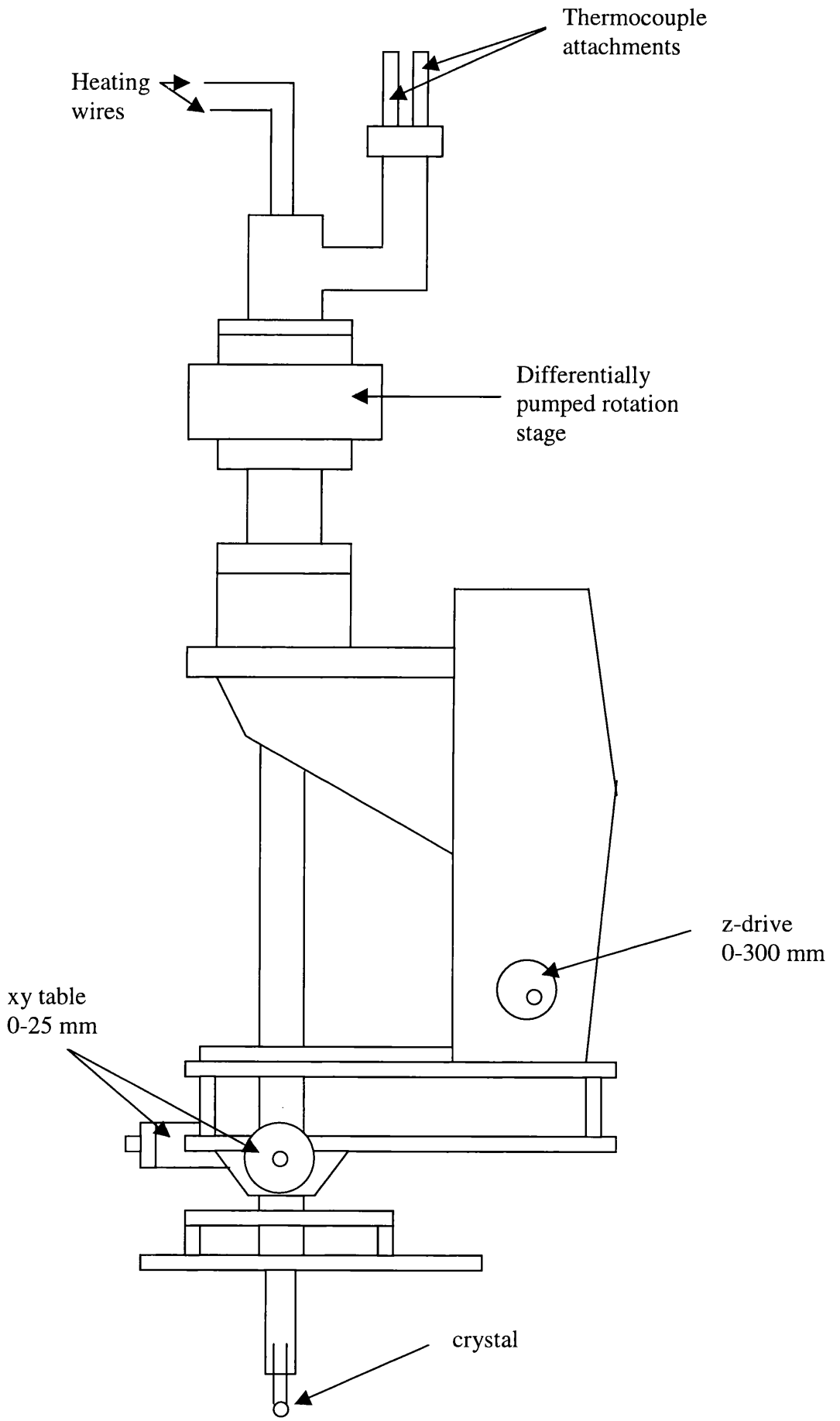

3.3 Experimental Procedures for the Glasgow experiments

3.3.1 TPD

TPD experiments were performed by firstly dosing the crystal at 122 K. Figure 6 shows a schematic diagram of the gas-line apparatus. The gas-line has a base pressure of $1x10^{-4}$ mbar and once the gas-line had been pumped to this pressure, the appropriate valves were closed off in order to isolate the line from the pumps when the line was filled with the dosing material. As thiophene, 3-chlorothiophene, 3-methylthiophene and 3-methoxythiophene are all liquids, this was achieved by simply opening the valves to the sample holders and allowing vapour into the gas line. Before dosing, the liquid in the sample that was to be dosed onto the crystal was subjected to three freeze/pump/thaw cycles in order to remove impurities.

Two dosing techniques were used in performing TPD experiments, namely "line-of-sight" and "back-filling". The line-of-sight technique involves placing the crystal 30 mm from the directional doser, which has a diameter of 1 mm and the back-filling technique involves dosing with the crystal at the roof of the chamber, well above the directional doser. In both experiments, after the dosing had taken place, the crystal was placed within a mm of the QMS, which was positioned using a linear drive. In order to prevent analysing molecules that desorb from the sample holder, the QMS is fitted with an aperture over the end of the instrument so that the crystal can be positioned directly in front of the QMS, figure 7.

3.3.2 AES

The electron gun of the AES instrument is fitted with a linear drive. This enables the gun to be placed very close to the crystal and also, to be moved away from the crystal when not in use. AES experiments were performed routinely on every clean surface prepared in order to check for surface cleanliness. Electron detection was by the use of an RFA.

Figure 6: *Schematic diagram of the gas-line used in Glasgow.*

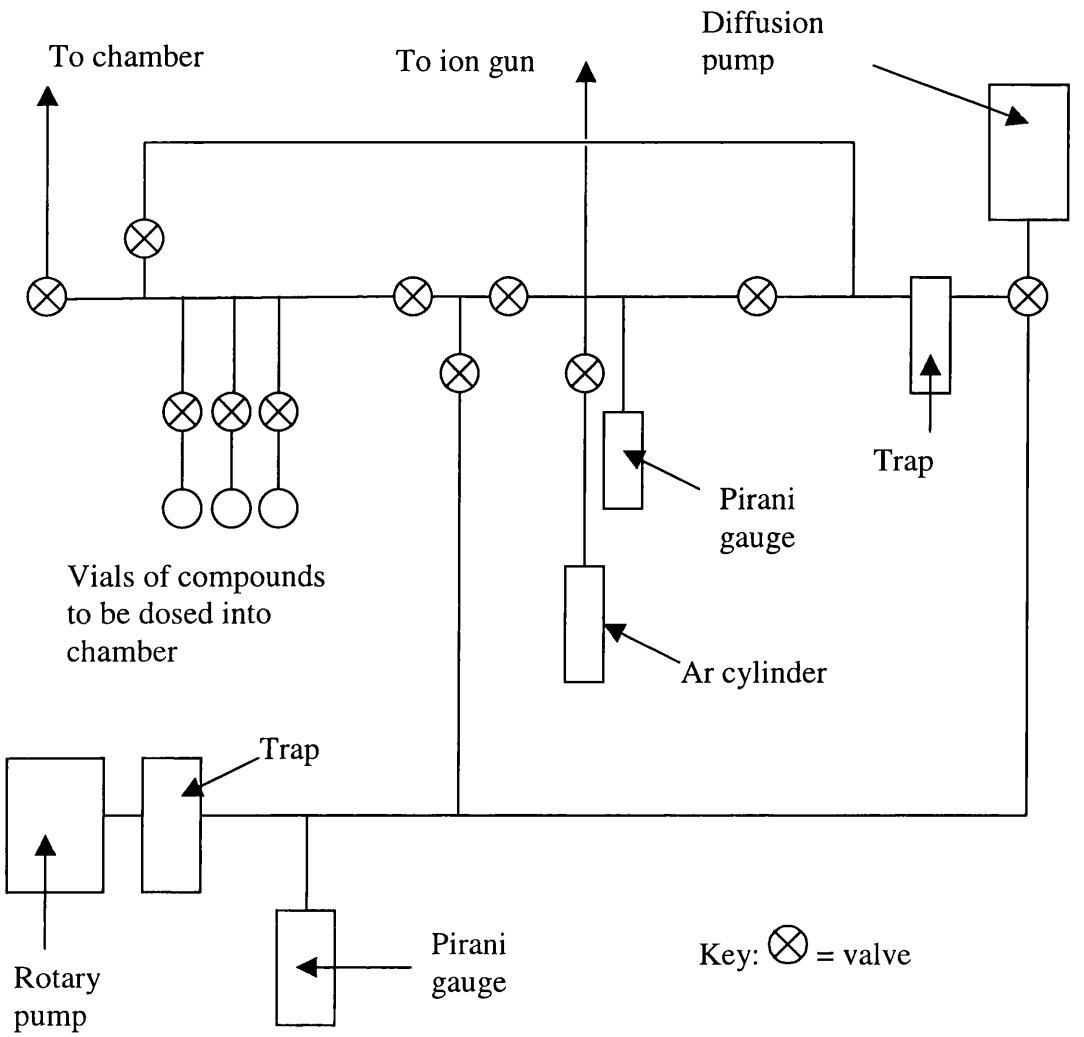

Figure 7: *Positioning of the crystal in TPD experiments. The welds and thermocouple connections on the crystal have been removed from the diagram for clarity.*

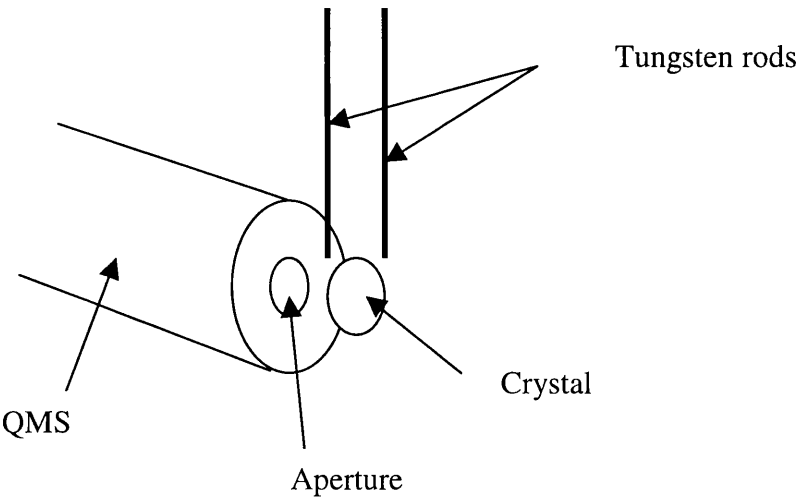

3.3.3 RFA electron detection in AES experiments

Figure 8 shows a schematic diagram of an RFA electron detector. In practice, a negative potential, the retard potential, which is close in value to the accelerating energy of the electron gun, is applied to the mesh closest to the screen. The other three meshes are earthed, the middle two being connected to each other. If the electron energy distribution is N(E) and the retarding potential is V_0, then the current arriving at the detector is:

$$\int_{E_0}^{\infty} N(E)dE \qquad (1)$$

As the highest energy beam electrons emitted have the primary beam energy E_P, the current can be expressed as:

$$\int_{E_0}^{E_P} N(E)dE \qquad (2)$$

Hence differentiation of the current results in the desired energy distribution, N(E). This is achieved in practice by modulating the retarding voltage V_0, by applying a sinusoidal voltage, $V_0+\Delta V\sin\omega t$. The collector current can be expressed as a sum of harmonics which comprise a d.c. term (equation 2) plus terms $\sin\omega t$, $\sin 2\omega t$ etc. The first harmonic, A_1, has amplitude:

$$A_1 = \Delta E N(E_0) + \frac{\Delta E^3}{8} N''(E_0) + \frac{\Delta E^5}{192} N''''(E_0) + \ldots \qquad (3)$$

The second harmonic, A_2, has amplitude:

$$A_2 = \frac{\Delta E^2}{4} N'(E_0) + \frac{\Delta E^4}{48} N'''(E_0) + \frac{\Delta E^6}{1536} N''''''(E_0) + \ldots \qquad (4)$$

In all AES experiments, it was the amplitude of the second harmonic that was measured by using a phase sensitive detector. This is due to the fact that the first harmonic signal measured at the collector can be very large due to the retarding grids

and the collector forming a hemispherical capacitor. The modulation voltage used in collecting AES spectra was 20 V_{p-p}.

3.3.4 RFA electron detection in LEED experiments

The RFA is modified in LEED experiments by setting the three grids that are earthed in the AES experiment to a slightly lower potential than the primary electron acceleration potential. This means that only elastically scattered electrons are able to reach the fluorescent screen.

Figure 8: *Schematic diagram of an RFA electron detector*

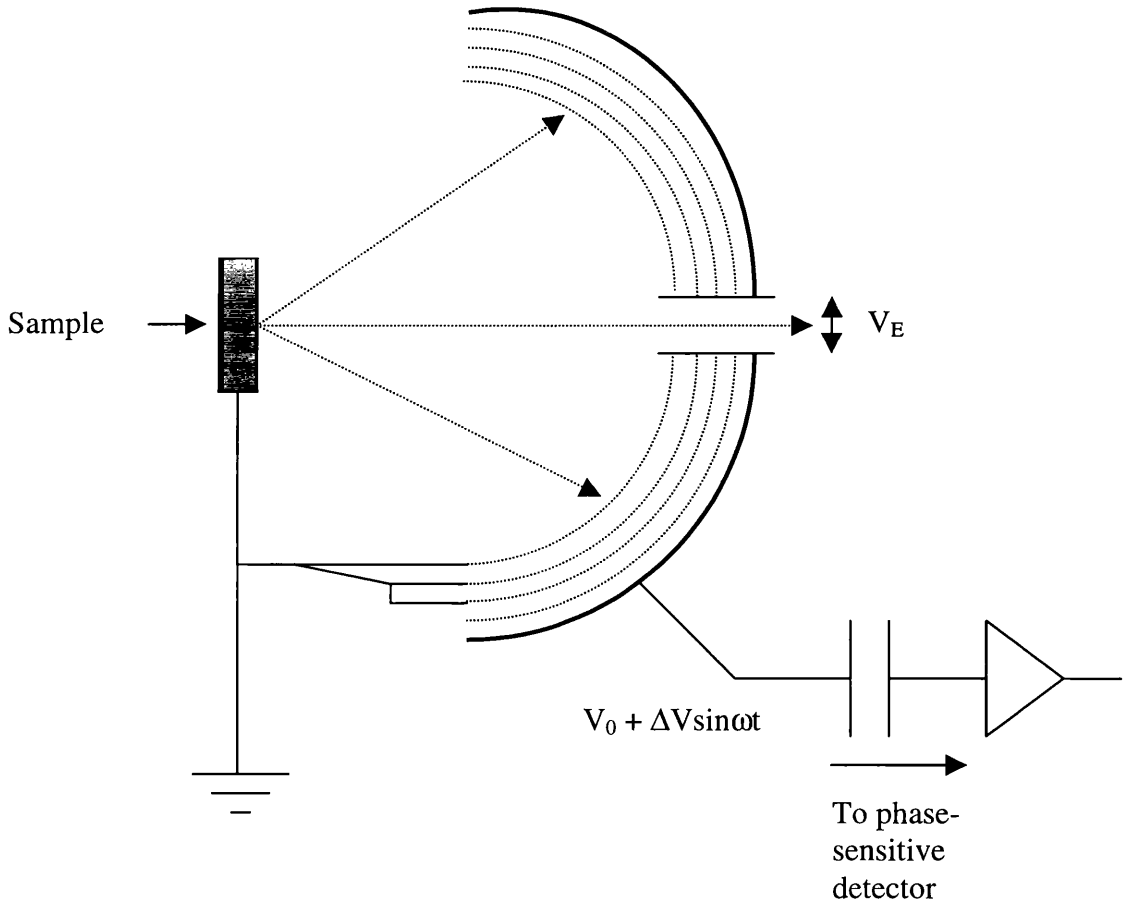

3.4 Experimental Procedures for the Daresbury experiments

Figure 9 shows a schematic diagram of the beam-line/UHV chamber interface at station 6.3 of the Daresbury Laboratory. The beamline and chamber of this station have been described previously[1] and only an outline of certain experimental procedures will be given here. All of the data from XPS, NIXSW and NEXAFS experiments was collected using a CHA. The raw data collected from each experiment was then divided by the beam monitor current, I_0'. The reason for this is that the intensity of the X-ray beam at the Daresbury Laboratory decreases with time. The I_0 current could not be used for this kind of standardisation for two reasons. In NIXSW experiments, the I_0 monitor is used as a measure of the XSW reflectivity as it is close to the crystal and therefore it is not a direct measure of the beam current. Also, the I_0 monitor was changed at some time during the course of this study and hence beam currents measured from different monitors at different beam-time allocation periods could not be compared. This had a very important consequence in calculating absolute coverages in ML from XPS data. Coverages were calculated as outlined in Chapter 4. All XPS data was background subtracted and normalised to the I_0' monitor current for comparison.

Figure 9: *Schematic diagram of the beamline/UHV chamber interface at station 6.3 of the Daresbury Laboratory (not to scale).*

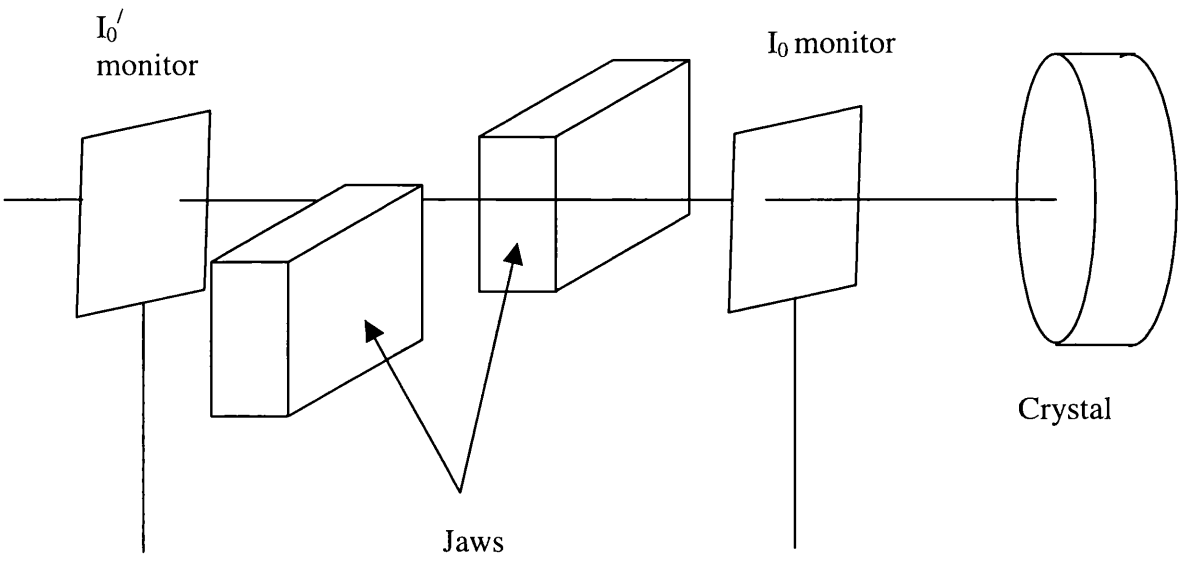

3.5 References

1. A.A. M^{c}Dowell, D. Norman, J.B. West, J.C. Campuzano and R.G. Jones, *Nuclear Instrumental Methods A,* 1986, **246**, 131.

Chapter 4. The adsorption of Thiophene on Cu(111)

4.1. Introduction

The adsorption of thiophene, C_4H_4S, on Cu(111) was studied using the techniques of TPD, AES, XPS, LEED, NIXSW and NEXAFS. The adsorption states were characterised by analysis of desorption features present in TPD spectra. AES, XPS and LEED were used to show that thiophene does not decompose on the Cu(111) surface and hence its molecular adsorption could be studied. A quantitative analysis of the different adsorption states in terms of monolayers (ML) was also obtained from AES, XPS and LEED. LEED was also able to show that thiophene does not form any structures with long range order at any coverage on Cu(111). Once these techniques established the nature of the adsorption, the different adsorption states, particularly at α-state (0.08±0.03 ML) and β-state (0.14±0.03 ML) coverage, were studied using the synchrotron techniques of NIXSW and NEXAFS. NEXAFS showed that at α-state coverage, the angle of orientation of the molecules prepared by a sequentially dosing method is 25±4 ° and at β-state coverage, the angle of orientation of the molecules is 45±6 °, thereby exhibiting a coverage dependent phase transition. Identical angles of orientation within experimental error were calculated from NEXAFS experiments from surfaces prepared by an annealing dosing method. NIXSW data showed that the adsorption site at α-state coverage is displaced atop when the surface was prepared by the annealed and the sequential dosing methods. However, at β-state coverage, the adsorption site is displaced atop using the annealed dosing method but either bridging, a mixture of 3-fold and atop sites or a mixture of all three sites when the sequential dosing method is used.

4.2. Results

4.2.1. Initial Characterisation

The initial characterisation of the adsorption behaviour of thiophene on Cu(111) at cryogenic temperatures was performed at Glasgow with AES, TPD and LEED. This data was then complimented with XPS experiments which were performed at station 6.3 of the Daresbury Laboratory.

Thiophene undergoes reversible molecular adsorption on Cu(111), as confirmed by AES measurements. AES spectra collected both before and after eight adsorption and desorption cycles are shown in figures 1 (a) and (b). If the desorption of thiophene is dissociative, then S and C would be present on the surface after cycles of TPD experiments. It is clear from the AES spectra shown in figure 1 that no S (figure 1 (a)) or C (figure 1 (b)) is present on the surface after desorption. The feature in figure 1 (a) at a kinetic energy of 264 eV in the pre-TPD (black) and post-TPD (red) spectra is a temperature dependent feature brought about by bulk secondary electrons and has been reported elsewhere in similar AES studies on Cu(111)[1]. This feature is very close to the C KLL kinetic energy range and the blue dashed spectrum was collected from a surface contaminated with C for comparison. The negative excursion in both the black and red spectra is much smaller than that of the blue spectrum, indicating that the feature does not actually represent C contamination on the surface. Also, the feature present in the black and red spectra decreased in intensity with increasing temperature, which is not concurrent with any strongly adsorbed carbonaceous fragments on the surface. The black data shown in figure 1 (a) was taken directly after annealing the crystal to 823 K. At lower temperatures, the feature is more pronounced. The feature present in the red data in figure 1 (b) (S LVV AES) at a kinetic energy of 184-195 eV is not due to adsorbed S as figures 7 and 8 quite clearly show. Figures 7 and 8 were collected from surfaces in which thiophene had been pre-adsorbed. They show that S is at a kinetic energy of 146-158 eV as this feature is changing in intensity with different adsorbed S coverages.

Figure 1 (a): *C KLL AES spectra taken before (red) and after (black) TPD experiments with a spectrum from a surface known to be contaminated with C (blue dashed) for comparison.*

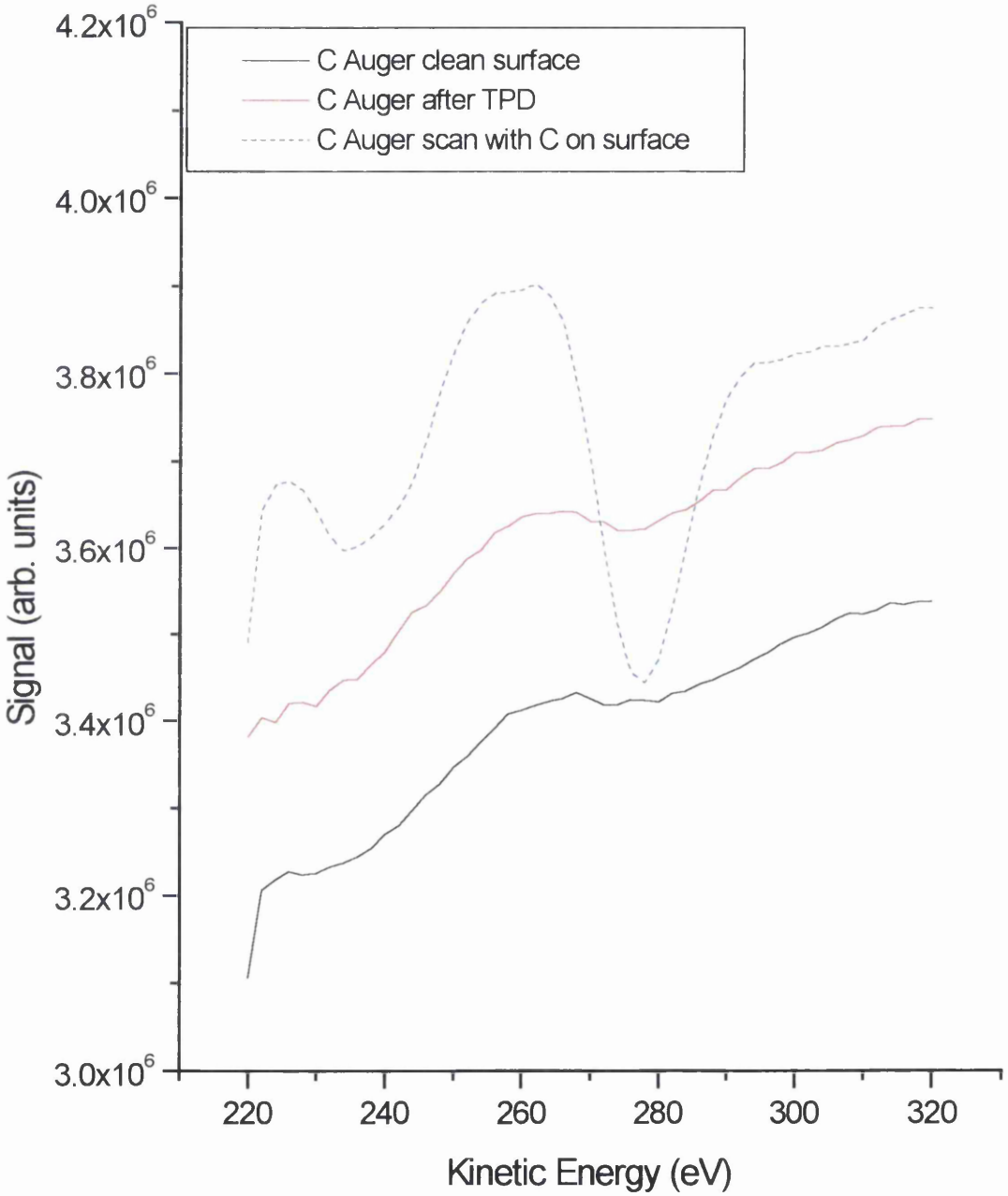

(b): *S LVV AES spectra taken before (red) and after (black) TPD experiments.*

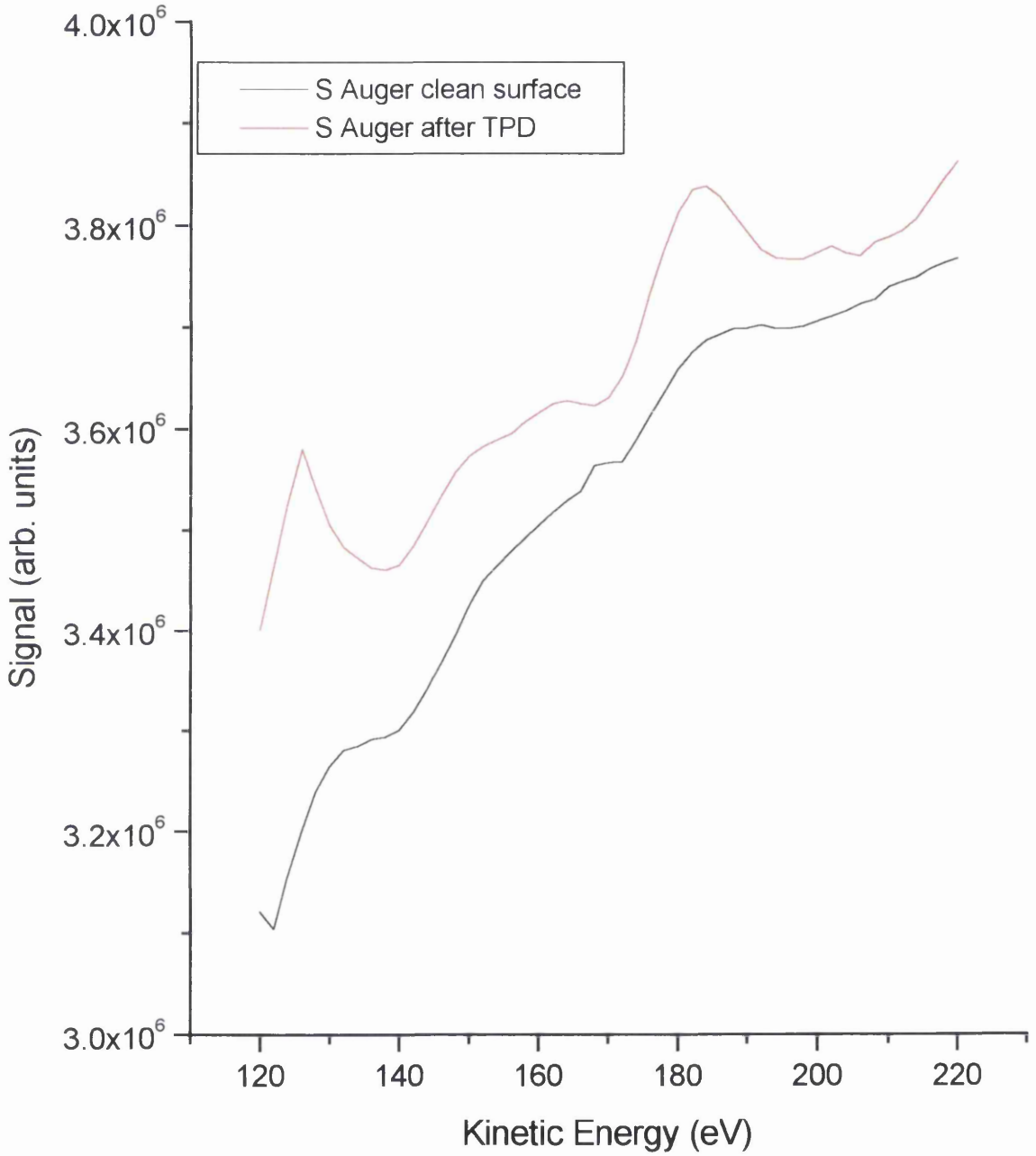

Figures 2 (a) and (b) show TPD spectra collected from surfaces with increasing thiophene coverage. In both figures, the heating rate used was 0.5 Ks^{-1}. In figure 2 (a), TPD spectra are shown from surfaces which had been dosed with thiophene using the backfilling method, which is described in detail in chapter 3. In figure 2 (b), TPD spectra are shown that were collected from surfaces which had been dosed with thiophene using the line-of-sight dosing method, which is also described in chapter 3. The advantage of line-of-sight dosing is that it can prepare multilayer surfaces without exposing the rest of the chamber to large amounts of thiophene. It must be remembered that the pressure of $3x10^{-9}$ mbar read on the ion gauge is lower than the actual pressure of thiophene that is incident on the crystal. By comparing two spectra of similar thiophene coverage, that is $1.2x10^{-5}$ mbar.s exposure (back-filling, orange) in figure 2 (a) and $5.4x10^{-7}$ mbar.s observed exposure (line-of-sight, blue) in figure 2 (b), it is possible to calibrate the two dosing techniques. In so doing, the line-of-sight dosing method deposits 22 times more thiophene than the back-filling method for an identical "exposure". From figure 2 (b) it is clear that increasing exposure of thiophene leads to the population of four desorption states. The first two desorption states to be populated are shown in the low coverage TPD spectra shown in figure 2 (a) (back-filling dosing method). With initial exposure ($6x10^{-7}$ mbar.s, figure 2 (a)) of thiophene, two desorption features are populated concurrently. The first of these features, which is observed at 297 K, is rapidly saturated after an exposure of $1.2x10^{-6}$ mbar.s and can be assigned to desorption from defect sites. Figure 3 shows two desorption spectra from surfaces that have been exposed to the same amount of thiophene ($1.44x10^{-6}$ mbar.s, back-filling method). The "roughened" spectrum was collected from a surface that was not previously annealed after an Ar^+ bombardment cycle. It shows a broad feature indicating desorption from a disordered crystal surface that has many defect sites. The broad feature in the "roughened" spectrum begins to tail off at the same temperature as the feature representing defect sites in the "annealed" spectrum and there is increased desorption at this temperature (297 K). Hence, the peak at 297 K in the TPD data in Figure 2 can be assigned to desorption from defect sites. A second feature at 234 K is present in the low exposure ($6x10^{-7}$ mbar.s) desorption data which will be referred to as the α-state. With increasing coverage, this feature gets larger

in intensity and shifts to lower temperatures. At saturation, an exposure of $6x10^{-6}$ mbar.s, the α-state peak is at 211 K.

Figure 2 (b) shows two more desorption features that are populated concurrently. At saturation of the α-state, another feature, hereby referred to as the β-state, is present at 173 K. Unlike the α-state, the β-state does not broaden and move to lower temperatures with increasing coverage. On saturation of the β-state, a fourth feature is present at 157 K which can be assigned to desorption from multilayers, as this peak does not saturate with continued dosing. Figure 4 shows the areas under each TPD spectrum in figure 2 (a) plotted against dosing time. The linear relationship represents a constant sticking co-efficient for thiophene.

The relative amounts of thiophene desorbing from the α- and β- states was determined in a separate series of TPD experiments. In these experiments, TPD spectra were collected from two surfaces which had both been prepared by removing multilayers of thiophene by annealing, figure 5. In figure 5, one surface was prepared by annealing to 157 K (black) and gives rise to a β-state desorption feature. The other surface was prepared by annealing to 173 K (red) and gives rise to an α-state desorption feature. The ratio of the integrated areas of these two spectra is the ratio of the amount of thiophene desorbing from β to that desorbing from α. The integrated area of the black spectrum in figure 5, β, is $1.7x10^{-8}$ mbarK and the area of the red spectrum, α, is $1.0x10^{-8}$ mbarK. Hence the ratio, β/α is 1.7.

LEED was used to determine whether thiophene formed any structures with long range order by preparing surfaces with α- and β-state coverages in the same way as in figure 5, but no structures were found at any coverage.

Figure 2: *TPD spectra of thiophene on Cu(111). Spectrum (a) shows TPD data collected using the "back-filling" dosing method and spectrum (b) shows TPD collected using the "line-of-sight" dosing method.*

(a)

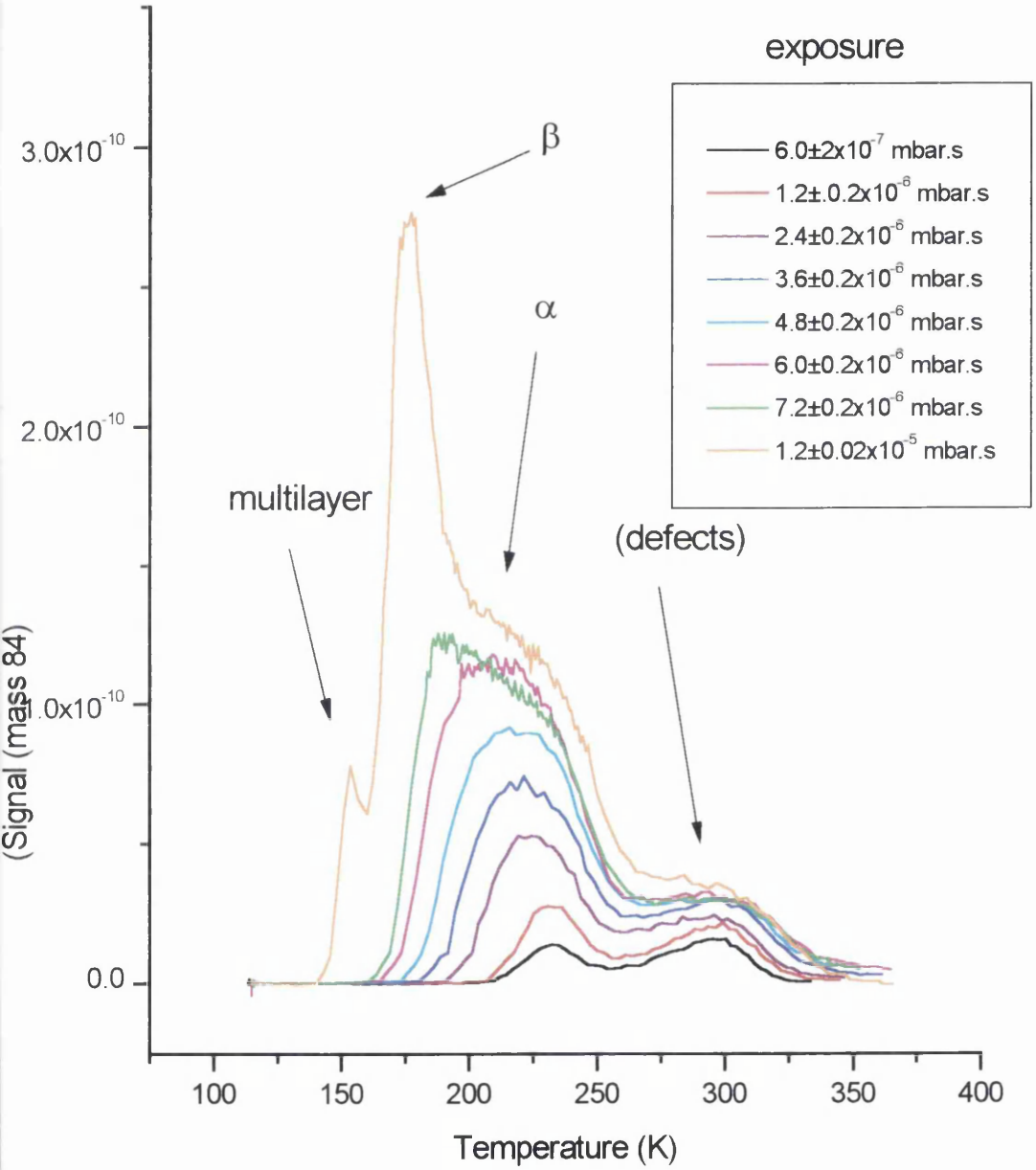

(b)

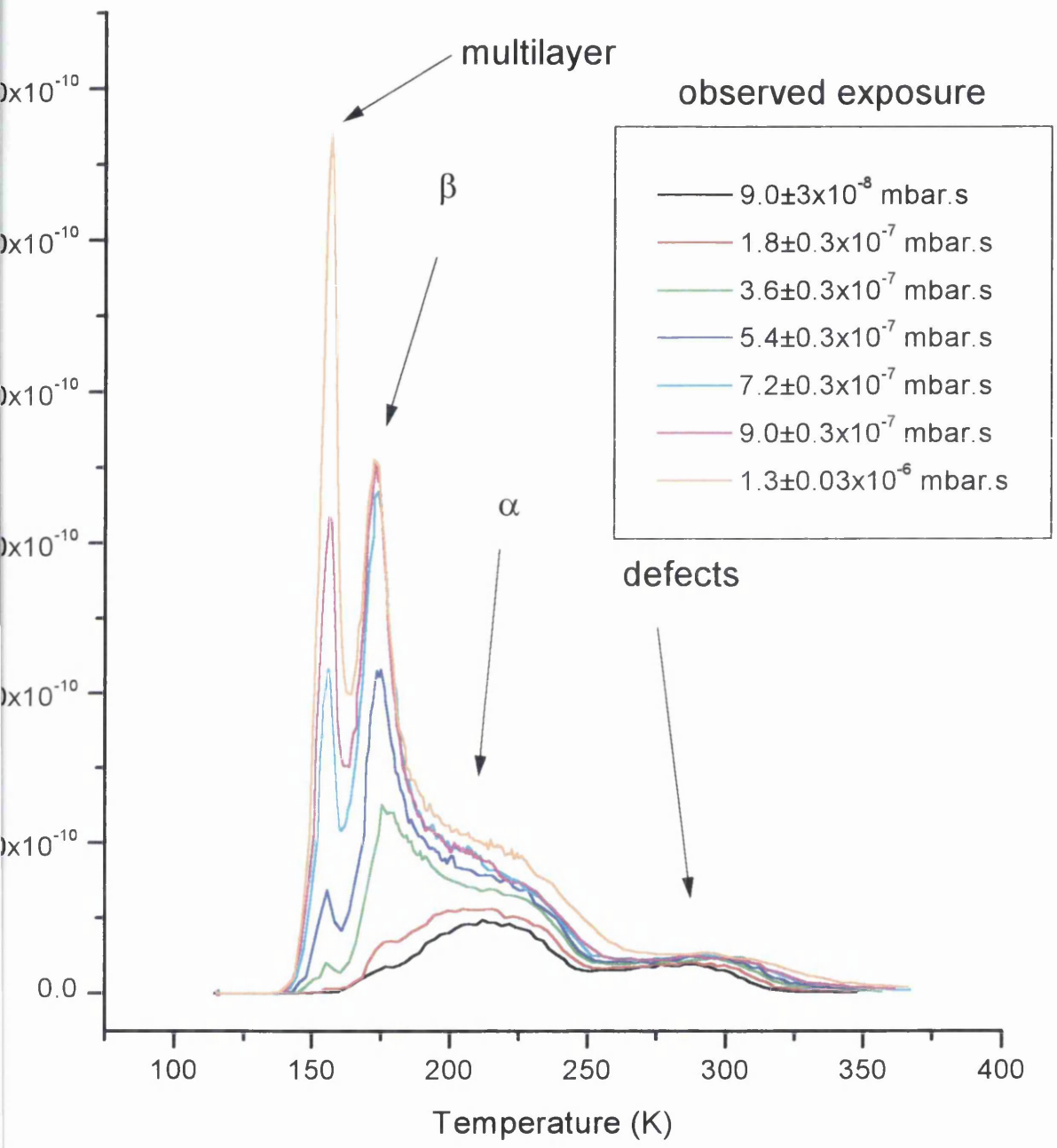
multilayer
observed exposure
β
α
defects
9.0±3x10-8 mbar.s
1.8±0.3x10-7 mbar.s
3.6±0.3x10-7 mbar.s
5.4±0.3x10-7 mbar.s
7.2±0.3x10-7 mbar.s
9.0±0.3x10-7 mbar.s
1.3±0.03x10-6 mbar.s
0.0
100
150
200
250
300
350
400
Temperature (K)

Figure 3: *TPD from surfaces in which the crystal had been prepared by Ar^+ bombardment and annealing to 823 K (black), and by Ar^+ bombardment without annealing (blue).*

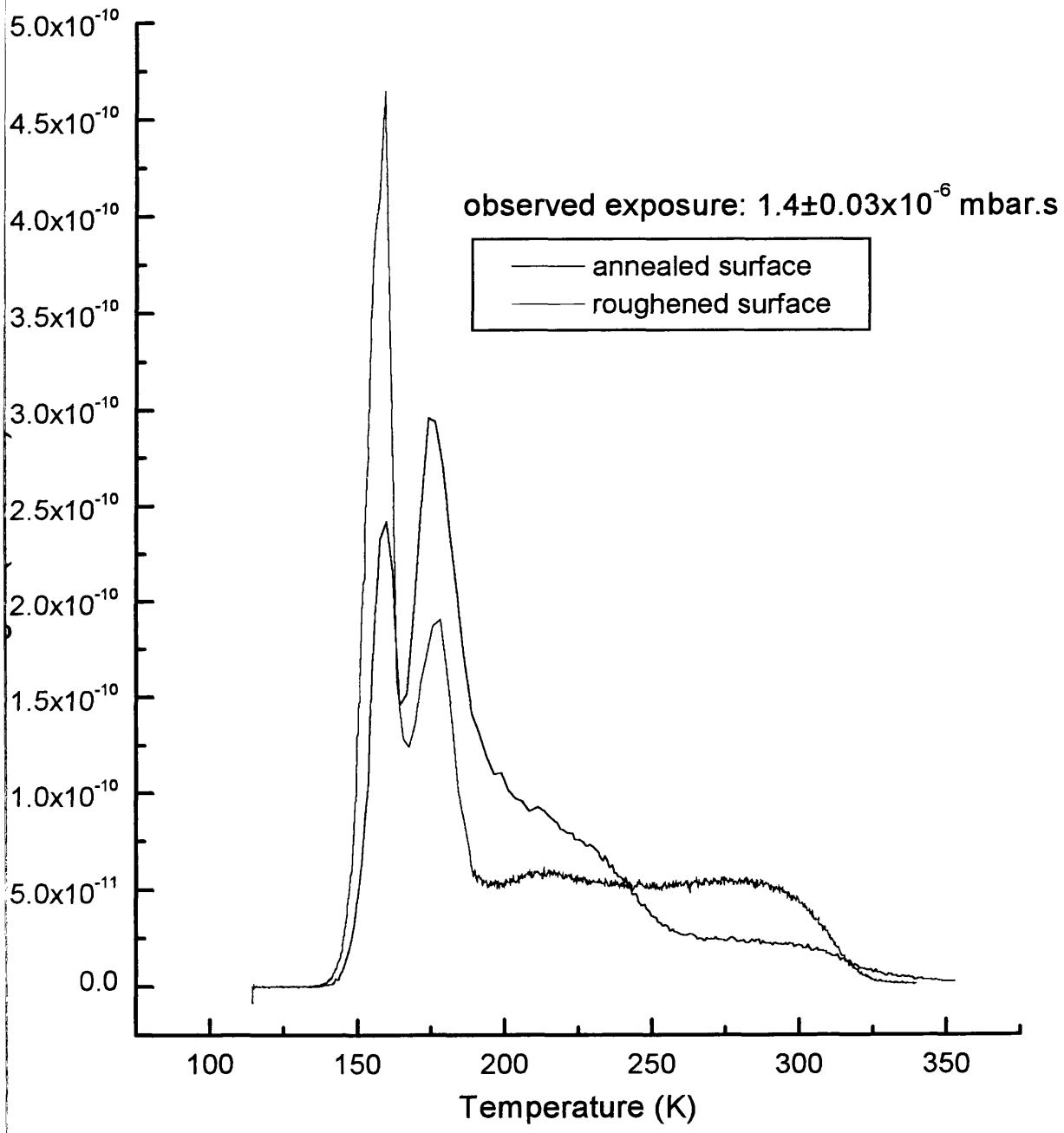

Figure 4: *Integrated areas for each of the TPD spectra shown in figure 2 (a) (back-filling method) showing a constant sticking co-efficient for thiophene on Cu(111).*

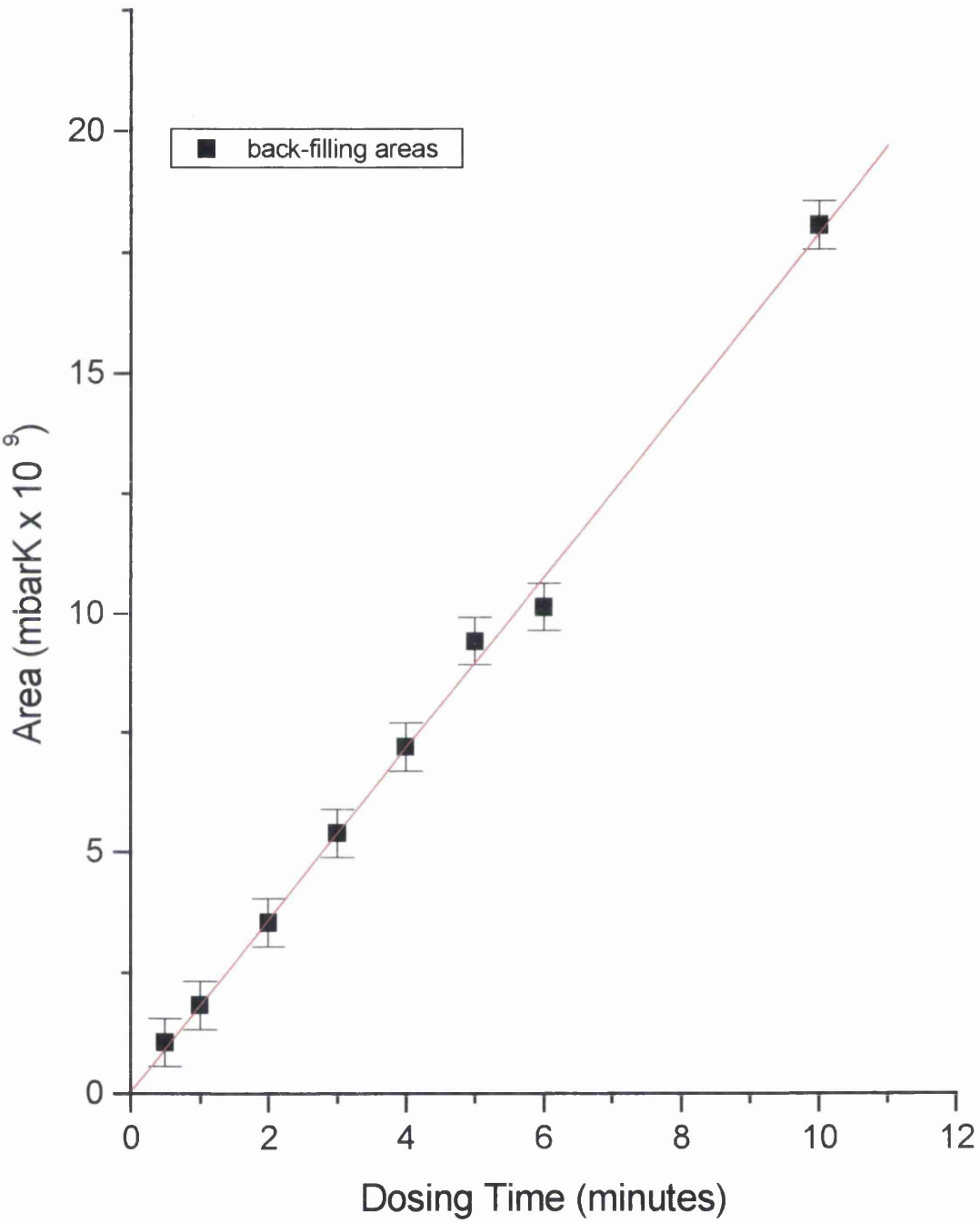

The absolute amount of thiophene in the α and β desorption states in terms of monolayers (ML) was obtained by collecting AES spectra of surfaces prepared with both α- and β-states and calibrating their peak heights against an AES spectrum of a surface with a known coverage. The term monolayer is used in this context to mean one sulfur atom for every copper atom. The surface with a known coverage that was used was the (√7x√7R19.1°)-S[2] surface which was prepared by dosing H_2S at 120 K and then annealing to 570 K for 20 minutes. An ordered (√7x√7R19.1°) LEED pattern was observed at a beam energy of 141 eV, as shown in figure 6 (b), and figure 7 shows a S AES spectrum of this surface. The (√7x√7R19.1°)-S surface has a coverage of 0.43 ML, that is for every seven copper atoms on the surface there are 3 adsorbed sulfur atoms. Analysis of S AES peak heights of surfaces dosed with thiophene and prepared with both α- and β- states, figure 8, compared to the (√7x√7R19.1°)-S AES peak height, figure 7, enables the absolute coverage in ML to be calculated. The coverage of the β state is therefore 0.14±0.03 ML and the coverage of the α state is 0.08±0.03 ML. Cu AES spectra are shown in figures 7 and 8 because the thiophene coverage is calculated by comparing the S:Cu ratios of α- and β- states with the S:Cu ratio of the (√7x√7R19.1°)-S surface.

Figure 5: *TPD data from surfaces prepared with β-state coverage (black) and α-state coverage (red). The ratio of the areas under the spectra shows that the ratio β/α is 1.7.*

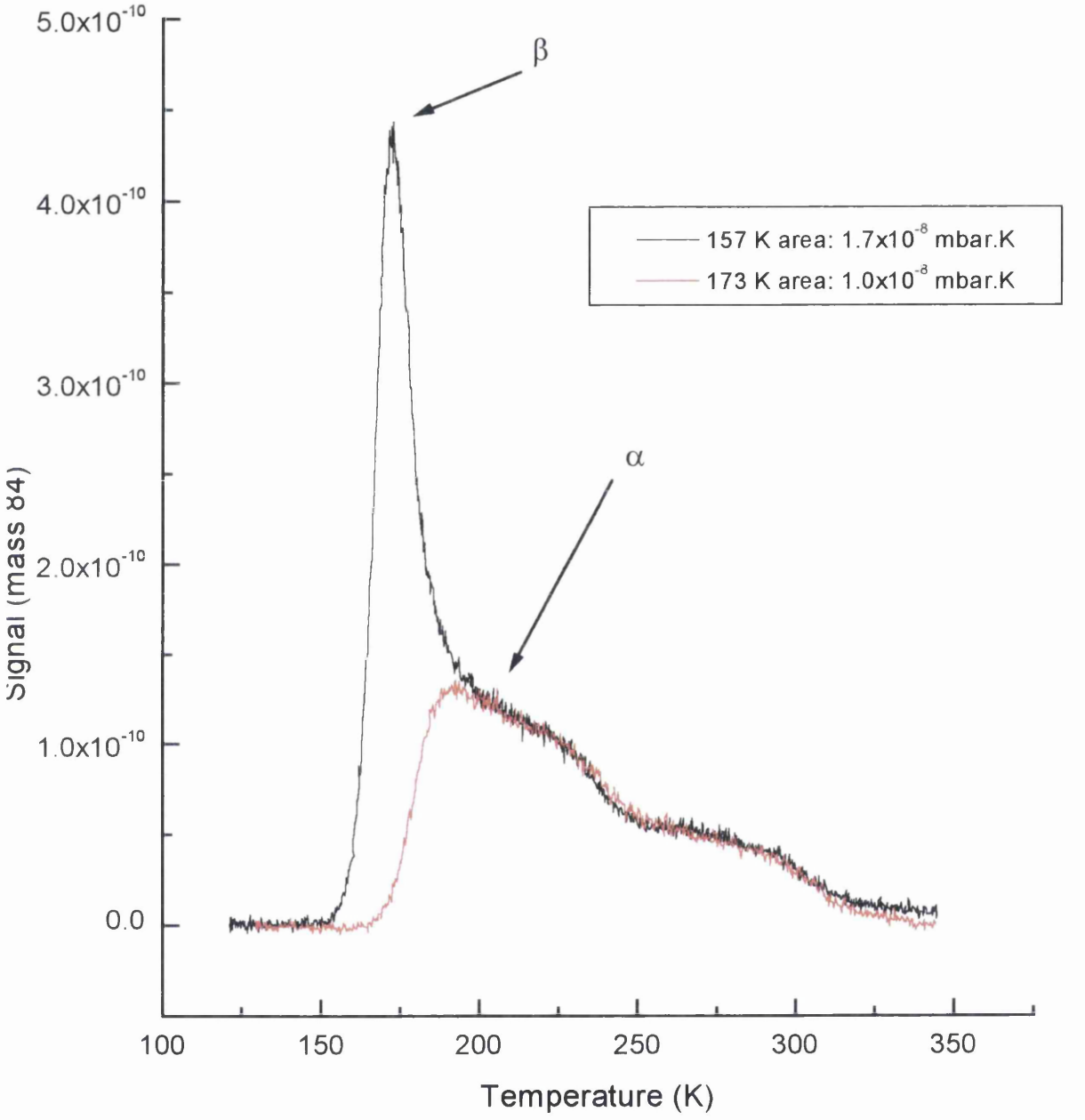

Figure 6: *Clean (1x1) and (√7x√7R19.1°)-S LEED patterns at 141 eV.*

(a) (1x1)

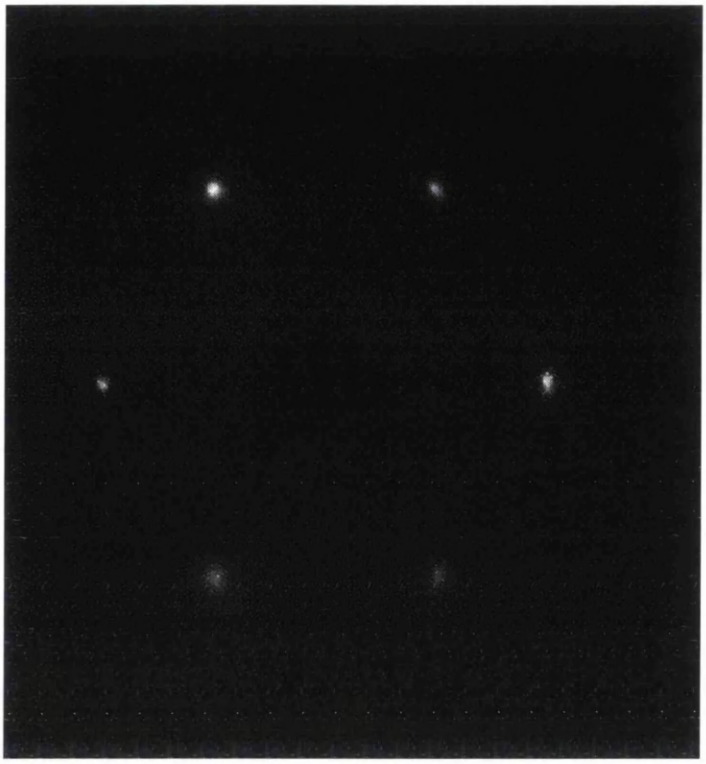

(b) (√7x√7R19.1°)-S

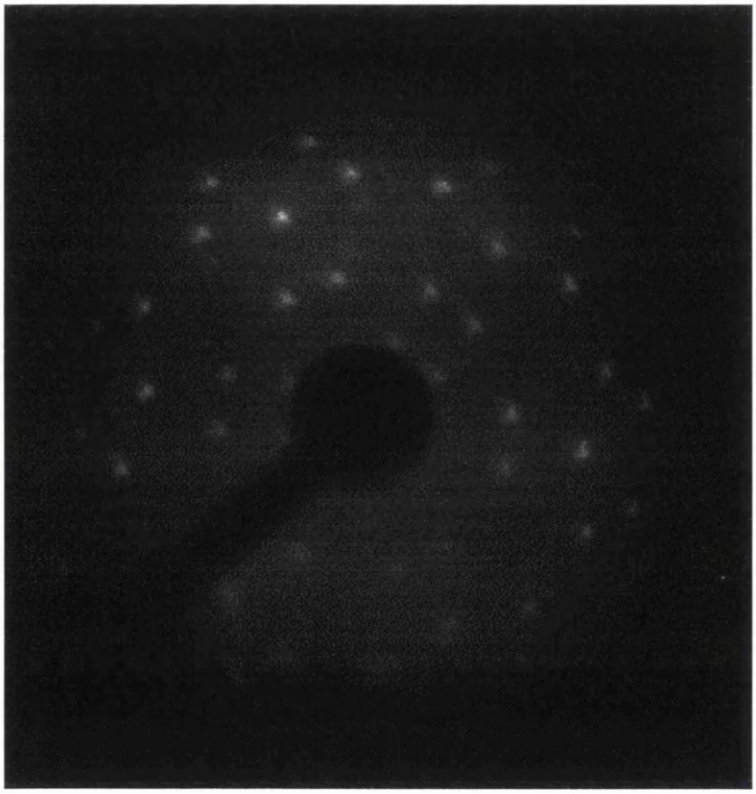

Figure 7: *S LVV Auger spectrum of a (√7x√7R19.1°)-S surface and a Cu LVV Auger spectrum. The Cu LVV Auger spectrum was collected before the preparation of the (√7x√7R19.1°)-S surface.*

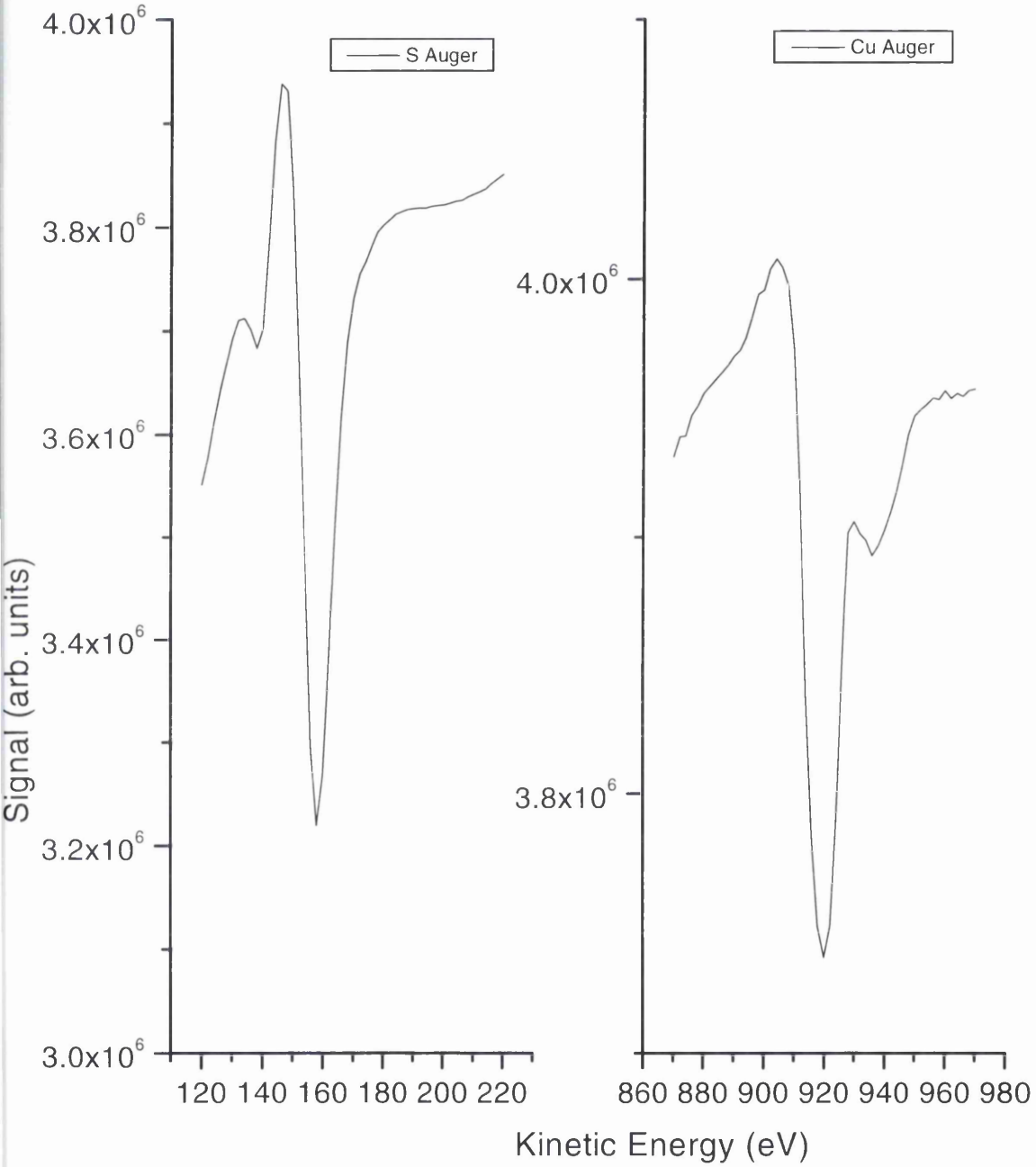

Figure 8: *S LVV Auger spectra of α-state (red) and β-state (black) surfaces. These two spectra were divided by their corresponding Cu Auger intensity and normalised for ease of comparison.*

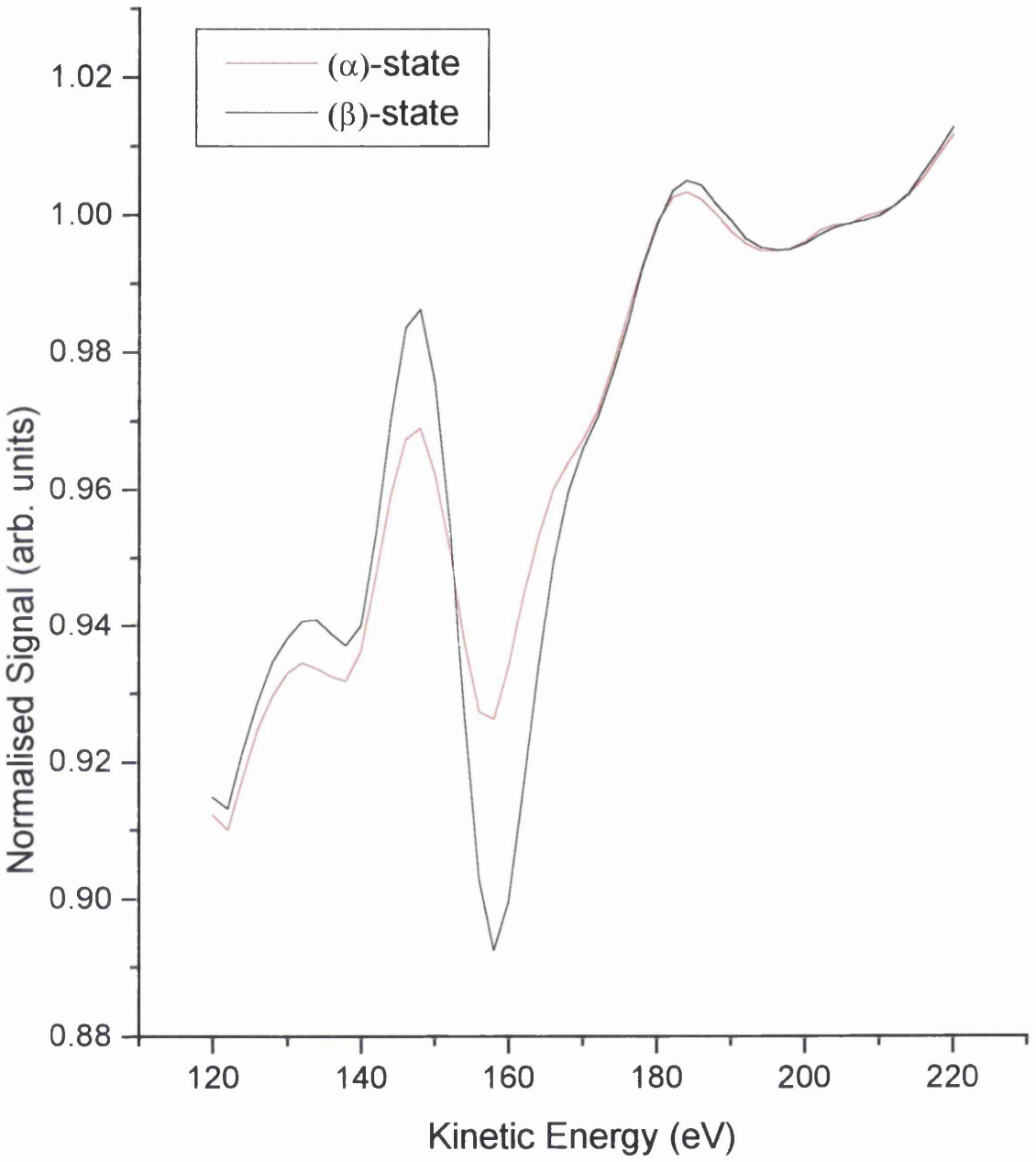

Characterisation of the adsorption at the Daresbury Laboratory was achieved by annealing multilayers of thiophene prepared by dosing at 120 K to specific temperatures. At each temperature, XPS experiments were performed. Although the coverage of each thiophene surface prepared can be calculated, care must be taken in assigning the coverage of α- and β- states because TPD experiments could not be performed at Daresbury.

In summary, TPD spectra of thiophene on Cu(111) show the presence of four desorption features. These are desorption from defect sites (297 K), from an α-state (234 K) a β-state (173 K) and multilayer desorption (157 K). AES shows that the desorption of thiophene on Cu(111) is molecular and reversible. AES and TPD both show that the ratio of α/β is 1.7. By calibrating S AES data with a known standard, the absolute coverage of the α-state is 0.08±0.03 ML and the absolute coverage of the β-state is 0.14±0.03 ML. LEED was able to show that thiophene does not form any ordered structures at any coverage.

Figure 9: *Plot showing variation in area under XPS spectra as a function of annealing temperature.*

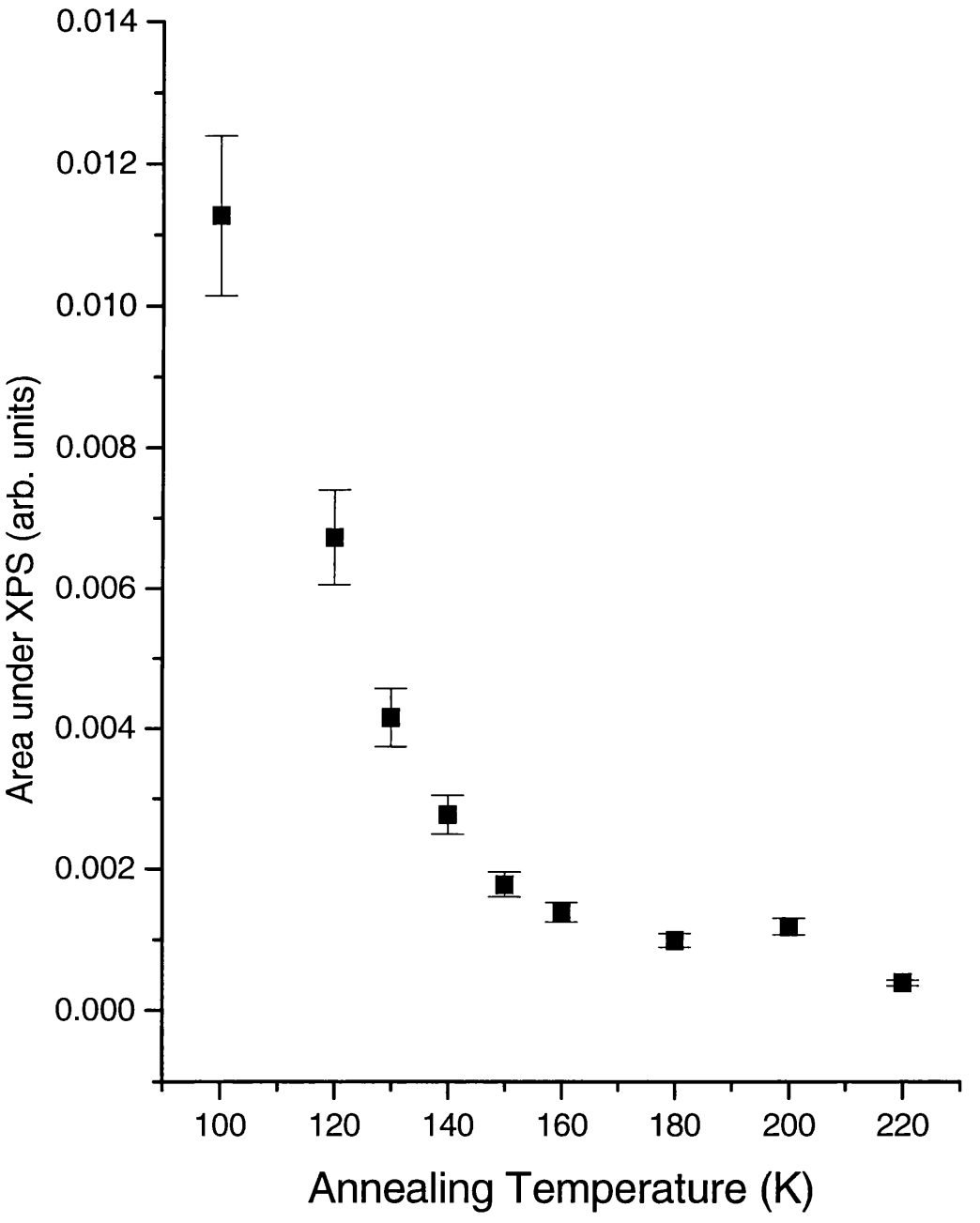

4.2.2 NEXAFS

NEXAFS experiments were performed in order to study the orientation of thiophene on Cu(111). The angle of inclination that can be derived from polarisation dependent NEXAFS experiments corresponds to the angle that the C_2 axis of the molecule makes with the surface. For example, if the molecule was oriented in a flat orientation with its π-ring roughly parallel to the surface, the angle of orientation would be close to 0 °. If the molecule was oriented with its π-ring perpendicular to the surface, the angle of orientation would be close to 90 °.

In particular, the coverage dependence of the orientation of the thiophene ring on Cu(111) was studied. Thiophene surfaces, of different coverages, were prepared by two different methods, "sequential dosing" and "annealing". In the sequential dosing method a small, typically sub-monolayer coverage, is prepared, NEXAFS data collected, and then higher coverages are prepared by sequential aliquot dosing. The benefit of using this dosing technique is that one can be confident that each surface prepared by this method has a higher coverage than the previous one. In effect the coverage is being "built-up" in sequential pieces and after each dose, NEXAFS data is collected and hence the orientational angle can be determined from low coverage up to multilayer coverage in small coverage increments. NEXAFS data collected from each surface prepared in this way is shown in figure 10. In figure 10, the first surface prepared had a coverage of 0.03 ML and after the seventh aliquot dose, the coverage had risen to 0.24 ML (multilayers).

Annealing experiments were also performed which involved dosing the crystal with sufficient amounts of thiophene at 120 K to form multilayers and then annealing the sample, with reference to figure 9, to study the coverage of interest, that is the α- or β- state. This was done to find out if surfaces prepared by the two different techniques, particularly at α- and β-state coverage, had the same orientational angle. All NEXAFS experiments were performed at beamline 6.3 of the Daresbury SRS.

4.2.3. Sequentially Dosed NEXAFS experiments.

The spectra shown in figure 10 represent data collected at two angles of X-ray incidence, grazing (19.5°) and normal (90°). The NEXAFS spectra in figure 10 were collected from surfaces that had been prepared by sequential dosing. These angles of X-ray incidence are also used in NIXSW experiments that will be described in the next section. All spectra shown in figure 10 are S K-edge NEXAFS spectra in which the intensity of the S (KLL) Auger electron (K.E. 2099 eV) was monitored as a function of photon energy and the data shown is normalised to the S K-edge jump.

The lowest coverage, 0.03 ML, spectrum (black) at grazing incidence exhibits a feature at 2467.8 eV. With increasing coverage, this feature decreases in intensity and broadens to higher photon energies. The corresponding normal incidence spectrum exhibits a feature at 2468.7 eV. With increasing coverage, this feature decreases in intensity and broadens to lower photon energies.

The feature in the grazing spectrum at 2467.8 eV is dominated by a π^* resonance and the feature in the normal spectrum at 2468.7 eV is dominated by a σ^* resonance.

These resonances were assigned with reference to a study by Stöhr *et al.*[3] who combined NEXAFS experiments on gas-phase thiophene and thiophene adsorbed on Pt(111) with theoretical calculations.

The qualitative dependence on polarisation of these two resonances, as outlined in detail in Chapter 2 indicates that the thiophene molecule is oriented with it's C_2 axis roughly parallel to the surface in a roughly flat geometry at a coverage of 0.03 ML. Other work concerning the adsorption of thiophene on Cu(111) studied by NEXAFS performed by Ohta *et al.*[4] shows similar NEXAFS spectra and resonance assignments. In all, six peaks can be assigned to the NEXAFS data. Figure 11 shows a plot of all the peak assignments used in this work (black) compared to that of Stöhr (red) and Ohta (blue). Stöhr assigns three features to 4s←1s, 4p←1s and 5p←1s transitions. These are present in our data and figure 11 shows how well the positions of these features compares with the work of Stöhr. Another feature was assigned in our data which is not noted by Stöhr but is featured in the work of Ohta. This is a small peak before the π^* resonance and may be a π^*-like transition originating from

the substrate[5]. Figure 11 shows that the peak assignments made in our data agree well with the work of both Stöhr and Ohta.

All of the six peaks in each of the spectra, grazing and normal, in figure 10 were fitted using Gaussian functions. Also used in the fitting procedure was a step function, in the form of a half-Gaussian, which was used to fit the nature of the S K-edge jump. The Gaussian functions used to fit the six peaks were of the form,

$$f(x)=\frac{A}{w}.\frac{\left(\sqrt{4\ln 2}\right)}{\pi}\exp(-4\ln 2).\frac{(x-x_c)^2}{w^2}$$

where A is the peak area, w is the FWHM and x_c is the peak centre. The ionisation potential was located at 2472.4 eV with reference to figure 12. Figure 12 shows a thiophene multilayer spectrum where the π^* and σ^* resonances have all but collapsed. This spectrum was chosen because the partial collapse of the π^* and σ^* resonances eases the assigning of the position of the ionisation potential to 2472.4 eV. The half-Gaussian step function (dotted blue line) used in figure 12 is derived from,

$$f(x)=\exp(x-2472.4)^2/7$$

where 2472.4 eV is the position of the ionisation potential and 7 is the width that represents a FWHM of 4.4 eV. The step function resulting from using this width is similar to that of Ohta *et al*[4]. Table 1 shows the positions of the seven features that were fitted, six peaks and a step.

Figure 10: *Nested sequentially dosed S K-edge NEXAFS experiments. Coverages and corresponding desorption states are shown. The dotted vertical lines represent the positions of π* and σ* resonances, as calculated by Stöhr et al.*[3]

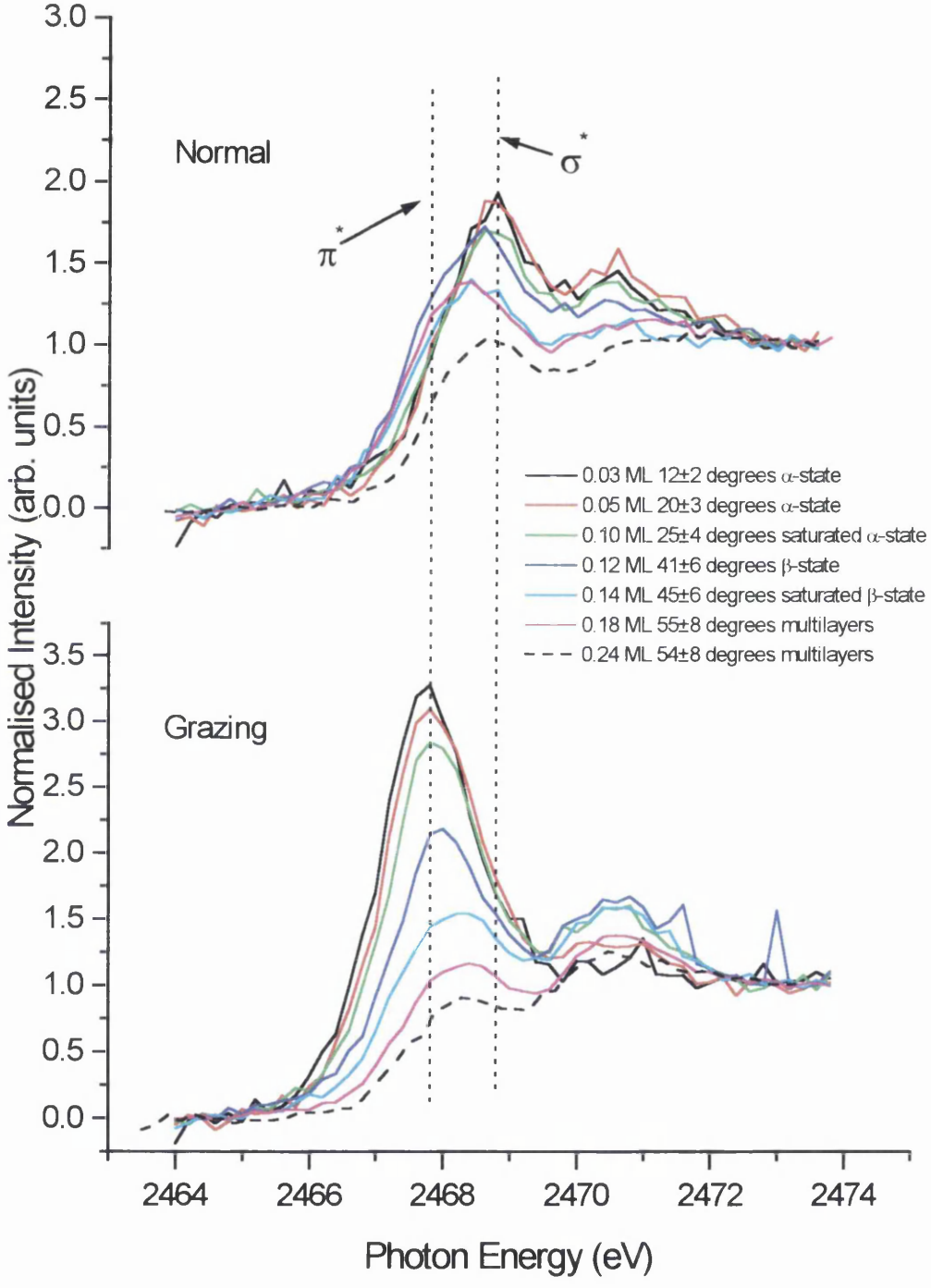

Figure 11: *Comparison of NEXAFS peak assignments for fitting procedure from this work and previous work*[3,4].

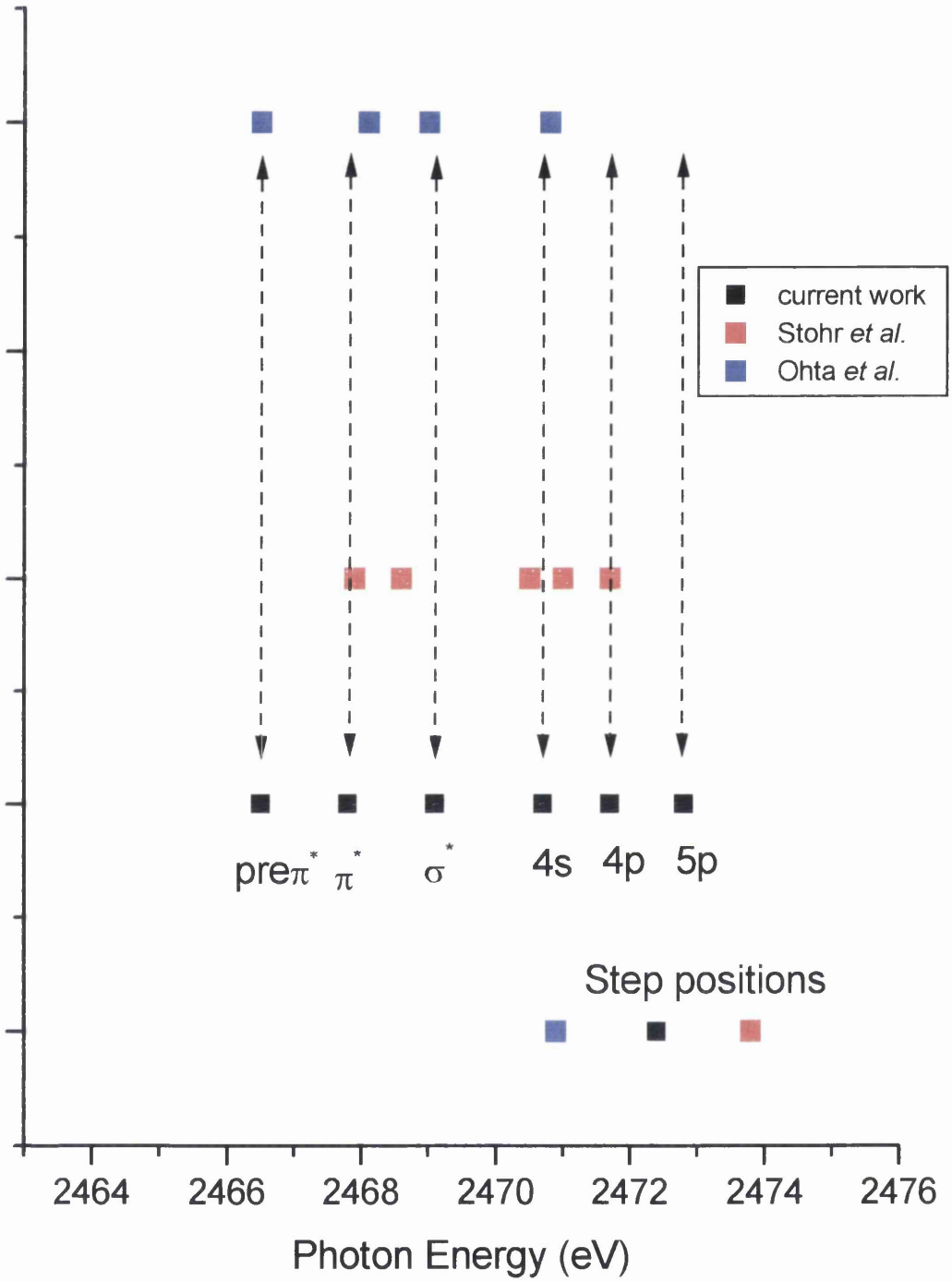

TABLE 1 *Positions of the seven features that were fitted in the data with the type of function that was used in the fitting procedure and the broadness used.*

Peak Position (eV)	Fitting Function	Assignment (ref.)	Broadness (eV)
2466.5	Gaussian	pre-π*	1.4
2467.8	Gaussian	π*	1.4
2468.7	Gaussian	σ*	1.4
2470.7	Gaussian	4s	1.4
2471.7	Gaussian	4p	1.4
2472.8	Gaussian	5p	1.4
2472.4	Step	Ionisation Threshold	4.4

TABLE 2 *Angles of inclination for coverages shown in NEXAFS data in figure 10 and corresponding TPD states.*

Coverage (ML)	π* area (grazing)	π* area (normal)	Ratio π*(g)/π*(n)	Angle (α) (°)	TPD state
0.03	4.29	0.10	42.90	12±2	α
0.05	3.85	0.28	13.75	20±3	α
0.10	3.52	0.44	8.00	25±4	Saturated α
0.12	2.32	0.93	2.49	41±6	β
0.14	1.73	0.91	1.90	45±6	Saturated β
0.18	1.12	1.14	0.98	55±8	multilayer
0.24	0.17	0.18	0.94	53±8	multilayer

As outlined in Chapter 2, the intensities of the π^* resonance in both grazing and normal NEXAFS spectra can be expressed as:

$$I(\theta) \propto \frac{1}{3} P[1+\frac{1}{2}(3\cos^2\theta-1)(3\cos^2\alpha-1)] \qquad (1)$$

where θ is the angle of X-ray incidence (19.5 or 90), P is the degree of X-ray polarisation (0.85)[6] and α represents the angle that the molecule makes with the surface.

The ratio of the intensity of the π^* resonance in a grazing spectrum, $I_{19.5}$, with the intensity of the π^* resonance in a normal spectrum, I_{90}, is a function of the angle of inclination that the molecule makes with the surface for a particular coverage.

All of the seven features identified in table 1 were used to fit each spectrum in figure 10 and a complete list of values derived from the fitting procedure such as peak position, broadness and area are listed in table 4 at the end of this section. The orientation of the thiophene molecule can be determined from the polarisation dependence of the π^* resonances. Although, in principle, the σ^* intensities could also be used to determine the molecular orientation. This approach was rejected on the grounds that there is a systematic error in the determination of both the positions and intensities of the σ^* resonances due to the step and the 4s←1s feature. This means that using the σ^* intensities proves unreliable for the purpose of calculating the angle of orientation that the thiophene molecule makes with the surface because significant errors in σ^* intensities would give inaccurate angles of orientation. The calculated intensities and ratios of π^* resonances for each of the seven coverages represented in figure 10 are shown in table 2.

Figure 12: *Determination of step function (blue dashed spectrum) from multilayer NEXAFS spectrum (black dots).*

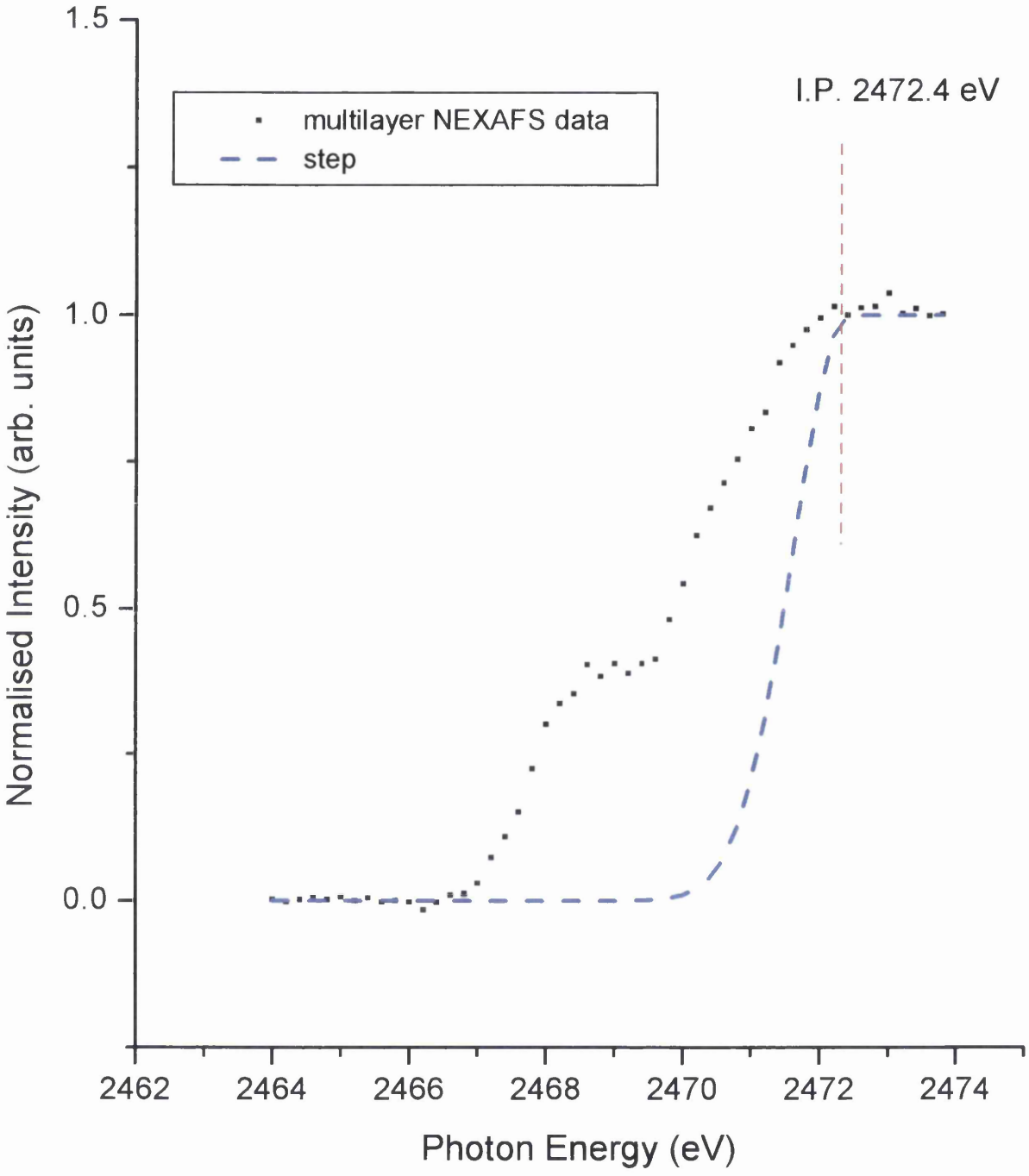

As the coverage increases from 0.03-0.18 ML, table 2 shows that the intensity of the π^* resonance decreases in the grazing data and increases in the normal data. At a coverage of 0.24 ML, multilayers have formed and the resonances collapse in intensity and appear as a broad feature (figure 10, dotted black data). Figure 13 shows the ratio $I\pi^*(g)/I\pi^*(n)$ plotted against coverage. It is clear that this ratio tends to unity with increasing coverage.

From table 4, the intensity of peak two, the π^* resonance, decreases as the coverage increases in the grazing incidence data. Also, the intensity of peak three, the σ^* resonance, decreases with increasing coverage in the normal incidence data. With a roughly flat orientation, the features expected to dominate NEXAFS spectra are a π^* resonance at grazing incidence and a σ^* resonance at normal incidence. This is observed in the low coverage (0.03 ML) data and the decrease in intensity of these two features as the coverage increases, as also shown in table 3, means that the orientation of the molecule is changing. The angles derived from the ratio $I\pi^*(g)/I\pi^*(n)$ shown in table 2 also show this.

At low coverage, 0.03 ML, the feature in the grazing data at 2467.8 eV can be fitted to 3 Gaussian functions, peaks 1, 2 and 3 in table 3, the one with the biggest intensity being at the position of the π^* resonance, peak 2. The feature in the normal data at 2468.7 eV at a coverage of 0.03 ML can be fitted to 3 Gaussian functions, peaks 1,2 and 3 in table 3, with the biggest intensity being at the position of the σ^* resonance, peak 3.

Figure 13: *Plot of $I_{\pi^*}(g)/I_{\pi^*}(n)$ for data in figure 10. The corresponding desorption states are also shown.*

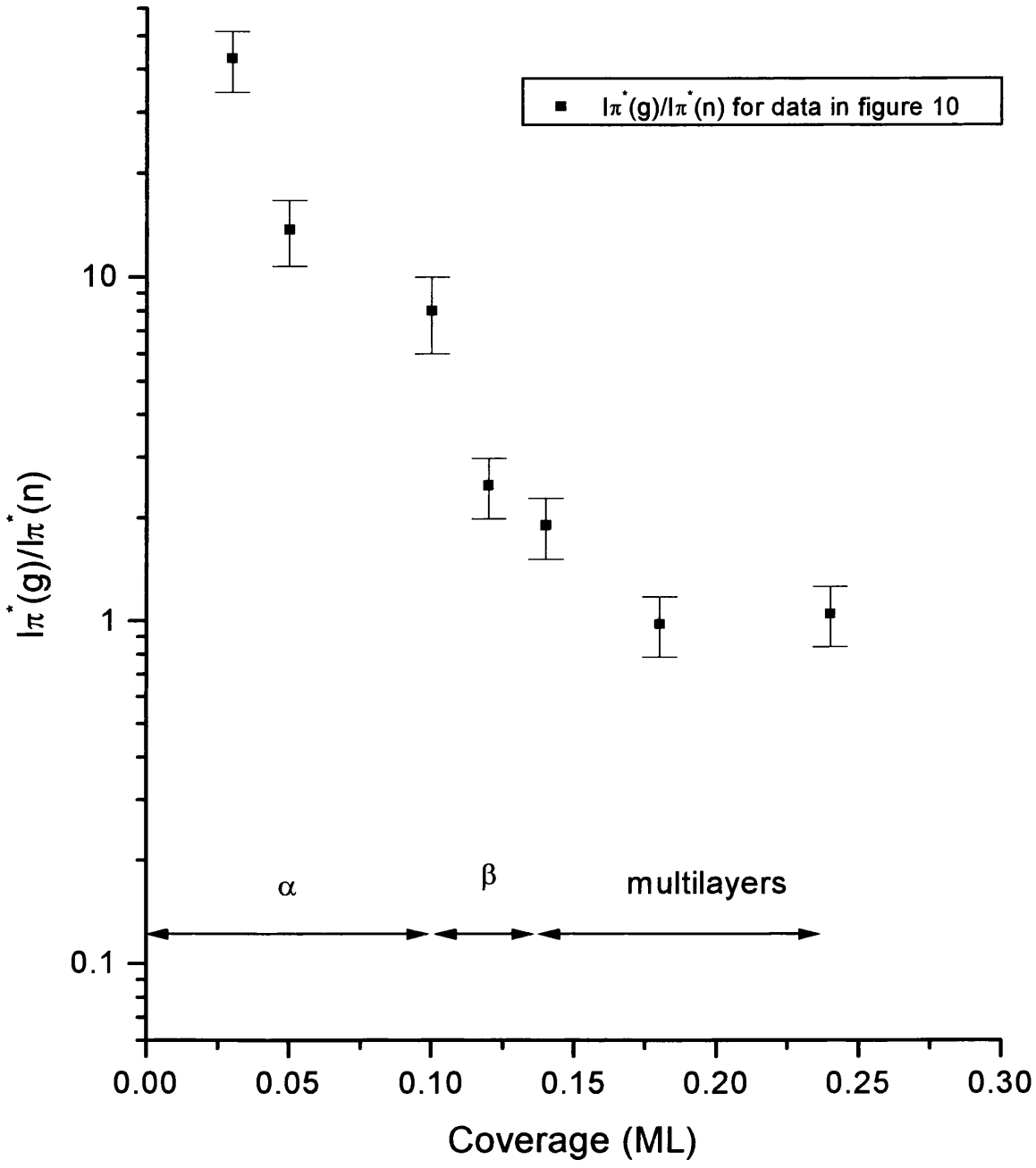

As the coverage increases, the features in both the grazing and normal spectra appear to broaden and this can be explained with reference to table 4. The broadening of the features noted above can be explained by an overall increased π^* contribution in the normal incidence data with increasing coverage, and an overall increased σ^* contribution in the grazing incidence data with increasing coverage.

Shown in figure 14 is a plot of the angles listed in table 2 against coverage which clearly shows that the angle that the molecule makes with the surface is changing as the coverage increases. The first three spectra, corresponding to coverages 0.03, 0.05 and 0.10 ML, all represent coverages that would give rise to an α-state desorption feature, as outlined in TPD results in the previous section. The angle of orientation that the thiophene ring makes with the surface over this small coverage range is increasing from an inclination of 12±2 ° (0.03 ML) to 20±3 ° (0.05 ML) to 25±4 ° (0.10 ML).

Coverages of 0.12 and 0.14 ML represent coverages that would give rise to a β-state desorption feature. At these coverages, the angle of inclination has risen to 41±6 ° and 45±6 ° respectively.

Figures 15 (a), (b) and (c) show fitted sequentially dosed S K-edge NEXAFS spectra at both normal and grazing incidence at 0.10 ML (saturated α-state), 0.14 ML (saturated β-state) and 0.24 ML (multilayer) coverages respectively.

Figure 14: *Plot of angles calculated for NEXAFS spectra shown in figure 10 and tabulated in table 1. The corresponding desorption states are also shown.*

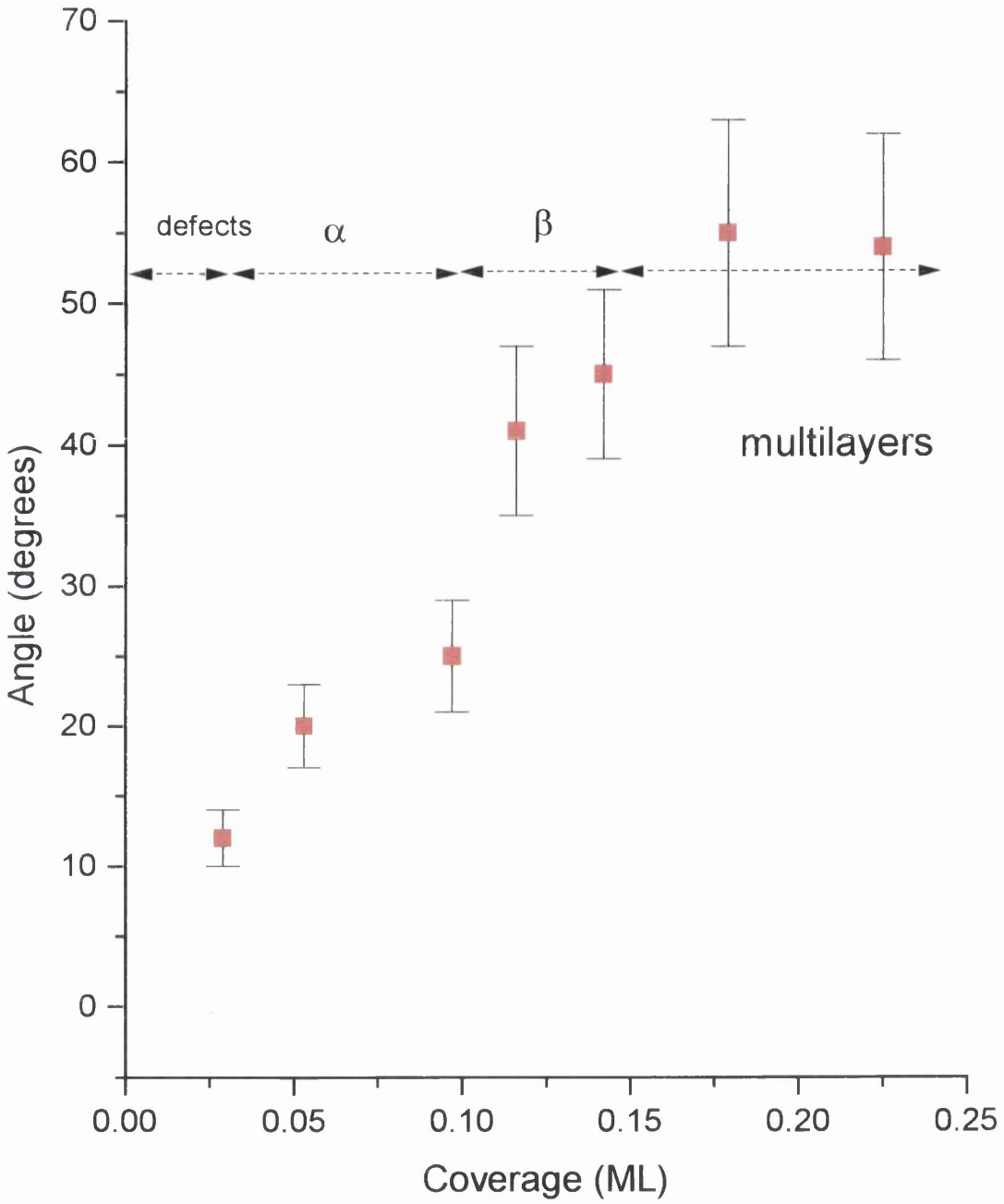

Figure 15: *Fitted sequentially dosed NEXAFS spectra for saturated α-state (a), saturated β-state (b), and multilayer coverages (c).*

(a) 0.10 ML

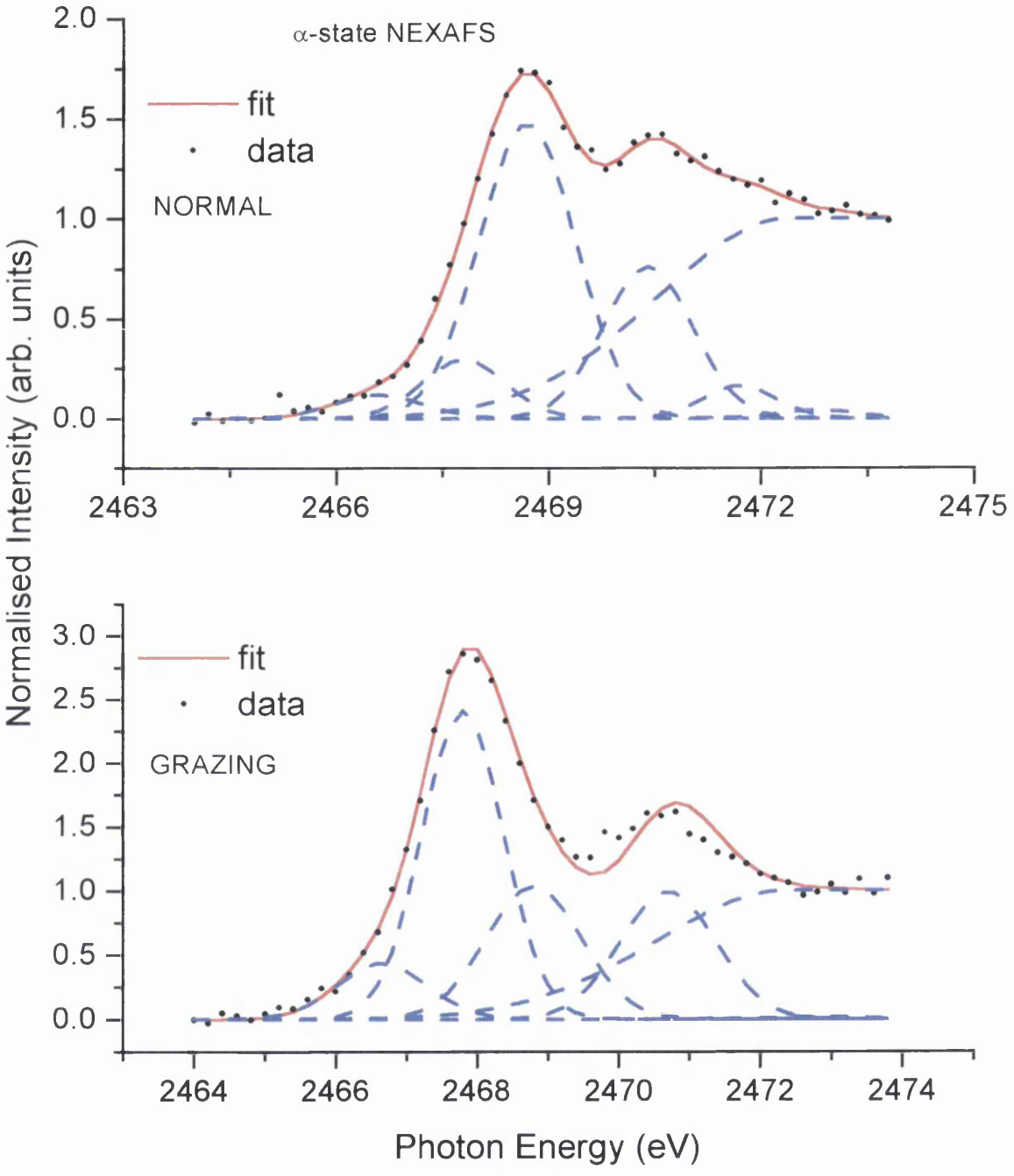

(b) 0.14 ML

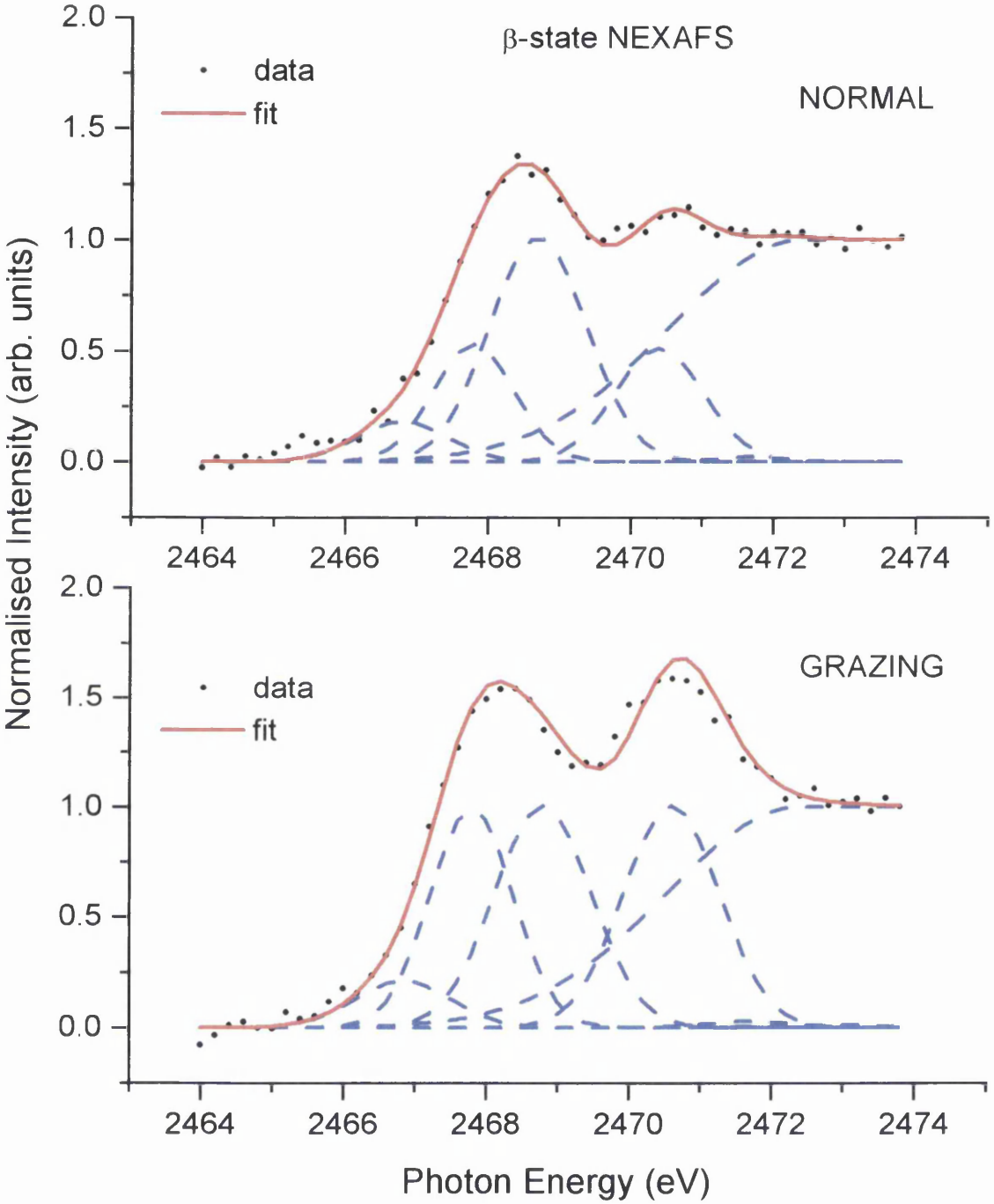
β-state NEXAFS
NORMAL
data
fit
GRAZING
data
fit
Normalised Intensity (arb. units)
Photon Energy (eV)
2.0
1.5
1.0
0.5
0.0
2464
2466
2468
2470
2472
2474

(c) 0.24 ML

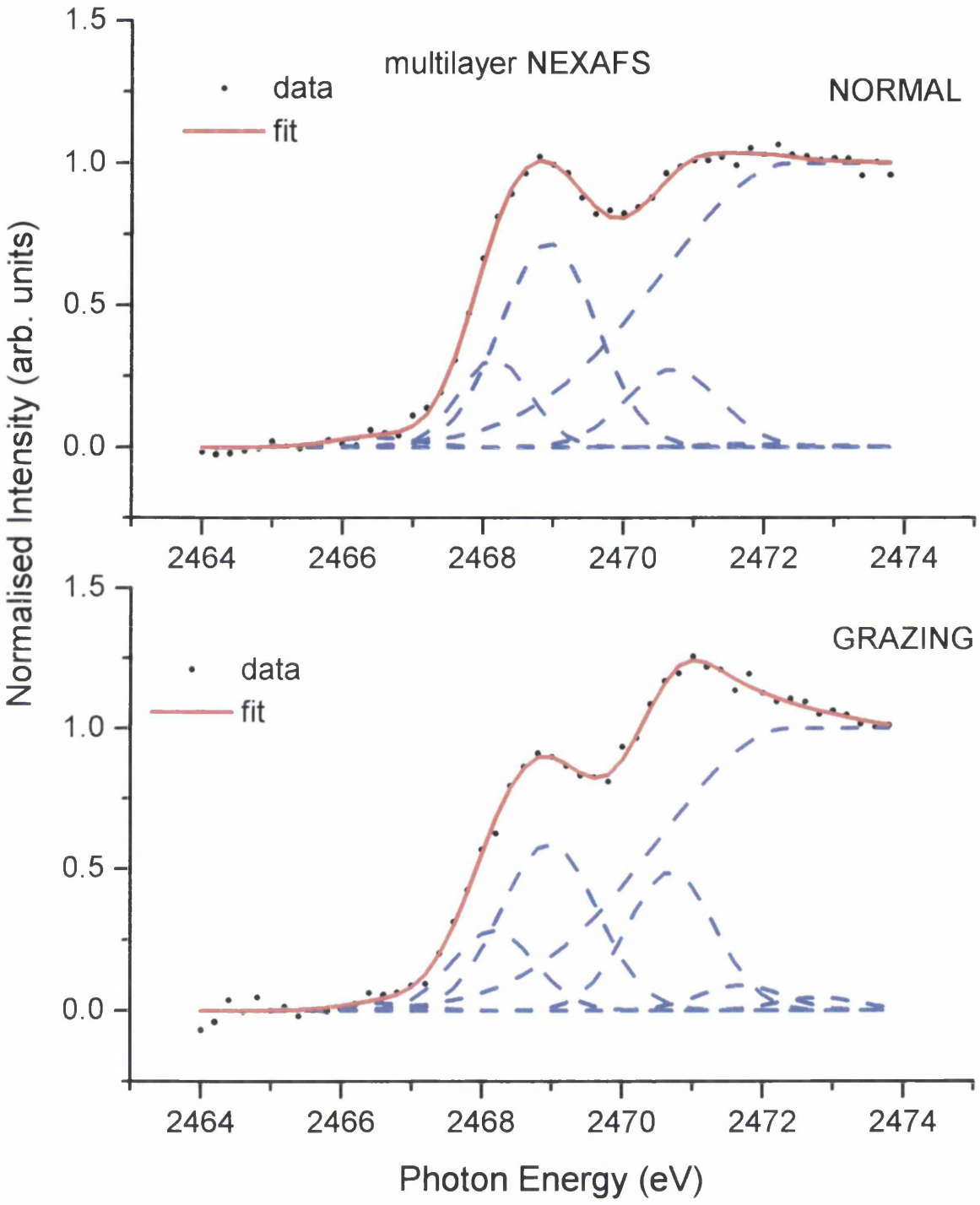
multilayer NEXAFS
NORMAL
data
fit
GRAZING
data
fit
Normalised Intensity (arb. units)
Photon Energy (eV)
1.5
1.0
0.5
0.0
2464
2466
2468
2470
2472
2474

4.2.4 Annealed NEXAFS experiments.

Thiophene surfaces were prepared by the annealing dosing method in order to study both the α and β states. The results of these experiments are listed in table 3. By analysis of XPS data at different annealing temperatures, the uncertainty associated with the coverage measurements using the annealed dosing method was calculated to be ±0.02 ML.

TABLE 3 *Angles of inclination for coverages shown in NEXAFS data in figure Whatever it is and show the fitted data.*

Coverage (ML)	π* area (grazing)	π* area (normal)	Ratio π*(g)/π*(n)	Angle (α) (°)	TPD states
0.09	3.32	0.81	4.10	34±5	Saturated α
0.11	4.66	0.92	5.07	31±5	Saturated α
0.14	2.77	1.11	2.50	41±6	Saturated β
0.18	4.13	2.76	1.49	49±7	Saturated β

From table 3 it is clear that the average angle at α-state coverage is 33+5 ° and the average angle at β-state coverage is 45±6 °. These angles are identical within experimental error to the angles calculated from sequential experiments, table 2. Fitted data at α- and β-state coverages is shown in figures 16 (a) and (b). This data was fitted in an identical way to the sequentially dosed data.

Figure 17: *Fitted NEXAFS spectra from annealed dosing experiments at α-state (a) and β-state (b) coverages.*

(a)

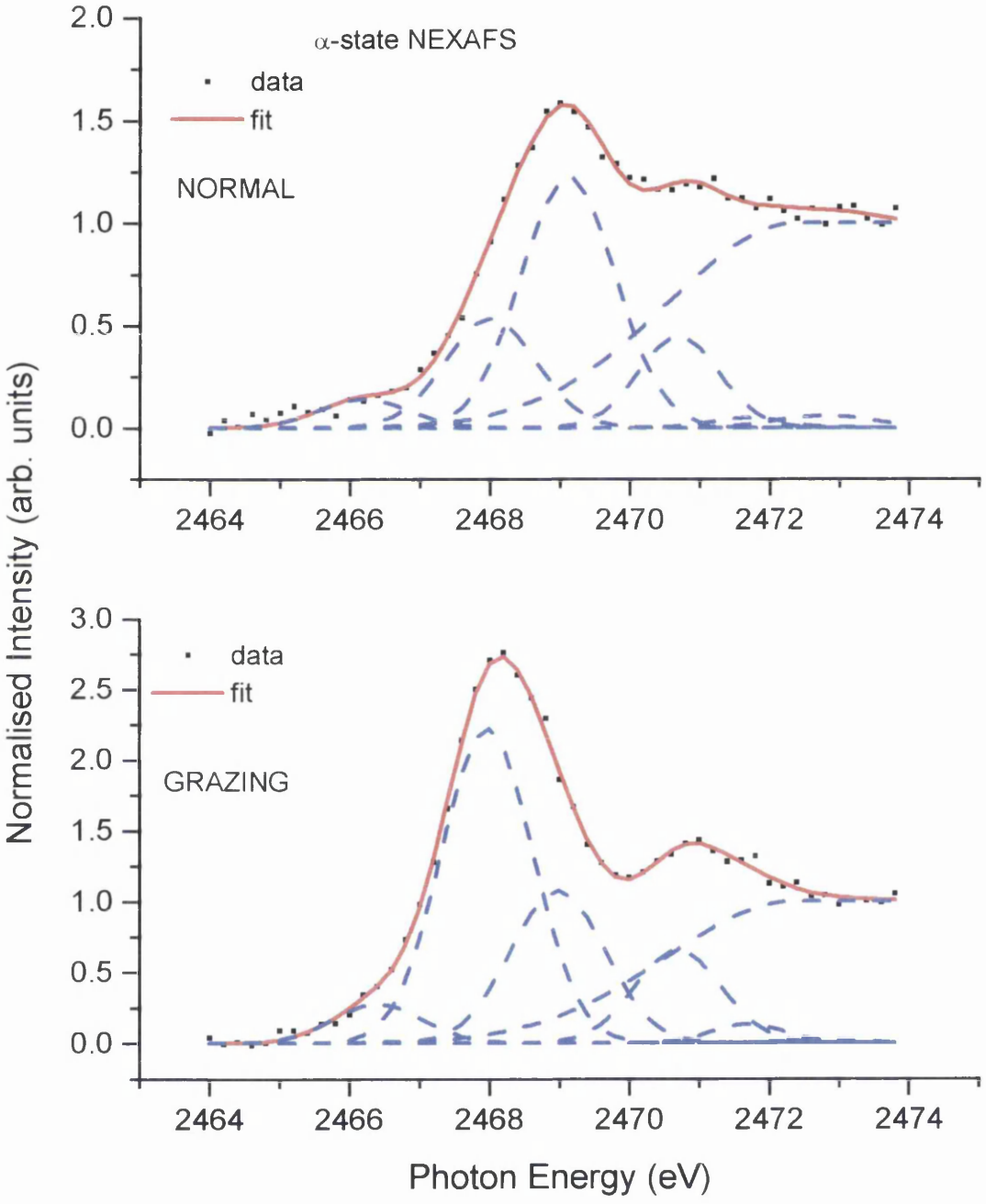

(b)

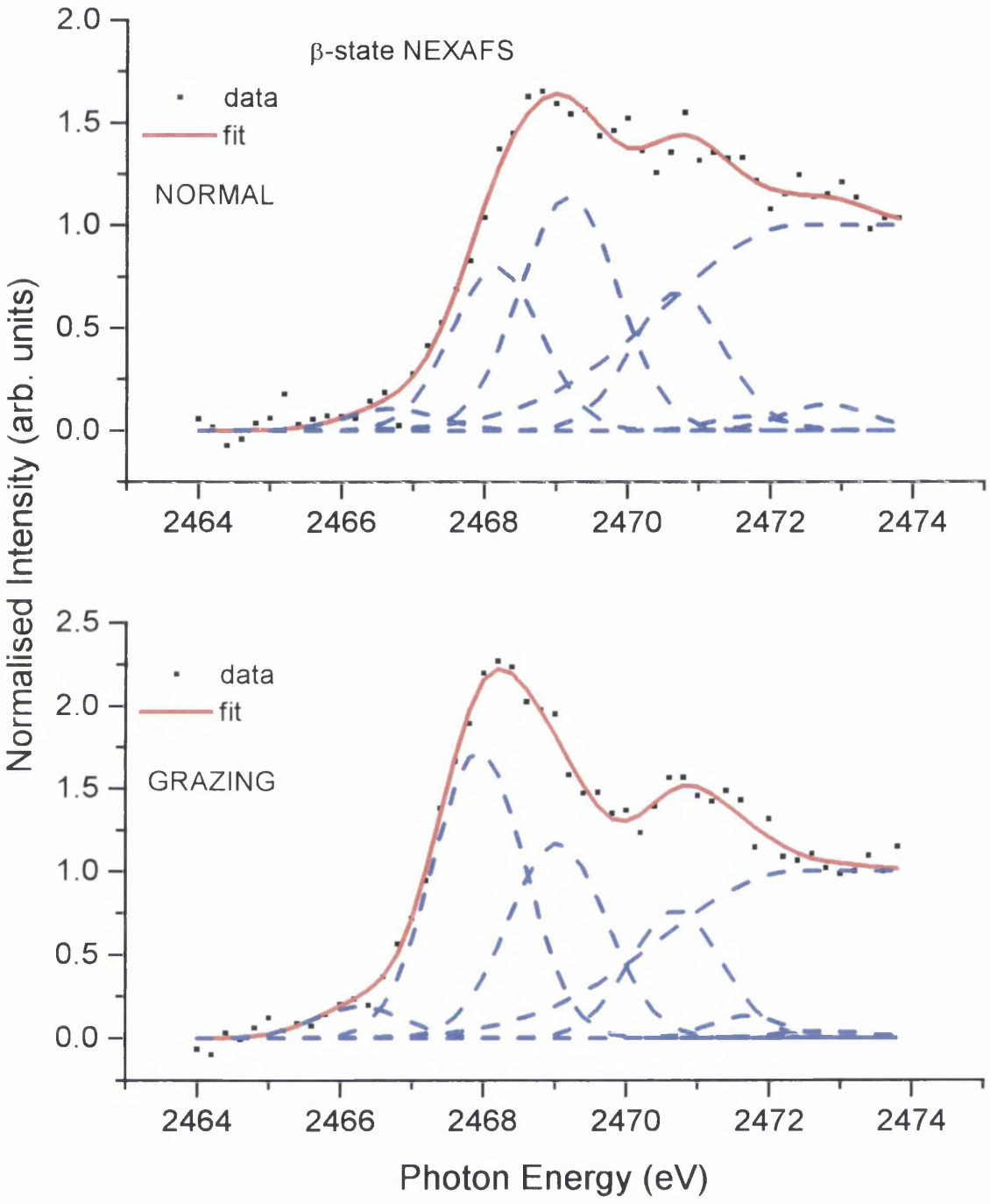
β-state NEXAFS
data
fit
NORMAL
GRAZING
Normalised Intensity (arb. units)
Photon Energy (eV)
2.0
1.5
1.0
0.5
0.0
2.5
2464
2466
2468
2470
2472
2474

TABLE 4 *Complete list of values obtained from fitting all data shown in figure 10 from seequentially dosed experiments.*

Peak one (grazing)	Position (eV)	Area	Broadness (eV)	Peak one (normal)	Position (eV)	Area	Broadness (eV)
Peak 1 (pre-π)							
0.03 ML (g)	2466.8	0.86	1.50	0.03 ML (n)	2466.8	0.37	1.60
0.05 ML (g)	2466.8	0.91	1.60	0.05 ML (n)	2466.6	0.22	1.50
0.10 ML (g)	2466.7	0.72	1.50	0.10 ML (n)	2466.6	0.19	1.50
0.12 ML (g)	2466.6	0.55	1.50	0.12 ML (n)	2466.6	0.31	1.50
0.14 ML (g)	2466.6	0.20	1.59	0.14 ML (n)	2466.6	0.24	1.50
0.18 ML (g)	2466.6	0.09	1.50	0.18 ML (n)	2466.6	0.15	1.50
0.24 ML (g)	2466.5	0.02	1.30	0.24 ML (n)	2466.3	0.02	1.30
Peak 2 (π*)							
0.03 ML (g)	2467.8	4.29	1.45	0.03 ML (n)	2467.8	0.10	1.34
0.05 ML (g)	2467.8	3.85	1.36	0.05 ML (n)	2467.8	0.28	1.36
0.10 ML (g)	2467.8	3.52	1.35	0.10 ML (n)	2467.8	0.44	1.39
0.12 ML (g)	2467.8	2.32	1.28	0.12 ML (n)	2467.8	0.93	1.27
0.14 ML (g)	2467.8	1.73	1.49	0.14 ML (n)	2467.8	0.91	1.49
0.18 ML (g)	2467.8	1.12	1.43	0.18 ML (n)	2467.9	1.13	1.45
0.24 ML (g)	2467.8	0.17	1.23	0.24 ML (n)	2467.8	0.18	1.20
Peak 3 (σ*)							
0.03 ML (g)	2468.8	1.24	1.20	0.03 ML (n)	2468.7	2.97	1.60
0.05 ML (g)	2468.8	1.89	1.60	0.05 ML (n)	2468.7	2.63	1.60
0.10 ML (g)	2468.8	1.64	1.60	0.10 ML (n)	2468.7	2.52	1.60
0.12 ML (g)	2468.8	1.83	1.60	0.12 ML (n)	2468.7	2.16	1.60
0.14 ML (g)	2468.8	1.01	1.60	0.14 ML (n)	2468.7	1.64	1.60
0.18 ML (g)	2468.8	1.20	1.60	0.18 ML (n)	2468.7	1.49	1.60
0.24 ML (g)	2468.8	1.22	1.60	0.24 ML (n)	2468.8	1.45	1.60
Peak 4 (4s←1s)							
0.03 ML (g)	2470.7	0.94	1.60	0.03 ML (n)	2470.7	1.21	1.48
0.05 ML (g)	2470.7	1.27	1.60	0.05 ML (n)	2470.7	1.22	1.45

0.10 ML (g)	2470.7	1.85	1.60	0.10 ML (n)	2470.7	1.21	1.49
0.12 ML (g)	2470.7	1.93	1.60	0.12 ML (n)	2470.7	1.04	1.56
0.14 ML (g)	2470.7	1.84	1.60	0.14 ML (n)	2470.7	0.82	1.59
0.18 ML (g)	2470.7	1.31	1.60	0.18 ML (n)	2470.7	0.92	1.60
0.24 ML (g)	2470.7	0.86	1.60	0.24 ML (n)	2470.7	0.50	1.60
Peak 5 (4p←1s)							
0.03 ML (g)	2471.7	0.00	0.00	0.03 ML (n)	2471.7	0.19	1.20
0.05 ML (g)	2471.7	0.00	0.00	0.05 ML (n)	2471.7	0.25	1.33
0.10 ML (g)	2471.7	0.00	0.00	0.10 ML (n)	2471.7	0.21	1.20
0.12 ML (g)	2471.7	0.00	0.00	0.12 ML (n)	2471.7	0.10	1.20
0.14 ML (g)	2471.7	0.00	0.00	0.14 ML (n)	2471.7	0.02	1.40
0.18 ML (g)	2471.7	0.00	0.00	0.18 ML (n)	2471.7	0.08	1.22
0.24 ML (g)	2471.7	0.08	1.40	0.24 ML (n)	2471.7	0.00	0.00
Peak 6 (5p←1s)							
0.03 ML (g)	2472.8	0.00	0.00	0.03 ML (n)	2472.8	0.03	1.60
0.05 ML (g)	2472.8	0.07	1.20	0.05 ML (n)	2472.8	0.00	0.00
0.10 ML (g)	2472.8	0.06	1.40	0.10 ML (n)	2472.8	0.04	1.30
0.12 ML (g)	2472.8	0.05	1.40	0.12 ML (n)	2472.8	0.04	1.60
0.14 ML (g)	2472.8	0.01	1.20	0.14 ML (n)	2472.8	0.01	1.60
0.18 ML (g)	2472.8	0.00	0.00	0.18 ML (n)	2472.8	0.06	1.60
0.24 ML (g)	2472.8	0.07	1.40	0.24 ML (n)	2472.8	0.01	1.20

4.2.5 NIXSW

The object of using Normal Incidence X-ray Standing Wavefield (NIXSW) in surface science is to determine the adsorption site occupied by an adsorbate[7]. This usually means describing which of the sites on the surface – atop, bridge, f.c.c., h.c.p. – or a combination of, is occupied by an adsorbate. The technique of NIXSW has been described previously in Chapter 2.

Standing wave profiles can be fitted to four experimental factors, namely the coherent fraction, f_{co}, the coherent position, D(hkl), the width of the X-rays used in the experiment, ΔE, and the mosaic spread of the crystal used. The coherent fraction and the coherent position are the parameters of most diagnostic value because they describe the nature of the adsorption. The coherent fraction f_{co} is a measure of the uncertainty in the position of the adsorption site and is a number between 0 – 1. A coherent fraction of 1 indicates that there is only one distinct adsorption site and a lower coherent fraction, for example 0.5, indicates disorder in the adsorption system brought about by either multiple site occupation or vibrational disorder, or both.

The coherent position, D(hkl), is the distance from the nearest scattering plane (hkl) to the adsorbate in Angstroms (Å), assuming no relaxation of the substrate surface layers. The Cu-S distance and Cu-S bond length can be calculated once the adsorption site has been determined. As X-ray standing waves propagate beyond the crystal surface creating hypothetical lattice planes, the coherent position derived from analysis of NIXSW data may not be relative to the surface plane. In the following results the coherent positions, Cu surface-S distances, obtained from analysis of NIXSW data give unfeasibly short distances for Cu-S bond lengths, irrespective of what the adsorption site is. The actual Cu-S distances, and subsequent Cu-S bond lengths, are then inferred as explained in the adsorbate NIXSW experiments section.

4.2.6 Substrate NIXSW experiments

Substrate NIXSW experiments were performed in order to fit the crystal mosaic spread and the width of the X-ray beam. As with every NIXSW experiment performed the standing wave profiles obtained from substrate experiments were also fitted with respect to the substrate coherent fraction and coherent position. All of the values obtained from fitting substrate NIXSW data are summarised in table 5. Also, the Bragg energy, which is required to fit the adsorbate NIXSW profiles, was derived from the substrate NIXSW data.

All clean surfaces prepared by the method outlined in Chapter 3 showed sharp (1x1) LEED patterns prior to dosing, as shown in figure 6 (a). A Cu LVV Auger (K.E. 909 eV) NIXSW standing wave profile from a clean, well ordered crystal surface would be expected to be fitted to a high coherent fraction and a coherent position of 0 Å. Figures 18 and 19 show standing wave profiles for the bulk copper substrate taken with respect to the (111) surface plane. The copper LVV Auger with a kinetic energy of 909 eV was monitored in each experiment. The fits of the standing wave profiles are shown in red.

Table 5: *Experimental values derived from substrate NIXSW experiments.*

	Coherent fraction	Coherent position (Å)	Broadness (eV)	Mosaic Spread (°)
Data One	0.85±0.05	0	0.95	0.1
Data Two	0.90±0.05	0	0.80	0.1

Data One and Data Two in Table 5 simply refer to two different experimental runs at beamline 6.3 of the Daresbury SRS. The two runs were two years apart and in that time, modifications were made to the beamline that had the effect of changing the broadness of the X-ray beam. This had no effect on the other experimental values derived such as the coherent fraction and the coherent position, and similarly prepared data from the two experimental runs can be directly compared. Table 5 shows that the

substrate standing wave profiles fit to a coherent position of 0 Å and a coherent fraction of 0.90±0.5. This means that the surface has a high degree of crystallographic order and that most of the surface atoms are located at f.c.c. lattice positions. The values obtained for X-ray broadness and crystal mosaic spread are fixed at these values in the subsequent analysis of adsorbate profiles. A complete list of intrinsic parameters used in the fitting process is listed in table 6:

Table 6: *Intrinsic parameters used in NIXSW fitting procedure.*

Real part of F_O	116.149
Imaginary part of F_O	13.646
Real part of F_H	88.708
Debye-Waller factor	1
Layer Spacing (Å)	2.08
Volume of Unit Cell ($Å^3$)	47.24

Thiophene NIXSW experiments were performed by monitoring S 1s photoemission. The standing wave profiles obtained from these experiments were then modelled using the parameters listed in table 6. A study by Woodruff *et al.*[8] has shown that in modelling standing wave profiles of 1s photoemission of elements such as C, N and O, non-dipole effects must be considered. In order to show that in the case of S 1s photoemission, there is no non-dipole excitation, it is necessary to compare S 1s photoemission and S KLL Auger emission NIXSW profiles from the same surface, figure 19. If non-dipole effects were present in the case of S 1s photoemission, the normalised intensity of the S 1s spectrum in figure 19 would be greater than that of the S KLL spectrum. As this is not the case, it has to be concluded that there are no non-dipole effects present in S 1s photoemission and that the fitting procedure used, as summarised in table 6, is valid.

Figure 17: *Substrate Cu LVV NIXSW profile fitted to a coherent fraction of 0.85, a coherent position of 0 Å, a mosaic spread of 0.1 ° and a broadness of 0.95 eV (table 5). This data was collected with respect to the (111) plane.*

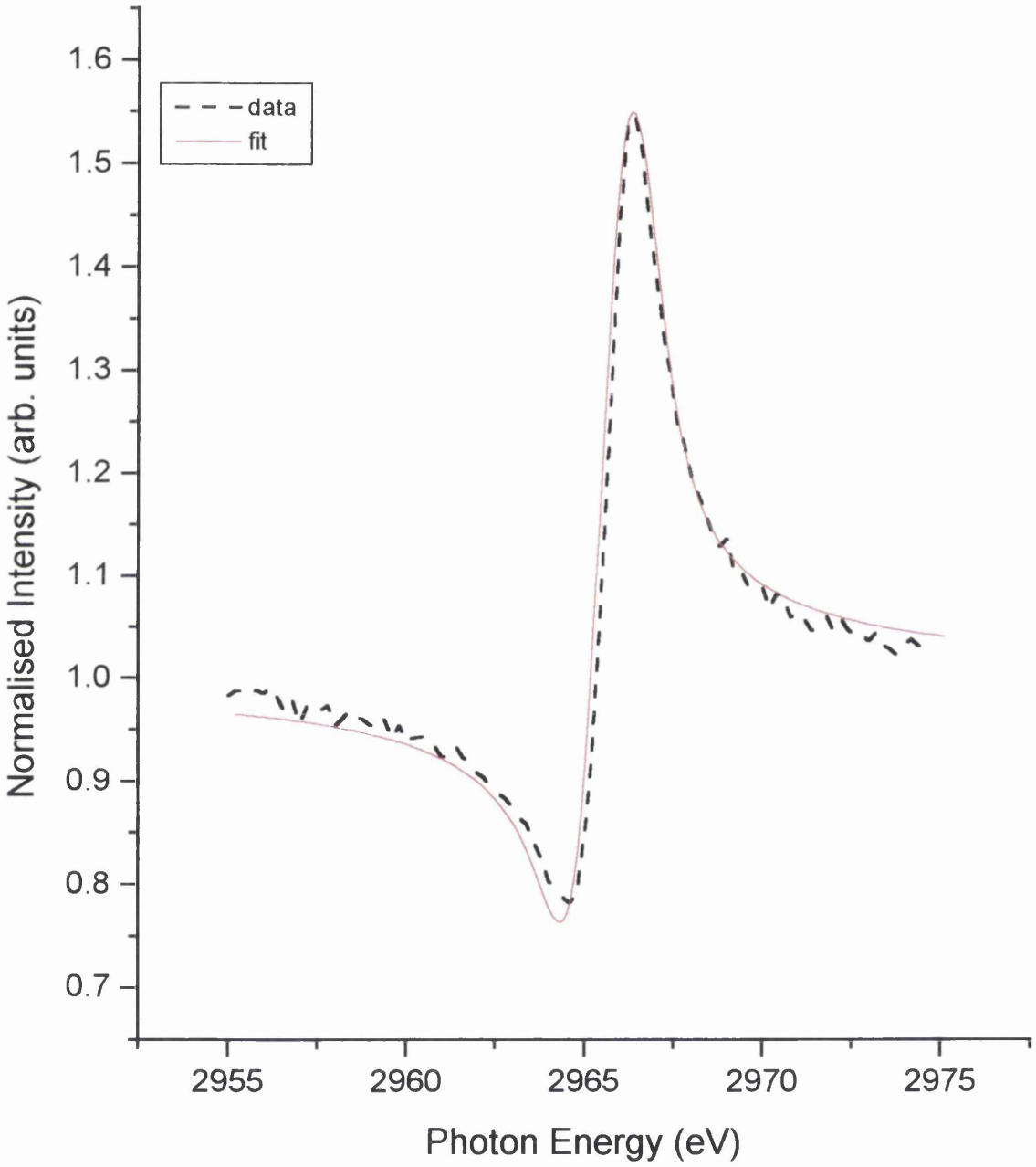

Figure 18: *Substrate Cu LVV NIXSW profile fitted to a coherent fraction of 0.90, a coherent position of 0 Å, a mosaic spread of 0.1 ° and a broadness of 0.80 eV (table 5). This data was collected with respect to the (111) plane.*

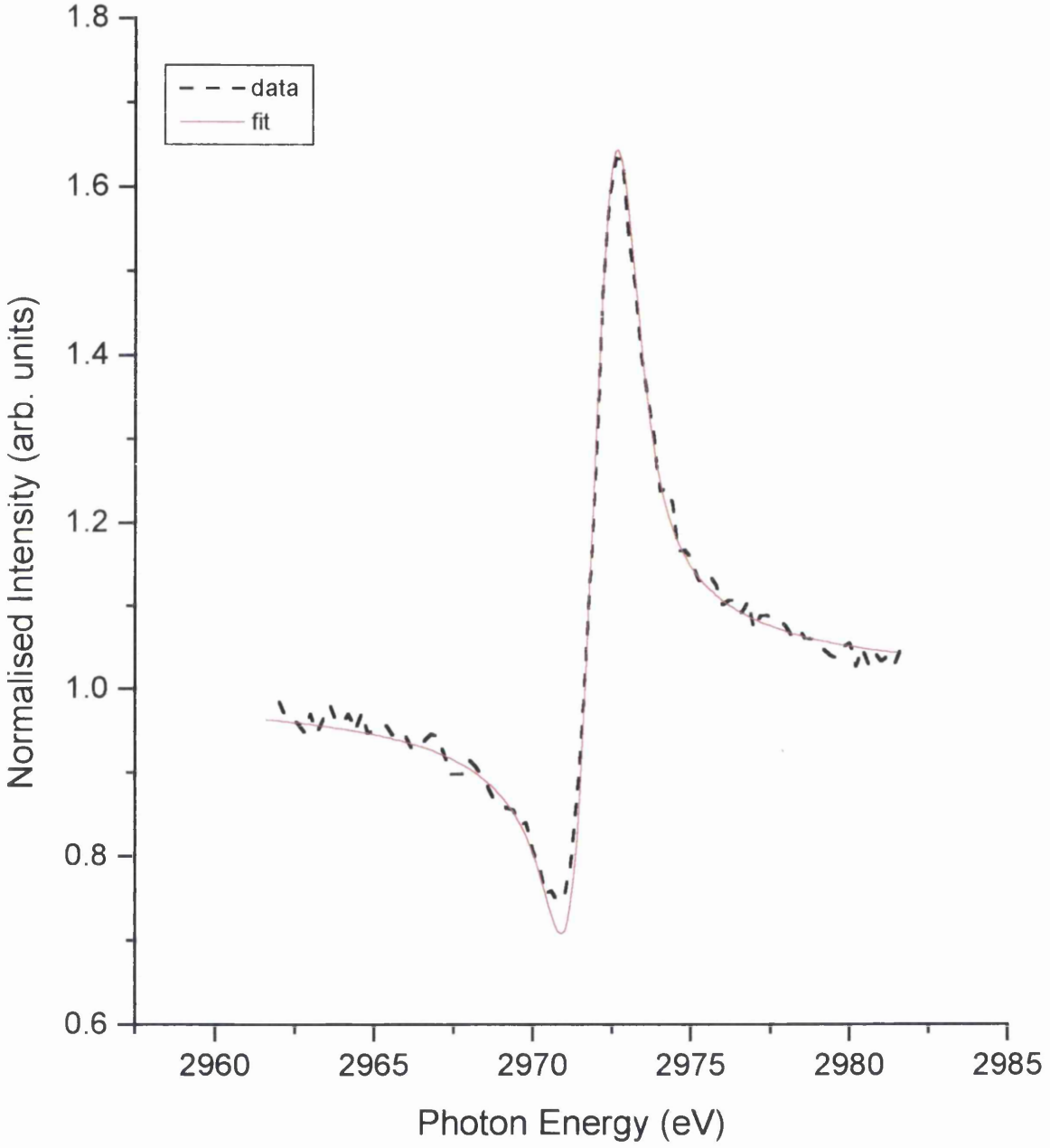

Figure 19: *S 1s photoemission (black) and S KLL Auger (blue) emission NIXSW data collected from the same surface. The similarity of these two spectra indicates the absence of non-dipole effects in S 1s photoemission.*

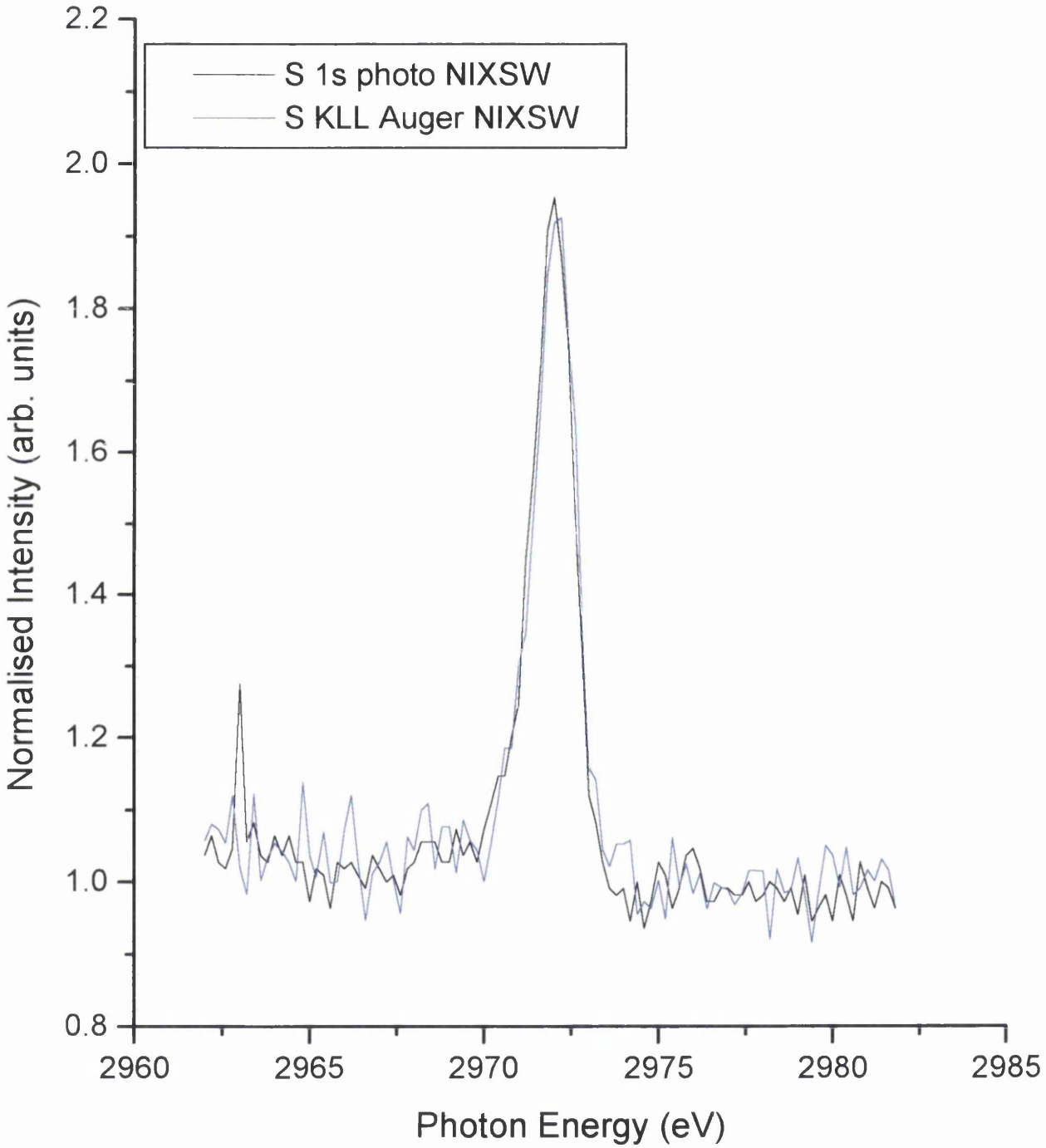

4.2.7 Adsorbate NIXSW experiments

To determine the adsorption site of thiophene on Cu(111), NIXSW experiments were performed which monitored S 1s photoemission. The standing wave profiles resulting from this, figures 20 and 21, look significantly different to the ones shown in figures 17 and 18. This is because the shape of standing wave profiles is very sensitive to the magnitude of the coherent position. The purpose of NIXSW experiments is to determine the adsorption site an adsorbate occupies on a surface. Firstly however, the distance from the surface to the adsorbate, in this case the height of the S in thiophene above the surface, is inferred from analysis of the coherent position data, as outlined in the next section. This height, the coherent position, is determined with respect to two planes, (111) and ($\bar{1}$11) and a triangulation technique is employed to unambiguously assign the adsorption site, as described in more detail in Chapter 2.

Two different methods were used in order to prepare thiophene surfaces with which to perform NIXSW experiments. These are "sequentially dosed" surfaces and "annealed" surfaces. Sequentially dosed surfaces were prepared in an identical manner to those described in the last section (NEXAFS). Annealed surfaces were prepared by dosing enough thiophene, at 120 K, to form multilayers. The crystal would then be annealed to specific temperatures to desorb the multilayers. The remaining adsorbed thiophene would then be subjected to NIXSW analysis. All surfaces prepared by both methods were subjected to XPS analysis in order for the coverage to be calculated in an identical method to the one described in the last section (NEXAFS). A complete list of data acquired from NIXSW experiments is shown in Table 7 (annealed data) and table 8 (sequential data).

NIXSW profiles using the annealed dosing method are shown in figures 20 (α-state) and 21 (β-state) and using the sequentially dosed method, in figure 22 (α- and β-state, (111) plane only).

Table 7: *S 1s NIXSW experiments performed for thiophene on Cu(111) using the annealed dosing method.*

Plane	Coverage	f_{co}	D(hkl) (Å)
111	0.08	0.90	0.55
111	0.09	0.90	0.55
111	0.09	0.90	0.55
111	0.09	0.80	0.50
111	0.11	0.90	0.55
111	0.14	0.55	0.80
111	0.15	0.65	0.80
$\bar{1}11$	0.09	0.85	0.80
$\bar{1}11$	0.11	0.70	0.75
$\bar{1}11$	0.16	0.60	0.80
$\bar{1}11$	0.17	0.67	0.80
$\bar{1}11$	0.19	0.50	0.90
$\bar{1}11$	0.19	0.60	0.80
$\bar{1}11$	0.24	0.35	0.70
$\bar{1}11$	0.26	0.33	0.80
$\bar{1}11$	0.30	0.40	0.75

Table 8: *S 1s NIXSW experiments performed for thiophene on Cu(111) using the sequential dosing method.*

Plane	Coverage	f_{co}	D(hkl) (Å)
111	0.02	0.90	0.40
111	0.04	0.90	0.45
111	0.07	0.90	0.47
111	0.10	0.90	0.50
111	0.13	0.60	0.50
111	0.15	0.45	0.50
111	0.22	0.25	0.35
111	0.25	0.15	0.35

The data shown in tables 7 and 8 is plotted in figures 23, 24, 25 and 26 in which the black data represents data from table 7 (annealed dosing data) and the red data represents data from table 8 (sequentially dosed data). Figure 23 shows how the coherent fraction in the (111) plane varies with increasing coverage. For both sequentially dosed and annealed experiments, the coherent fraction remains constant at a value of 0.90±0.05 up to coverages of 0.10 ML. At higher coverages, notably, 0.13-0.15 ML, the coherent fraction drops to values between 0.45-0.65, and at coverages above 0.20 ML, the coherent fraction has dropped to 0.1-0.2. This means that at thiophene coverages from 0–0.10 ML there is a single distinct adsorption site for both annealed and sequentially dosed experiments. From 0.13-0.15 ML the coherent fraction has dropped, but the adsorption would still be expected to be reasonably well defined in terms of adsorption site occupation. At coverages above 0.20 ML, the coherent fraction has dropped to such an extent due to the formation of multilayers that there is no unique adsorption site occupied at this high coverage.

Figure 24 shows how the coherent position in the (111) plane varies with increasing coverage. For the annealed data, at coverages up to 0.10 ML, the coherent position remains constant at a value of 0.54±0.03 Å. At higher coverages, notably 0.14 ML, the coherent position has risen to 0.80±0.07 Å. However, the sequentially dosed data shows that the coherent position is 0.50±0.05 Å at coverages from 0-0.14 ML.

Figure 20: *S 1s NIXSW profiles of 0.09 ML thiophene (α-state) with respect to (111) and ($\bar{1}11$) planes prepared by the annealed dosing method.*

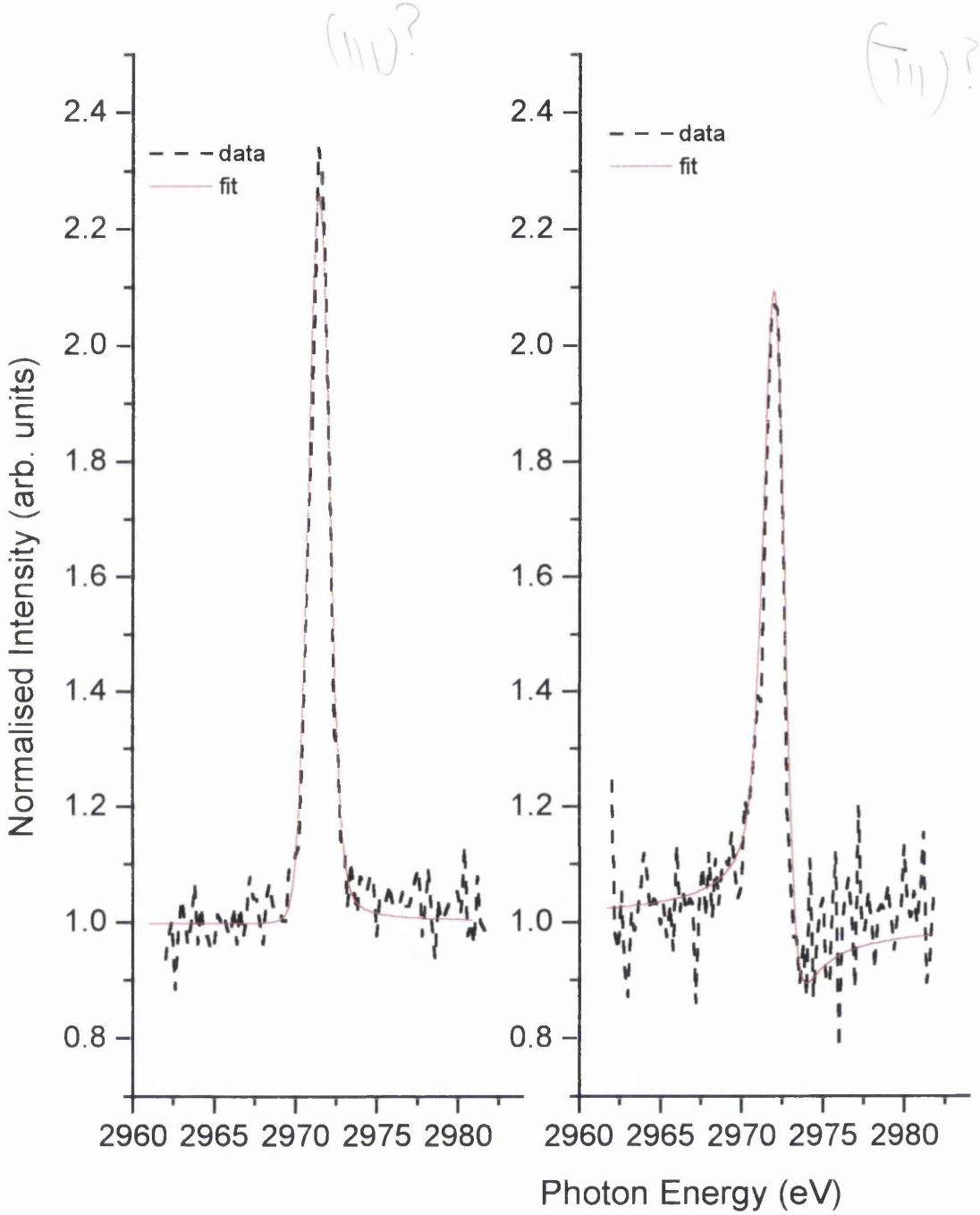

Figure 21: *S 1s NIXSW profiles of 0.14 ML thiophene (β-state) with respect to (111) and ($\bar{1}11$) planes prepared by the annealed dosing method.*

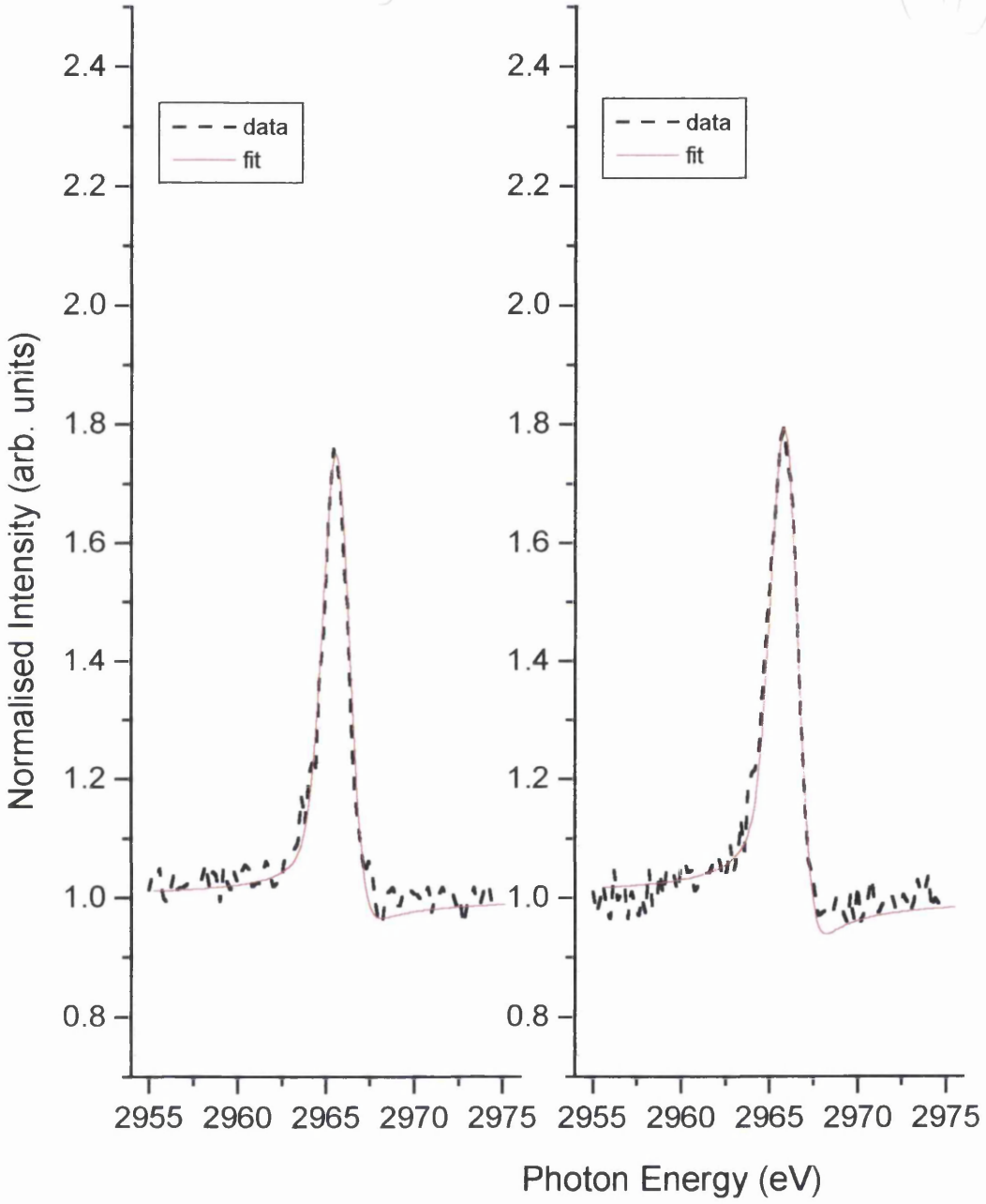

Figure 22 : *Sequentially dosed NIXSW profiles at α- (0.10 ML) and β-state (0.15 ML) coverages.*

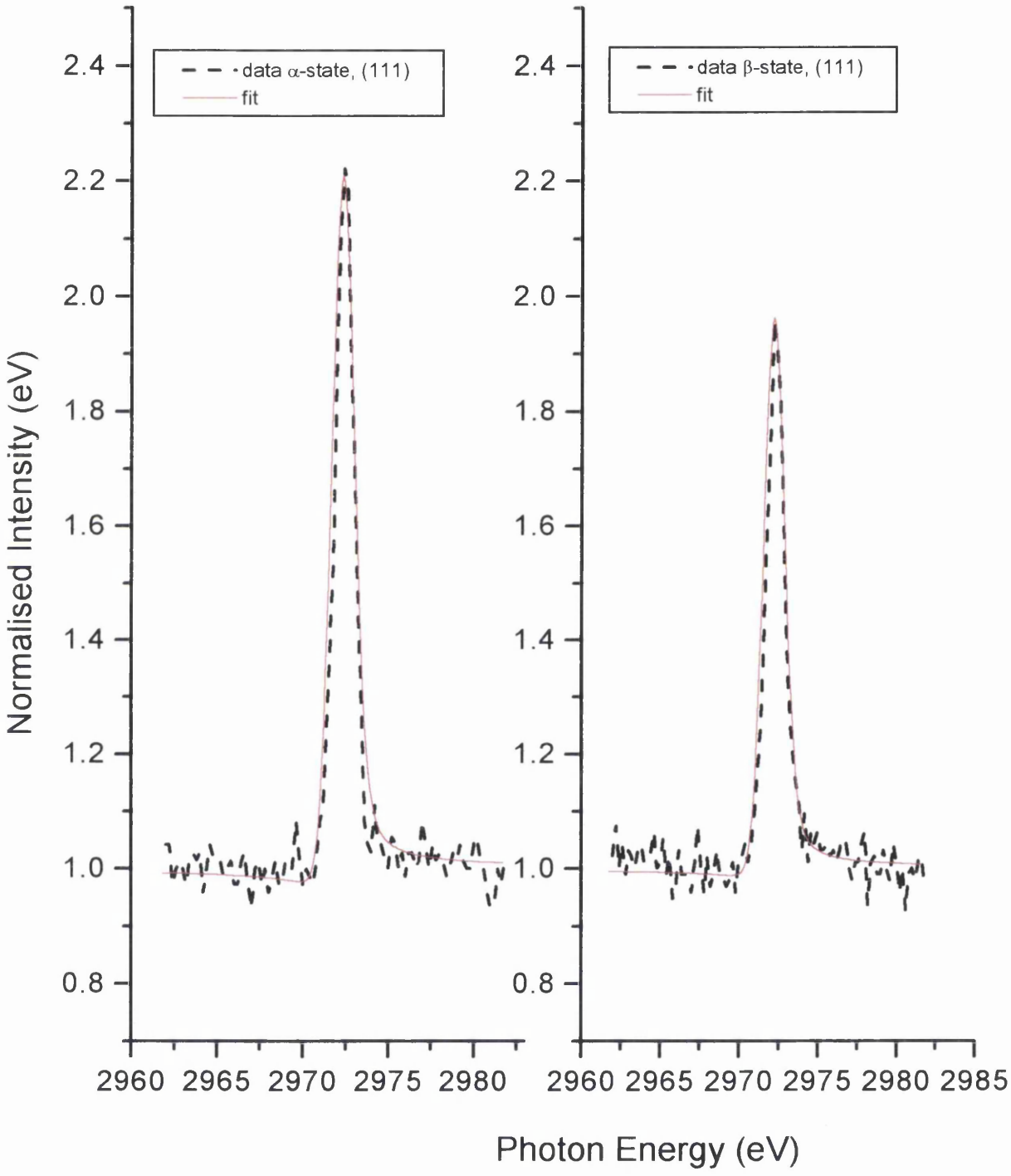

Figure 23: *Plot showing how coherent fraction varies with coverage with respect to the (111) plane.*

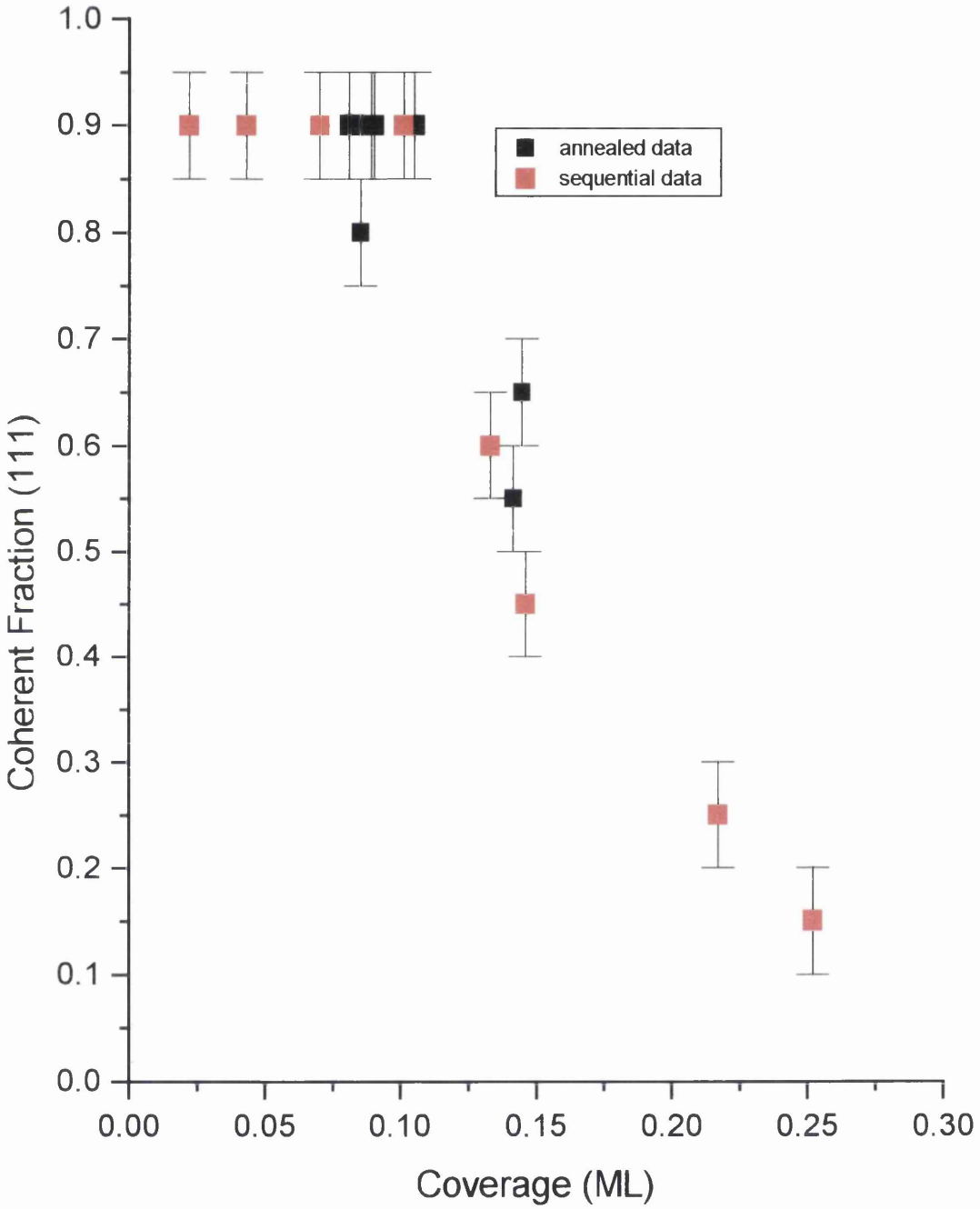

Figure 24: *Plot showing how coherent position varies with coverage with respect to the (111) plane.*

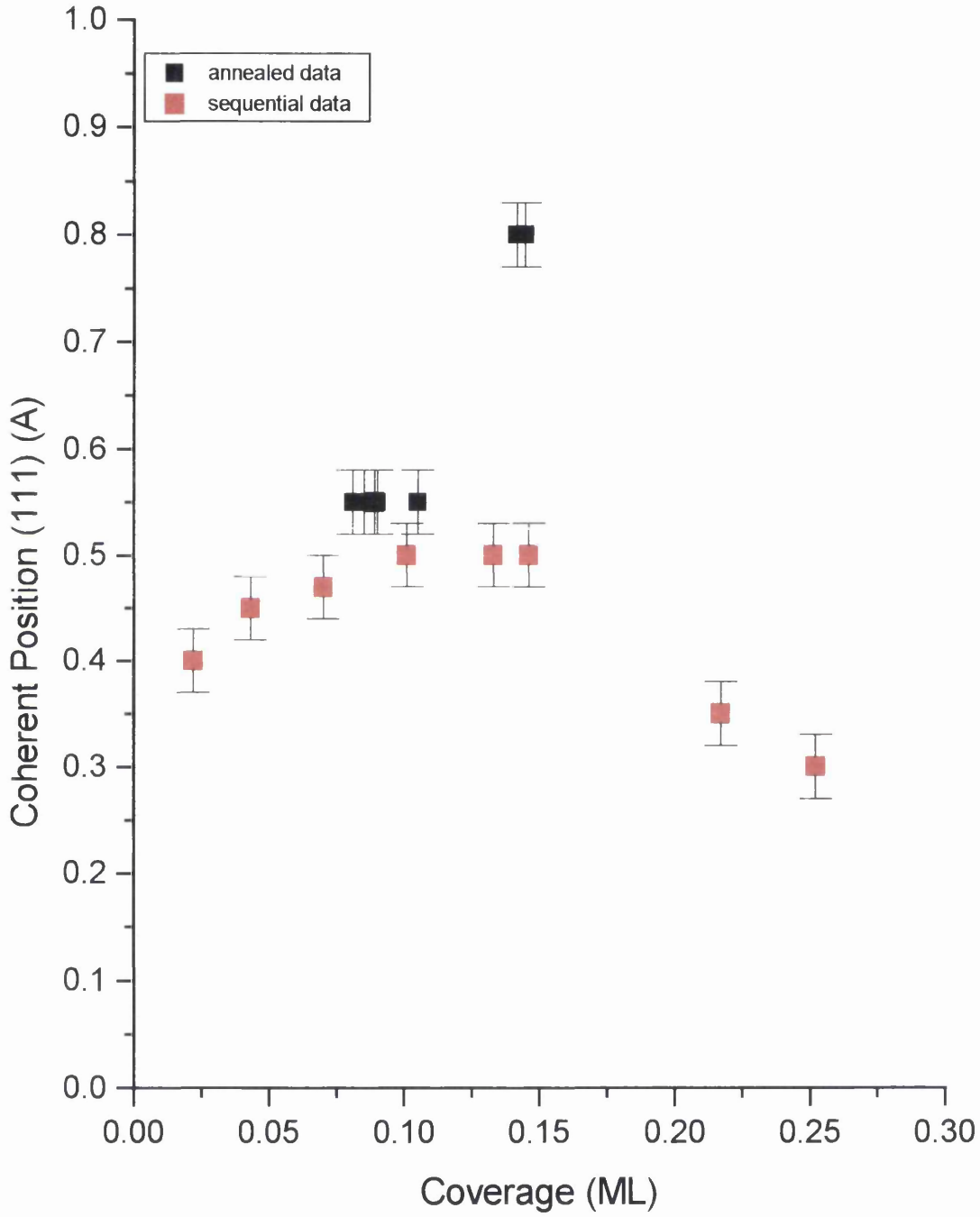

Figure 25: *Plot showing how coherent fraction varies with coverage with respect to the ($\bar{1}11$) plane.*

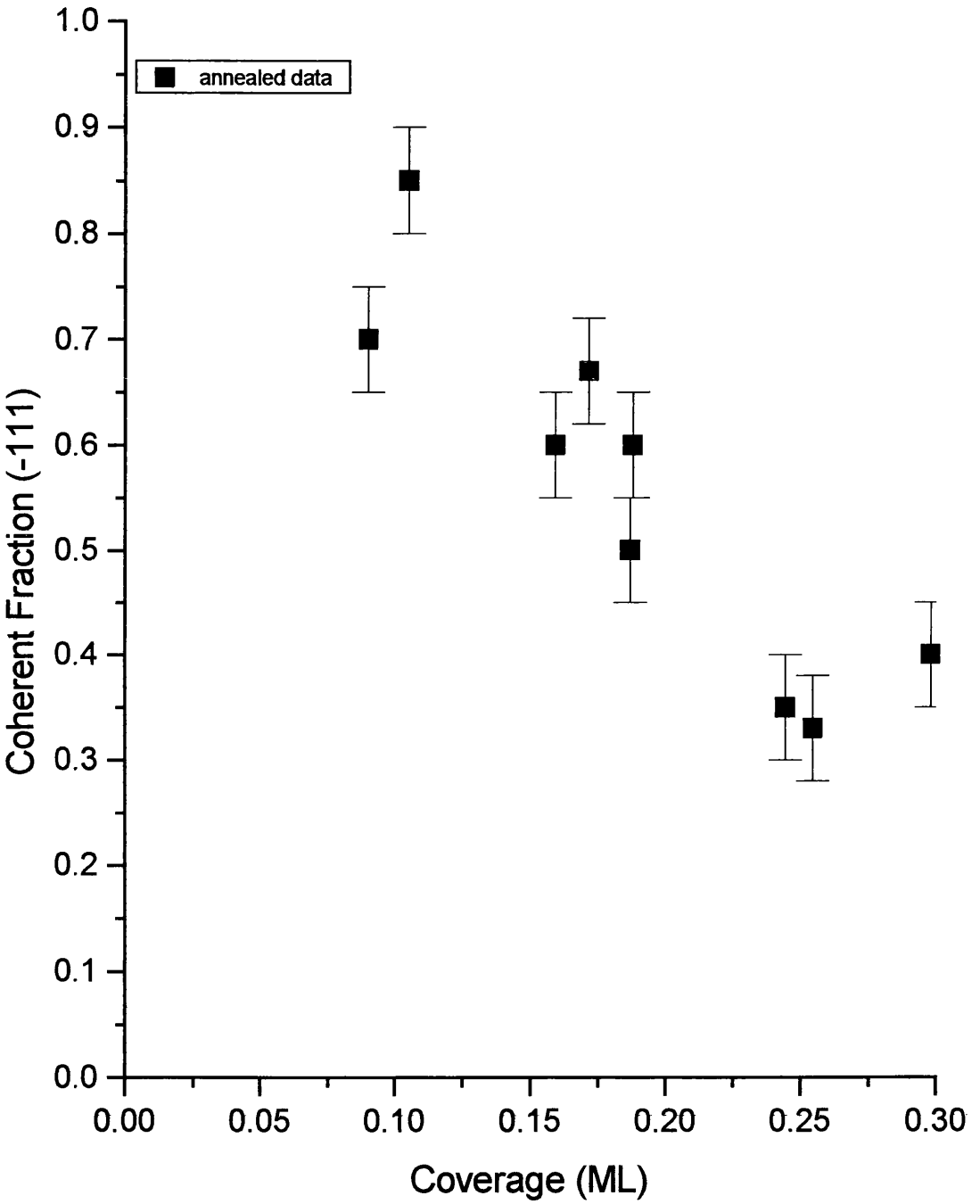

Figure 26: *Plot showing how coherent position varies with coverage with respect to the ($\bar{1}11$) plane.*

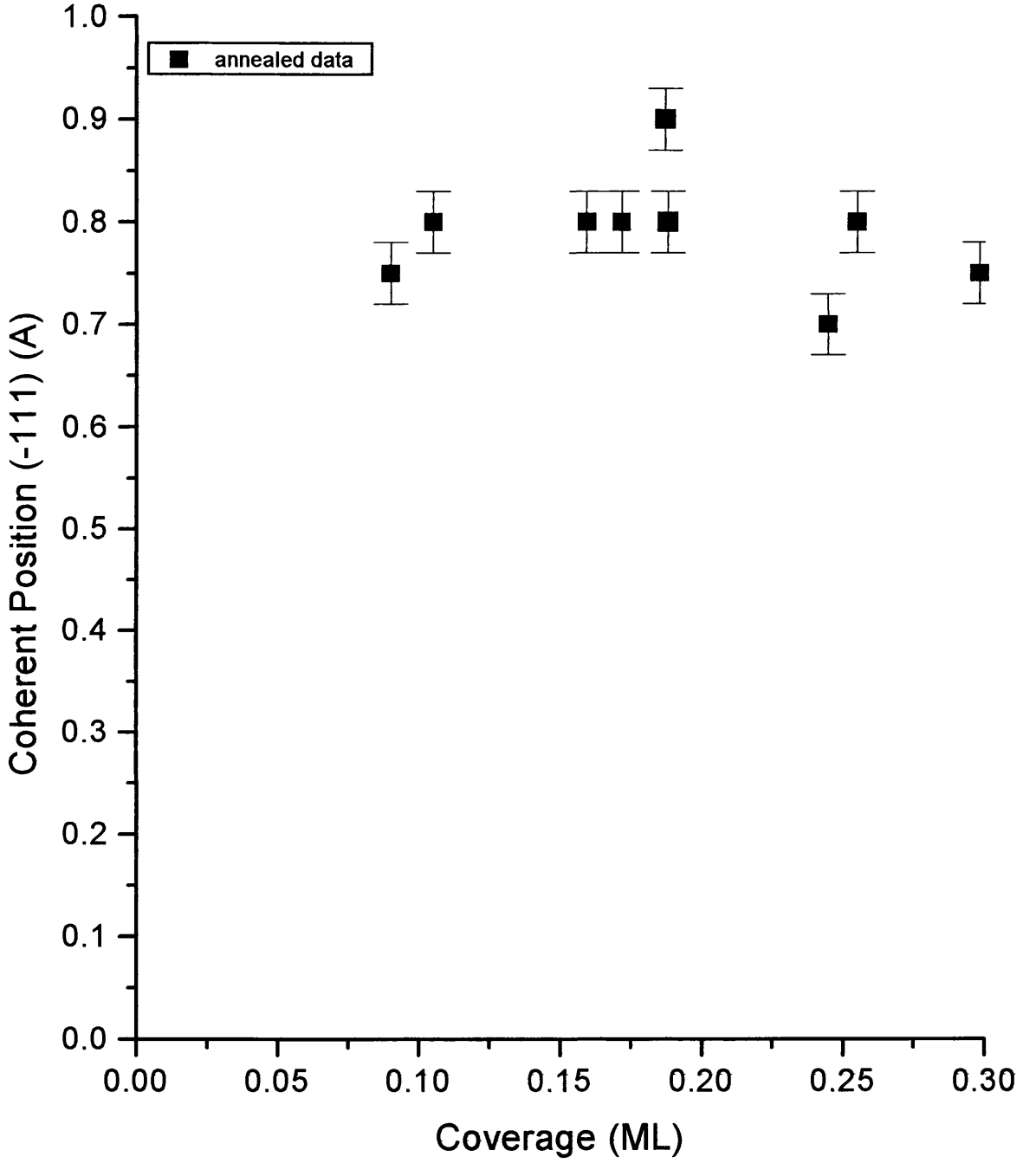

It was not possible to perform sequentially dosed experiments with respect to the ($\bar{1}11$) plane. Therefore figures 25 and 26 show how the coherent fraction and coherent position in the ($\bar{1}11$) plane respectively, vary with increasing coverage for annealed surfaces only. Figure 25 shows that the coherent fraction falls with increasing coverage. At coverages up to 0.10 ML, the coherent fraction is 0.85±0.05 and at 0.16 ML the coherent fraction is 0.60±0.05. Figure 26 shows that the coherent position doesn't change significantly over the coverage range shown. At coverages up to 0.10 ML, the coherent position is 0.80±0.05 Å and at 0.16 ML the coherent position is 0.80±0.05 Å. Coverages up to 0.10 ML and between 0.12-0.16 ML are of the most interest because these are the coverages that correspond to the desorption states described in TPD results. A coverage of 0.10±0.02 ML represents a thiophene coverage that would give rise to a saturated α-state desorption feature and a coverage of 0.14±0.02 ML represents a thiophene coverage that would give rise to a β-state desorption feature. Therefore, because the NIXSW data is coverage dependent, it can now be interpreted in terms of desorption features noted in TPD results. Table 9 shows a summary of all of the NIXSW data collected using both the sequential and annealing dosing techniques.

Table 9: *NIXSW data tabulated in terms of α- and β desorption states.*

α-state (annealed)	
Coherent fraction (111)	0.89±0.05
Coherent position (111) (Å)	0.54±0.03
Coherent fraction ($\bar{1}$11)	0.78±0.05
Coherent position ($\bar{1}$11) (Å)	0.78±0.03
β-state (annealed)	
Coherent fraction (111)	0.60±0.07
Coherent position (111) (Å)	0.80±0.05
Coherent fraction ($\bar{1}$11)	0.64±0.07
Coherent position ($\bar{1}$11) (Å)	0.80±0.05
α-state (sequential)	
Coherent fraction (111)	0.90±0.05
Coherent position (111) (Å)	0.50±0.03
β-state (sequential)	
Coherent fraction (111)	0.53±0.07
Coherent position (111) (Å)	0.50±0.05

The errors shown in this table are calculated from the errors involved in fitting the data. Small changes in the fitting procedure in fitting the shape of the standing wave profile to a coherent position, result in differences in coherent fractions represented by the errors shown in the table. Also, because of the signal to noise exhibited in figures 19 and 20 there has to be a degree of uncertainty as to the coherent position and coherent fraction of each fit. The errors increase with increasing coverage because the coherent fraction drops with increasing coverage.

4.3 Discussion

In the current work, TPD was only used to characterise the different adsorption states and to determine their relative coverages. No structural information was inferred from the TPD data. Similarly to the previous work in this field, other techniques, in this case NIXSW and NEXAFS, were used to gain information on the structure of the α- and β-states. This was done principally by sequential dosing NIXSW and NEXAFS experiments in which a whole range of coverages, from sub-monolayer to multilayer was studied. Annealed experiments were performed in order to study just the α- and β- states. It is possible that the differing preparatory techniques could provide different structures for the α- and β- states and this could in turn, be probed by NIXSW and NEXAFS. Previous work on related systems, such as thiophene on Ag(111)[9], benzene on Cu(111)[10], pyrrole and furan on Cu(100)[11] and furan on Ag(111)[12] all show TPD results that exhibit desorption features similar to that found in figure 2. That is, desorption features from an α-like and β-like state as well as from multilayers and defect sites.

4.3.1 Structure of thiophene on Cu(111) at α-state coverage

The principal feature of interest in the TPD data concerning the α-state is the broadening and moving to lower desorption temperatures of its desorption feature, figure 2 (a). Previous work in this field has proposed two reasons for this. Bent *et al.* who studied the adsorption of benzene on Cu(111)[10] proposed that the broadening to lower temperatures of the monolayer peak was due to the molecules tilting slightly as the coverage increased. The molecules would be in a flat orientation at very low coverages, and as the coverage increased up to the saturation of the α-state, the tilt angle that the molecules make with the surface would increase so as to produce a corrugated, or scaled[13] surface of adsorbed molecules. In this model, the angle of orientation of the molecules in the monolayer is constantly changing, because there is a constant addition of benzene molecules, until saturation monolayer coverage. Broadening to lower desorption

temperatures of an α-like feature is also observed in a TPD study[14] of benzene on Cu(110) by Lambert *et al.* who assign, by HREELS[15], the structure of benzene to be slightly tilted at all coverages.

Weiss *et al.*[16] also studied the adsorption of benzene on Cu(111) and STM results from this study suggest that there is no appreciable change in orientational angle and that the broadening to lower temperatures of the α-state peak from TPD measurements is caused by the adsorbed molecules forming islands. In this model the islands that the molecules form all have different sizes, and hence the molecules contained within the islands all have slightly different binding energies due to the different numbers of molecules surrounding them. Lots of different sized islands would therefore desorb at different temperatures forming a broad α-state desorption feature as seen in figure 2(a).

In order to ascertain which of these models fits the current work, or indeed if the NIXSW and NEXAFS data can provide an alternative model, it is necessary to analyse the sequentially dosed NIXSW and NEXAFS data up to α-state coverage. This could then show how increasing the coverage in small increments up to saturated α-state coverage affects, if at all, both the angle of orientation and the adsorption site and provide an explanation for the observed shift and broadening of the α-state feature in the TPD data.

Table 2 shows that at coverages of 0.03, 0.05 to 0.10 ML the corresponding orientational angles are 12±2 °, 20±3 ° and 25±4 °. At first sight it would appear that the orientational angle is changing within the monolayer, thus agreeing with the work of Bent *et al.*[10] However, STM work by Weiss *et al.* concerning benzene on Cu(111)[16] and Hamers *et al.* concerning thiophene on Ag(111)[17] suggests that at very low coverages, such as 0.03 ML, the majority of adsorbed molecules that are adsorbed to defect sites are in very flat orientations. A coverage of 0.03 ML represents an exposure of approximately $3.6\pm0.2\times10^{-6}$ mbar.s in figure 2 (a) (dark blue data). Figure 2 (a) shows that at this coverage a significant percentage of the adsorbed molecules are bonded to defect sites. The orientational angle calculated at this coverage is 12±2 ° and, if at this coverage, as the TPD data suggests, there exists molecules bonded to α-state sites and defect sites,

then the calculated angle of 12±2 ° is the average orientational angle of the α-state and defect sites. The angle at α-state coverage is 25±4 ° and previous STM work suggests that the molecules that are very strongly bonded to defect sites have angles close to 0 °. It is clear that a dosed surface containing a significant proportion of molecules bonded to defect sites would have an average angle close to 12±2 °.

Within experimental error, the difference in orientational angle over the coverage range 0.05-0.10 ML could be as much as 12 °. It is therefore possible that the orientation of the thiophene molecules that are not bonded to defect sites, over the whole coverage range 0.03-0.10 ML, is changing but is changing in increments that are too small to be detected by the NEXAFS technique. Similarly, it is possible that the observed shift and broadening to lower desorption temperatures of the α-state feature as shown in figure 2 (a) is due to islanding, but neither the NEXAFS or NIXSW techniques are suitable probes for investigating the presence of islanding.

The NEXAFS data does not provide any conclusive proof for either of the two models proposed to explain the broadening and shifting to lower desorption temperatures of the α-state desorption feature in figure 2(a).

4.3.2 Adsorption Site Determination by Real Space Triangulation

NIXSW experiments were performed with respect to two surface planes, (111) and ($\bar{1}11$) in order to determine the adsorption site of thiophene at saturated α-state coverage. This was achieved by analysis of NIXSW data collected from surfaces prepared by the annealed dosing method. Subsequent NIXSW experiments were performed by using the sequential dosing method but only with respect to the (111) plane. The annealed dosing data was analysed using a triangulation procedure in order to determine which of the four sites, atop,.bridging, f.c.c.or h.c.p., is occupied[18] as outlined in more detail in Chapter 2.

This procedure involves deriving D($\bar{1}11$) from D(111) using the following equations:

$$\text{Atop: } D(\bar{1}11) = D(111)/3$$

$$\text{Bridge: } D(\bar{1}11) = D(111)/3 + d(111)/2$$

$$\text{F.C.C.: } D(\bar{1}11) = (D(111) + 2d(111))/3$$

$$\text{H.C.P.: } D(\bar{1}11) = (D(111) + d(111))/3$$

4.3.3 Adsorption site of Thiophene at α-state coverage as prepared by the annealed dosing method

The high coherent fraction in the (111) plane for thiophene adsorbed onto Cu(111), table 9, means that there is only one distinct adsorption site that the thiophene molecule occupies. The D($\bar{1}11$) values in table 10 are derived using a D(111) value from table 9 (0.54 Å) plus a lattice spacing (2.08 Å). The reason for this is that the scattering plane that this coherent position is measured from does not go through the surface and in fact, the coherent position in this case is measured from a hypothetical lattice plane, a lattice spacing – 2.08 Å – from the surface. Hypothetical lattice planes are formed by the standing wave propagating outwards from the bulk crystal, as the periodicity of a standing wave is equal to a lattice spacing - d_H. In the analysis, the value that is obtained is the distance from the nearest lattice plane to the adsorbate, which in this case, is not the surface lattice plane.

Table 10: *D($\bar{1}11$) values derived from experimental D(111) (2.62 Å)values at α-state coverage, as prepared by the annealed dosing method.*

Site	D($\bar{1}11$) (Å)	f_{co}
Atop	0.87	0.89
Bridging	1.91	0.30
f.c.c.	2.44	0.89
h.c.p.	1.57	0.89
experimental	***0.78***	***0.78***

So in this case, a lattice spacing - 2.08 Å – must be added to this value, to give a value of 2.62±0.03 Å. Previous work on thiophene on Cu(111) as studied by Ohta *et al.*[4] using the technique of SEXAFS gives a Cu-S separation distance of 2.50±0.02 Å. From table 9, the experimental D($\bar{1}11$) value is 0.78 Å, and with reference to the derived values in table 10, the nearest fit is to the atop position (0.87 Å). The coherent fraction with respect to the ($\bar{1}11$) plane, 0.78±0.05, is slightly lower than the coherent fraction with respect to the (111) plane, 0.89±0.05. This is probably due to the molecules having a small amplitude of vibration parallel to the (111) plane, thereby having a larger amplitude of vibration perpendicular to the ($\bar{1}11$) plane, reducing the coherent fraction with respect to the ($\bar{1}11$) plane. Also, the molecules could be slightly displaced from the idealised atop position, thereby also reducing the magnitude of the coherent fraction with respect to the ($\bar{1}11$) plane. In reality, both these static and vibrational disorders are probably occuring and hence the adsorption site of thiophene in the α-state, as prepared by the annealed method, can be described as being "displaced atop".

An Argand diagram, figure 27, can be constructed where each of the derived ($\bar{1}11$) coherent position values, for atop, bridge, h.c.p. and f.c.c., are represented by vectors. The length of each vector is given by the coherent fraction in the (111) plane. This is because the ($\bar{1}11$) coherent positions listed in table 10 are derived from (111) data and hence the length of each vector in the Argand diagram is described by the (111) data. The angle that each vector makes is given by 2π D($\bar{1}11$)/d_H (See Woodruff *et*

al.[18]). Figure 27 shows a vector representation of each of the derived values shown in table 10 for atop, bridge, f.c.c. and h.c.p. adsorption sites. It is clear that the nearest fit to the experimental vector is the atop vector and hence the adsorption site can be described as being "displaced atop". Hence in this case, matching the atop D($\bar{1}11$) value in table 10 with the experimental value and matching the atop vector in figure 27 to the experimental vector are analogous procedures because they are both determined by the magnitude of D($\bar{1}11$). In this case, the Argand diagram approach has not yielded any information not afforded by simply matching up the derived ($\bar{1}11$) data with the experimental ($\bar{1}11$) data.

4.3.4 Adsorption site of Thiophene at α-state coverage as prepared by the sequential dosing method

As previously noted, it was not possible to perform sequentially dosed NIXSW experiments with respect to the ($\bar{1}11$) plane. However, for the (111) plane, the saturated α-state coverage sequentially dosed data is identical within experimental error to the (111) annealed data with respect to the coherent fraction and coherent position (table 9). It can then safely be assumed that the adsorption site occupation in a saturated α-state prepared by the sequential dosing method is identical to that of a surface prepared by the annealing method, as previously discussed. This means that the adsorption site occupied by thiophene on Cu(111) prepared by sequential dosing in a saturated α-state is "displaced atop".

Figure 24 shows how the coherent position varies with increasing sequentially dosed coverage with respect to the (111) plane. Over the coverage range 0.02, 0.04, 0.07, 0.10 ML, the coherent position appears to be rising from 0.40±0.03 Å to 0.50±0.03 Å. As noted before in the discussion about the angle of orientation of thiophene at very low coverages, at a coverage of 0.02 ML, a significant proportion of the molecules are adsorbed to defect sites. Molecules bonded to defect sites are much more strongly bound than to non-defect sites, such as atop, bridging, f.c.c. or h.c.p. and the Cu surface-S bond distances would be expected to be much shorter in the case of defect site

Figure 27: *Argand Diagram showing experimental ($\bar{1}11$) value and the four derived values (green), table 10, for annealed α-state data. The length of the experimental vector (blue) is the coherent fraction (0.78) and the angle is given by $2\pi D(\bar{1}11)/d_H$. The nearest fit to the experimental data is the atop vector (not drawn to scale).*

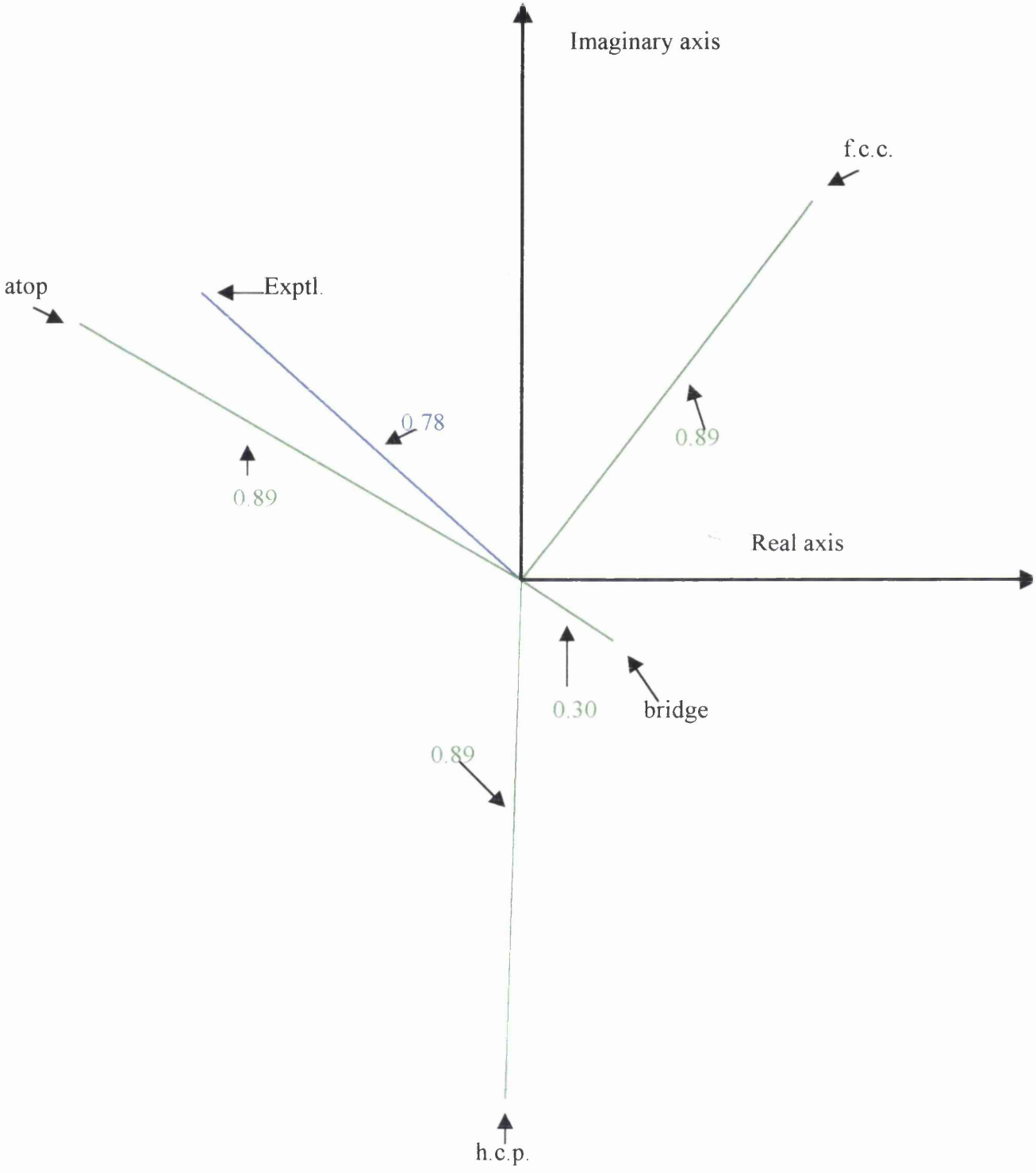

adsorption as a result of this. Therefore, the shorter coherent position of 0.40 Å at 0.02 ML is due to a significant number of the molecules bonding to defect sites at this coverage. The other coverages, 0.04, 0.07, 0.10 ML all exhibit coherent positions that are identical within experimental error. This also shows that there is no change in adsorption site occupation up to saturated α-state coverage and hence the broadening to lower desorption temperatures of the α-state in the TPD data is not due to the adsorption site changing up to the saturated α-state coverage.

4.3.5 Structure of thiophene on Cu(111) at β-state coverage

The presence of the β-state in the TPD data poses some interesting questions. The most obvious of these is the identity of the β-state and its subsequent structure. The techniques of NEXAFS and NIXSW are ideal techniques to answer these questions as they can provide a complete picture of the orientation of the molecule at β-state coverage and the adsorption site occupation. Postulations can then be made about why the β-state forms at all.

There are two reported explanations for the presence of a β-like desorption feature published in previous work. Umbach *et al.* who studied thiophene adsorption on Ag(111)[9], assign the β-like state in their TPD data, using XPS, to desorption of thiophene that has undergone a phase transition, figure 28. This model involves the re-orientation of adsorbed thiophene molecules from a roughly flat π-bonded geometry to a more inclined geometry with increasing coverage. This is possible with a molecule like thiophene because it can bond to the surface via the π-ring and/or via the S lone pair. The β-state would exhibit a larger S lone pair bonding contribution than the α-state in the phase transition model because the π-ring of the molecule is sufficiently tilted from the surface.

Bent *et al.* who studied benzene adsorption on Cu(111)[10] assign the β-like state in their TPD data to desorption of benzene from a bilayer using NEXAFS. In this context, the β-state represents a separate stable benzene layer above the monolayer. The

bilayer model is also proposed by Sexton[11] who studied pyrrole and furan on Cu(100) using TPD and HREELS.

Figure 28: *Possible structures giving rise to a β-like desorption state.*

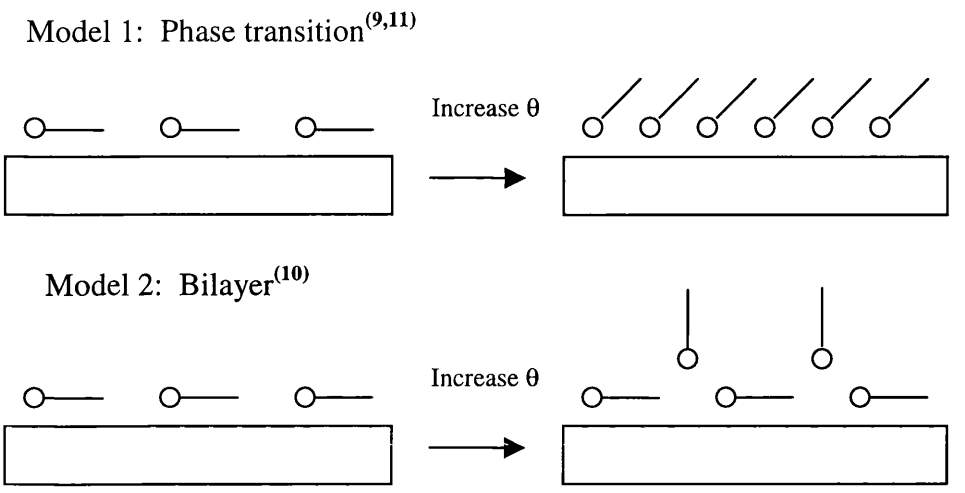

These two differing models both explain the presence of a β-like state in TPD data very well. In the phase transition model, the β-state desorption feature contains both a feature attributable to desorption from the α-state and one from the β-state, figure 5. If, in the current work, the β-state represents a phase transition, the β-state coverage spectrum in figure 5 which consists of two features, one at 173 K and one at 234 K, represent two different structural states at different coverages. At saturated β-state coverage, all of the molecules, represented by the entire two-component β-state feature in figure 5 are at an inclined geometry. During the TPD heating ramp, when sufficient molecules from the β-peak have desorbed at 173 K to leave an α-state coverage, the remaining adsorbed molecules at α-state coverage, are oriented in a roughly flat geometry. Thus there is a coverage dependent phase transition. The β-state has a lower desorption temperature because the inclined molecules are bonded via the thiophene S lone pair and hence are less strongly bound than the roughly flat molecules that are π-bonded in the α-state.

The two features in the β-state desorption spectrum in figure 5 can also be explained in terms of bilayer formation. In this model, the α-state is fully occupied by

thiophene molecules and the β-state represents a separated second layer above the first layer. The second layer is much more weakly bound than the first layer because it is further away from the surface, and hence has a lower desorption temperature and appears as a separate peak in the TPD data. Further evidence for bilayer formation, figure 28, in the benzene on Cu(111) study[10] and furan on Cu(100)[11] study comes from X-ray crystal structures of benzene and furan in which the molecules are arranged in the unit cell in T-shaped arrays.

NEXAFS data, particularly figure 14 and table 2 show that there is a change in orientational angle from 25±4 ° to 41±6 ° as the coverage changes from 0.10 ML to 0.12 ML. This is a substantial change in angle over a very small coverage range. If the β-state shown in the TPD spectra in figure 2 (b) was indicative of a bilayer, then it would be expected that the second layer (bilayer) would be occupied in a step-wise fashion. This would result in a gradual change in orientational angle as the second, more upright layer, is added. A second layer having a flat orientation is ruled out on the basis of the average angle of orientation of the molecules at this coverage (41±6 °). The bilayer model is not consistent with the sudden change in angle noted from NEXAFS results from a 0.02 ML coverage rise. This points to the phase transition model. The β-state in this work is indicative of a phase transition because there is a very large change in orientational angle over a very small coverage range. It can be envisaged that, at absolute saturation of the roughly flat α-state, more thiophene deposited on this surface simply leads to the adsorbed molecules "flipping" to a more inclined angle (41±6 °). The driving force for this could be that with a more inclined geometry, it is possible to pack more adsorbates onto the surface. Also, adsorbate-adsorbate interactions in the form of π-stacking may help to stabilise the adsorbed layer in this orientation.

Table 3 shows that the change in orientational angle from α- to β-state when the annealed dosing method is used is 33±5 ° to 45±6 °. Within experimental error this is identical behaviour to that of the sequentially dosed study. Hence, the two differing methods, annealed and sequentially dosed, do not prepare different surfaces in terms of the orientational angle of the molecules. The phase transition is therefore purely

coverage driven and at β-state coverage, the molecules are at an inclined geometry irrespective of which method was used to prepare the surface.

4.3.6 Adsorption site of thiophene at β-state coverage as prepared by the annealed dosing method.

Using an analogous procedure to the one described previously for the α-state data, the adsorption site for the β-state can be derived and the possible values are shown in table 11. Similarly to the α-state data, a lattice spacing, 2.08 Å, has to be added to the experimentally obtained (111) coherent position (0.80 Å).

Table 11: *D($\bar{1}11$) values derived from experimental D(111) (2.88 Å) values at β-state coverage using the annealed dosing method.*

Site	D($\bar{1}11$) (Å)	f_{co}
Atop	0.96	0.60
Bridging	2.00	0.20
f.c.c.	2.35	0.60
h.c.p.	1.65	0.60
experimental	***0.80***	***0.64***

As can be seen from both table 11 and an Argand diagram representation of this data, figure 29, the adsorption site for the β-state can also be described as being "displaced atop".

The annealed NIXSW data shows that the coherent position rises from 0.54±0.03 to 0.75±0.05 Å as the coverage rises from α-state to β-state. This is not indicative of any change in adsorption site however, as the S atom in the thiophene molecule is bonded to a slightly displaced atop site at both coverages. This represents a significant increase in Cu-S bond length of 0.21±0.08 Å. The lower coherent fractions from annealed experiments with respect to both planes at β-state coverage (0.60±0.07 with respect to the

Figure 29: *Argand Diagram showing experimental ($\bar{1}11$) value and the four derived values (green), table 10, for annealed β-state data. The length of the experimental vector (blue) is the coherent fraction (0.64) and the angle is given by $2\pi D(\bar{1}11)/d_H$. The nearest fit to the experimental data is the atop vector (not drawn to scale).*

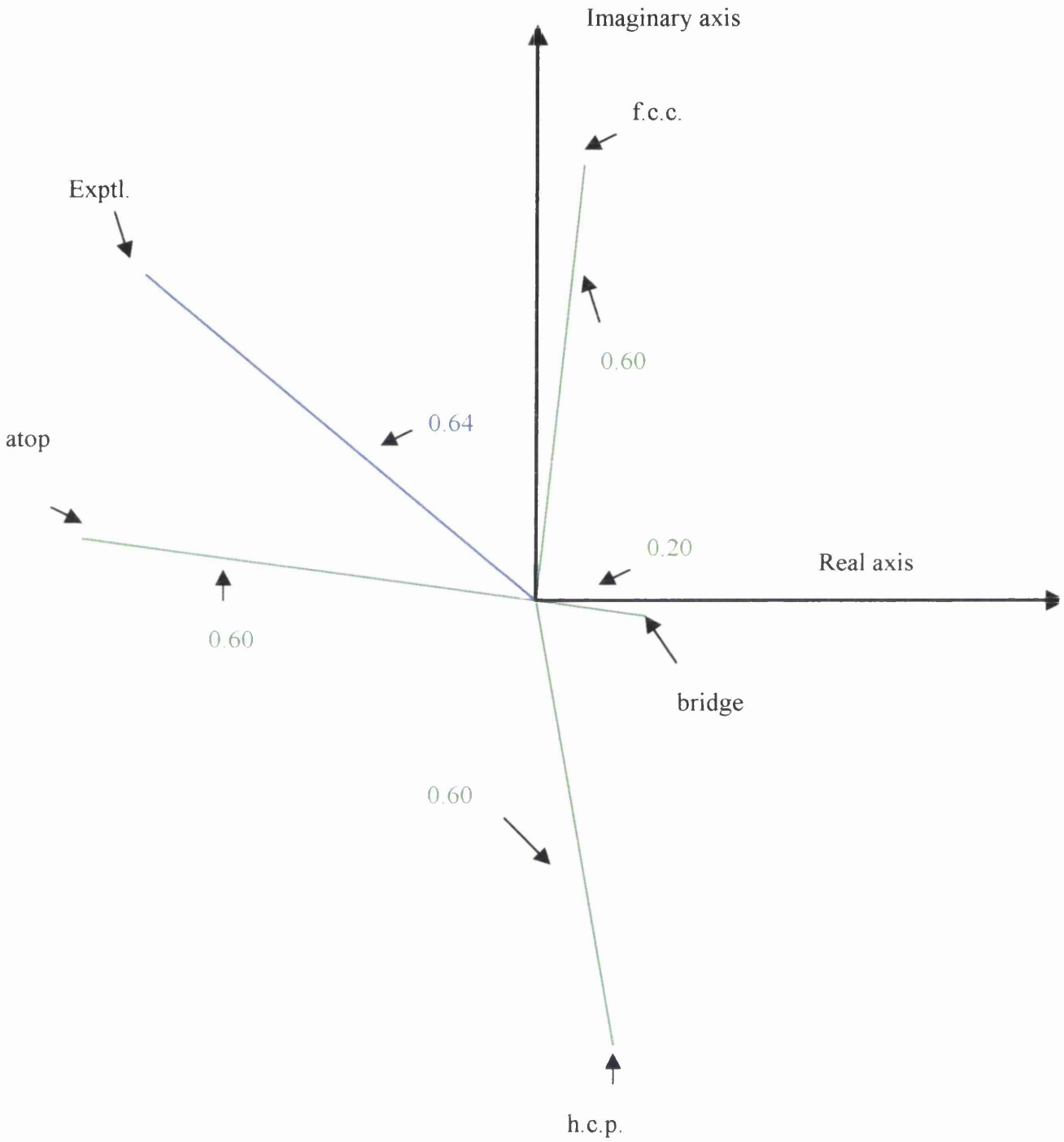

(111) plane at β-state coverage compared to 0.89±0.05 at α-state coverage) and α-state coverage (0.64±0.07 with respect to the ($\bar{1}$11) plane at β-state coverage compared to 0.78±0.05 at α-state coverage) are as a result of the bond lengthening at β-state coverage. As the molecules in the β-state are farther away from the surface, they interact less strongly with the surface and are less strongly bound than at α-state coverage. Again, both static and vibrational disorder, as discussed at α-state coverage, play a big part in lowering the coherent fraction with respect to both planes and hence, increasing the uncertainty in the adsorption position.

4.3.7 Adsorption site of thiophene at β-state coverage as prepared by the sequential dosing method.

At β-state coverage, the two dosing methods, annealed and sequential, give significantly different values for the coherent position and coherent fraction. At β-state coverage, the coherent position with respect to the (111) plane from the sequential dosing experiments is 0.50±0.05 Å and for the annealed experiments is 0.80±0.05 Å. The coherent fraction with respect to the (111) plane from the sequential dosing experiments is 0.53±0.05 and for the annealed experiments is 0.60±0.07. The differences in coherent position are outwith experimental error and the differences in coherent fraction are at the very limits of the experimental error. Therefore it cannot be assumed, in the absence of ($\bar{1}$11) data, that the adsorption site occupation of the β-state is the same for sequentially dosed experiments as it is for annealed experiments.

The annealed data standing wave profiles can be fitted to higher coherent fractions than the corresponding coverage sequential data, at β-state coverage. Therefore the adsorbed thiophene molecules have well-defined adsorption sites when the adsorbed surfaces are prepared by this method (annealed). An explanation for this could be that the annealing of the surface orders the adsorbed layer, and the adsorbed molecules are given enough energy to move to the most energetically favourable sites, particularly at the higher coverage β-state. There is no difference between the sequentially dosed data and the annealed data for the α-state because there are fewer molecules on the surface

and this means that there is enough bare atop substrate sites for the molecules to bond to. This is not the case at the β-state coverage. A model can be envisaged where a thiophene coverage corresponding to a β-state is prepared by sequential dosing. From TPD measurements, this is a significantly higher coverage than the α-state. Without annealing, this adsorbed layer is essentially adsorbed on a weakly corrugated surface and all of the adsorption sites could be occupied.

A sequentially dosed layer of thiophene of β-state coverage can be envisaged to occupy all possible adsorption sites, atop, bridging and 3-fold. For the purposes of this part of the discussion, it will be assumed that the two 3-fold sites are energetically equivalent. In the annealing process, the adsorbed layer orders so that only the atop (displaced) site is occupied. In the sequentially dosed case, if the Cu-S bond length in each of the atop, bridge and 3-fold sites is the annealed coherent position, 2.88 Å, it is possible to show that the coherent position value of 2.58 Å obtained from sequentially dosing experiments is the average of all 3 sites being occupied with a Cu-S bond length of 2.88 Å (from annealed experiments) (figure 28). Using trigonometry, it can be shown that with a Cu-S bond length of 2.88 Å and a Cu-Cu bond length of 2.55 Å, the coherent positions above the surface are as shown in figure 30. The experimental coherent position at β-state coverage is 2.58±0.05 Å (0.50 + 2.08 Å). The nearest to this in figure 30 is the bridging site (2.58 Å), but also a combination of atop and 3-fold sites, 2.88 Å and 2.48 Å would also give an average bond length of 2.50±0.05 Å. It is entirely possible, that all sites are occupied to some extent at β-state coverage when the sequentially dosed method is used at 120 K, and on annealing, the adsorbed layer orders and moves to a displaced atop site.

Figure 30: *Diagram showing possible Cu-S coherent positions for each of the adsorption sites using a Cu-S bond lengths of 2.88 Å (table 12). Yellow balls indicate S and blue balls indicate Cu.*

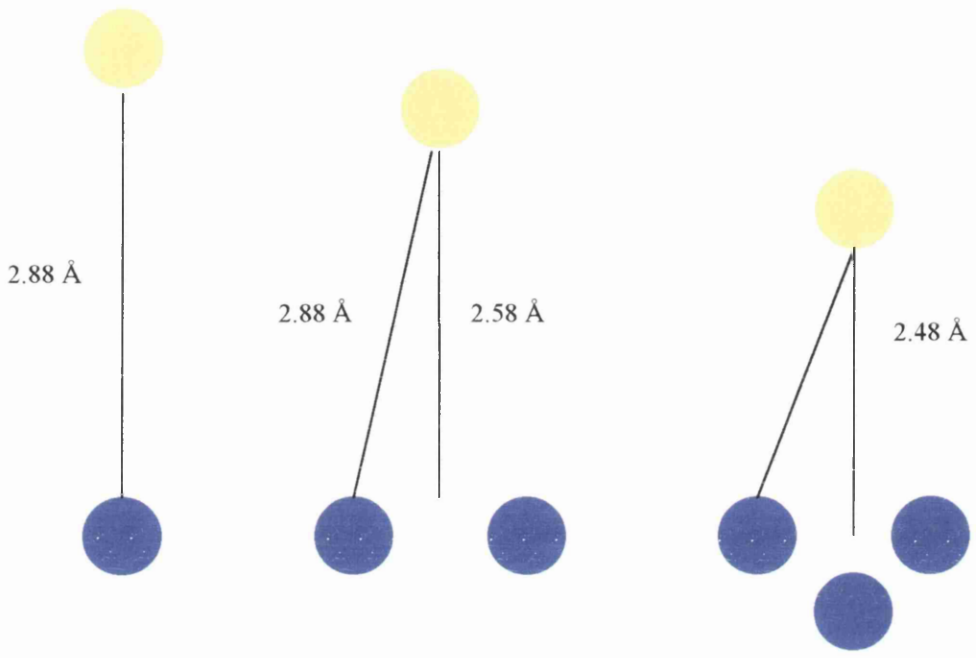

4.4 Conclusion

The NIXSW data shows that there is a difference in coherent fraction and coherent position in the (111) plane in the annealed data in comparing the α-state coverage and β-state coverage. However, this does not lead to any corresponding change in adsorption site (displaced atop) but it does lead to a bond elongation of 0.21±0.08 Å. The change from α-state coverage to β-state coverage in the sequentially dosed data leads to a very small change in adsorption site from displaced atop to either bridge or a combination of atop and 3-fold or even a combination of all three sites.

Figure 14 shows that there is a significant change in orientational angle of the adsorbed thiophene molecules over the coverage range 0.10-0.14 ML, that is, from α-state to β-state using the sequentially dosed method. The angles change over this small coverage range from 25±4 ° to 45±6 °. Table 3 shows that the annealed dosing method prepares surfaces with identical angles of orientation at α- and β-state coverages, in which the angles change from 33±5 ° to 45±6 °. The phase transition that exists from the α-state to the β-state is purely a function of coverage, as noted in similar work on pyridine on Ag(111)[19, 20] and the driving force for the phase transition is due to the fact that more thiophene molecules can pack onto the surface in an upright geometry than in a flat geometry. The sequential and annealed dosing methods therefore produce surfaces with identical angles of orientation but with slightly different adsorption sites, at β-state coverage only.

4.5. References

1. N.K. Singh, R.G. Jones and D.P. Woodruff, *Surface Science Letters,* 1990, **232**, L228-L231.
2. J.L. Domange and J. Oudar, *Surface Science,* 1968, **11**, 124-142.
3. A.P. Hitchcock, J.A. Horsley and J Stöhr, *Journal of Chemical Physics,* 1986, **85** (9), 4835-4848.
4. A. Imanishi, S. Yagi, T Yokoyama, Y. Kitajima and T. Ohta, *Journal of Electron Spectroscopy and Related Phenomena*, 1996, **80**, 151-154.
5. J. Stöhr, *NEXAFS Spectroscopy,* 1996, pp. 234-237.
6. A.A. M^{c}Dowell, D. Norman, J.B. West, J.C. Campuzano and R.G. Jones, *Nuclear Instrumental Methods A,* 1986, **246**, 131.
7. D.P. Woodruff, *Progress in Surface Science*, 1998, **57** (1), 1-60.
8. C.J. Fisher, R. Ithin, R.G. Jones, G.J. Jackson, D.P. Woodruff and B.C.C. Cowie, *Journal of Physics: Condensed Matter,* 1998, **10**, L629.
9. K.M. Baumgårtner, M. Volmer-Uebing, J. Taborski, P. Båuerle and E. Umbach, *Berichte der Bunsengellschaft fur Physikalische Chemie*, 1991, **95**, 1488-1495.
10. M. Xi, M.X. Yang, S.K. Jo and B.E. Bent, *Journal of Chemical Physics*, 1994, **101**, 9122-9131.
11. B.A. Sexton, *Surface Science*, 1985, **163**, 99-113.
12. J.L. Solomon, R.J. Madix and J. Stöhr, Journal of Chemical Physics, 1991, **94** (5), 4012-4023.
13. E. Umbach, *Progress in Surface Science*, 1990, **35**, 113-127.
14. J.R. Lomas, C.J. Baddeley, M.S. Tikhov and R.M. Lambert, *Langmuir*, 1995, **11**, 3048-3053.
15. J.R. Lomas, C.J. Baddeley, M.S. Tikhov and R.M. Lambert, *Chemical Physics Letters*, 1996, **263**, 591-596.
16. S.J. Stranick, M.M. Kamna and P.S. Weiss, *Surface Science*, 1995, **338**, 41-59.
17. X. Chen, E.R. Frank and R.J. Hamers, *Journal of Vacuum Science and Technology B*, 1996, **14** (2), 1136-1140.

18. D.P. Woodruff, B.C.C. Cowie and A.R.H.F. Ettema, *Journal of Physics: Condensed Matter,* 1994, **6**, 10633-10645.

19. M. Bader, J. Haase, K.-H. Frank, A. Puschmann and A. Otto, *Physical Review Letters*, 1986, **56** (18), 1921-1924.

20. J.E. Demuth, K. Christmann and P.N. Sanda, *Chemical Physics Letters,* 1980, **76** (2), 201-206.

Chapter 5. The adsorption of 3-chlorothiophene on Cu(111)

5.1. *Introduction*

The adsorption of 3-chlorothiophene was studied by TPD, AES, XPS, LEED, NIXSW and NEXAFS, in a similar way to the previous chapter (thiophene). NIXSW was used to determine the adsorption site of both the S and Cl in the molecule at monolayer coverage, however only the adsorption site with respect to the S atom in 3-chlorothiophene could be determined. It was found that both the Cu-S bond length, the adsorption site and the angle of orientation of 3-chlorothiophene at saturated monolayer coverage is identical within experimental error to that of thiophene at saturated α-state coverage. The height above the surface of the Cl with respect to the (111) surface plane for 3-chlorothiophene was shown to be 3.51±0.15 Å which corresponds to a physisorption distance. However, it was not possible to assign the adsorption site of the Cl-group. NEXAFS was used to determine the tilt angle of the molecule with respect to the surface as a function of coverage, and as in the case of thiophene, there is no change in orientation within the monolayer. The orientation was also calculated once the heights of S and Cl above the (111) plane were determined, and a model for the adsorption structure proposed.

5.2. *Results*

5.2.1. *Initial characterisation*

Figures 1 (a) and (b) show TPD spectra collected from surfaces with increasing 3-chlorothiophene coverage. The 3-chlorothiophene surfaces represented in figures 1 (a) and (b) were prepared by using the line-of-sight dosing method. The heating rate used in the TPD experiments represented by figures 1(a) and (b) was 0.5 Ks^{-1}.

Figure 1 (a) shows TPD spectra collected from low coverage 3-chlorothiophene surfaces. It shows three main features signifying desorption from three distinct desorption states. The main peak of interest shown in the $9.0\pm3x10^{-8}$ mbar.s observed exposure (black) data is at 235 K which at saturation coverage, $2.1\pm0.3x10^{-7}$ mbar.s observed exposure (green), has moved to 225 K. This peak will be referred to as an α-state and the $2.1\pm0.03x10^{-7}$ mbar.s observed exposure (green) spectra in figure 1 (a), represents desorption from a saturated α-state of 3-chlorothiophene. The shift of 10 K to lower desorption temperatures is a considerably smaller shift to lower desorption temperatures than in the corresponding α-state desorption feature in thiophene where the shift from low coverage to saturation coverage is from 234 K to 211 K. There is no significant broadening of the α-state peak shown in figure 1 (a) as the coverage is increased from the black data to the green data. Also shown in figure 1 (a) is evidence of desorption from defect sites at 287 K. This feature was assigned by comparing the spectra to a thiophene TPD spectra at similar coverage (Chapter 4, figure 3 (a), black data), that also exhibits desorption from defect sites. Desorption from defect sites is relatively small in the case of 3-chlorothiophene. The ratio of peak heights, saturated α-state:defect sites, in the case of thiophene is 3.6 and in the case of 3-chlorothiophene is 10.5 indicating that in the case of 3-chlorothiophene there is relatively much less desorption from defect sites. The reason for this will be outlined with respect to AES experiments (figure 3).

The $5.4\pm0.3x10^{-7}$ mbar.s observed exposure (blue) data in figure 1 (a) represents a coverage of slightly more than a saturated α-state as there is another peak appearing at 182 K. Figure 1 (b) shows TPD spectra from surfaces prepared with substantially more than α-state coverage. It is clear from Figure 1 (b) that the peak at 182 K that is starting to form in figure 1 (a) represents multilayer desorption. The peak at 182 K does not saturate with increasing coverage.

The TPD data in figures 1 (a) and (b) differ from the thiophene study in which TPD data showed the presence of two distinct sub-multilayer states, the α-state and the β-state. As there is no evidence of any β-like state in the present (3-chlorothiophene) study, the α-like state shown in figures 1(a) and (b) will simply be referred to as a monolayer state. Figure 2 shows the integrated areas for each of the TPD spectra in figure 1 (b) plotted as a function of dosing time. The linear dependence indicates a constant sticking co-efficient for 3-chlorothiophene.

Unlike thiophene, there is a small amount of dissociation of 3-chlorothiophene, shown by the presence of S, Cl and C on the surface after TPD experiments, figures 3 and 4. The relatively small amount of desorption from defect sites is due to this small amount of dissociation. It is likely that the majority of dissociation occurs at defect sites, hence a relatively lower amount of intact 3-chlorothiophene molecules desorb from defect sites compared to the thiophene study. Figure 5 shows AES spectra collected from a monolayer of 3-chlorothiophene (black) over the kinetic energy range covering S and Cl, and a spectrum over the same kinetic energy range after a TPD experiment where a monolayer was deposited and desorbed (red).

It is clear from figure 5 that there is both S and Cl on the surface after desorption of a monolayer of 3-chlorothiophene. The coverage of a monolayer of 3-chlorothiophene can be calibrated against a known coverage in a similar way to the method used to calibrate the coverages of the α- and β- states concerning thiophene, figure 6. The calculated coverage of a monolayer of 3-chlorothiophene with respect to this is 0.11 ± 0.03 ML.

Figure 1 (a): *TPD spectra of 3-chlorothiophene on Cu(111) prepared by the line-of-sight dosing method showing the presence of desorption from defect sites, monolayer state and multilayers.*

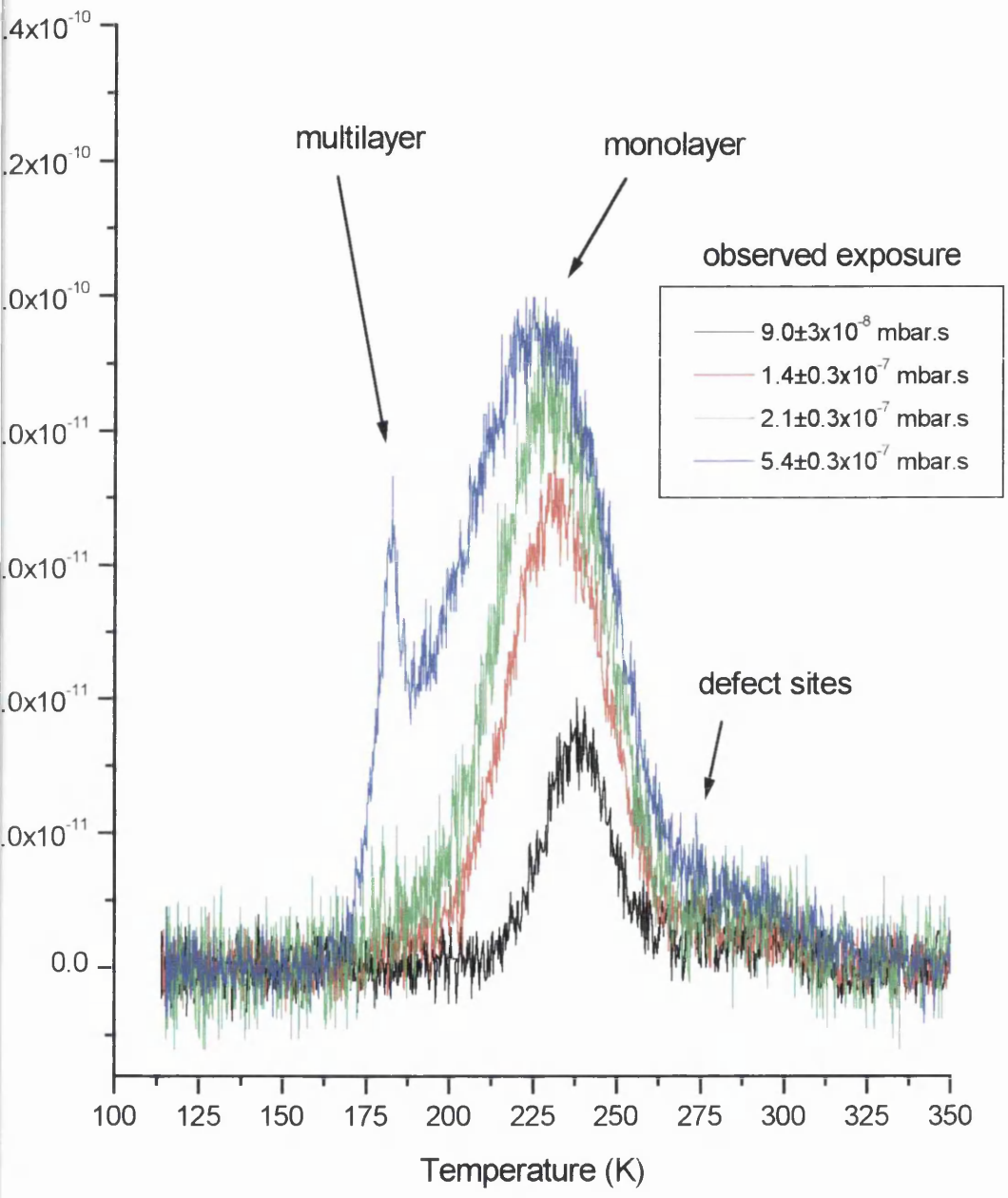

(b): *TPD spectra of 3-chlorothiophene prepared by the line-of-sight dosing method. This data shows that the peak at 182 K represents multilayer desorption.*

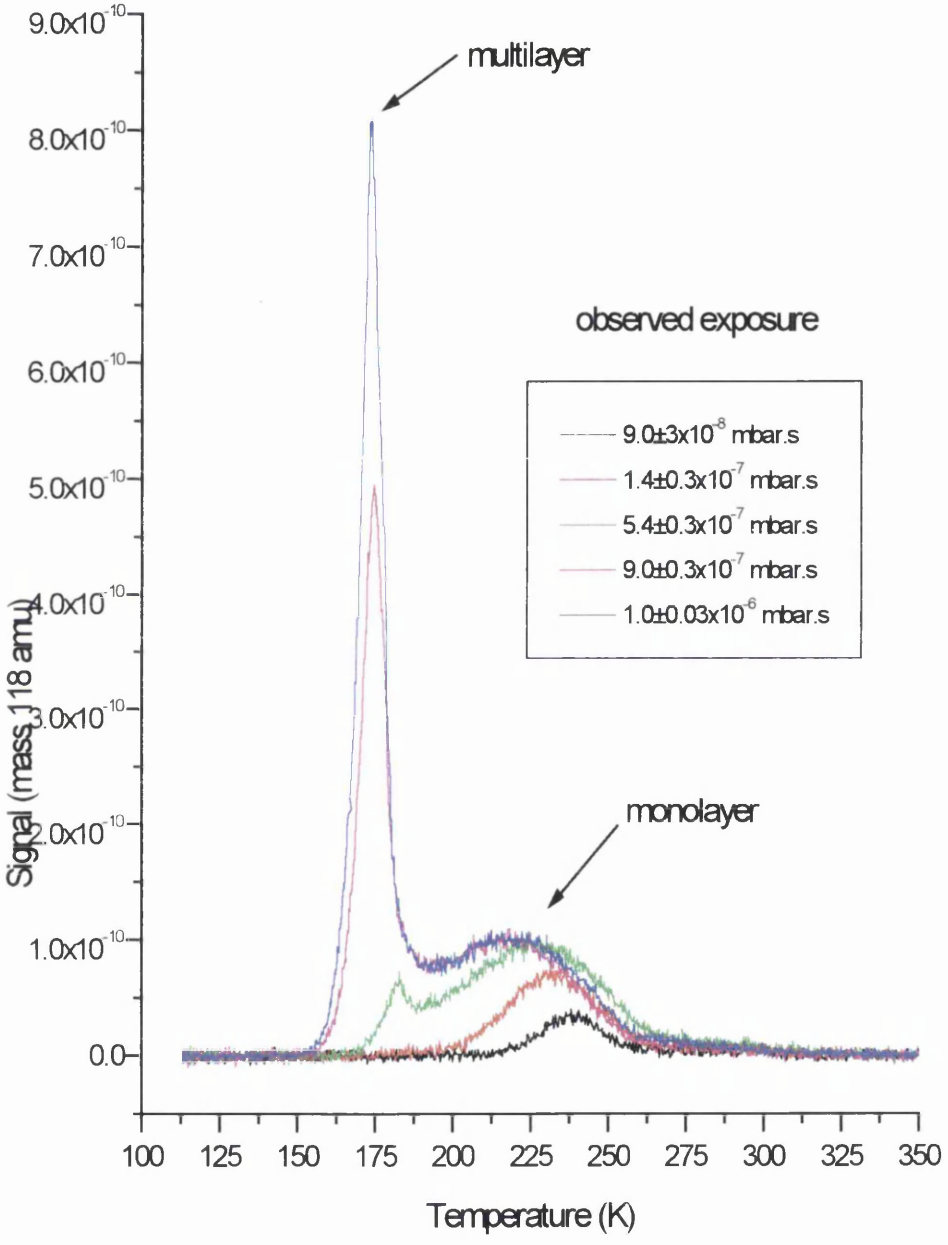

Figure 2: *Integrated areas for each of the TPD spectra shown in figure 1(b).*

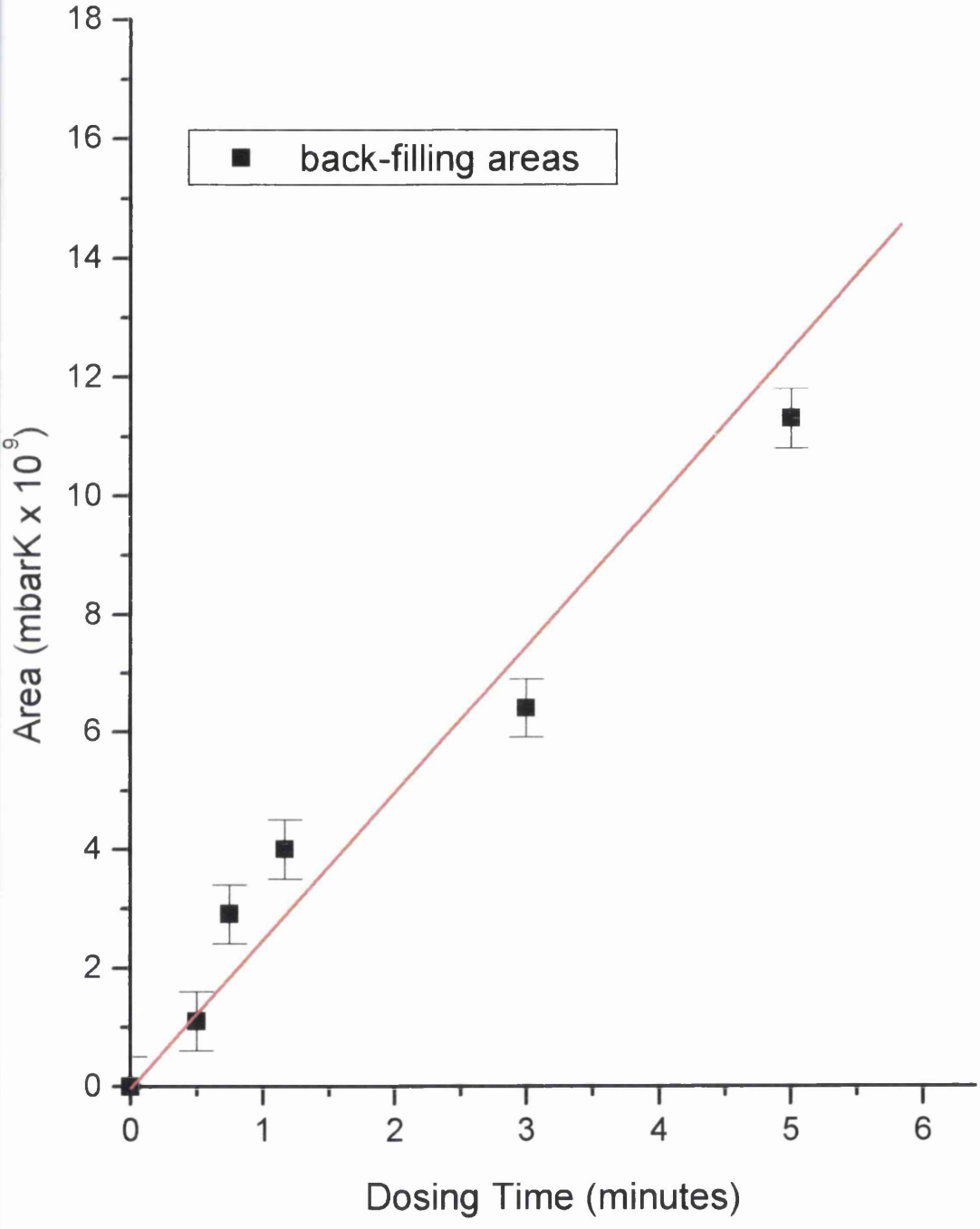

Figure 3: *S AES spectra collected both before (black) and after (red) TPD experiments showing the presence of S and Cl on the surface and hence that 3-chlorothiophene dissociates on the surface.*

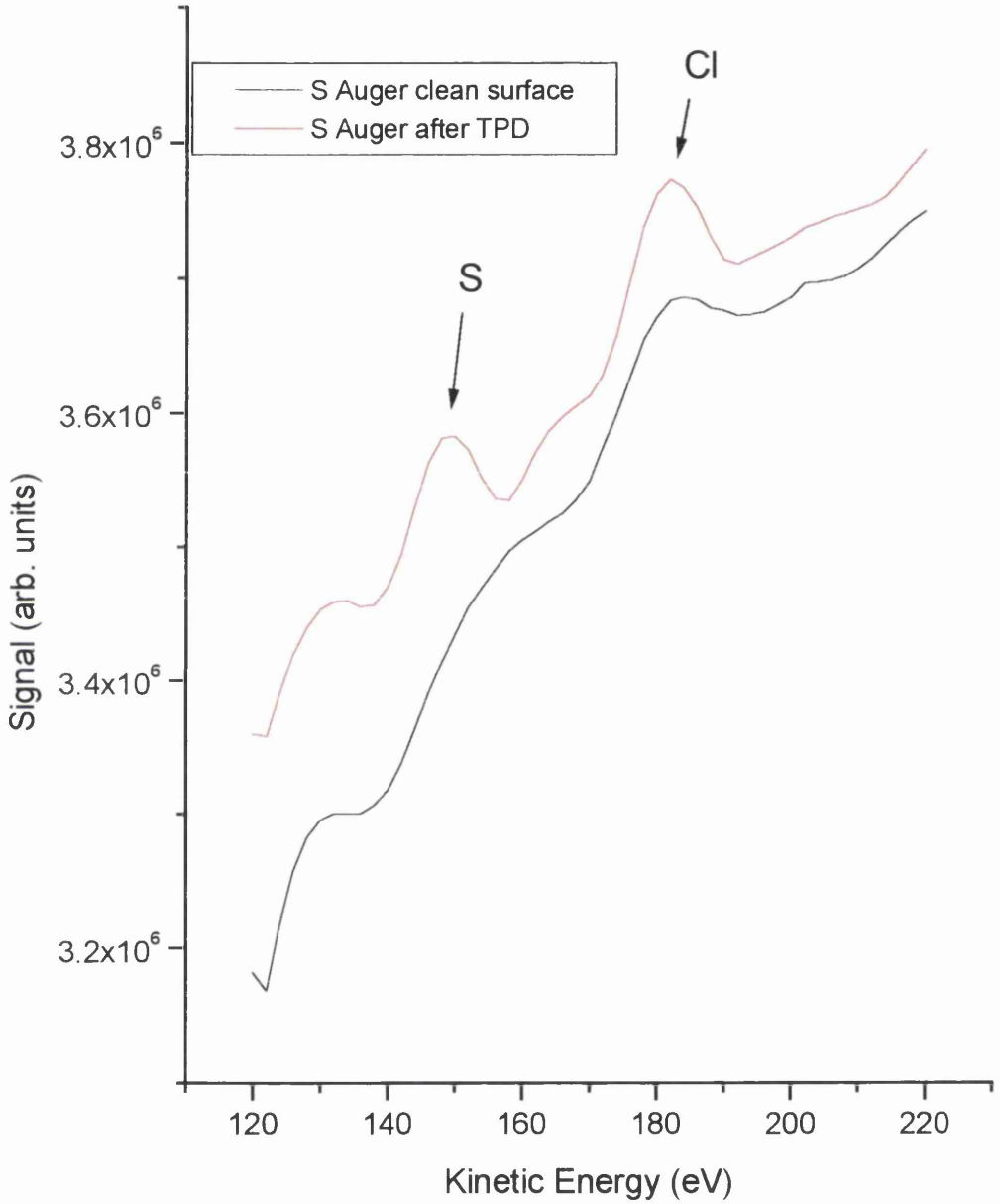

Figure 4: *C AES data collected both before (black) and after (red) TPD experiments showing the presence of C on the surface after TPD experiments and that 3-chlorothiophene dissociates on the surface.*

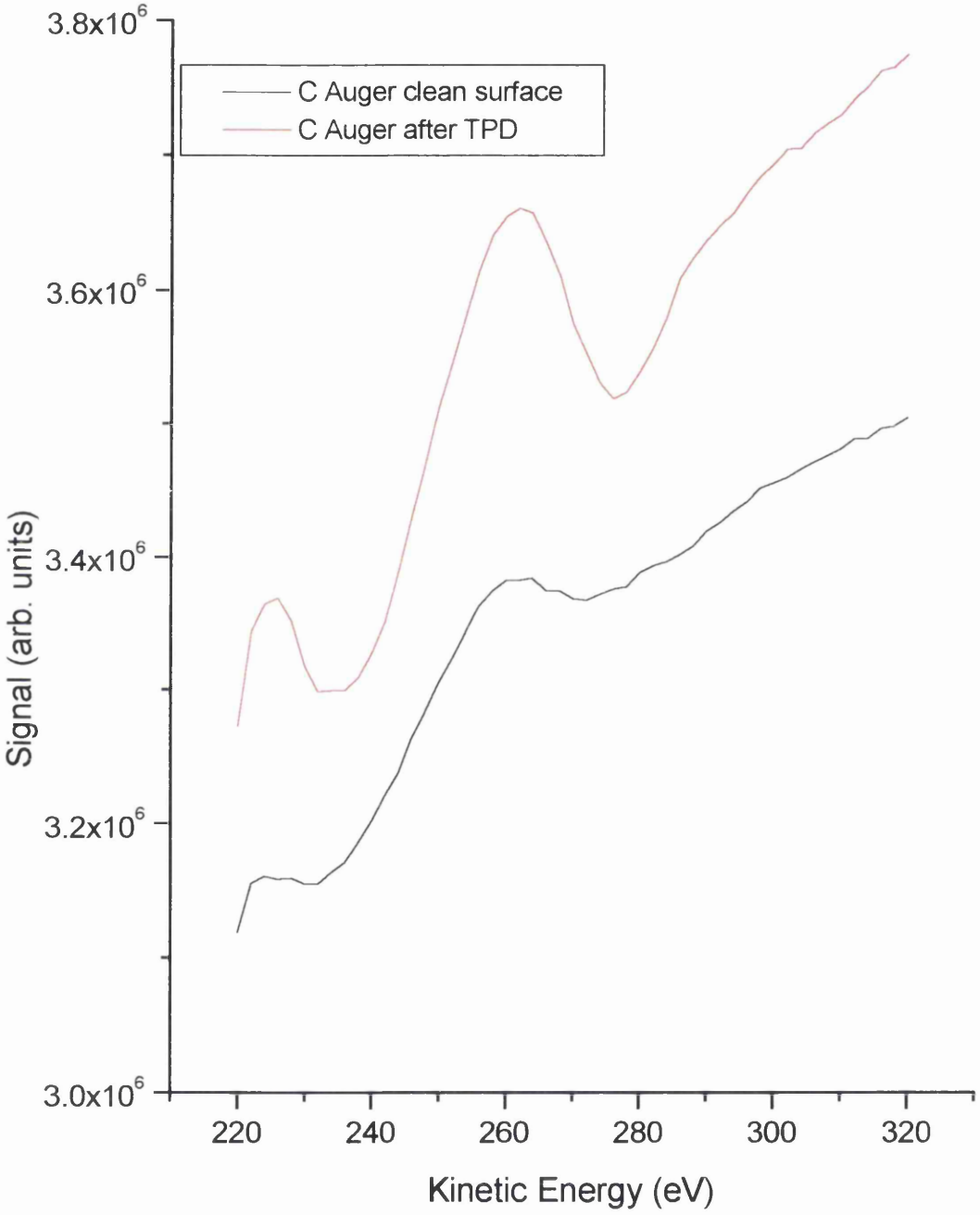

Figure 5: *AES spectra showing S and Cl from a surface of monolayer coverage (black) and from a surface in which a monolayer had been deposited and then desorbed (red). The spectra in this figure have been divided by their corresponding Cu Auger intensity and normalised for ease of comparison.*

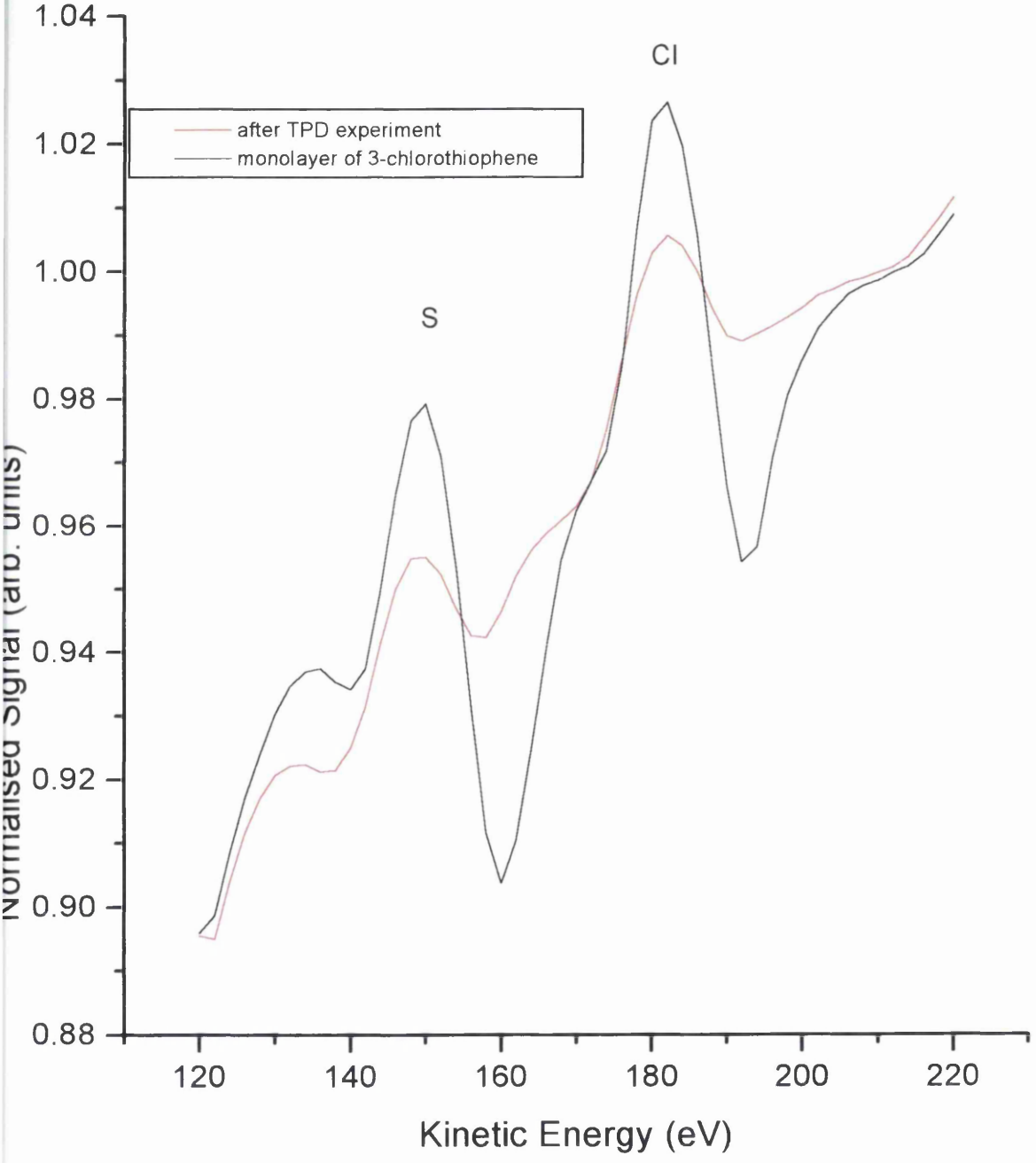

Figure 6: *S AES spectrum of (√7x √7R19.1°)-S surface (blue) which has a coverage of 0.43 ML, and S AES spectrum of a monolayer of 3-chlorothiophene which has a calculated coverage of 0.11±0.03 ML. The spectra in this figure have been divided by their corresponding Cu Auger intensity and normalised for ease of comparison.*

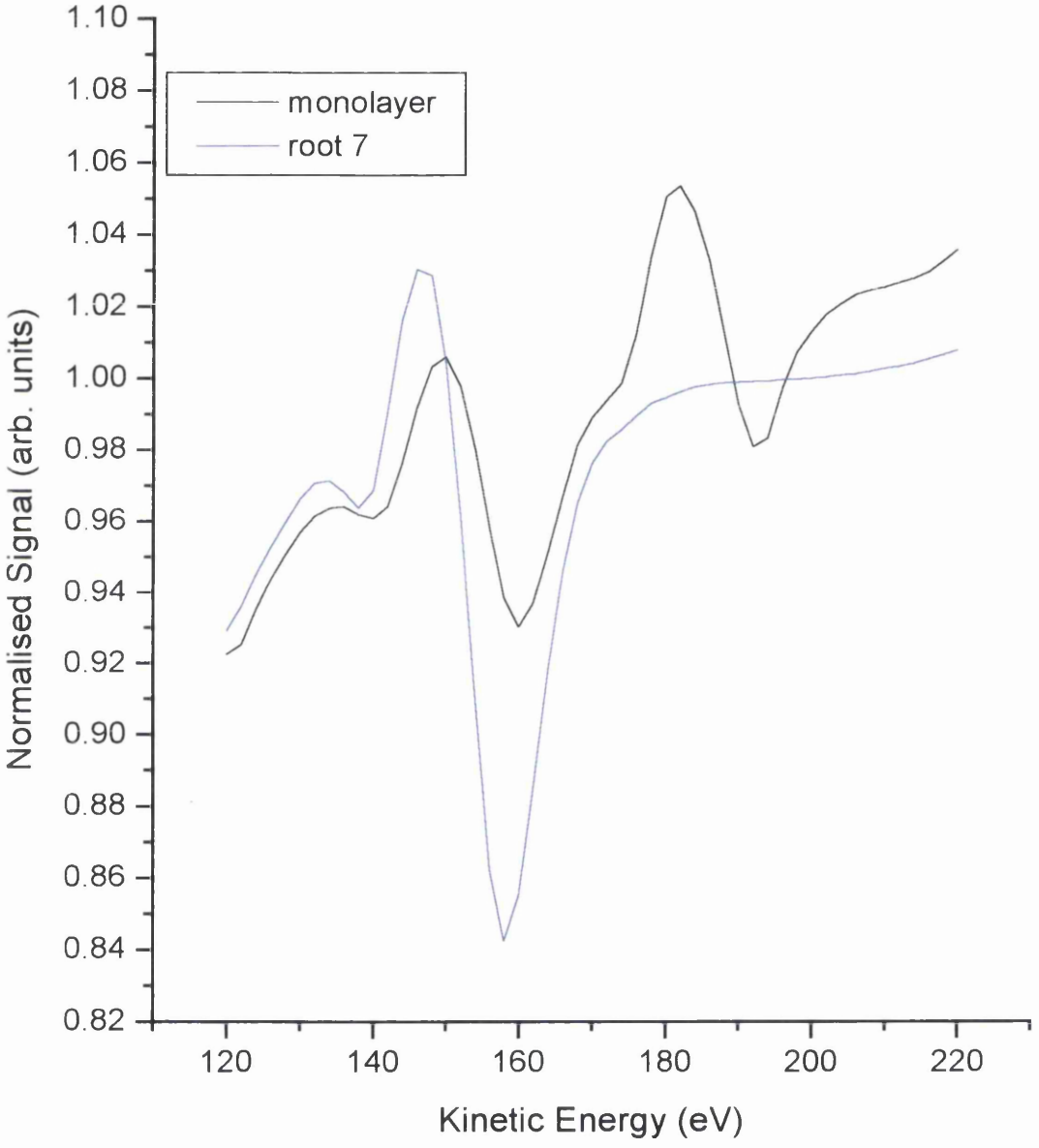

The red data in figure 5, which represents S and Cl left on the surface after a TPD experiment where a monolayer of 3-chlorothiophene was deposited, can be compared to the ($\sqrt{7}$x$\sqrt{7}$R19.1°-S) surface also. The amount of dissociation of 3-chlorothiophene on Cu(111) can be represented in terms of ML and the height of the S peak in the black data in figure 3 represents a coverage of 0.02 ML. This means that approximately 18 % of the monolayer, which has a coverage of 0.11±0.03 ML, dissociates.

Figure 7 shows that Cl left on the surface after desorption undergoes electron stimulated desorption (ESD). A coverage of 3-chlorothiophene corresponding to a saturated monolayer was dosed onto the surface and then desorbed. The black spectrum in figure 7 shows S and Cl left on the surface and was taken immediately after desorption. The electron beam from the AES electron gun was then left on and AES spectra were taken after 55 minutes (red spectrum) and 75 minutes (green spectrum). The spectra in figure 7 clearly show that there is a decrease in Cl intensity over this time period, whereas the S intensity remains constant. Cl is well known to undergo ESD from Cu surfaces[1]. As in the thiophene study, only the S AES spectra were used for coverage calculations. C and Cl AES spectra were collected to ensure that dissociation had taken place. No organic fragments, such as C4, C3 or C2 moieties could be detected using the QMS in TPD experiments. This is because the amount of dissociation is small and also that on adsorption, the 3-chlorothiophene decomposes, primarily at defect sites, to leave strongly bound C and S containing fragments that cannot be removed by heating.

S 1s XPS data was taken at the Daresbury Laboratory by dosing multilayer coverages of 3-chlorothiophene and then annealing the surfaces to different temperatures. Coverages of each surface prepared in this way were determined in the same way as described in Chapter 3. A plot of coverage versus annealing temperature is shown in figure 6 which can be used as a guide in subsequent experiments to prepare annealed surfaces of a known coverage.

LEED was used to detect any 3-chlorothiophene structures with long range order and similarly to thiophene, no structures were found at any coverage. LEED also showed that the decomposition products on the surface do not form any long range ordered structures.

Figure 7: *AES spectra of S and Cl showing electron stimulated desorption of Cl. The numbers in parenthesis indicate the total exposure to the electron beam in minutes.*

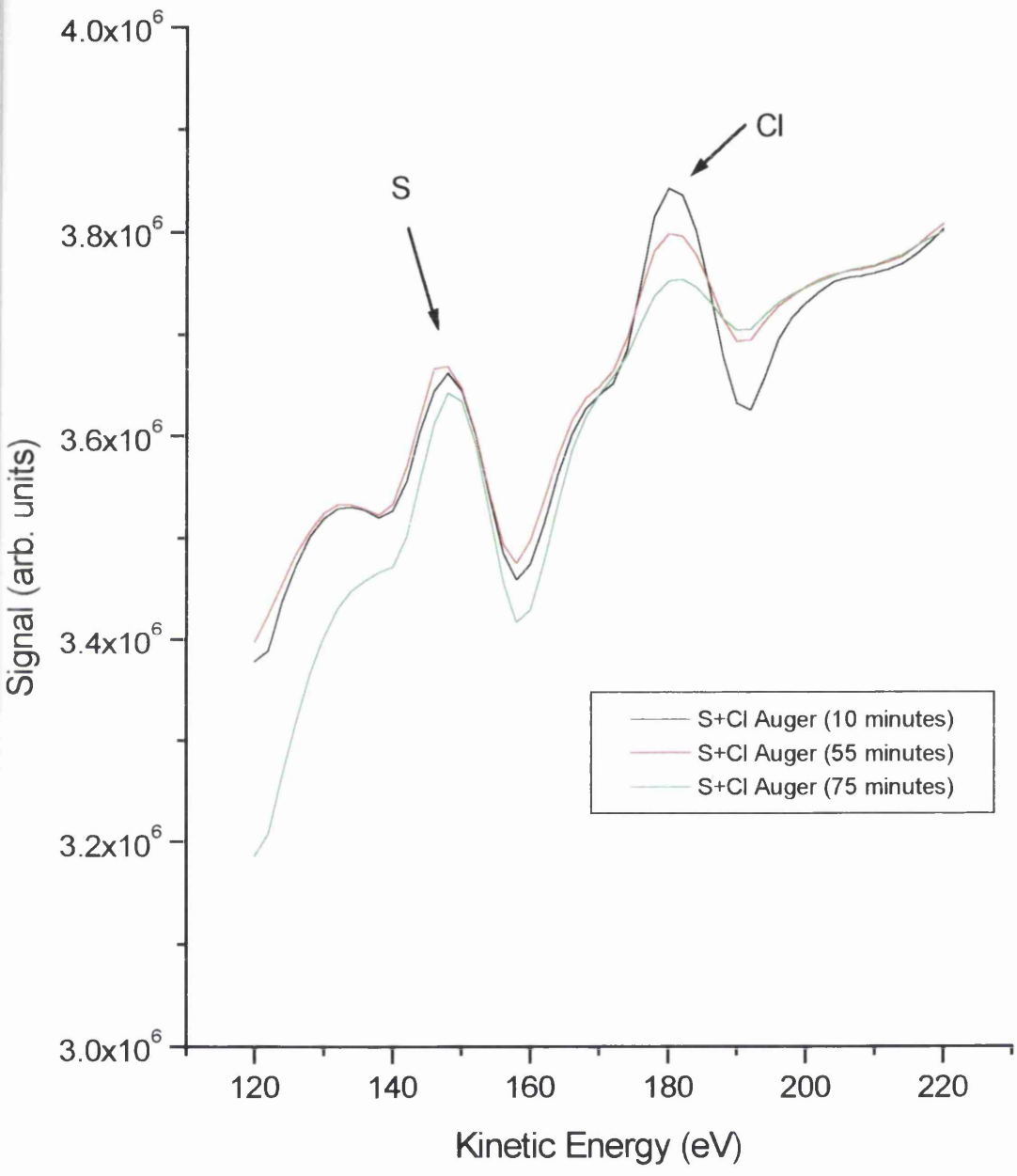

Figure 8: *Plot of coverage, as calculated by XPS, versus annealing temperature for 3-chlorothiophene.*

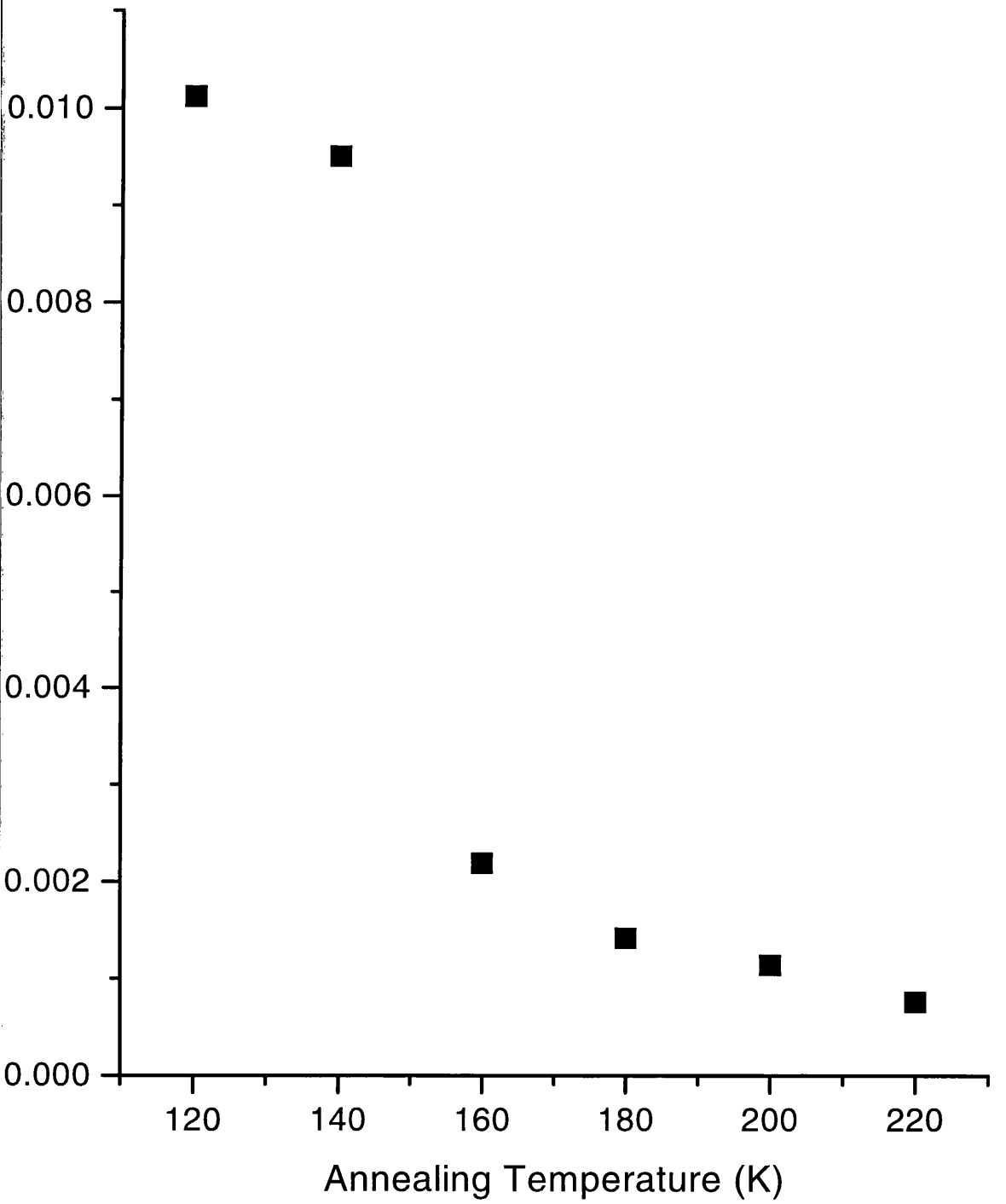

5.2.2. NEXAFS

NEXAFS experiments were performed in order to study the orientation of 3-chlorothiophene on Cu(111). As in the thiophene study, NEXAFS was used to probe the coverage dependence of the orientation of 3-chlrothiophene on Cu(111). This was done by performing sequentially dosed NEXAFS experiments. These experiments were performed in an identical manner to those described in Chapter 3.

5.2.3 Sequentially dosed NEXAFS experiments

The spectra shown in figure 9 represent data collected at two angles of X-ray incidence, normal (90°) and grazing (19.5°). All spectra shown in figure 9 are S K-edge NEXAFS spectra. Therefore, the intensity of the S (KLL) Auger electron, which has a kinetic energy of 2099 eV, was monitored as a function of photon energy and the data shown is normalised to the S K-edge jump.

The lowest coverage (black, 0.05 ML) spectrum in figure 9 exhibits a feature at 2467.3 eV at grazing incidence. The corresponding normal incidence spectrum at this coverage exhibits a feature at 2468.2 eV. Contrasting with NEXAFS data collected for thiophene, there is no discernible broadening of any of the features with increasing coverage. The features present in the low coverage data, at 2467.3 eV and 2468.2 eV respectively, are at similar positions to the π^* and σ^* resonances that were assigned in the previous chapter concerning thiophene. At low coverage, thiophene NEXAFS spectra indicate the presence of a π^* resonance at 2467.8 eV and a σ^* resonance at 2468.7 eV.

There are no reported S KLL NEXAFS spectra regarding 3-chlorothiophene, hence the features present in the spectra in figure 9 could not be assigned with reference to previous work as in the case of thiophene. However, the features present in the current work are qualitatively similar to that of thiophene, and although no calculations were performed, assignments can be made due to the similarities of the NEXAFS spectra (compare figure 11 in chapter 4 and figure 9 below).

Figure 9: *Sequentially dosed nested S KLL NEXAFS spectra for 3-chlorothiophene on Cu(111).*

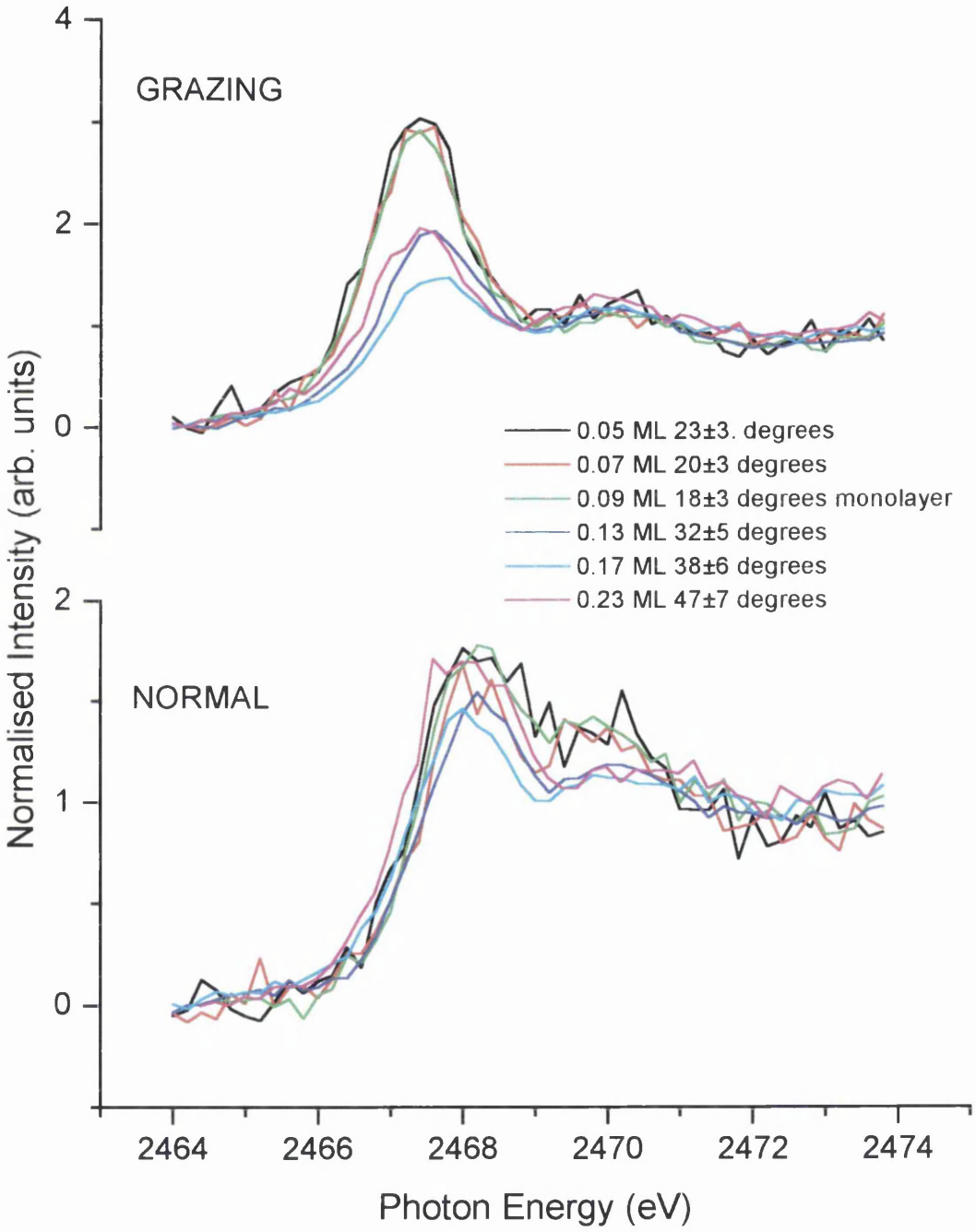

The feature at 2467.3 eV in the grazing incidence spectrum at 0.05 ML can be assigned predominantly to a π^* resonance and the feature at 2468.2 eV in the normal incidence spectrum can be assigned predominantly to a σ^* resonance. Polarisation dependence[2] of these resonances indicates that the 3-chlorothiophene molecules are oriented in a roughly flat geometry on the surface, at a coverage of 0.05 ML. In all, seven features can be identified in the NEXAFS data shown in figure 9, six peaks and a step, and these are listed and assigned in table 1. The assignments of the other features was also made by comparing the spectra and the relative positions of the features to work performed on thiophene. The data was fitted using an identical procedure to the one used in the case of the thiophene NEXAFS data. The identified features and functions used in the fitting are summarised in table 1 and the ratio $I\pi^*(g)/I\ \pi^*(n)$ and subsequent derived angles are summarised in table 2. A complete list of all the values used in the fitting procedure can be found in table 3.

AES and TPD data shows that a saturated monolayer of 3-chlorothiophene has a coverage of 0.11±0.03 ML. Figure 10 shows that the angle of inclination of the adsorbed 3-chlorothiophene does not change within experimental error for the first four coverages studied, 0.05, 0.06, 0.07 and 0.09 ML. The quoted coverages are very close but due to the sequential dosing technique being employed, each surface prepared in this way has a higher coverage than the previous surface. Figure 10 shows that at coverages between 0.05-0.09 ML, the angle of orientation is at a constant value of 20±3 °. At a coverage of 0.13 ML, the angle of orientation is 32±5 °. This shows that up to monolayer coverage there is no change in molecular orientation. At coverages of 0.13 ML and higher, multilayer formation means that the angle of orientation is increasing, in this case from 32±5 to 47±7 ° over the coverage range 0.13-0.23 ML. Figure 11 shows a plot of the ratio $I\pi^*(g)/I\pi^*(n)$, which as expected, approaches unity with increasing coverage.

TABLE 1 *Positions of the seven features that were fitted in the data with the type of function that was used in the fitting procedure and the broadness used.*

Peak Position (eV)	Fitting Function	Assignment	Broadness (eV)
2465.0	Gaussian	pre-π*	1.4
2467.1	Gaussian	π*	1.4
2468.0	Gaussian	σ*	1.4
2469.1	Gaussian	4s	1.4
2470.9	Gaussian	4p	1.4
2471.5	Gaussian	5p	1.4
2472.4	Step	Ionisation Threshold	4.4

TABLE 2 *Angles of inclination for NEXAFS data in figure 9 and corresponding TPD states.*

Coverage (ML)	π* area (grazing)	π* area (normal)	Ratio π*(g)/π*(n)	Angle (α) (°)	TPD state
0.05	4.26	0.43	9.91	23±3	Monolayer
0.06	3.66	0.18	20.33	17±3	Monolayer
0.07	4.24	0.31	13.68	20±3	Monolayer
0.09	4.23	0.25	16.92	18±3	Saturated Monolayer
0.13	2.16	0.46	4.70	32±5	Multilayer
0.17	1.69	0.54	3.13	38±6	Multilayer
0.23	2.53	1.5	1.69	47±7	Multilayer

Figure 10: *Plot of angles from table 2 versus coverage derived from sequentially dosed 3-chlorothiophene NEXAFS experiments.*

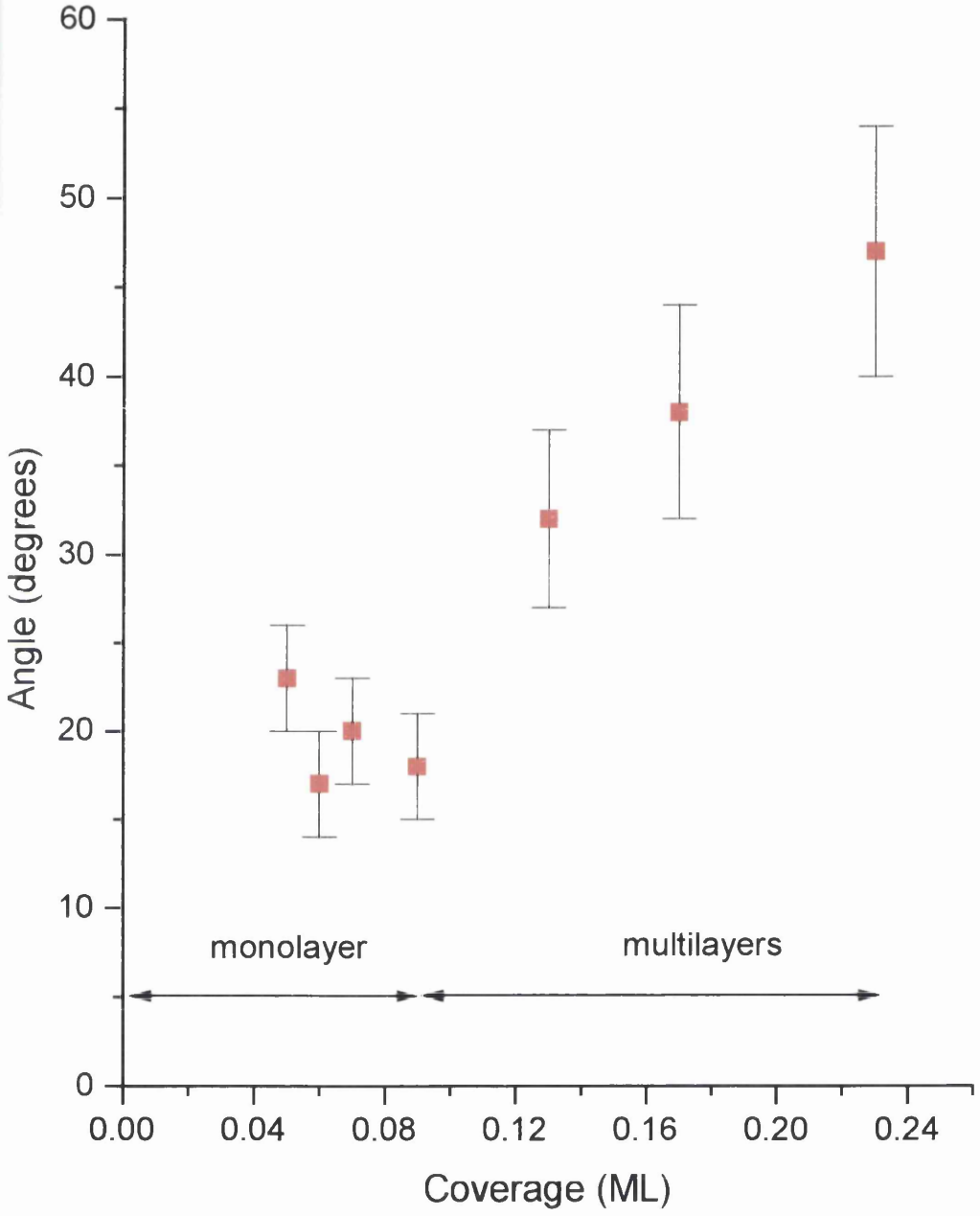

Figure 11: *Plot of ratio Iπ*(g)/Iπ*(n) from table 2 for sequentially dosed 3-chlorothiophene experiments.*

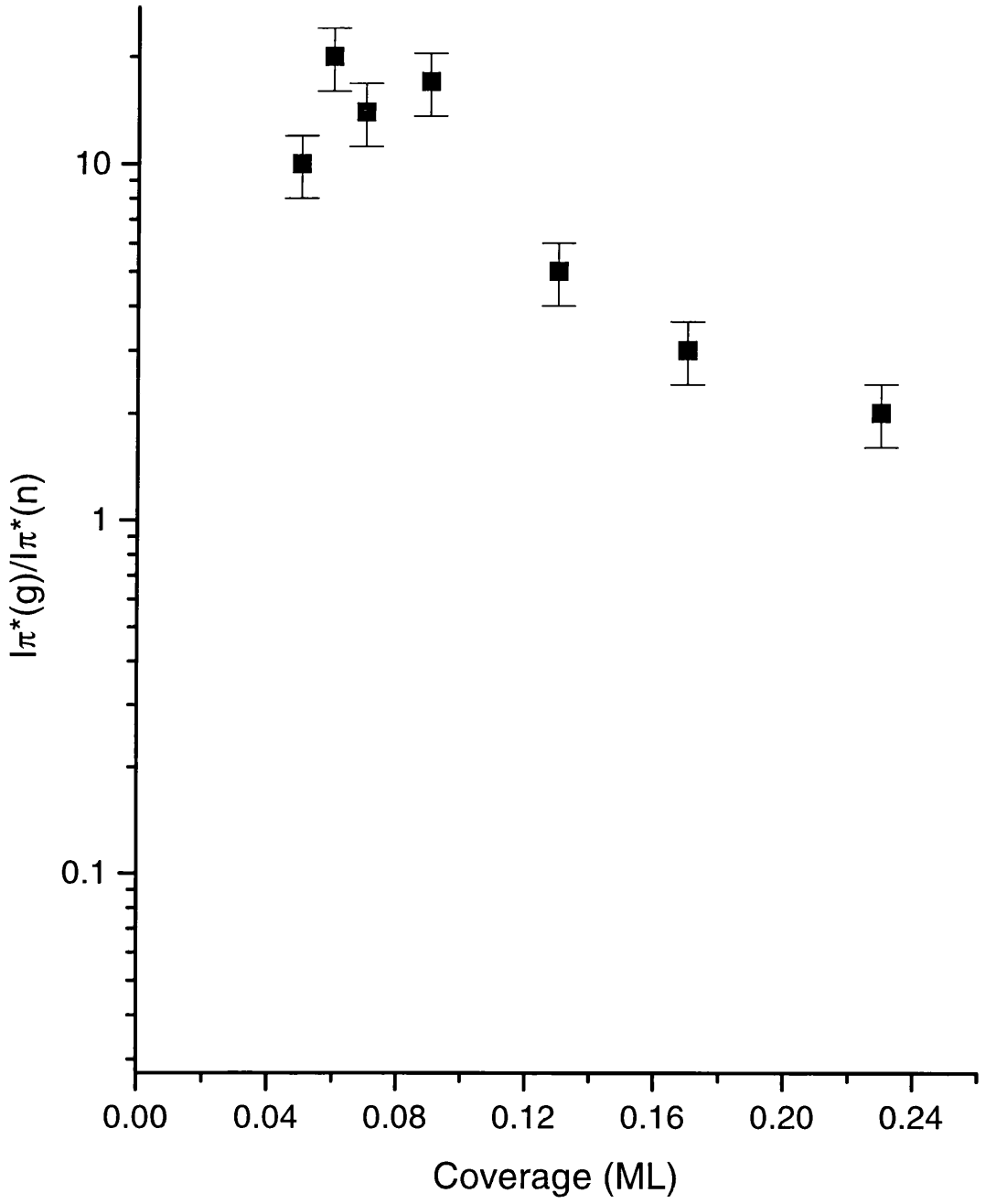

Figures 12 (a), (b) and (c) show fitted NEXAFS spectra at grazing and normal incidence at coverages of 0.05, 0.13 and 0.23 ML respectively. Figure 12 (a) shows that the grazing spectrum is clearly dominated by a distinct π^* resonance and that the normal spectrum is clearly dominated by a σ^* resonance. With increasing coverage, figure 12 (b), the features dominated by π^* and σ^* resonances are starting to broaden slightly and lower in intensity. In figure 12 (c), the features at grazing and normal incidence have lowered yet further in intensity and look very similar. The reason for this is that there is an overall increased σ^* contribution in the grazing incidence NEXAFS data and an overall increased π^* contribution in the normal incidence NEXAFS data, with increasing coverage. The net effect of this is an increased inclination of the molecules from a coverage of 0.13-0.23 ML as shown in figure 10.

Figure 12 (a): *Fitted NEXAFS spectra at grazing and normal incidence at a coverage of 0.05 ML.*

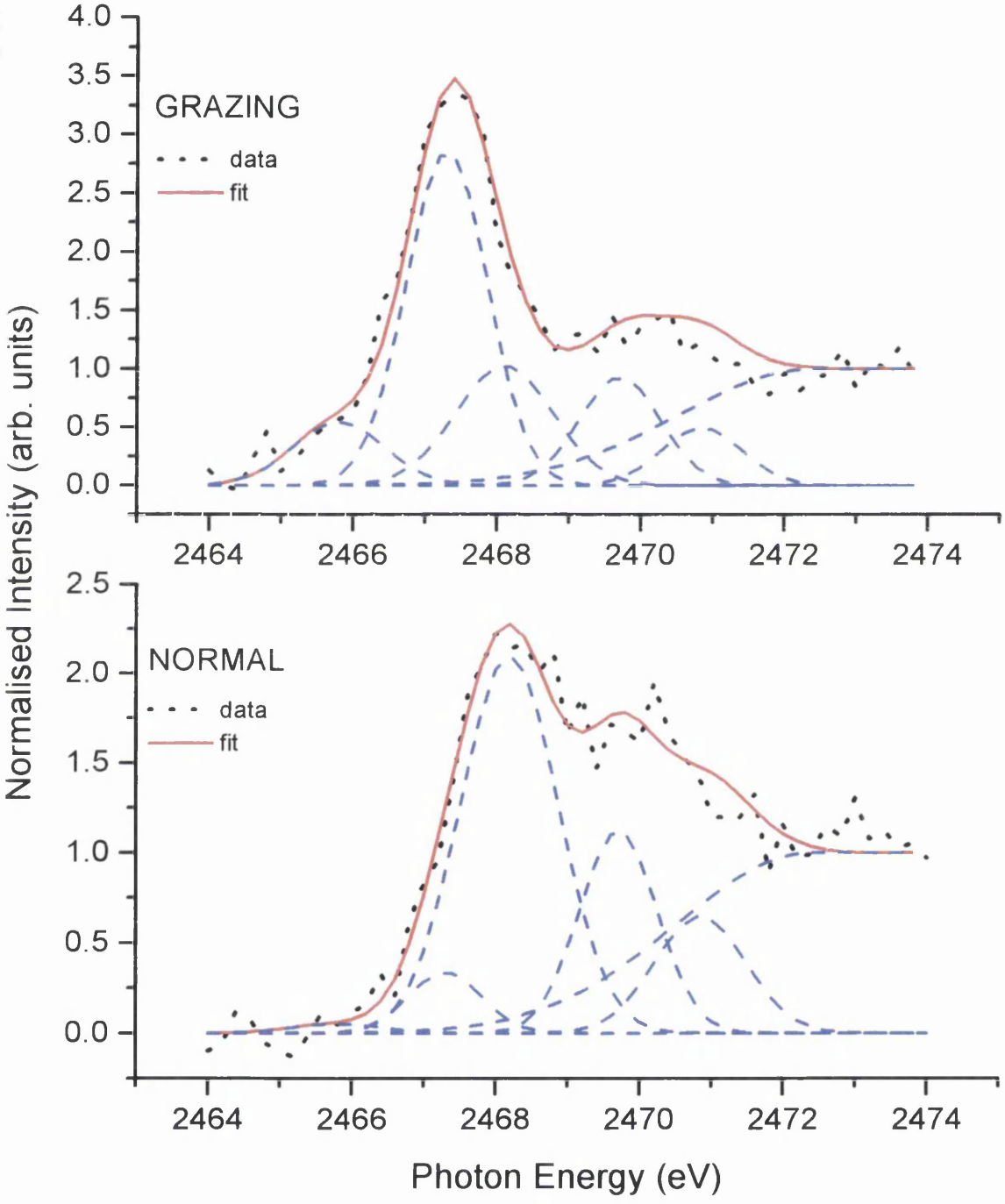

(b): *Fitted NEXAFS spectra at grazing and normal incidence at a coverage of 0.13 ML.*

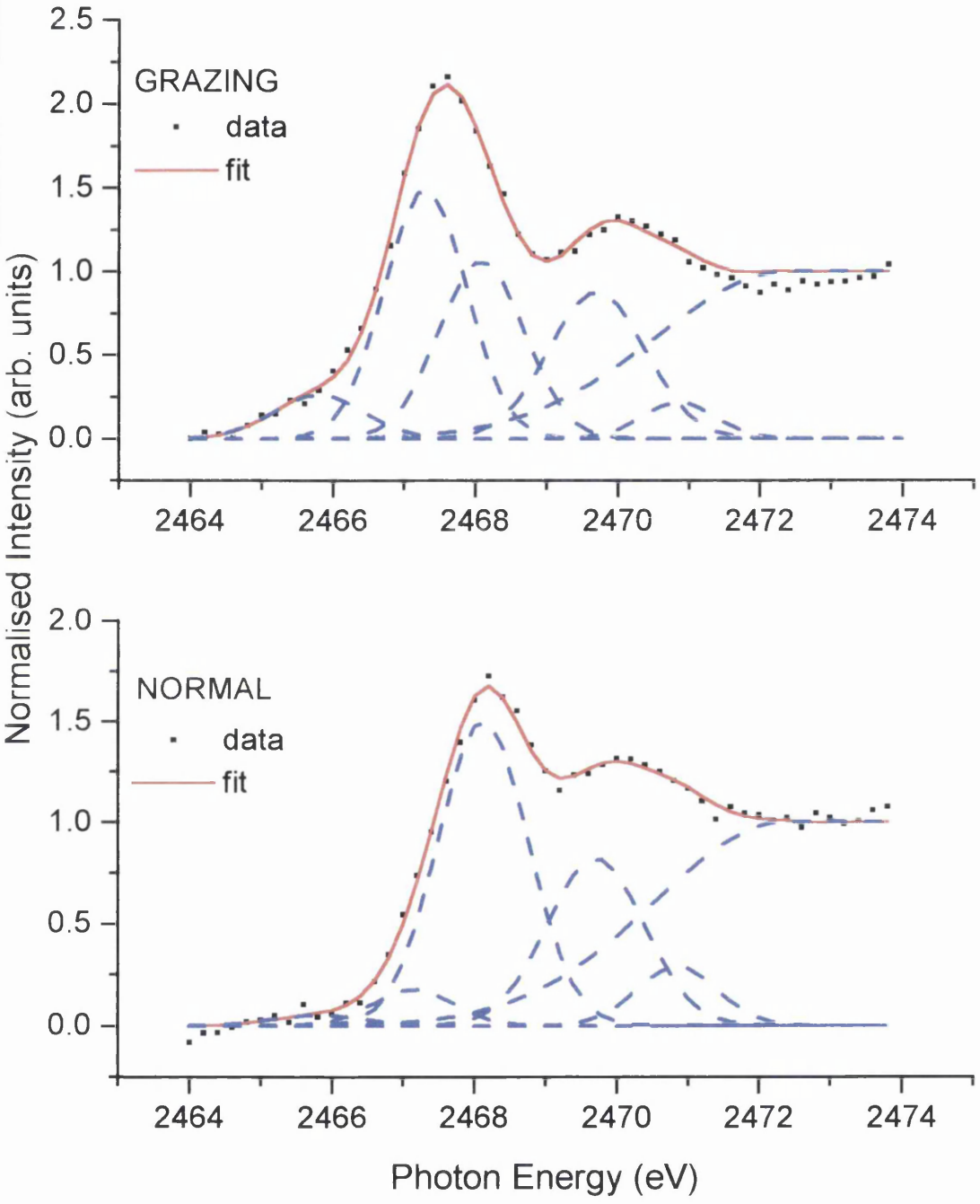

(c): *Fitted NEXAFS spectra at grazing and normal incidence at a coverage of 0.23 ML (multilayer).*

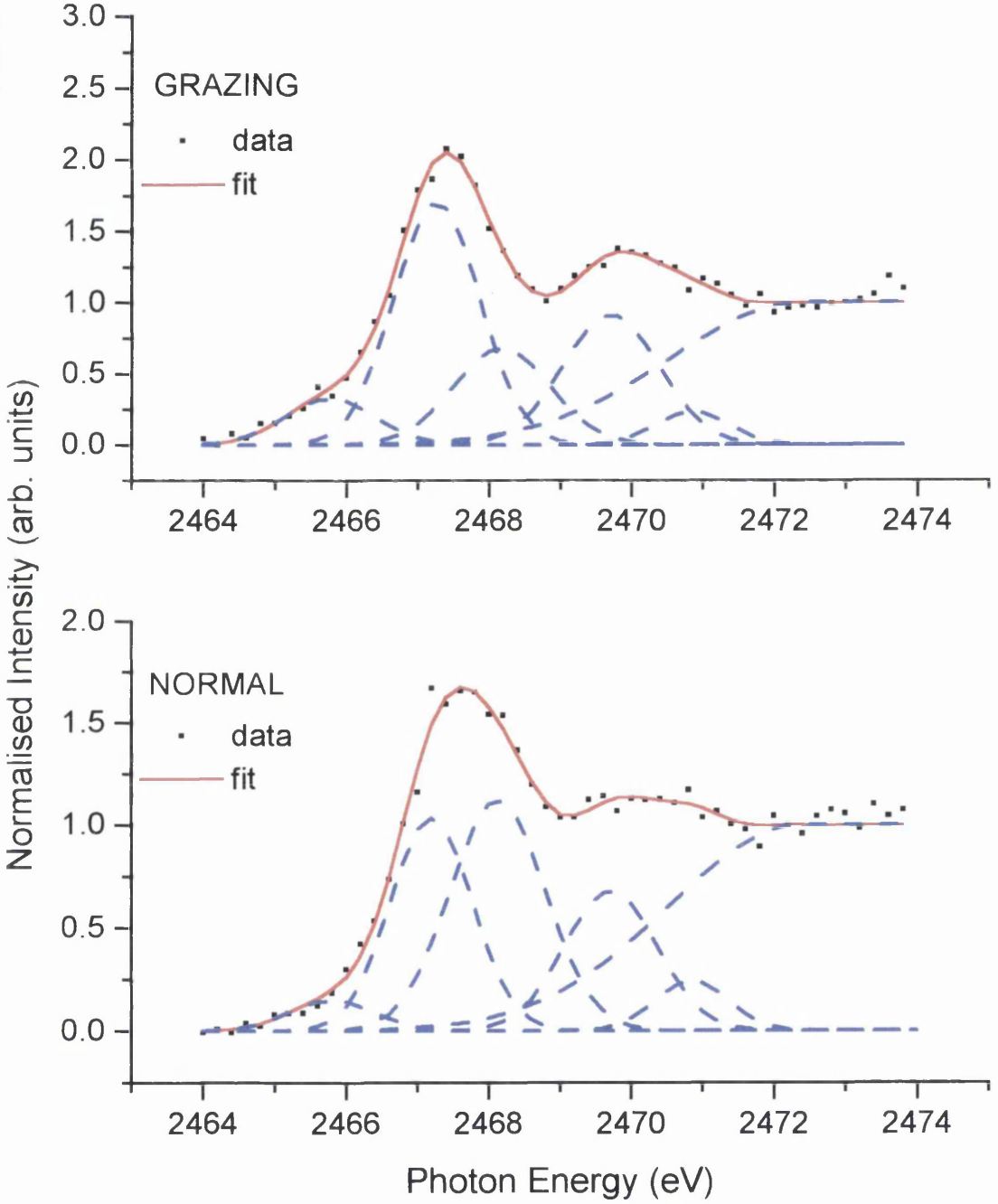

TABLE 3 *Complete list of values obtained from fitting all data shown in figure 10.*

Peak one (grazing)	Position (eV)	Area	Broadness (eV)	Peak one (normal)	Position (eV)	Area	Broadness (eV)
Peak 1 (pre-π)							
0.05 ML	2465.8	0.81	1.50	0.05 ML	2465.8	0.08	1.50
0.06 ML	2465.8	0.48	1.30	0.06 ML	2465.8	0.08	1.50
0.07 ML	2465.8	0.46	1.30	0.07 ML	2465.7	0.17	1.50
0.09 ML	2465.8	0.71	1.50	0.09 ML	2465.8	0.06	1.50
0.13 ML	2465.8	0.42	1.50	0.13 ML	2465.7	0.06	1.30
0.17 ML	2465.7	0.35	1.50	0.17 ML	2465.8	0.11	1.50
0.23 ML	2465.8	0.50	1.30	0.23 ML	2465.8	0.20	1.50
Peak 2 (π*)							
0.05 ML	2467.3	4.26	1.37	0.05 ML	2467.3	0.43	1.50
0.06 ML	2467.3	3.66	1.35	0.06 ML	2467.2	0.18	1.33
0.07 ML	2467.3	4.24	1.34	0.07 ML	2467.1	0.31	1.40
0.09 ML	2467.3	4.23	1.38	0.09 ML	2467.2	0.25	1.20
0.13 ML	2467.3	2.16	1.36	0.13 ML	2467.2	0.46	1.23
0.17 ML	2467.3	1.69	1.40	0.17 ML	2467.2	0.54	1.53
0.23 ML	2467.3	2.53	1.35	0.23 ML	2467.2	1.50	1.50
Peak 3 (σ*)							
0.05 ML	2468.2	1.62	1.60	0.05 ML	2468.2	3.59	1.60
0.06 ML	2648.2	1.71	1.49	0.06 ML	2468.1	3.00	1.49
0.07 ML	2468.2	2.12	1.60	0.07 ML	2468.2	2.98	1.53
0.09 ML	2468.2	1.53	1.60	0.09 ML	2468.2	3.31	1.60
0.13 ML	2468.1	1.61	1.60	0.13 ML	2468.2	2.18	1.38
0.17 ML	2468.1	1.36	1.48	0.17 ML	2468.1	1.97	1.52
0.23 ML	2468.2	1.16	1.49	0.23 ML	2468.1	1.87	1.49
Peak 4 (4s←1s)							
0.05 ML	2469.7	1.50	1.53	0.05 ML	2469.7	1.52	1.27

0.06 ML	2469.7	1.55	1.60	0.06 ML	2469.7	1.80	1.60
0.07 ML	2469.7	2.12	1.60	0.07 ML	2469.7	1.53	1.25
0.09 ML	2469.7	1.53	1.60	0.09 ML	2469.7	1.42	1.27
0.13 ML	2469.7	1.50	1.60	0.13 ML	2469.7	1.39	1.60
0.17 ML	2469.7	1.45	1.60	0.17 ML	2469.7	1.07	1.45
0.23 ML	2469.7	1.58	1.60	0.23 ML	2469.7	1.16	1.60
Peak 5 (4p←1s)							
0.05 ML	2470.9	0.37	1.20	0.05 ML	2470.9	1.03	1.50
0.06 ML	2470.9	0.22	1.20	0.06 ML	2470.9	0.57	1.33
0.07 ML	2470.9	0.40	1.20	0.07 ML	2470.9	0.75	1.34
0.09 ML	2470.9	0.40	1.29	0.09 ML	2470.9	0.76	1.50
0.13 ML	2470.9	0.28	1.20	0.13 ML	2470.9	0.43	1.44
0.17 ML	2470.9	0.37	1.40	0.17 ML	2470.9	0.33	1.20
0.23 ML	2470.9	0.29	1.20	0.23 ML	2470.9	0.34	1.33
Peak 6 (5p←1s)							
0.05 ML	2471.5	0.01	1.60	0.05 ML	2471.5	0.01	1.60
0.06 ML	2471.5	0.01	1.20	0.06 ML	2471.5	0.01	1.60
0.07 ML	2471.5	0.15	1.60	0.07 ML	2471.5	0.06	1.60
0.09 ML	2471.5	0.01	1.60	0.09 ML	2471.5	0.11	1.60
0.13 ML	2471.5	0.01	1.20	0.13 ML	2471.5	0.01	1.60
0.17 ML	2471.5	0.01	1.20	0.17 ML	2471.5	0.01	1.60
0.23 ML	2471.5	0.01	1.20	0.23 ML	2471.5	0.01	1.60

5.2.4. NIXSW

NIXSW experiments were performed in order to study the adsorption structure of 3-chlorothiophene on Cu(111). In particular, as with thiophene, the Cu-S bond length was derived from S 1s photoemission NIXSW data collected from (111) and ($\bar{1}11$) planes, assuming no relaxation of the surface Cu atoms. From this the adsorption site was derived by a triangulation procedure as detailed in chapter 2. The wider scope of the current study is that of substituent effects, and in this particular case, the effects of the electron withdrawing Cl- group at the 3-position of the thiophene ring. In a complex molecule like 3-chlorothiophene, it would be expected that the presence of the Cl-group at the 3-position would have either a steric or electronic effect, or even both, over a similar coverage range to the thiophene study. For the purposes of NIXSW experiments however, 3-chlorothiophene data can be directly compared to the previously well characterised thiophene data and any changes or similarities accounted for. This is facilitated by NEXAFS experiments, but also NIXSW experiments that reveal structural information about the Cl- group itself. In a directly analogous method, both experimental and in the process of data analysis, NIXSW experiments were performed which monitored Cl KLL Auger emission simultaneously to S 1s photoemission experiments. All that is required to ascertain the adsorption site for the entire molecule is the S 1s photoemission NIXSW experiments, as with thiophene. Knowledge of the Cl height above the surface is further structural information, in which the angle of orientation of the molecule can be calculated, assuming molecular planarity, and compared to that calculated from NEXAFS.

5.2.5 *Substrate NIXSW experiments*

Substrate NIXSW experiments were performed by monitoring Cu LVV Auger emission. A Cu substrate NIXSW profile is shown in figure 13. The data was analysed using the same fitting procedure as outlined in chapter 3. The experimental values of interest from fitting the substrate profiles, notably the coherent fraction, f_{co}, the coherent position, D(hkl), the width of the X-ray beam, ΔE, and mosaic spread of the crystal are tabulated in table 4.

As expected, the data is fitted to a very high coherent fraction, indicating a high degree of crystallographic order on the Cu(111) surface. The X-ray broadness of 0.7 eV differs to that of substrate thiophene NIXSW experiments because the 3-chlorothiophene data was collected at a different time. In an analogous procedure to the thiophene NIXSW data, the adsorbate profiles were subsequently fitted using a broadness of 0.7 eV and a mosaic spread of 0.1 °.

Table 4: *Experimental values derived from substrate NIXSW experiments.*

	Coherent fraction (f_{co})	Coherent position (D(111) (Å)	Broadness (ΔE) (eV)	Mosaic Spread (°)
Data	0.90±0.05	0	0.7	0.1

Figure 13: *Cu LVV NIXSW profile (black) with fit (red) with respect to the (111) plane.*

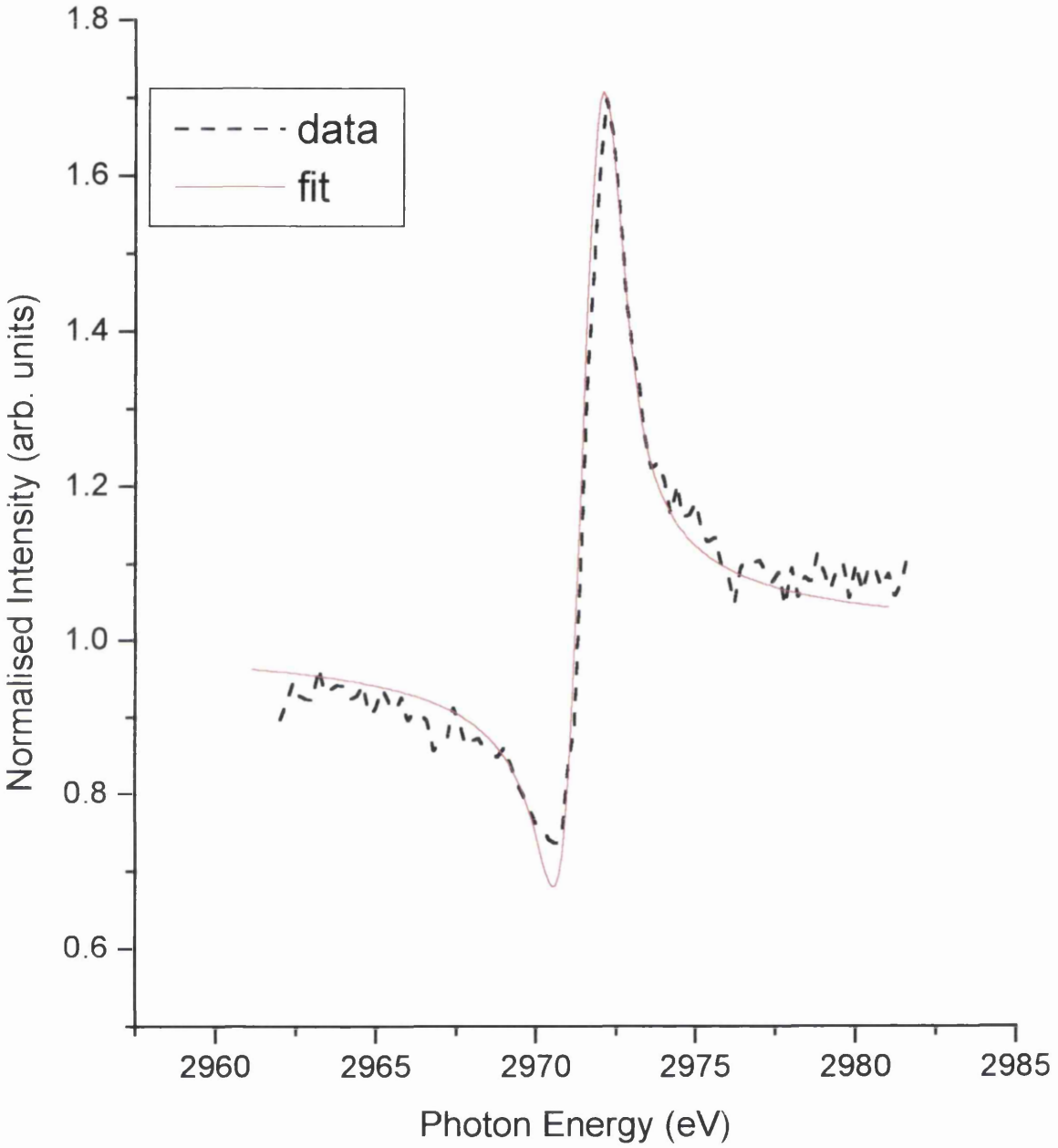

5.2.6 *S 1s Adsorbate NIXSW experiments using the annealed dosing method*

3-chlorothiophene surfaces were prepared by the annealed dosing method and the coverage of each surface prepared was determined as described in chapter 4. S 1s NIXSW experiments were performed at different coverages and table 5 shows a summary of the results obtained by the annealing dosing method at monolayer coverage. An error of 0.02 ML was calculated by considering the areas under each XPS spectrum for each surface and the annealing temperature. A complete list of the experiments performed is in table 6. Fitted S 1s NIXSW data is shown in figures 14 and 15.

Table 5: *Summary of values obtained from fitting S 1s and Cl KLL NIXSW data at monolayer coverage.*

Data	Plane	f_{co}	D(hkl) (Å)
S 1s	(111)	0.90±0.05	0.54±0.03 (2.62±0.03)
S 1s	($\bar{1}$11)	0.70±0.05	0.85±0.03
Cl KLL	(111)	0.80±0.10	1.43±0.15 (3.51±0.15)
Cl KLL	($\bar{1}$11)	0.20±0.10	0.40±0.15

Figure 14: *S 1s NIXSW profile (black) with fit (red) at monolayer coverage with respect to (111) plane, as prepared by the annealed dosing method.*

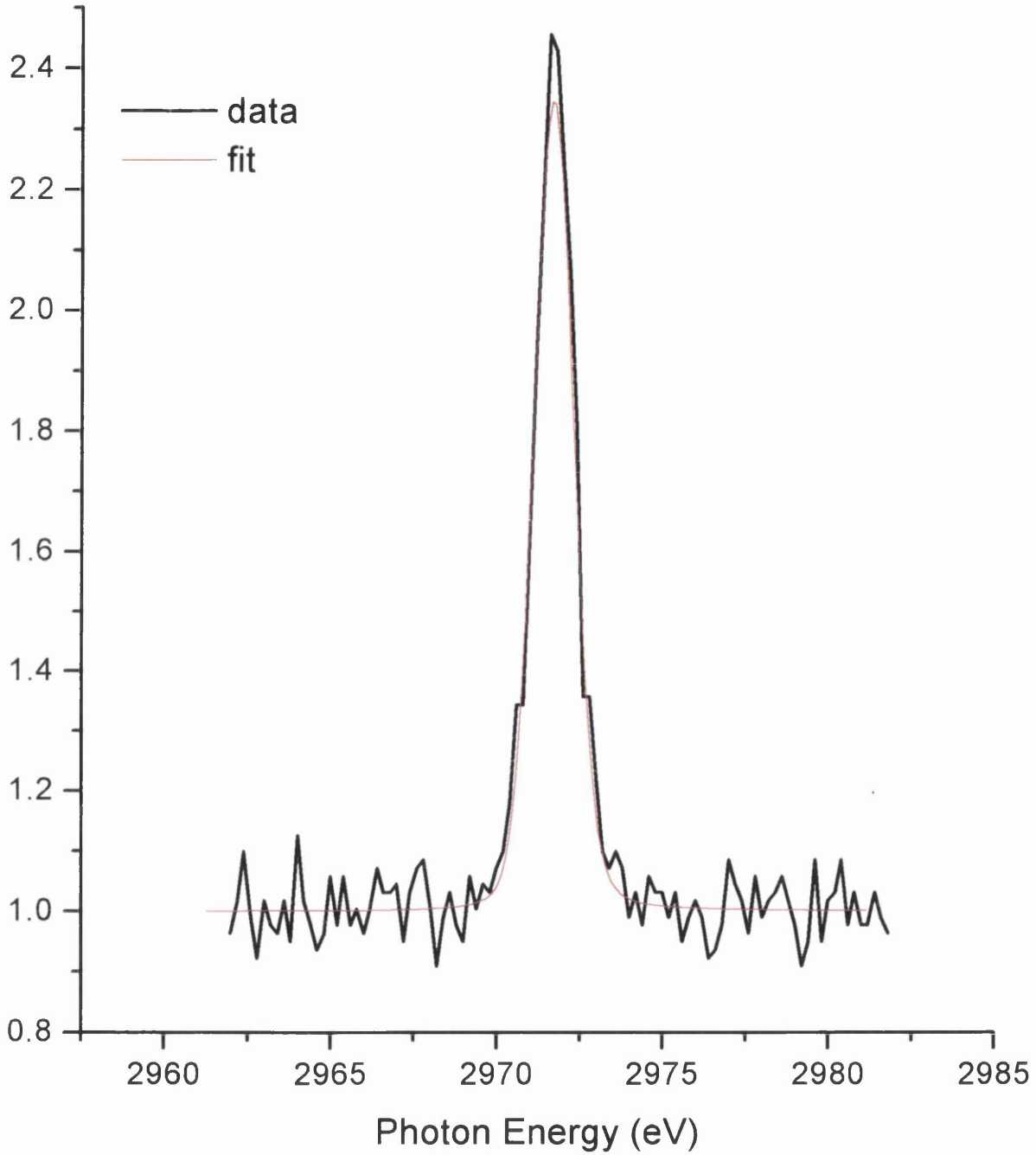

Figure 15: *S 1s NIXSW profile (black) with fit (red) at monolayer coverage with respect to ($\bar{1}11$) plane, as prepared by the annealed dosing method.*

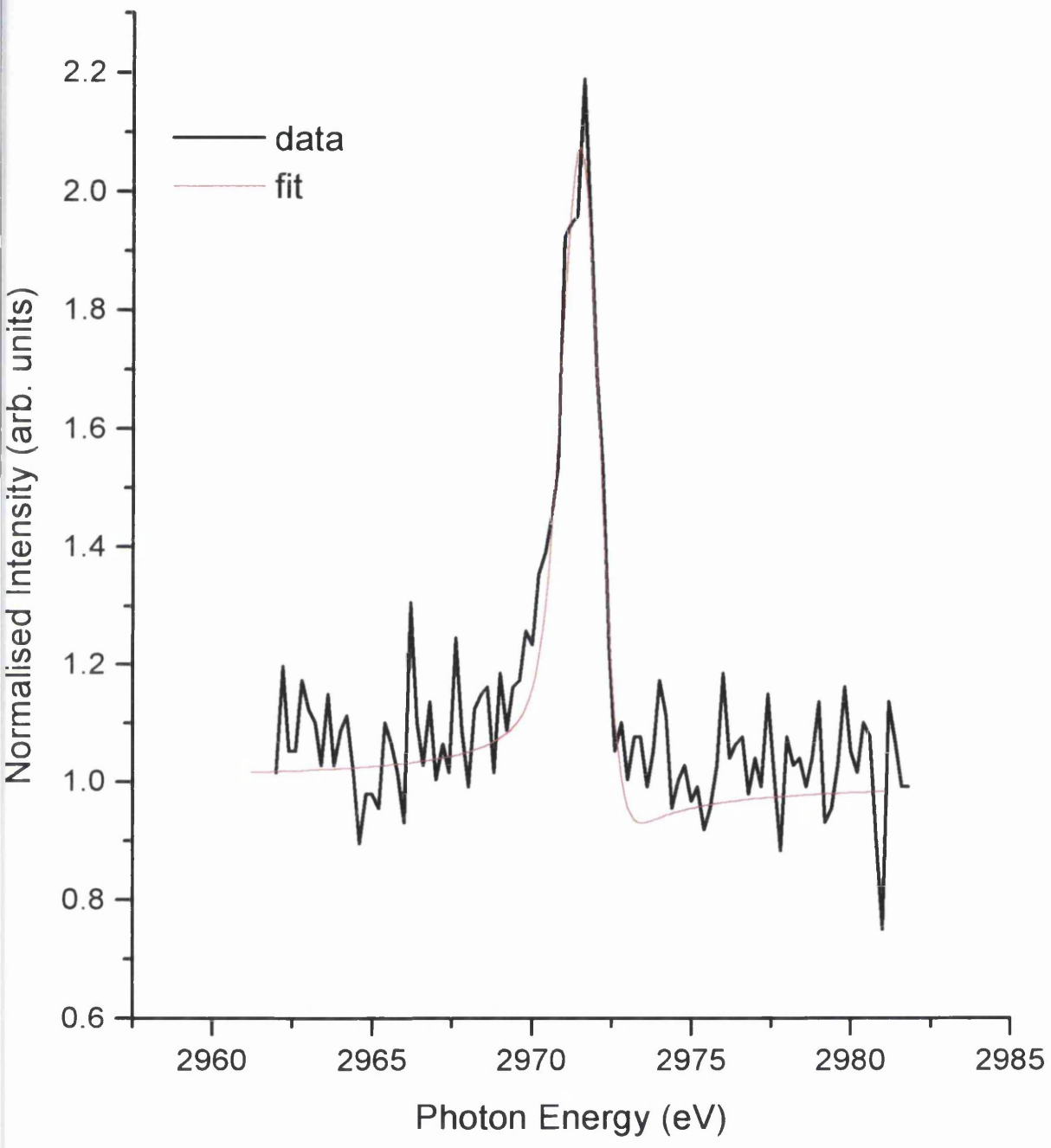

5.2.7 *Cl KLL Adsorbate NIXSW experiments using the annealed dosing method*

Cl KLL NIXSW experiments were performed in an analogous way to S 1s NIXSW experiments in that the surfaces were also prepared by the annealed dosing technique. A summary of the values derived from Cl KLL NIXSW experiments performed at monolayer coverage is shown in table 5. A complete list of the experiments performed is in table 7. Fitted Cl KLL NIXSW data is shown in figures 16 and 17.

From table 5, it is clear that the coherent positions of the S and Cl with respect to the (111) plane are different. This would imply that the heights above the surface of the S and Cl in the adsorbed 3-chlorothiophene are different also. The adsorption site cannot be inferred however from just comparing the coherent positions in the (111) plane, and this is deferred until the "Discussion" section.

The errors shown in table 5 concerning Cl KLL NIXSW data are much larger than the corresponding errors for S 1s NIXSW data because the Cl KLL NIXSW spectra is of much poorer quality.

Figure 16: *Cl KLL NIXSW profile (black) with fit (red) at monolayer coverage with respect to (111) plane, as prepared by the annealed dosing method.*

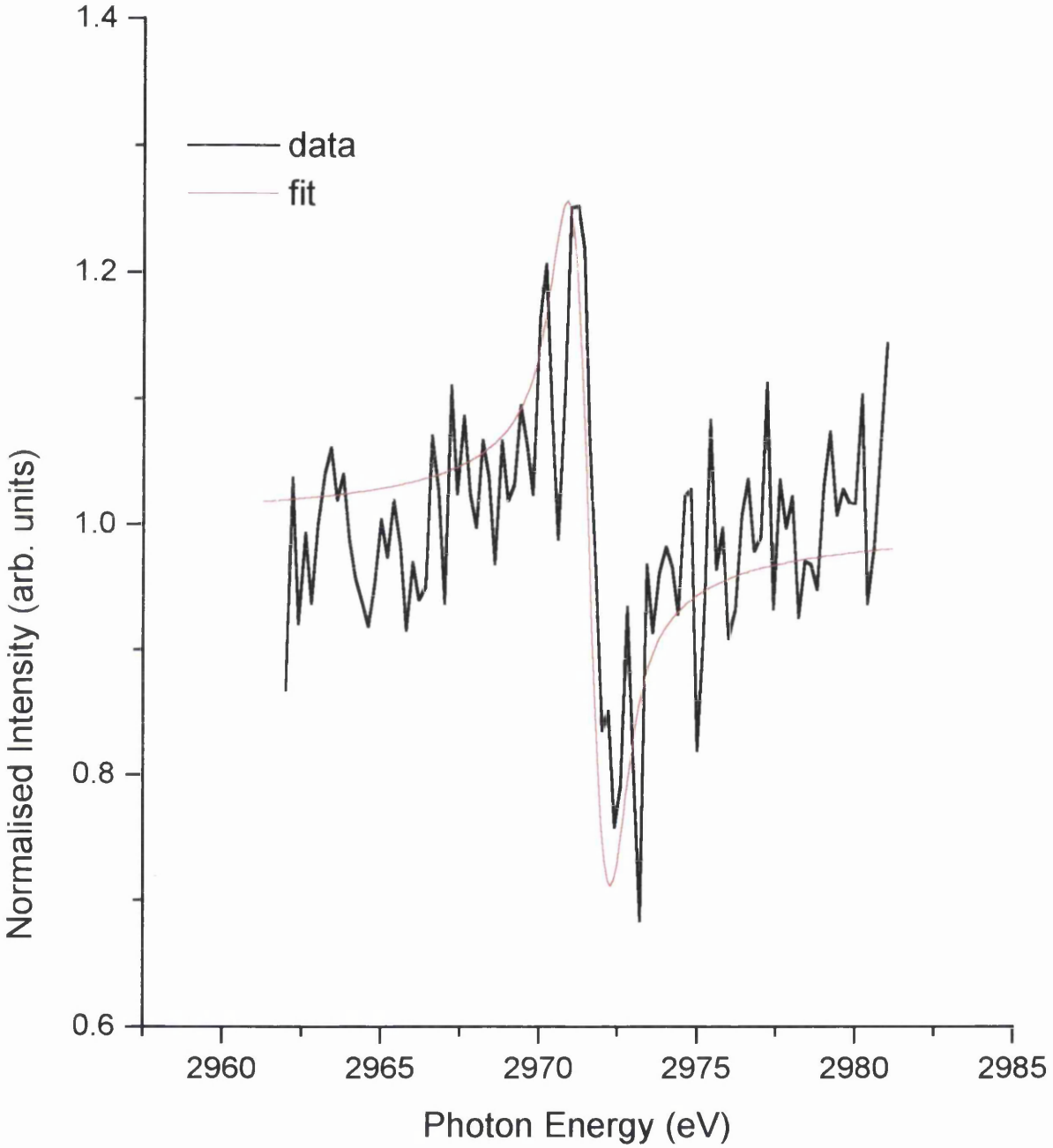

Figure 17: *Cl KLL NIXSW profile (black) with fit (red) at monolayer coverage with respect to ($\bar{1}11$) plane, as prepared by the annealed dosing method.*

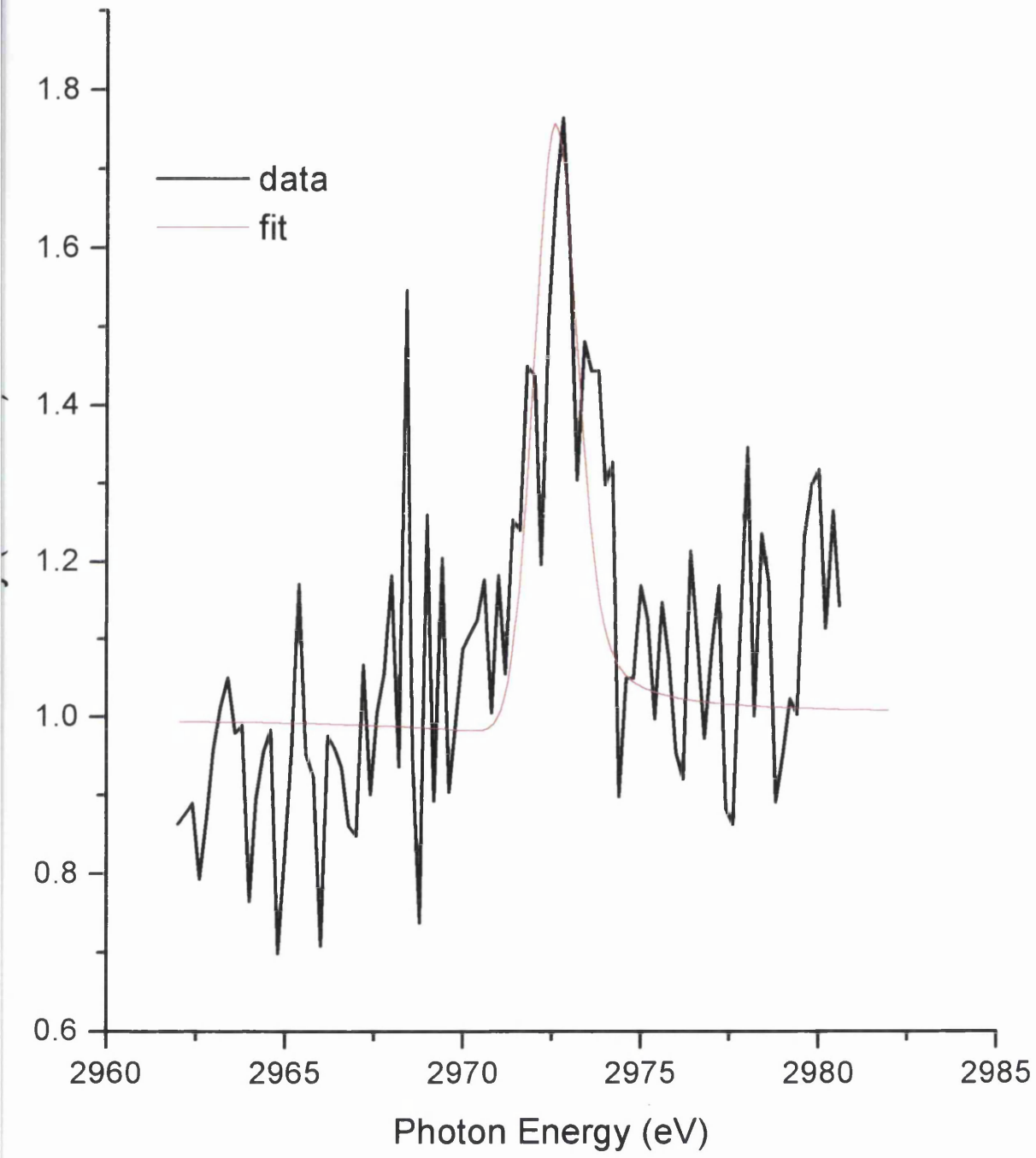

Table 6: *Complete list of S 1s NIXSW experiments at monolayer coverage as prepared by the annealed dosing method.*

Coverage (ML)	Plane	f_{co}	D(hkl) Å	Broadness (eV)
0.07±0.02	(111)	0.90	0.50	0.70
0.07±0.02	(111)	0.90	0.57	0.70
0.11±0.02	(111)	0.70	0.55	0.70
0.12±0.02	(111)	0.80	0.55	0.70
0.09±0.02	($\bar{1}$11)	0.70	0.85	0.70
0.12±0.02	($\bar{1}$11)	0.70	0.77	0.70
0.13±0.02	($\bar{1}$11)	0.55	0.75	0.70

Table 7: *Complete list of Cl KLL NIXSW experiments at monolayer coverage as prepared by the annealed dosing method.*

Coverage (ML)	Plane	f_{co}	D(hkl) Å	Broadness (eV)
0.08±0.02	(111)	0.80	1.43	0.70
0.08±0.02	(111)	0.80	1.43	0.70
0.08±0.02	($\bar{1}$11)	0.30	0.40	0.70
0.09±0.02	($\bar{1}$11)	0.10	0.40	0.70
0.12±0.02	($\bar{1}$11)	0.25	0.40	0.70

5.3 *Discussion*

As in the study of thiophene on Cu(111), the techniques of NIXSW and NEXAFS can be used to provide structural models in order to explain the observed features in TPD data of 3-chlorothiophene on Cu(111). It is clear from figures 1 (a) and (b) that 3-chlorothiophene gives rise to only three desorption features. That is, desorption from defect sites at 287 K, monolayer desorption at 225 K and multilayer desorption at 182 K. Therefore, the presence of the Cl-group at the 3-position on the thiophene ring is prohibiting the gross re-organisation of the molecule in the form of a phase transition.

This is the first surface science study of 3-chlorothiophene on any substrate. However, the current work can be compared and contrasted to previous work concerning the similar molecule chlorobenzene on different substrates. The monolayer peak for 3-chlorothiophene at saturation coverage is at 225 K and the corresponding α-state peak in the case of thiophene is at 211 K, also at saturation coverage. Studies of chlorobenzene on Ag(111)[3] by White *et al.* and Si(111)7x7[4] by Xu *et al.* both show that the desorption temperature of chlorobenzene is 20 K higher than benzene on the corresponding substrates. White *et al.* attribute this temperature difference to the interaction of the Cl-group with the surface but Xu *et al.* attribute it to the electrophilic substitution effect of Cl on the benzene ring. White *et al.* also observed in their TPD study that the monolayer peak moved to lower desorption temperatures by 10 K, as also noted in the TPD study of 3-chlorothiophene. The reason for the difference in the desorption temperatures of 3-chlorothiophene and thiophene on Cu(111) is due to the interaction of Cl on the surface, as the following discussion of the NIXSW data will show. This interaction can also explain why there is significantly less broadening of the monolayer peak when comparing 3-chlorothiophene to thiophene. In the thiophene study it was not possible to ascertain the cause of the broadening and moving to lower desorption temperatures of the α-state peak. It is clear from NEXAFS data, figure 10, that there is no change in orientational angle of 3-chlorothiophene within the monolayer, however, as in the thiophene study, there may be very small changes that are insensitive to the NEXAFS technique. In the islanding model [5] described in Chapter 4, the authors state that the molecules that they studied (thiophene and 2,5-dimethylthiophene) were sufficiently mobile on the surface to

form islands. In the case of 3-chlorothiophene, there is evidence for a surface-Cl interaction and hence 3-chlorothiophene, on initial adsorption, may not be as mobile as thiophene. Instead, the Cl-group would appear to be weakly interacting with the surface, "locking" the orientation of the molecule at an angle of 20±3 °. The addition of more 3-chlorothiophene onto the surface is having no effect on the orientation of pre-adsorbed molecules.

The decomposition of 3-chlorothiophene on Cu(111) can also be explained by the presence of the Cl-group. Figure 1 (a) shows TPD spectra in which the relative amount of desorption from defect sites of 3-chlorothiophene compared to monolayer desorption is considerably less than the case for thiophene. This is because the interaction of the Cl-group is much stronger at defect sites, such as step edges, than with the (111) surface. The bonding of 3-chlorothiophene to defect sites is so strong that either on adsorption or on desorption (heating), the molecule fragments and very few intact 3-chlorothiophene molecules desorb intact from defect sites.

Therefore, a model can be proposed in which on initial exposure, 3-chlorothiophene bonds to the surface with an orientational angle of 20±3 °. Further exposure of 3-chlorothiophene up to saturated monolayer coverage does not change the angle of orientation, as shown by NEXAFS data in figure 10.

5.3.1 Adsorption site determination by real space triangulation

NIXSW experiments were performed on 3-chlorothiophene in order to determine the adsorption sites of both S and Cl at monolayer coverage. NIXSW profiles at monolayer coverage are shown in figures 14-17, and a summary of the values obtained is given in table 5.

The coherent positions with respect to the (111) plane for both S 1s and Cl KLL NIXSW experiments from the fitting procedure do not lead to reasonable Cu-S and Cu-Cl bonded distances. For this reason, as in the analysis of S 1s thiophene NIXSW data, a lattice spacing, 2.08 Å, is added to each of these values and these values are given in table 5 in parenthesis.

NIXSW experiments were performed with respect to two planes, the (111) and ($\bar{1}$11) planes. As outlined in chapter 2, a triangulation method can then be employed that derives D($\bar{1}$11) from D(111) for each of the possible adsorption sites of atop, bridge, f.c.c. and h.c.p. In the case of lower coherent fractions than 0.90±0.05, and the possibility of multiple site occupation, Argand diagrams are used to derive the adsorption site.

5.3.2 Adsorption site determination for S in 3-chlorothiophene at monolayer coverage.

In the case of S 1s NIXSW data at monolayer coverage, using D(111) = 2.62 Å in the above equations gives the following possible values for D($\bar{1}11$) (table 8):

Table 8: *Possible D($\bar{1}11$) and f_{co} values for the four adsorption sites and the experimentally obtained value from S 1s NIXSW experiments at monolayer coverage.*

Site	Atop	Bridge	F.C.C.	H.C.P.	Experimental
D($\bar{1}11$) (Å)	0.87	1.91	2.26	1.57	0.85±0.03
f_{co}	0.90	0.30	0.90	0.90	0.70±0.05

The experimentally derived D($\bar{1}11$) value from ($\bar{1}11$) NIXSW data is 0.85±0.03 Å and the closest match to this is the "atop" site (0.87 Å). As in the thiophene study, the adsorption site is termed "displaced atop" due to the slightly smaller coherent fraction with respect to the ($\bar{1}11$) plane. An Argand diagram representation of how the data best fits to the atop site is shown in figure 18. The lengths and angles of each of the vectors in figure 18 were calculated as described in Chapter 4 and are summarised in table 9.

Table 9: *Length and angle of each vector in figure 18.*

Site	Atop	Bridge	F.C.C.	H.C.P.	Experimental
Vector length (cm)	0.90	0.30	0.90	0.90	0.70
Vector angle (°)	151	331	31	272	147

Figure 18 shows that the nearest fit to the experimental vector (red) is the "atop" vector, thus reinforcing the assignment made by simply matching up the derived D($\bar{1}11$) value for the atop site with the experimental D($\bar{1}11$) value. In the atop geometry, a coherent position with respect to the (111) plane of 2.62 Å means that the Cu-S bond length is also 2.62 Å. This is identical to the value calculated for the Cu-S bond length in thiophene adsorption at α-state coverage, when the surface was prepared by the annealing method. It would appear that putting a substituent Cl- group at the 3-position of the thiophene ring has had no effect whatsoever on the mode of bonding to the surface, in that the molecule bonds in the atop position at monolayer coverage.

Figure 18: *Argand diagram representation of the data listed in table 9. Each angle is given by $2\pi.D(\bar{1}11)/d(111)$ and the length of each vector is given by the magnitude of the corresponding coherent fraction. The experimental data is in red. Not shown to scale.*

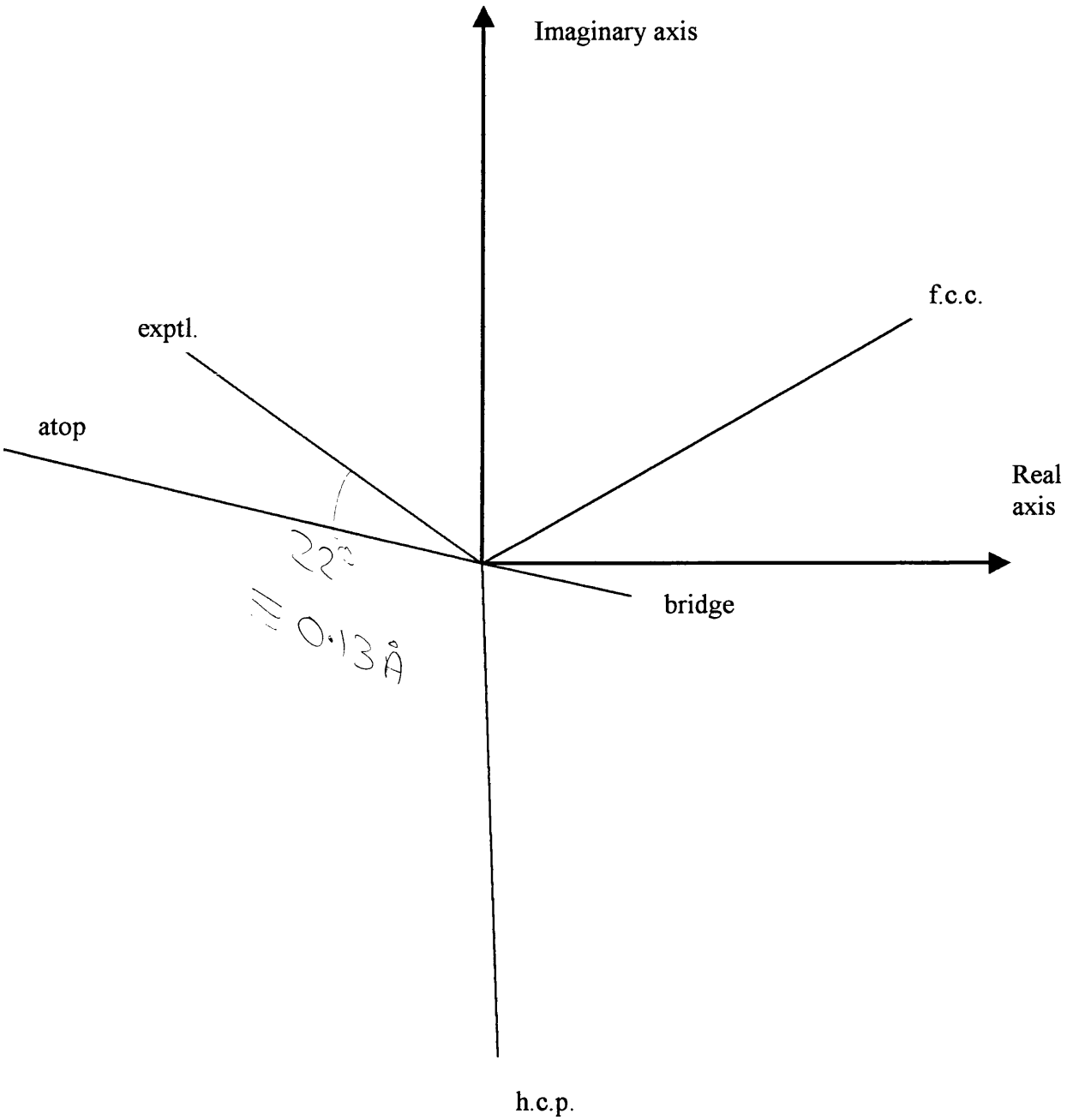

5.3.3 Adsorption site determination for Cl in 3-chlorothiophene at monolayer coverage.

At monolayer coverage, table 10 shows the D($\bar{1}11$) values that can be derived for each of the four adsorption sites, atop, bridge, f.c.c. and h.c.p. in order to ascertain which of these sites is occupied by Cl in 3-chlorothiophene.

Table 10: *Possible D($\bar{1}11$) values for the four adsorption sites and the experimentally obtained value from Cl KLL NIXSW experiments at monolayer coverage.*

Site	Atop	Bridge	F.C.C.	H.C.P.	Experimental
D($\bar{1}11$) (Å)	1.17	2.21	2.56	1.86	0.40±0.15 (2.48±0.15 Å)
f_{co}	0.80	0.27	0.80	0.80	0.20±0.10

The best fit to the experimental value of 2.48±0.15 Å, in which a lattice spacing has been added to the original value for the same reasons as before, is the f.c.c. value of 2.56 Å. However, it is not accurate in this case to say that the f.c.c. site is occupied by Cl at monolayer coverage. The reason for this lies in the very low coherent fraction with respect to the ($\bar{1}11$) plane. This is shown in more detail by an Argand diagram representation of the data in table 10, shown in figure 19.

Table 11: *Length and angle of each vector in figure 19.*

Site	Atop	Bridge	F.C.C.	H.C.P.	Experimental
Vector length (cm)	0.80	0.27	0.80	0.80	0.20
Vector angle (°)	203	23	83	322	69

Figure 19: *Argand diagram representation of the data listed in table 11. Each angle is given by $2\pi.D(\bar{1}11)/d(111)$ and the length of each vector is given by the magnitude of the corresponding coherent fraction. The experimental data is in red. Not shown to scale.*

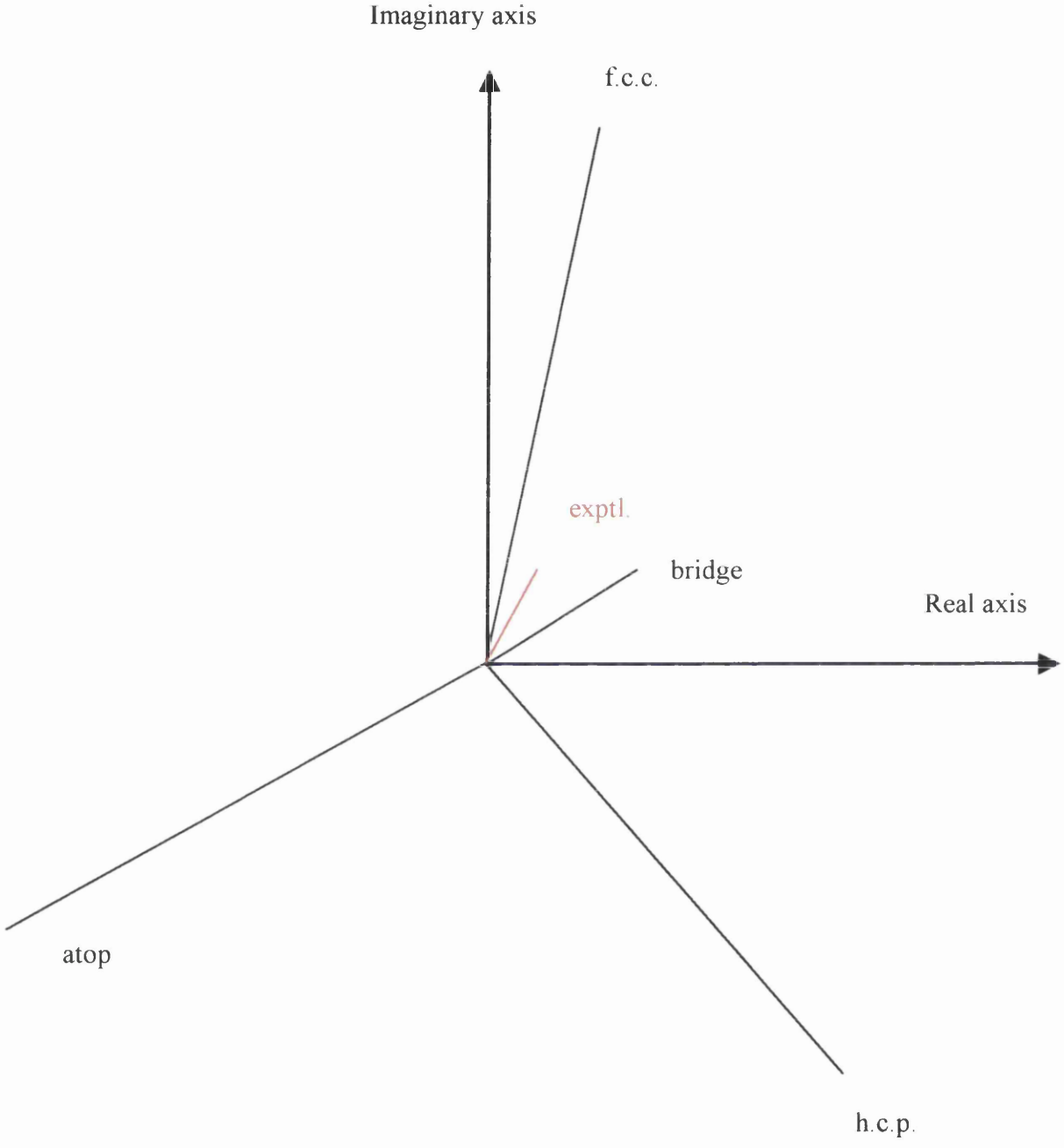

The coherent fraction with respect to the ($\bar{1}11$) plane is 0.2±0.10. In practice this makes it impossible to assign the adsorption site to any unique site because a combination of a number of the vectors in figure 19 matches the experimental vector in red. Figure 19 shows quite clearly the need for Argand diagram analysis of NIXSW data when dealing with low coherent fractions. A low coherent fraction with respect to the ($\bar{1}11$) plane means that there cannot be one single unique adsorption site and in this case, the coherent fraction with respect to the ($\bar{1}11$) plane is so low that it is not possible to state what the adsorption site is.

The coherent fraction with respect to the (111) plane is 0.80±0.10. This means that the coherent position of 3.51±0.15 Å is a well-defined Cu-Cl distance and amounts to a physisorbed Cl group, even if it is not known which adsorption site it is referring to. The sum of the Van der Waal's radii of Cu and Cl is 3.15 Å and this would be expected to be close to a physisorption distance. A NIXSW study of 1-bromo-2-chloroethane on Cu(111) by Jones *et al.*[6] gives a physisorption Cu surface-Cl height of 3.48±0.10 Å. A chemisorption Cu surface-Cl height, from a NIXSW study of Cl on Cu(111) also by Jones *et al.*[7], is 1.88±0.03 Å. By using the bond lengths and angles from a study of 3-chlorothiophene using microwave spectroscopy[8] it is possible to calculate the angle of orientation of the molecule if the Cu-S and Cu-Cl distances are known, assuming molecular planarity on adsorption. A model for the bonding of 3-chlorothiophene can now be proposed based on the NIXSW results (figure 20).

Figure 20: *Adsorption model for 3-chlorothiophene on Cu(111) at monolayer coverage.*

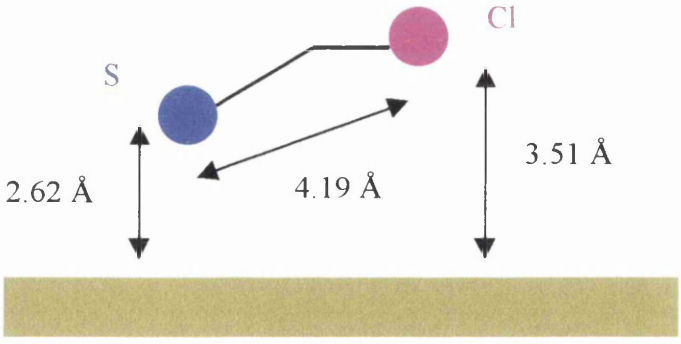

Assuming that the adsorbed 3-chlorothiophene molecule is planar and has the same bond lengths and angles as the microwave spectroscopy study, the tilt angle can be calculated by calculating the S-Cl "cross-molecule" distance of 4.19 Å. The tilt angle in this case is 12±2 °.

NEXAFS data, figure 10, shows that at monolayer coverage the tilt angle is 20±3 °. These two tilt angles, 12±2 ° and 20±3 °, differ by outwith any reasonable experimental error but are both valid tilt angles for the adsorbed molecule. The reason that the two angles are different is because the tilt angle measured by NEXAFS and the tilt angle that can be derived from knowing the S and Cl heights in the adsorbed molecule are not the same if the molecule is twisted about the pseudo-C_{2v} axis (in this case, the pseudo- C_{2v} axis in 3-chlorothiophene is directly analogous to the C_{2v} axis in thiophene). The 3-chlorothiophene molecule bonds to the surface with the S in a slightly displaced atop adsorption site and an orientational angle of 20±3 °. Interaction between the Cl and the surface means that the Cl is pulled toward the surface slightly, thereby twisting the molecule about the pseudo-C_{2v} axis, which remains at 20±3 ° to the surface, and giving an angle of 12±2 ° with respect to the S-Cl "cross molecule" distance. It must be stressed that this model assumes that the molecule remains planar on adsorption.

5.4 Conclusion

The substituent group has an effect on the bonding of 3-chlorothiophene to Cu(111) because it forbids the re-orientation of the molecule as seen in the phase transition evident in the thiophene study. The reason for this is that the Cl-group interacts weakly with the surface but strongly enough to stop further tilting within the monolayer as the coverage is increased, as shown by the NEXAFS results, and certainly prevents any major re-orientation of the molecule as exhibited by thiophene. The angle of orientation calculated at saturated monolayer coverage is 20±3 ° from sequentially dosed experiments and this compares to 25±4 ° in the case of thiophene (sequentially dosed). The adsorption site for 3-chlorothiophene is "displaced atop" with respect to S and the Cu-S bond length is 2.62 Å. This is identical to the thiophene study and as the angle of orientation is within experimental error of the angle of orientation of thiophene at similar coverage, it must be concluded that at monolayer coverage, the presence of Cl- is having little effect on the surface structure of the molecule.

The Cl- group causes a twist of the molecule rather than a tilt, which is a much more subtler re-orientation than a tilt or a complete re-orientation like a phase transition, as probed by the heights of S and Cl at monolayer coverage from NIXSW results. This is due again, to the Cl- group interacting with the surface and pulling the Cl- group nearer to the surface than in the case with thiophene where there is a H- at the 3-position. Primarily at defect sites, the Cl-group causes the dissociation of the molecule, but most of the 3-chlorothiophene molecules, as shown in the TPD and AES results, desorb intact from the surface.

5.5 References

1. W.K. Walter and R.G. Jones, *Journal of Physics – Condensed Matter,* 1989, **1**, SB201-SB202.
2. J. Stöhr, *NEXAFS Spectroscopy,* 1996, pp. 234-237.
3. X. –L. Zhou and J.M. White, *Journal of Chemical Physics,* 1990, **92** (9), 5612-5621.
4. Y. Cao, J.F. Deng and G. Q. Xu, *Journal of Chemical Physics*, 2000, **112** (10), 4759-4767.
5. X. Chen, E.R. Frank and R.J. Hamers, *Journal of Vacuum Science and Technology B*, 1996, **14** (2), 1136-1140.
6. M.F. Kadodwala, A.A. Davis, G. Scragg, B.C.C. Cowie, M. Kerkar, D.P. Woodruff and R.G. Jones, *Surface Science,* 1997, **392**, 199-211.
7. D.P. Woodruff, D.L. Seymour, C.F. McConville, C.E. Riley, M.D. Crapper, N.P. Prince and R.G. Jones, *Physical Review Letters*, 1987, **58** (14), 1460-1462.
8. W. Caminati, B. Velino, F. Caccinelli, R.S. Cataliotti, S.M. Murgia, G. Paliani and A. Santucci, *Journal of Molecular Structure*, 1998, **174**, 285-290.

Chapter 6. The adsorption of 3-methylthiophene and 3-methoxythiophene on Cu(111)

6.1. Introduction

The adsorption of both 3-methoxythiophene and 3-methylthiophene on Cu(111) was studied using the techniques of TPD, AES, XPS, LEED, NIXSW and NEXAFS. In the case of 3-methylthiophene, TPD results show evidence for desorption from monolayer, multilayer and defect sites and in the case of 3-methoxythiophene there is evidence for desorption from multilayer and monolayer sites and very little desorption from defect sites. As with the 3-chlorothiophene study, there was no β-state-like peak present in the TPD data of either molecule. NIXSW data showed that the adsorption site at monolayer coverage for both molecules was found to be displaced atop using the annealed dosing method. NEXAFS data showed that the angle of orientation at monolayer coverage for 3-methylthiophene is 24±4 ° and for 3-methoxythiophene is 26±4 °.

6.2 Results

6.2.1 Initial characterisation of 3-methylthoiphene

3-methylthiophene undergoes reversible molecular adsorption on Cu(111) as shown by the AES spectra in figures 1 (a) and (b). Figure 1 (a) shows S AES spectra taken both before and after TPD experiments. The post-TPD data (red) was collected after seven adsorption/desorption cycles that are represented by the TPD data shown in figure 2 (a). The absence of any features in the post-TPD spectrum in figure 1 (a) over the K.E. range 140-160 eV shows that no S is present on the surface after desorption, inferring that 3-methylthiophene desorbs molecularly. Figure 1(b) shows C AES spectra taken both before and after TPD experiments. As there is no evidence for S on the surface after TPD experiments, there cannot be any decomposition of 3-methylthiophene.

Figure 1(a): *S LVV AES spectra taken before (red) and after (black) TPD experiments of 3-methylthiophene. The lack of any feature over the kinetic energy range, 140-160 eV in the red data shows that after TPD experiments, there is no S present on the surface.*

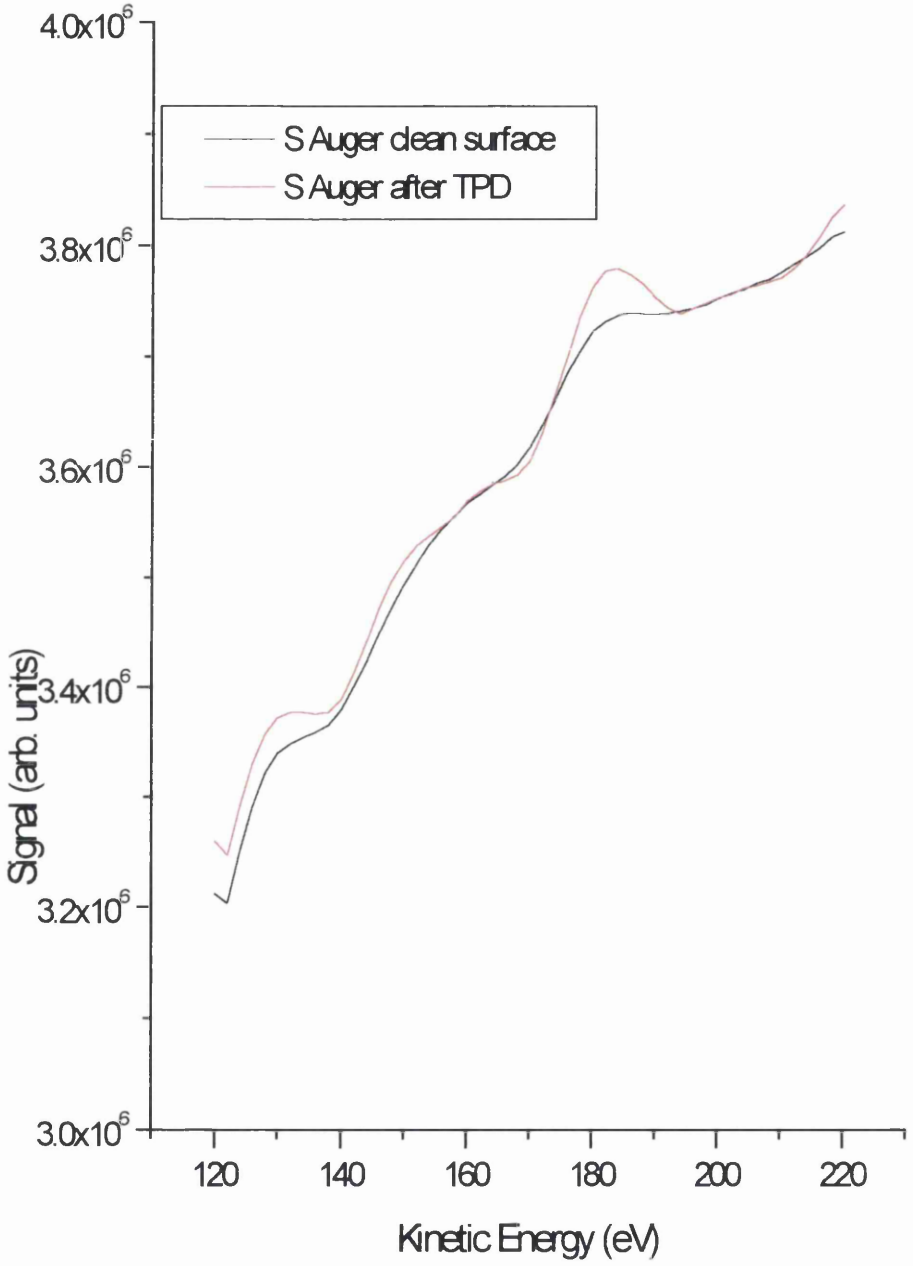

(b): *C KLL AES spectra taken before (red) and after (black) TPD experiments of 3-methylthiophene. As outlined in Chapter 4, the red data represents a surface clean of C contamination.*

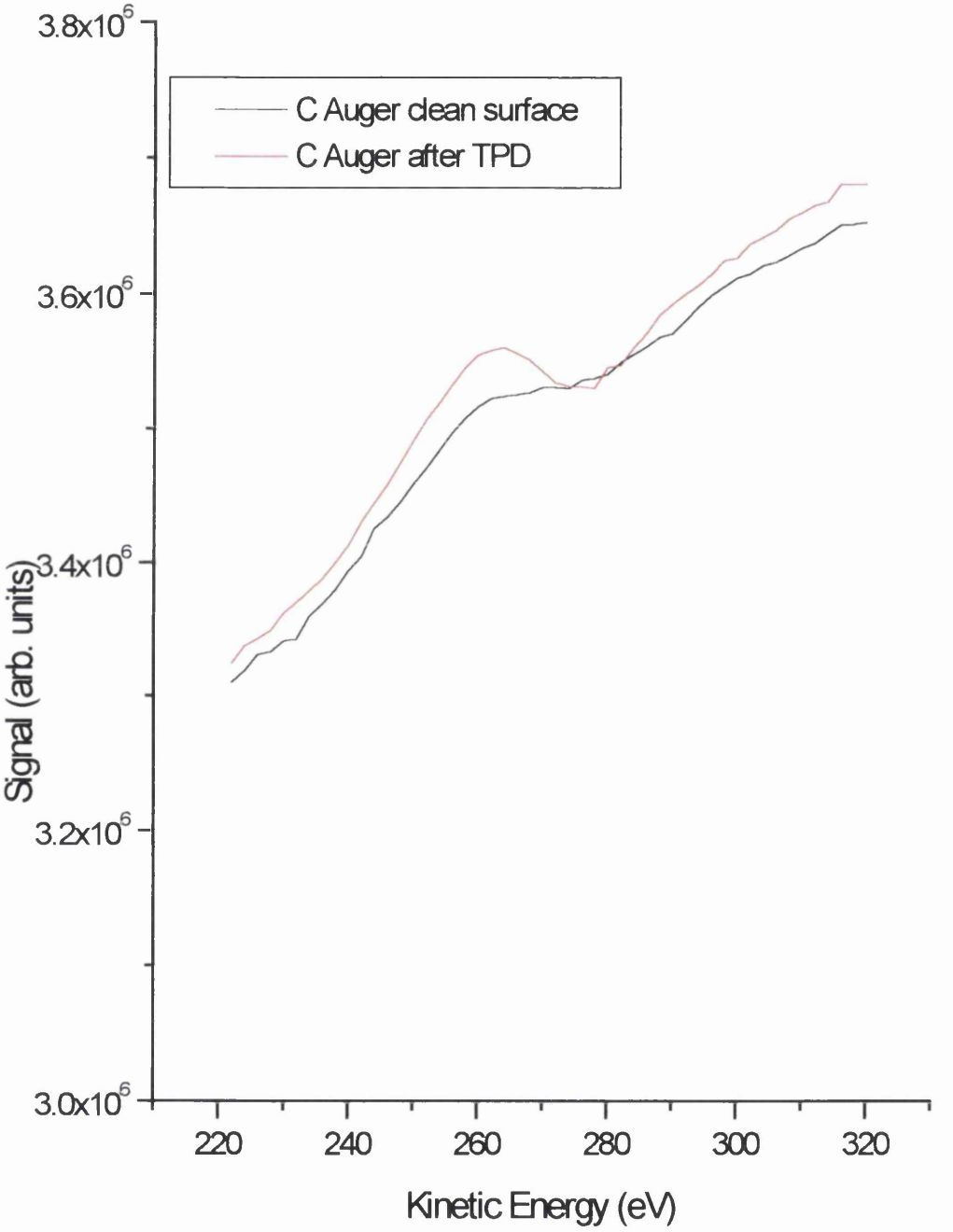

The feature present in figure 1(b) at 260-280 eV in the red data is caused by secondary electrons[1], as noted in Chapter 4 (thiophene), and is temperature dependent. As there is no adsorbed S on the surface and no adsorbed C on the surface after desorption, it can be concluded that the desorption of 3-methylthiophene is molecular and reversible.

Figures 2 (a) and (b) show TPD spectra of 3-methylthiophene. In figure 2 (a), the heating rate used was 1.5 K s^{-1} and in figure 2 (b) it was 0.5 K s^{-1}. Figure 2 (a) shows that, with increasing exposure, using the back-filling dosing method, two desorption states are populated. The data at an exposure of $6x10^{-7}$ mbar.s (black) exhibits two main features, one at 265 K and one at 318 K. The feature at 318 K, within the noise level of the data, saturates at an exposure of $6x10^{-7}$ mbar.s. This feature at 318 K can be assigned to desorption of 3-methylthiophene from defect sites. This assignment was made by comparing the feature at 318 K with figure 3 in Chapter 4. The feature present at 265 K increases in intensity with increasing coverage, moves to a lower desorption temperature and becomes significantly broader. At the highest exposure shown, $5.4x10^{-6}$ mbar.s, the feature has moved to 235 K. This desorption feature is analogous to the α-state feature in the thiophene study. Due to the absence of any β-state-like feature it will be referred to as representing monolayer desorption.

Figure 2 (b) shows TPD data collected from surfaces with substantially higher coverages, that were prepared using the line-of-sight dosing technique. The data at an observed exposure of $1.8\pm0.3x10^{-7}$ mbar.s (red, figure 2 (b)) represents desorption from a saturated monolayer of 3-methylthiophene. It is clear that the feature at 168 K that does not saturate with increasing exposure, represents multilayer desorption.

Figure 2: *TPD spectra of 3-methylthiophene on Cu(111). Spectrum (a) shows data collected using the "back-filling" method and spectrum (b) shows data collected using the "line-of-sight" method.*

(a)

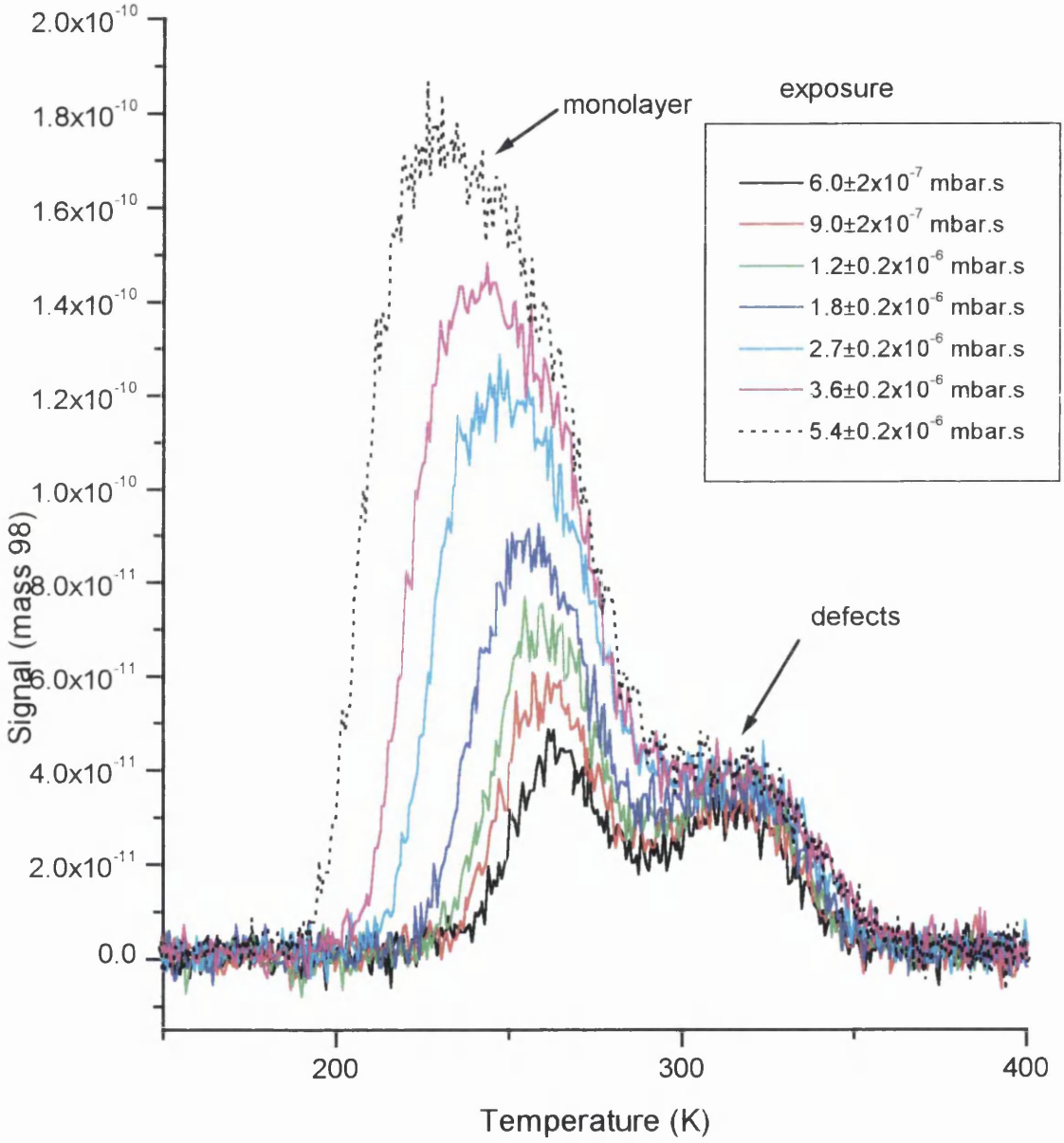

(b)

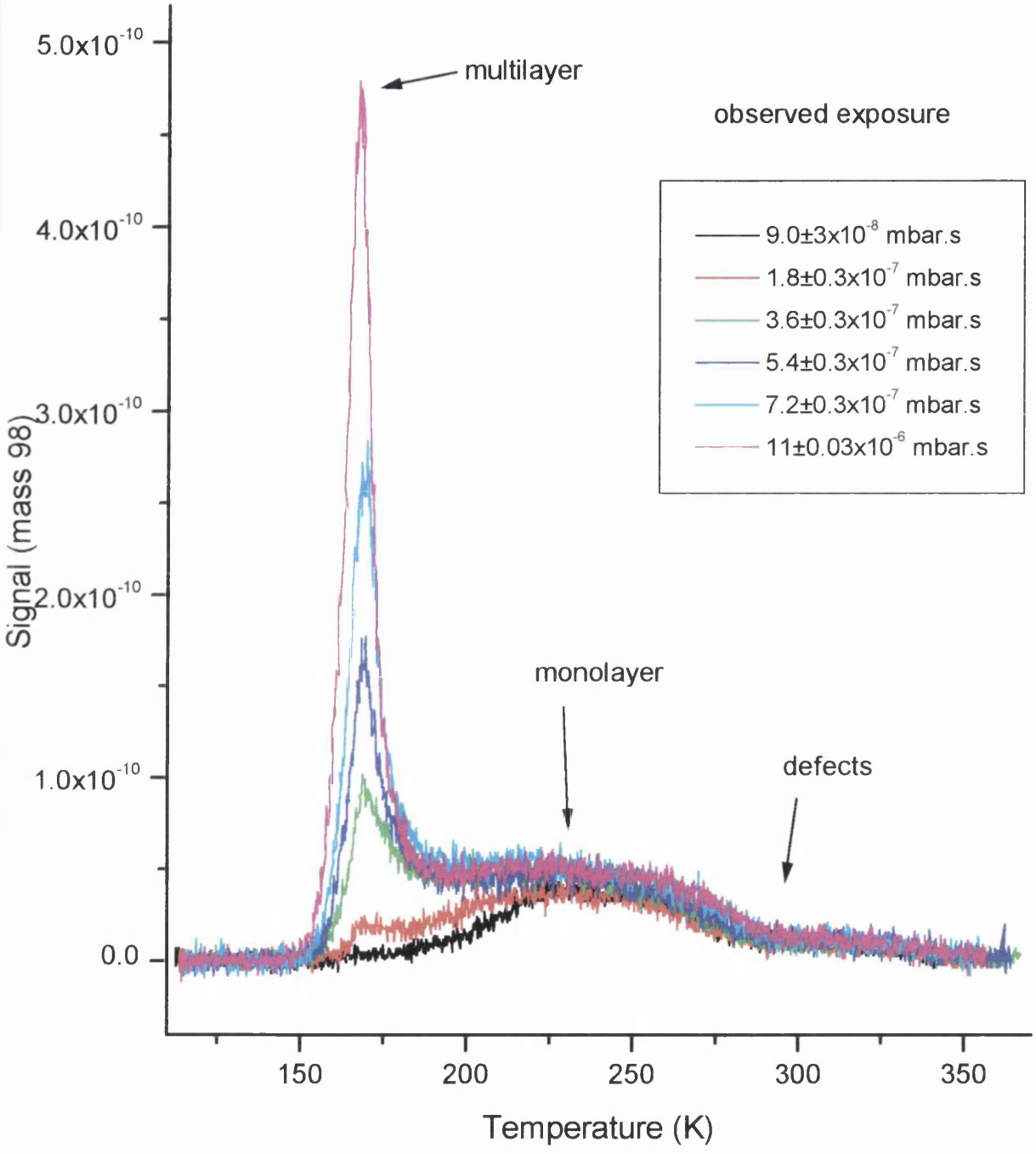
5.0x10-10
4.0x10-10
3.0x10-10
2.0x10-10
1.0x10-10
0.0
Signal (mass 98)
multilayer
monolayer
defects
observed exposure
9.0±3x10-8 mbar.s
1.8±0.3x10-7 mbar.s
3.6±0.3x10-7 mbar.s
5.4±0.3x10-7 mbar.s
7.2±0.3x10-7 mbar.s
11±0.03x10-6 mbar.s
150
200
250
300
350
Temperature (K)

Figure 3 shows a plot of the area under each TPD spectrum in figure 2 (a) plotted against dosing time. The linear relationship represents a constant sticking co-efficient for 3-methylthiophene.

The coverage of a saturated monolayer of 3-methylthiophene was calculated in an identical manner to that described in Chapter 4. Figure 4 shows a S AES monolayer spectrum plotted with a S AES spectrum collected from a ($\sqrt{7}$x$\sqrt{7}$R19.1°)-S surface. Analysis of the peak heights shows that a monolayer of 3-methylthiophene has a coverage of 0.11±0.03 ML.

LEED was used to detect the presence of any long range ordered structures of 3-methylthiophene on Cu(111), but no structures were found at any coverage.

At the Daresbury Laboratory, each surface prepared was subjected to XPS analysis and the coverage of each surface was determined as described in Chapter 4. Experiments were performed in which multilayers were formed at 100 K. The crystal was then annealed in 20 K increments to 240 K and after each 20 K anneal, XPS data was collected. Figure 5 shows that there is a significant drop in the area under XPS spectra between 140-160 K. This is due to multilayer desorption occuring when the crystal is annealed from 140-160 K. TPD data from Glasgow however, shows that multilayer desorption occurs at 168 K. Figure 5 shows essentially the same information as the TPD data except that the temperatures do not exactly match up. This anomaly in the thermocouple readings is not a problem however, because AES data at Glasgow shows that the saturated monolayer coverage is 0.11±0.03 ML. All surface studied at Daresbury were subjected to XPS analysis, so all surfaces studied at Daresbury can be represented in terms of ML also.

Figure 3: *Integrated areas for each of the TPD spectra shown in figure 2 (a). The linear relationship indicates a constant sticking co-efficient for 3-methylthiophene.*

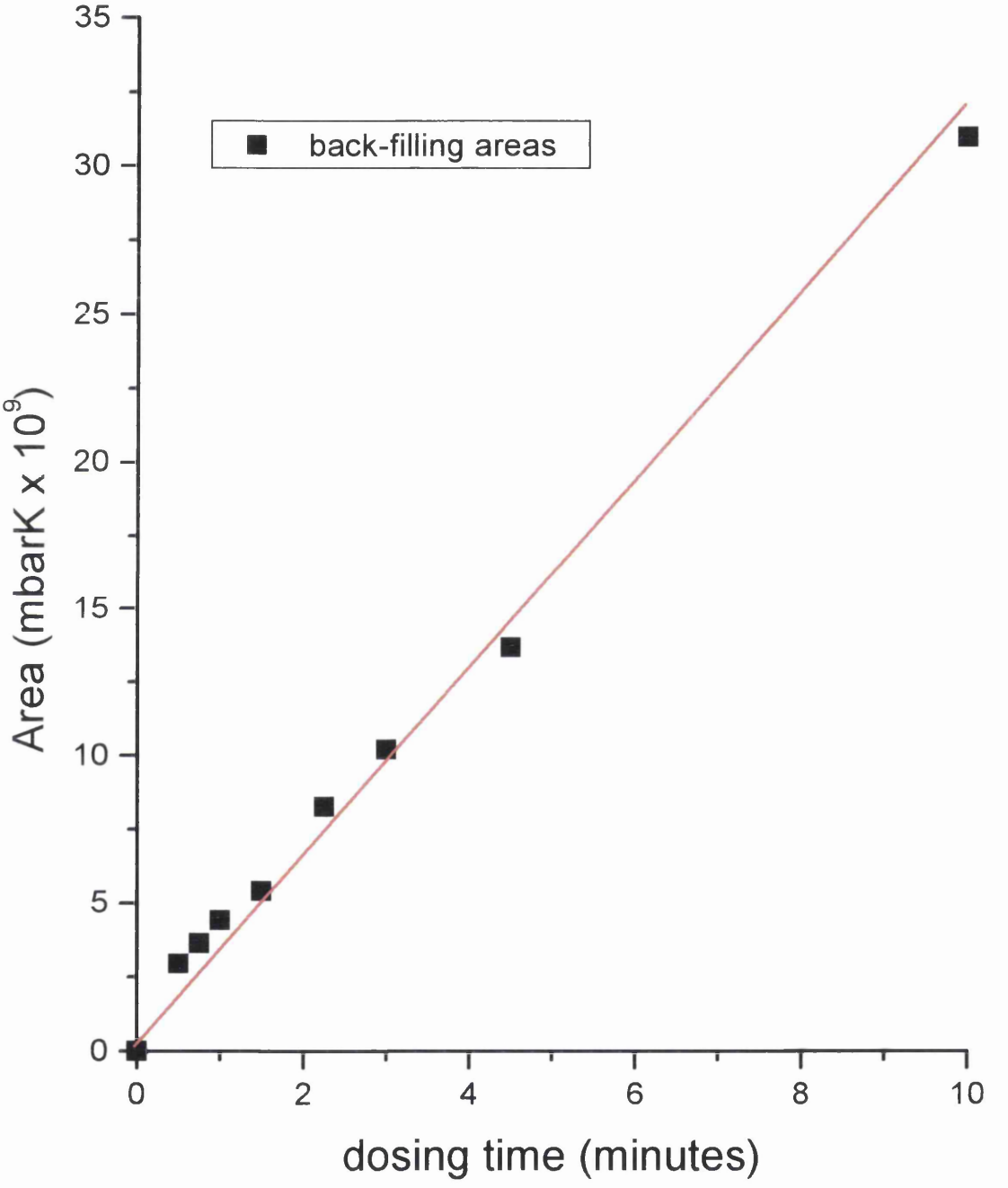

Figure 4: *Plot showing S AES from monolayer coverage (red) and a (√7x√7R19.1°)-S surface (black). The data shown has been divided by the corresponding Cu AES intensity and normalised for ease of comparison. Analysis of the peak heights shows that a monolayer of 3-methylthiophene has a coverage of 0.11±0.03 ML.*

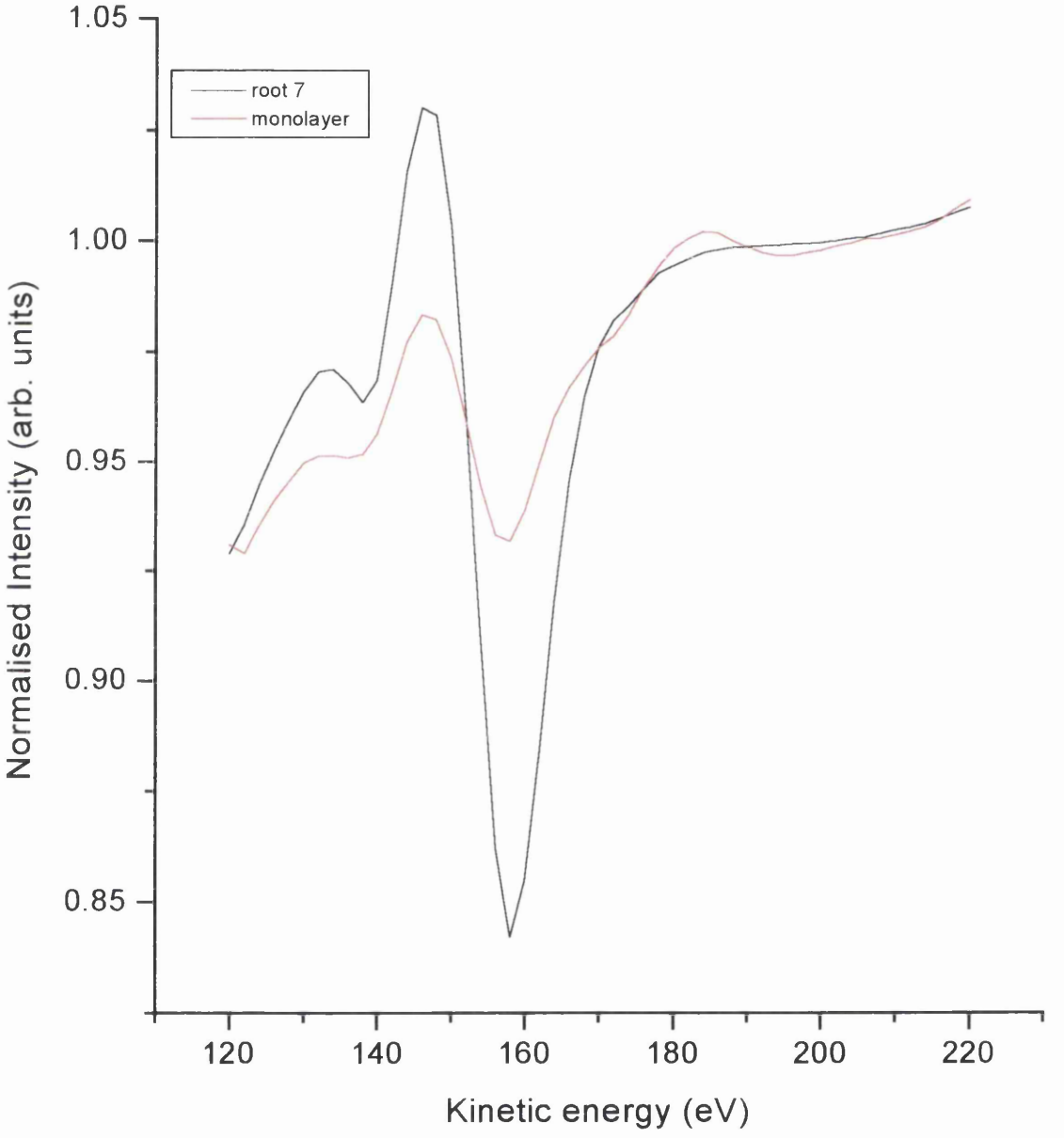

Figure 5: *Area under XPS spectra at 20 K intervals from 100-240 K.*

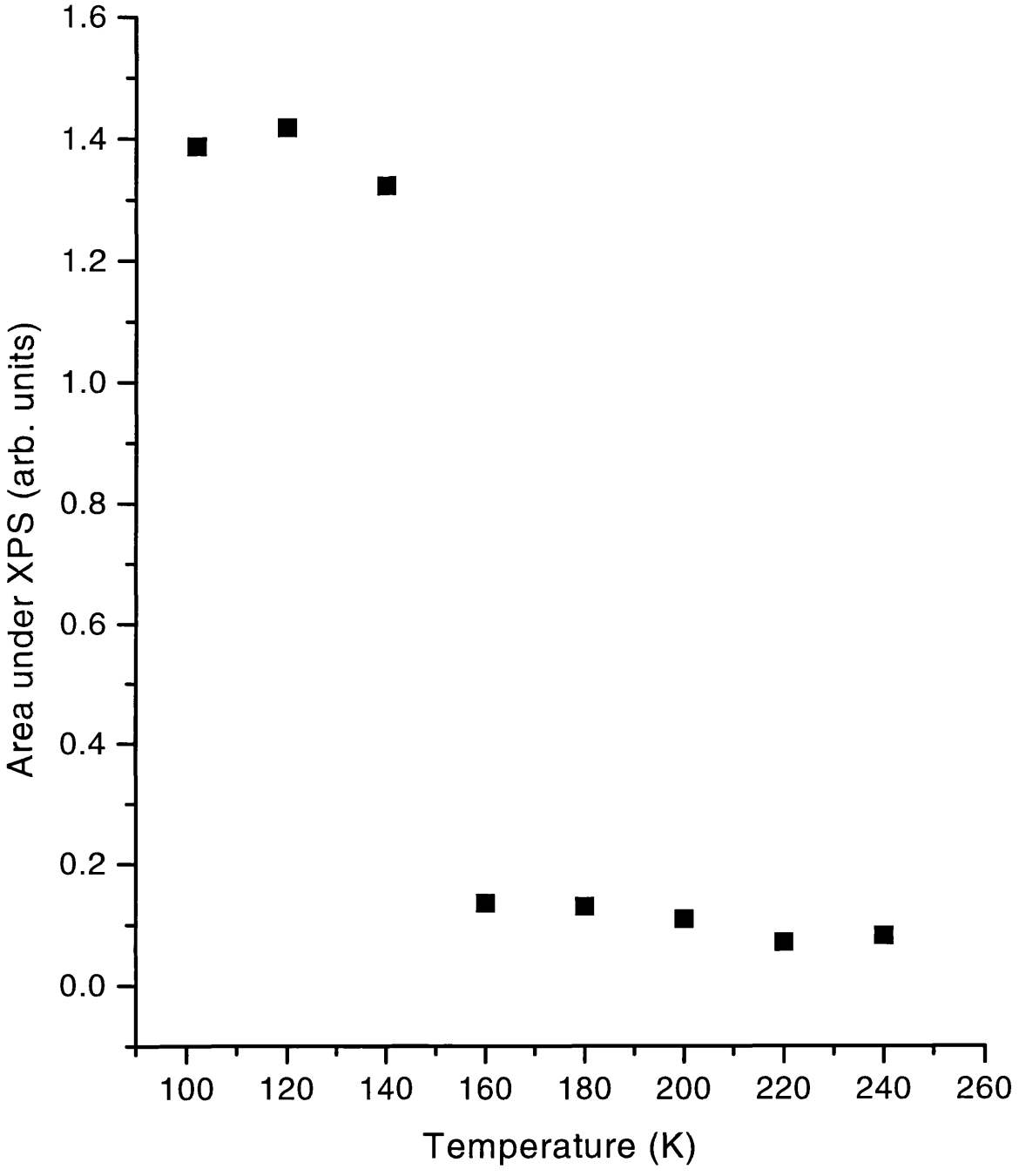

6.2.2 Initial characterisation of 3-methoxythiophene

Figures 6 (a) and (b) show TPD data collected for 3-methoxythiophene. In both cases, the line-of-sight dosing technique and a heating rate of 0.5 $degs^{-1}$ was used. Figure 6 (a), ($6x10^{-7}$ mbar.s exposure (black)) shows evidence of desorption from two desorption states. The first of these is at 325 K, and as in the case of 3-methylthiophene, can be assigned to desorption from defect sites, although within the noise level of the data, there is very little desorption from defect sites. The other feature in the black data in figure 6 (a) is at 255 K and can be assigned to desorption from a monolayer state. Desorption from a saturated monolayer state occurs at an initial exposure of $7.2x10^{-6}$ mbar.s (green data) where the T_{max} is 251 K. At an exposure of $9.6x10^{-6}$ mbar.s (blue data), a small shoulder is evident at 195 K. At an exposure of $1.4x10^{-5}$ mbar.s (pink data) and from an inspection of figure 6 (b), it is clear that the shoulder at 195 K in the blue data, which becomes a separate peak at 181 K in the pink data, represents the formation of multilayers. Figure 6 (b) shows TPD data collected from surfaces with significantly higher coverages. It shows that not only does the multilayer peak at 181 K observed in figure 6 (a) not saturate, it splits into three distinct peaks at 180, 186 and 196 K respectively. This may be due to the presence of three distinct isomers of 3-methoxythiophene, s-cis, gauche and s-trans[2] in the multilayer that all have slightly different inter-molecular interactions and hence, slightly different desorption temperatures. Figure 7 shows a plot of the area of TPD spectra versus dosing time for the data shown in figure 6 (a). The linear relationship shown represents a constant sticking co-efficient for 3-methoxythiophene.

The reduced desorption from defect sites shown in figure 6 (a) is similar to figure 1 (a) in Chapter 5 (3-chlorothiophene). The reason for this in the case of 3-chlorothiophene was that there was a small amount of dissociation, particularly at defect sites. Figures 8 (a) and (b) show C and S AES spectra from before and after a desorption experiment where a surface representing a monolayer coverage was prepared. Figure 8 (a) shows quite clearly that C is left on the surface after desorption due to the feature at 261-276 eV in the post-TPD (red) spectrum.

Figure 6: *TPD spectra of 3-methoxythiophene on Cu(111). Both spectra (a) and (b) were prepared using the "line-of-sight" method.*

(a)

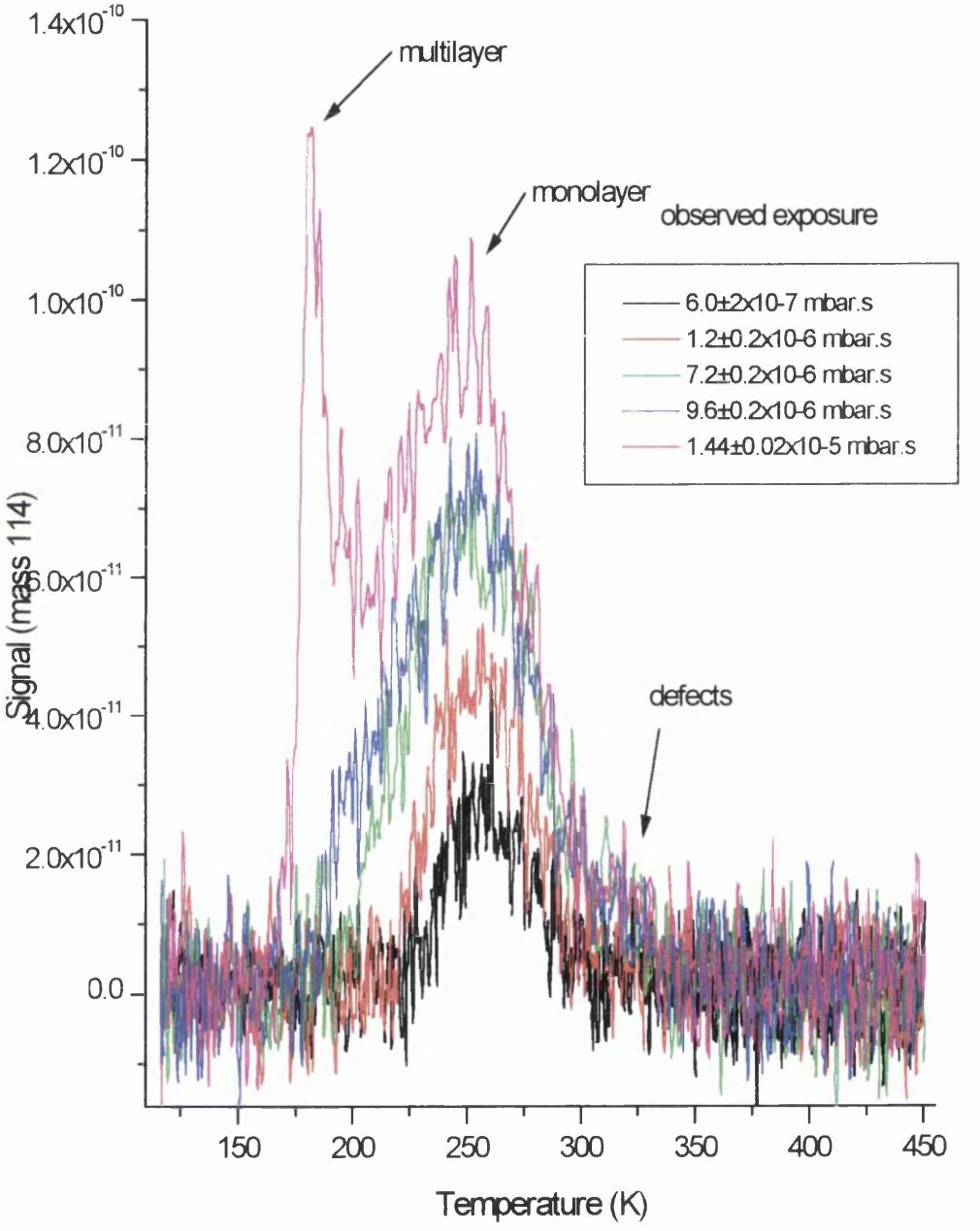

(b)

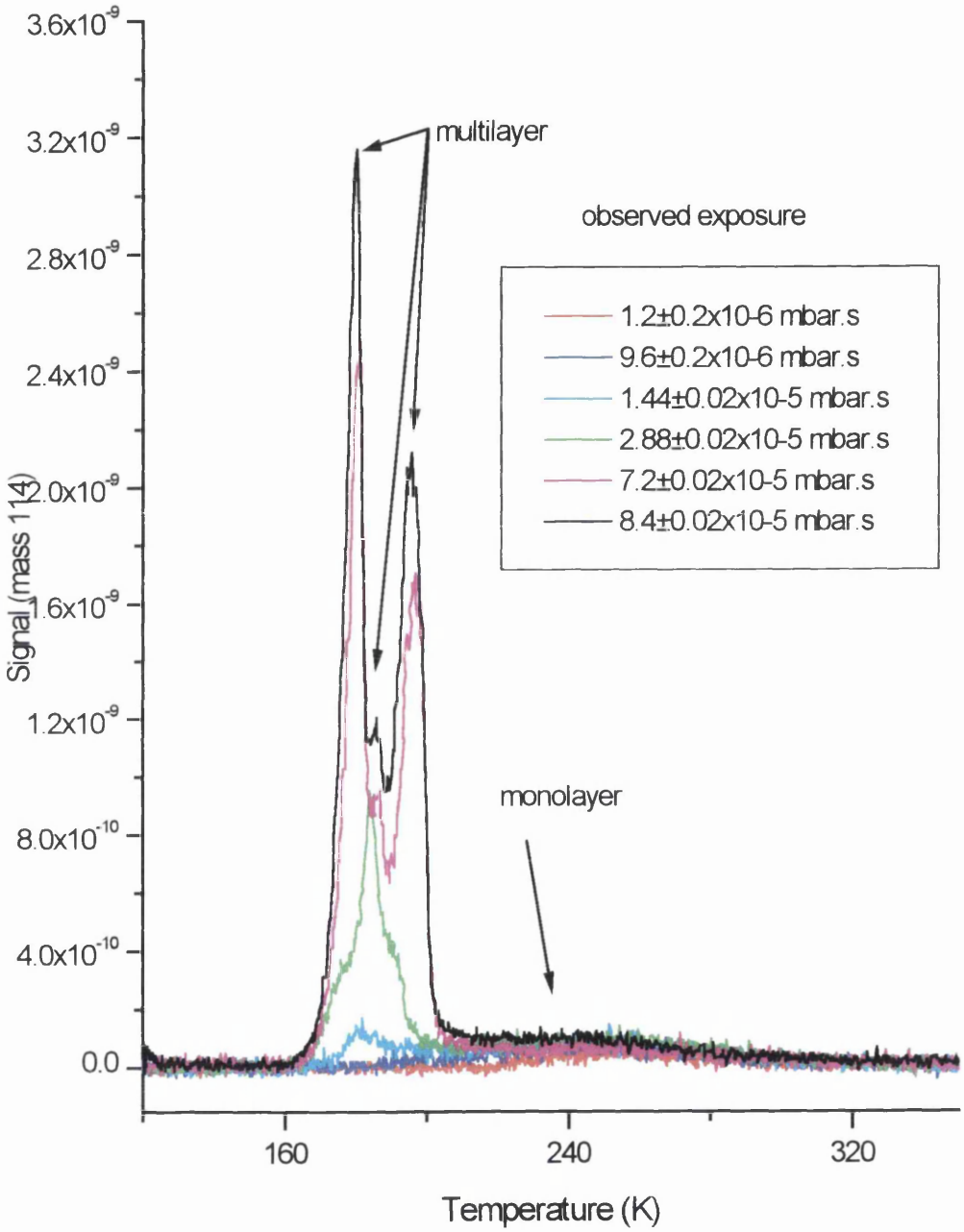
3.6x10-9
3.2x10-9
2.8x10-9
2.4x10-9
2.0x10-9
1.6x10-9
1.2x10-9
8.0x10-10
4.0x10-10
0.0
Signal (mass 114)
160
240
320
Temperature (K)
multilayer
monolayer
observed exposure
1.2±0.2x10-6 mbar.s
9.6±0.2x10-6 mbar.s
1.44±0.02x10-5 mbar.s
2.88±0.02x10-5 mbar.s
7.2±0.02x10-5 mbar.s
8.4±0.02x10-5 mbar.s

Figure 7: *Integrated areas for each of the TPD spectra shown in figure 6 (a). The linear relationship represents a constant sticking co-efficient for 3-methoxythiophene.*

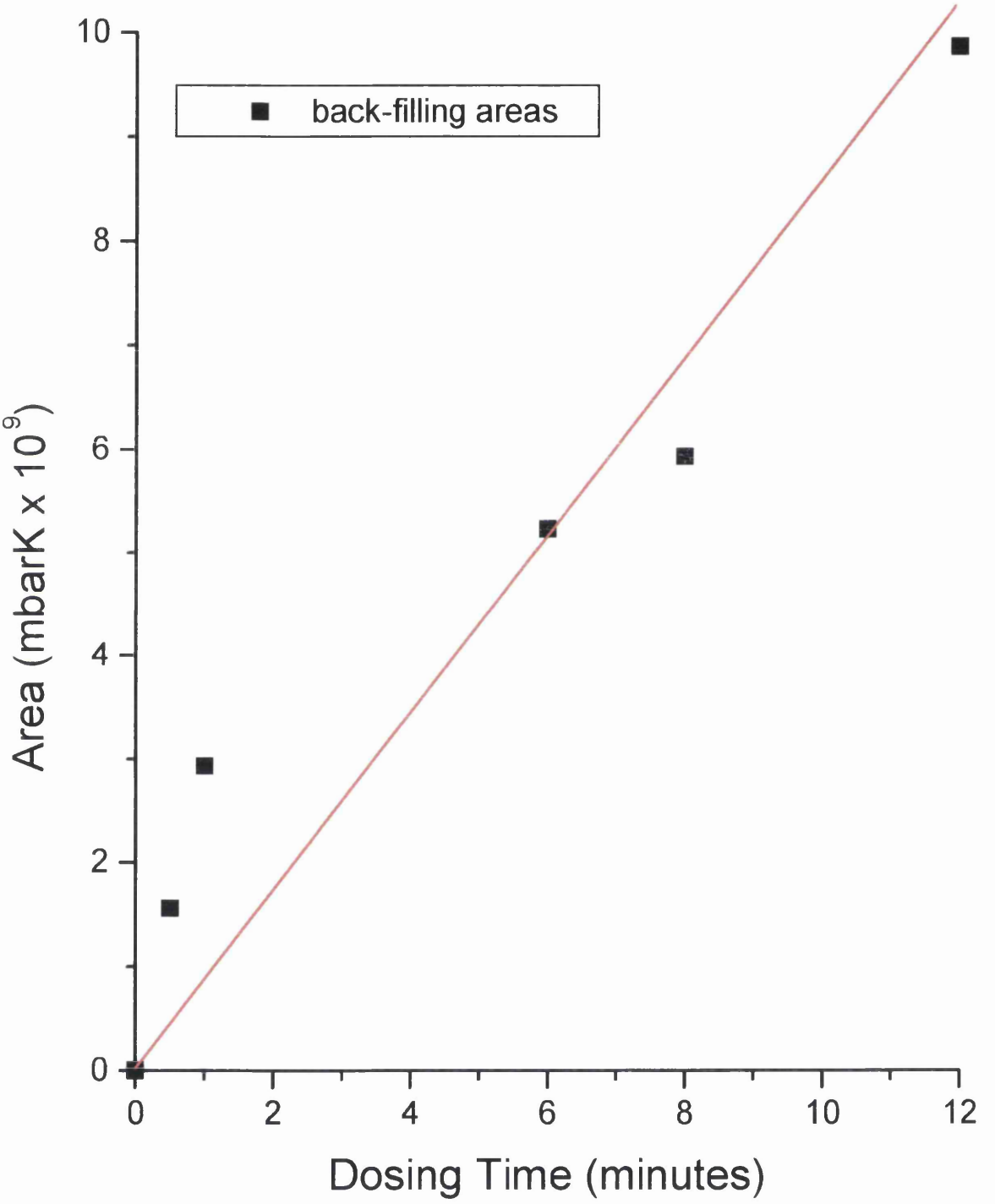

Figure 8(a): *C KLL AES spectra taken before (black) and after (red) TPD experiments. The feature present in the red spectrum at 261-276 eV shows that there is C on the surface after desorption of 3-methoxythiophene.*

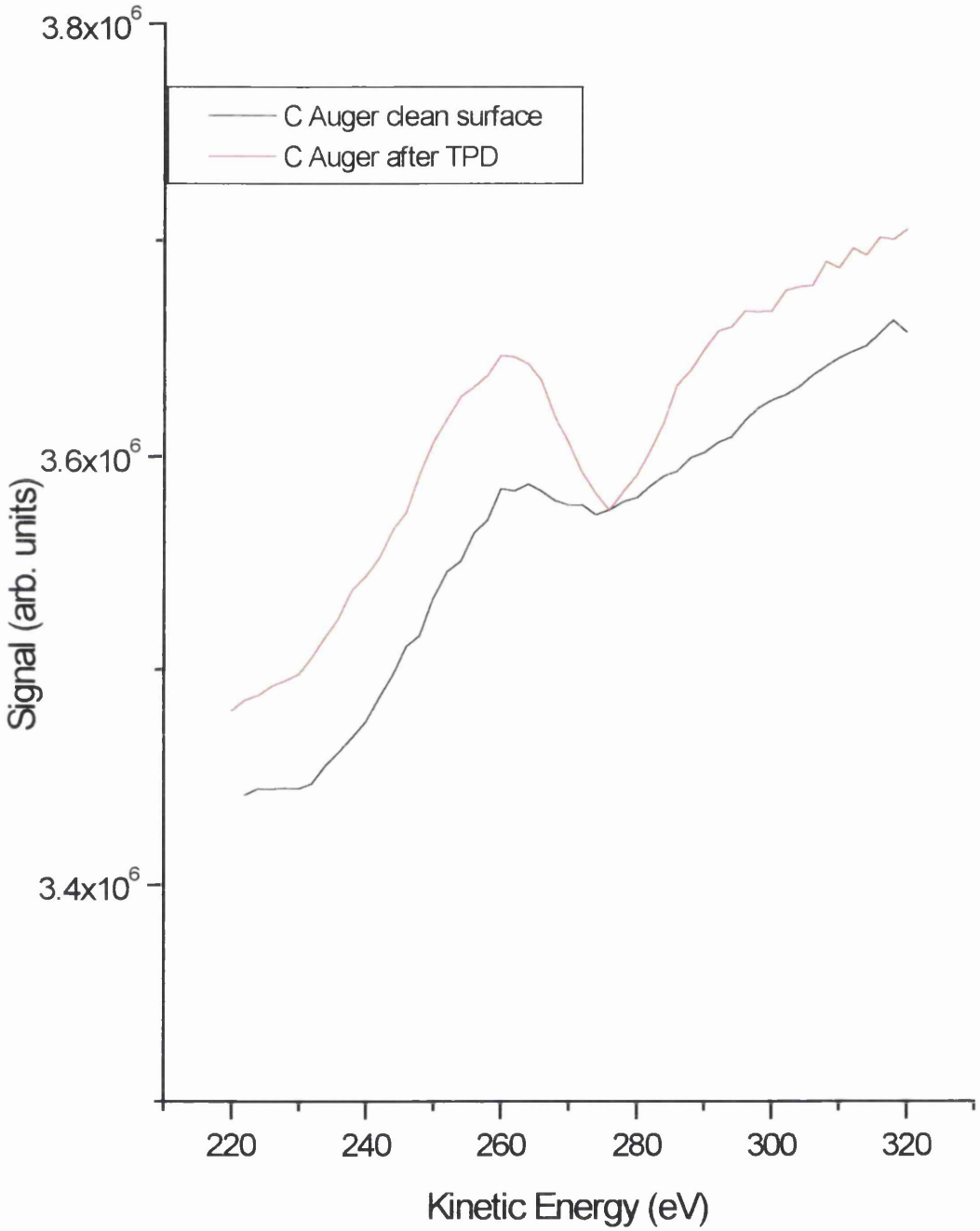

Figure 8(b): *S LVV AES spectra taken before (red) and after (black) TPD experiments. The feature present in the red spectrum at 149-156 eV shows that there is S present on the surface after desorption of 3-methoxythiophene.*

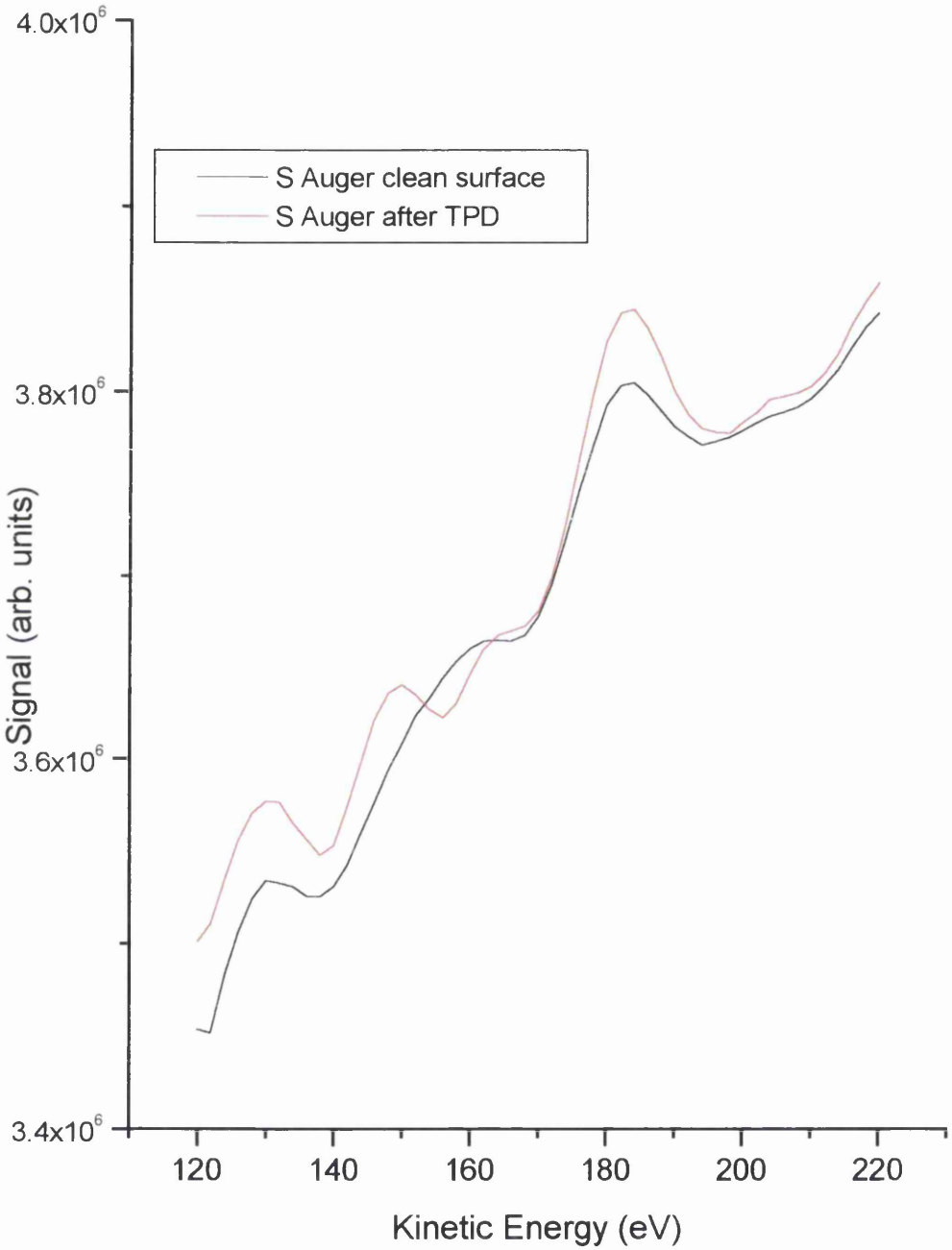

Figure 8 (a) also shows the clear difference between a clean surface (black data) and a surface contaminated with C. Although a feature is present in the clean surface spectrum, as detailed previously[1], this is not due to C contamination.

Figure 8 (b) shows that S is also present on the surface due to the feature at 149-156 eV. The presence of both S and C on the surface after desorption indicates that 3-methoxythiophene decomposes on the surface to leave S and C fragments. No H or any organic fragments could be detected by the QMS desorbing from the surface, indicating both that the amount of desorption is very small and that the fragments that are left on the surface after decomposition are very strongly bound to the surface.

The coverage, in ML, of both the saturated monolayer coverage of 3-methoxythiophene and of the amount of decomposition was calculated as described in Chapter 4. Figure 9 shows S AES spectra of a saturated monolayer (red) and a ($\sqrt{7}$x$\sqrt{7}$R19.1°)-S surface (black). From figure 9, the coverage of a saturated monolayer of 3-methoxythiophene is 0.12±0.03ML. Figure 10 shows S AES from a surface in which a monolayer coverage was prepared and then desorbed (blue data). This data, labelled "decomposition" is shown with the monolayer data from figure 4 (black). From figure 10, the amount of decomposition of 3-methoxythiophene corresponds to 0.02 ML.

LEED was used in order to determine if 3-methoxythiophene formed any structures with long-range order at monolayer coverage, but no structures could be detected by LEED at this, or any other coverage. Similarly, LEED was used to determine whether the decomposition products formed any structures with long range order, but no structures could be detected.

Figure 9: *Plot showing S AES from monolayer coverage (red) and a (√7x√7R19.1°)-S surface (black). The data shown has been divided by the corresponding Cu AES intensity and normalised for ease of comparison. Analysis of the peak heights shows that a monolayer of 3-methylthiophene has a coverage of 0.12±0.03 ML.*

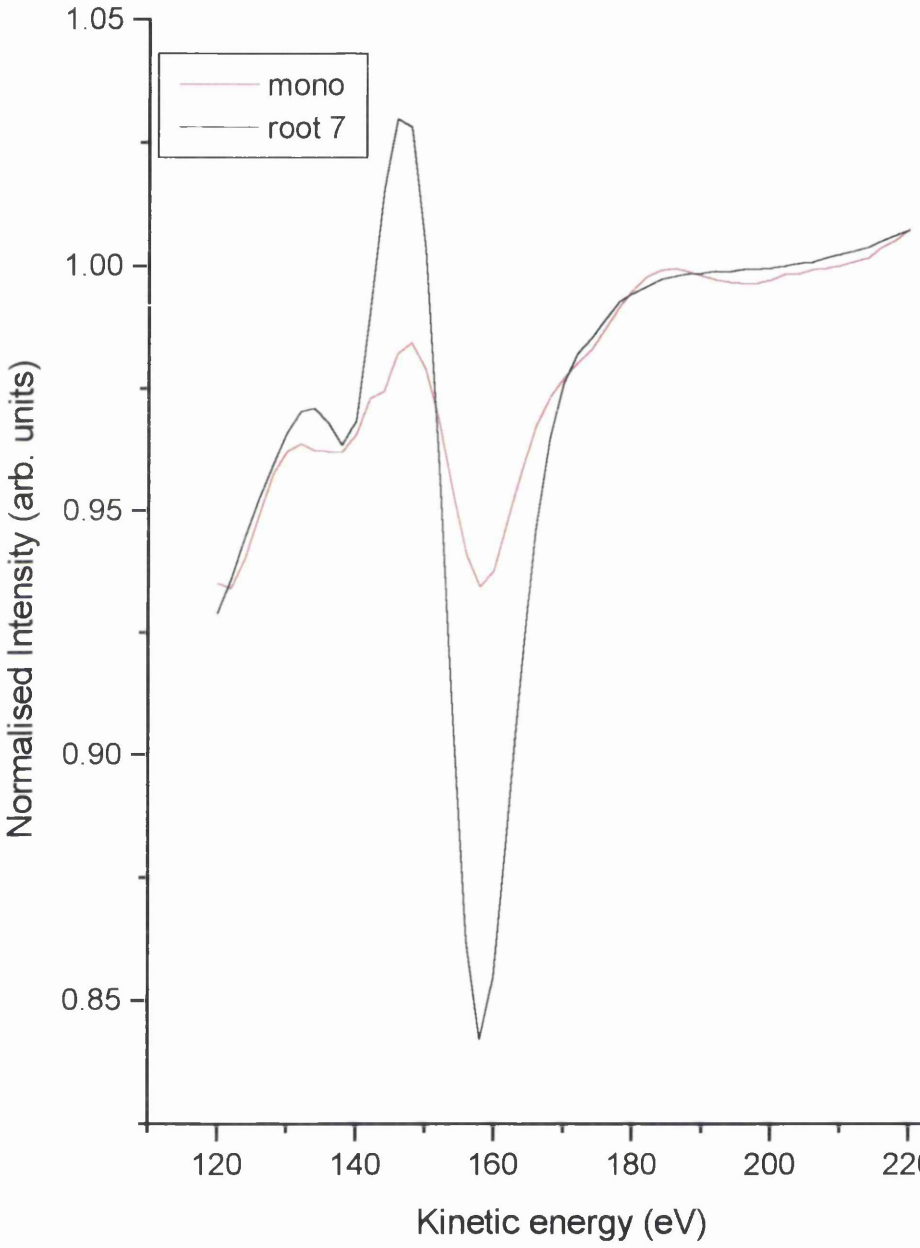

Figure 10: *Plot showing S AES from monolayer coverage (red) and a surface in which a monolayer had been desorbed to show the amount of dissociation (black). The data shown has been divided by the corresponding Cu AES intensity and normalised for ease of comparison. Analysis of the peak heights shows that the amount of decomposition corresponds to 0.02 ML*

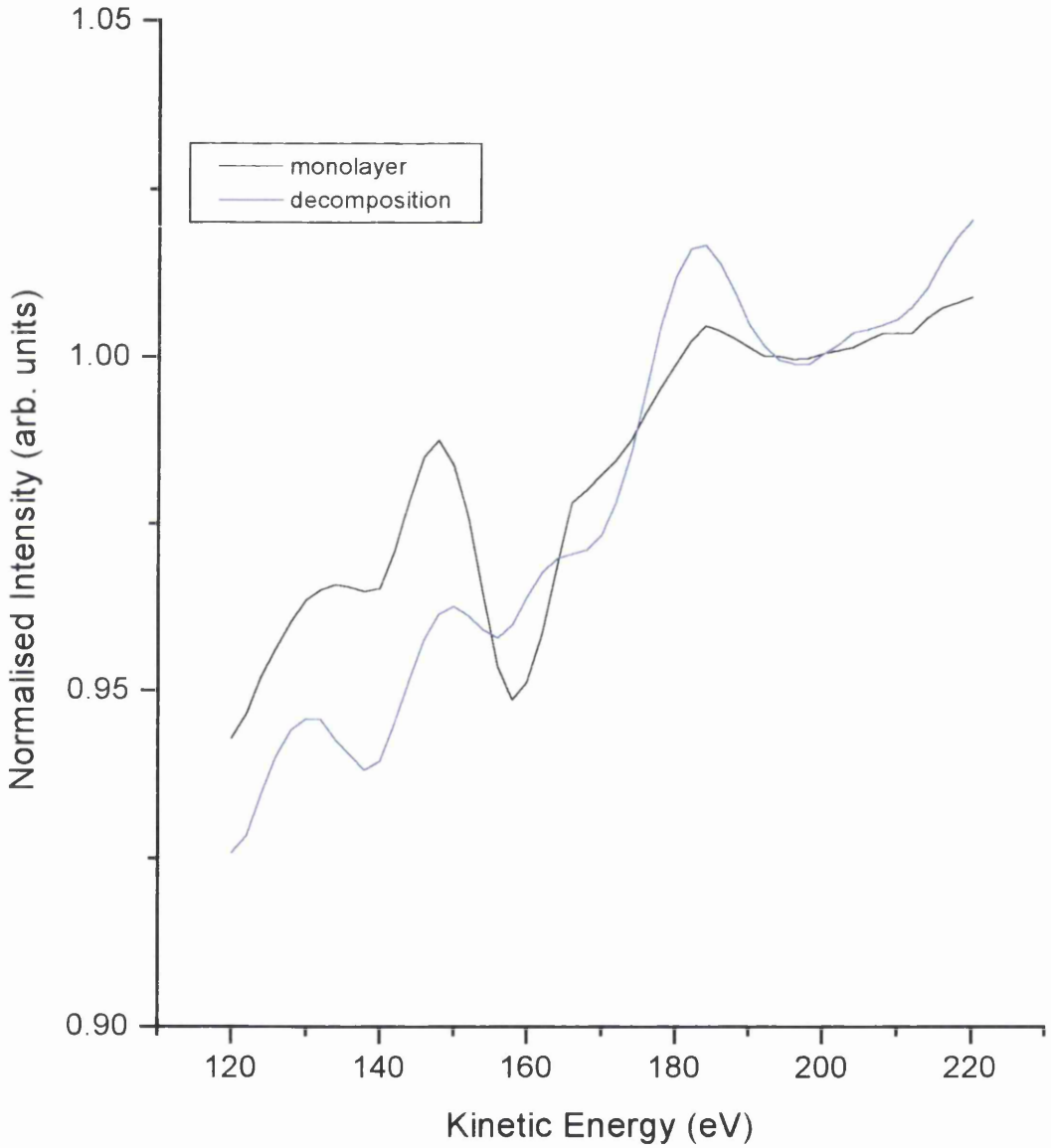

In an analogous procedure to figure 5 (3-methylthiophene), figure 11 shows the area under XPS spectra taken every 20 K from 100-260 K after multilayers of 3-methoxythiophene had been deposited at 100 K. At a temperature of 140 K there is a drop in XPS area due to the onset of multilayer desorption, and by 180 K, the multilayers have desorbed altogether. As with the study of 3-methylthiophene, this method is a rather crude way of determining the multilayer desorption temperature. However, as with all of the molecules studied in the current work, coverages were calculated for each surface prepared at the Daresbury Laboratory, as described in Chapter 4.

Figure 11: *Area under XPS spectra at 20 K intervals from 100-280 K.*

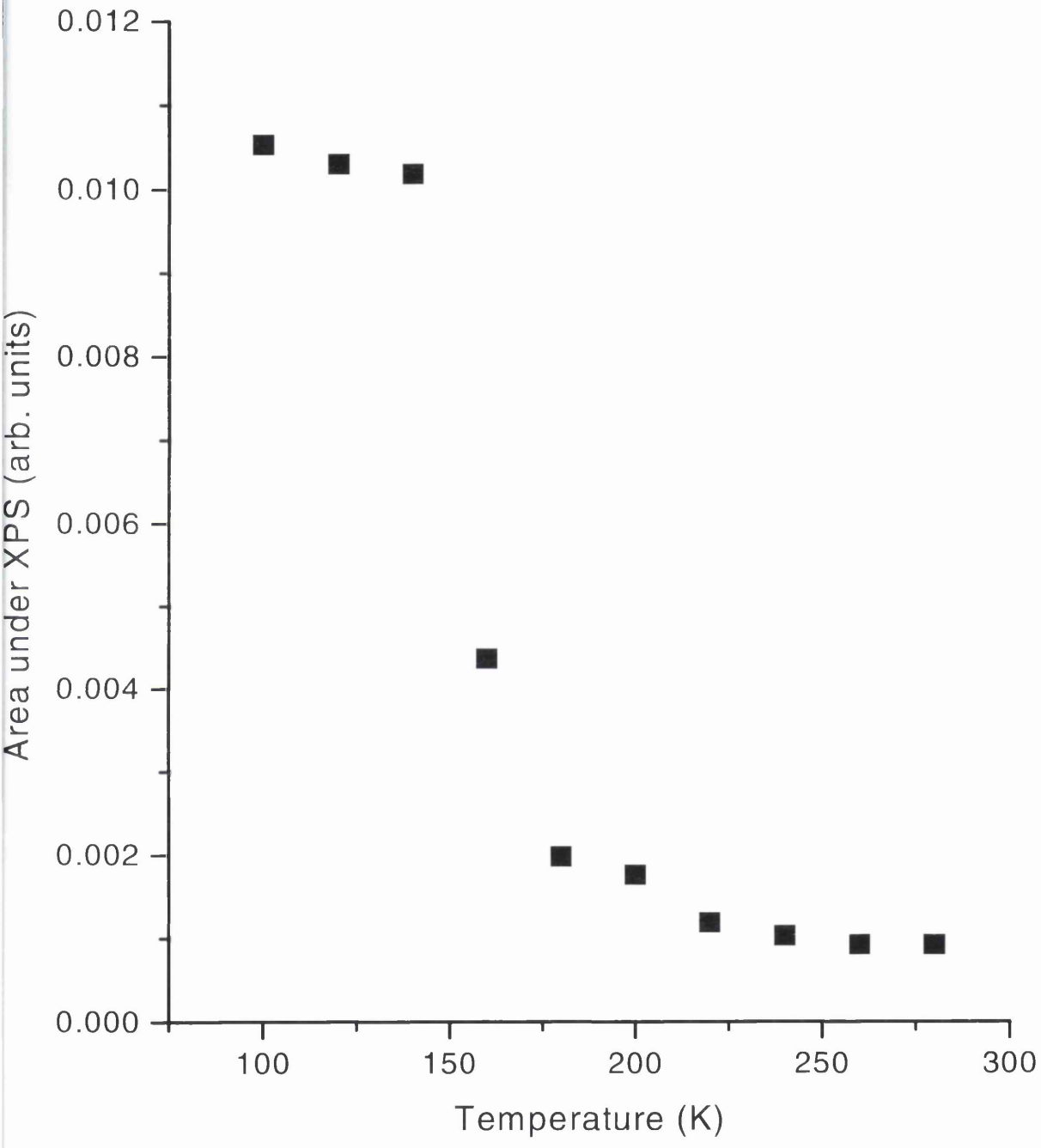

6.2.3 NEXAFS

NEXAFS was used to determine the angle of orientation of both 3-methylthiophene and 3-methoxythiophene on Cu(111). The angle of orientation was determined over a range of coverages, from sub-monolayer to multilayer, for both 3-methylthiophene and 3-methoxythiophene by performing sequentially dosed NEXAFS experiments. The coverage of each surface was determined in an identical way to that described in Chapter 4.

6.2.4 Sequentially dosed NEXAFS experiments of 3-methylthiophene

The S K-edge NEXAFS spectra shown in figure 12 were collected and analysed using an identical procedure to that described in Chapter 4. The lowest coverage spectra (0.03 ML) in the grazing data exhibits a feature at 2467.9 eV. With increasing coverage to 0.07 ML there is a slight decrease in intensity of this feature and by 0.11 ML, this feature has decreased significantly and is broader. With increasing coverage the feature lowers in intensity and at coverage of 0.19 ML has collapsed entirely. The lowest coverage spectra (0.03 ML) in the normal data exhibits a feature at 2468.7 eV. This feature appears almost identically in the 0.07 ML data in size, position and shape. However, by 0.11 ML, the feature has broadened to lower photon energies and at coverages of 0.16 ML and higher, the feature decreases in intensity, eventually collapsing at a coverage of 0.23 ML.

There is no previous published work concerning the assignment of features present in S K-edge 3-methylthiophene NEXAFS data. However, as in the case of 3-chlorothiophene, assignments can be made due to the similarity of the data with that of thiophene. The features present in the thiophene S K-edge NEXAFS data in Chapter 4 were assigned with reference to a study by Stöhr, *et al.*[3] The spectra shown in figure 12 are qualitatively similar to both the present thiophene study and the work of Stöhr.

Figure 12: *Sequentially dosed nested S K-edge NEXAFS data for 3-methylthiophene at different coverages, as shown. The data shown is normalised to the S K-edge jump.*

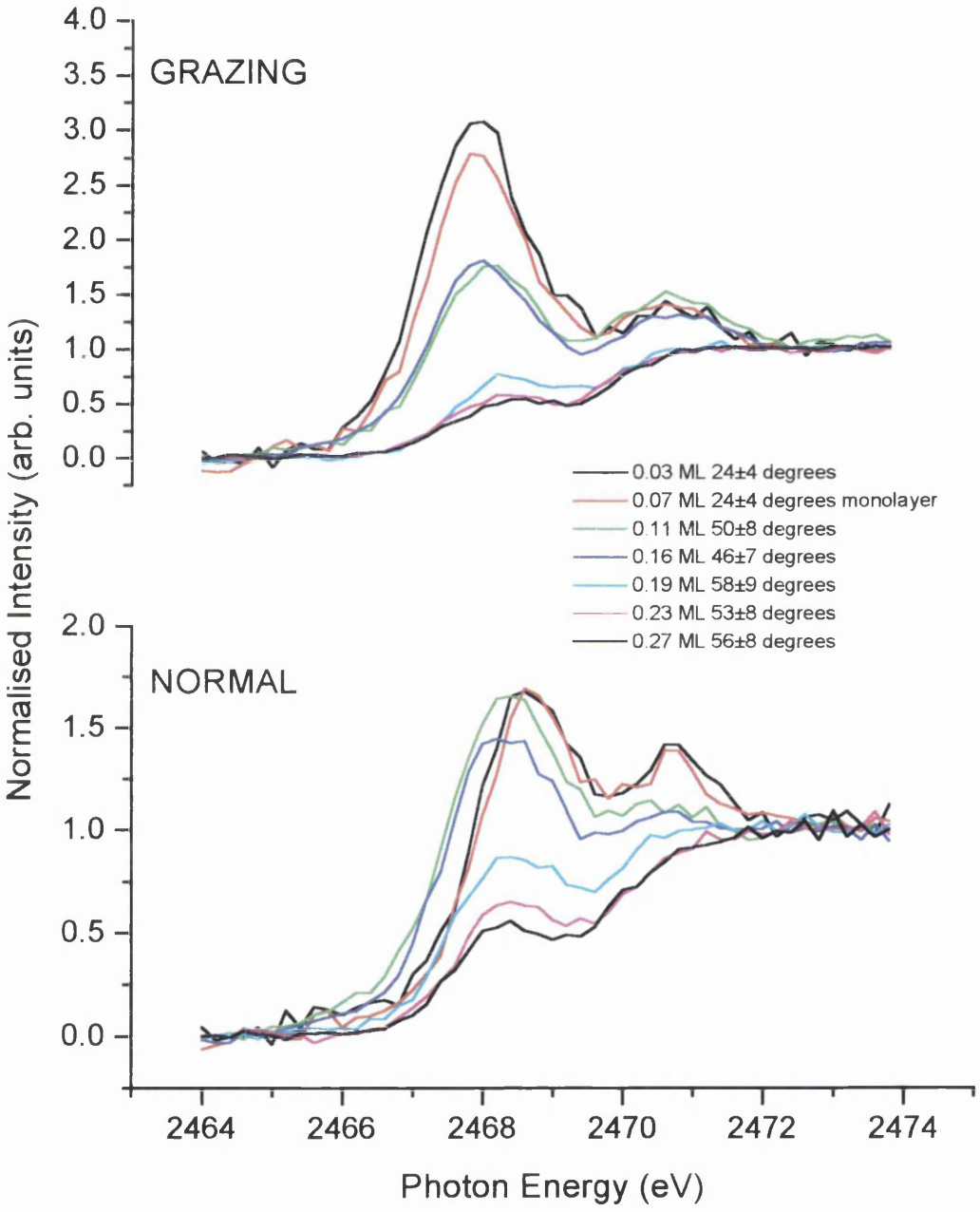

TABLE 1 *Positions of the seven features that were fitted in the data with the type of function that was used in the fitting procedure and the broadness used.*

Peak Position (eV)	Fitting Function	Assignment (ref.)	Broadness (eV)
2465.9	Gaussian	pre-π*	1.4
2467.9	Gaussian	π*	1.4
2468.8	Gaussian	σ*	1.4
2470.4	Gaussian	4s	1.4
2470.9	Gaussian	4p	1.4
2471.6	Gaussian	5p	1.4
2472.4	Step	Ionisation Threshold	4.4

TABLE 2 *Angles of inclination for NEXAFS data in figure 2 and corresponding TPD states.*

Coverage (ML)	π* area (grazing)	π* area (normal)	Ratio π*(g)/π*(n)	Angle (α)	TPD state
0.03	5.47	0.58	9.43	24±4	Monolayer
0.07	4.41	0.47	9.38	24±4	Monolayer
0.11	2.41	1.79	1.35	50±8	Multilayer
0.16	2.91	1.68	1.73	46±7	Multilayer
0.19	0.65	0.80	0.81	58±9	Multilayer
0.23	0.64	0.55	1.16	53±8	Multilayer
0.27	0.48	0.53	0.91	56±8	Multilayer

Therefore, the same assignments made in Chapter 4 with regard to the thiophene work can also be made here.

The feature at 2467 9 eV in the 0.03 ML grazing incidence NEXAFS spectra in figure 2 is dominated by a π^* resonance. The feature at 2468.7 eV in the 0.03 ML normal incidence spectra in figure 12 is dominated by a σ^* resonance. Polarisation dependence of these resonances indicates that 3-methylthiophene adopts a roughly flat geometry on the surface at a coverage of 0.03 ML.

In all, each of the spectra, grazing and normal incidence in figure 12 were fitted in the same way as in Chapter 4. Seven functions, six Gaussians and a step, were used to fit the seven features that can be identified in the data. This is summarised in table 1. A complete list of the values obtained from fitting all of the data shown in figure 12 can be found at the end of this section in table 3.

As in the previous studies of thiophene and 3-chlorothiophene, the ratio of the intensities of the π^* resonances, $I\pi^*(g)/I\pi^*(n)$, can be used to determine the angle of orientation. This ratio, shown plotted in figure 13, and subsequently the angle of orientation was determined for each of the coverages shown in figure 12, and is summarised in table 2.

AES data shows that a surface of coverage 0.11±0.03 ML represents a saturated monolayer of 3-methylthiophene. The first two data sets in table 2 at coverages of 0.03 and 0.07 ML are clearly of sub-monolayer coverage and the angles of orientation calculated for these two coverages are both 24±4 °. However, at a coverage of 0.11 ML, the angle of orientation has risen to 50±8 °. This is due to the onset of multilayer formation and although this coverage matches exactly that of a saturated monolayer, the error involved in the AES coverage measurement is so large that in fact, smaller coverages than 0.11 ML represent monolayer and sub-monolayer coverages, and higher coverages, as shown by the angles in table 2, represent multilayer coverages. Table 2 and figure 14 quite clearly show that there is no change in orientational angle within the monolayer. At coverages above 0.07 ML, the orientational angle rises from 24±4 ° to 50±8 °. Figures 15 (a), (b) and (c) show fitted NEXAFS data at coverages of 0.03, 0.11 and 0.23 ML respectively.

Figure 13: *Ratio Iπ*(g)/Iπ*(n) for each 3-methylthiophene NEXAFS spectra shown in figure 12. As expected, this ratio approaches unity with increasing coverage.*

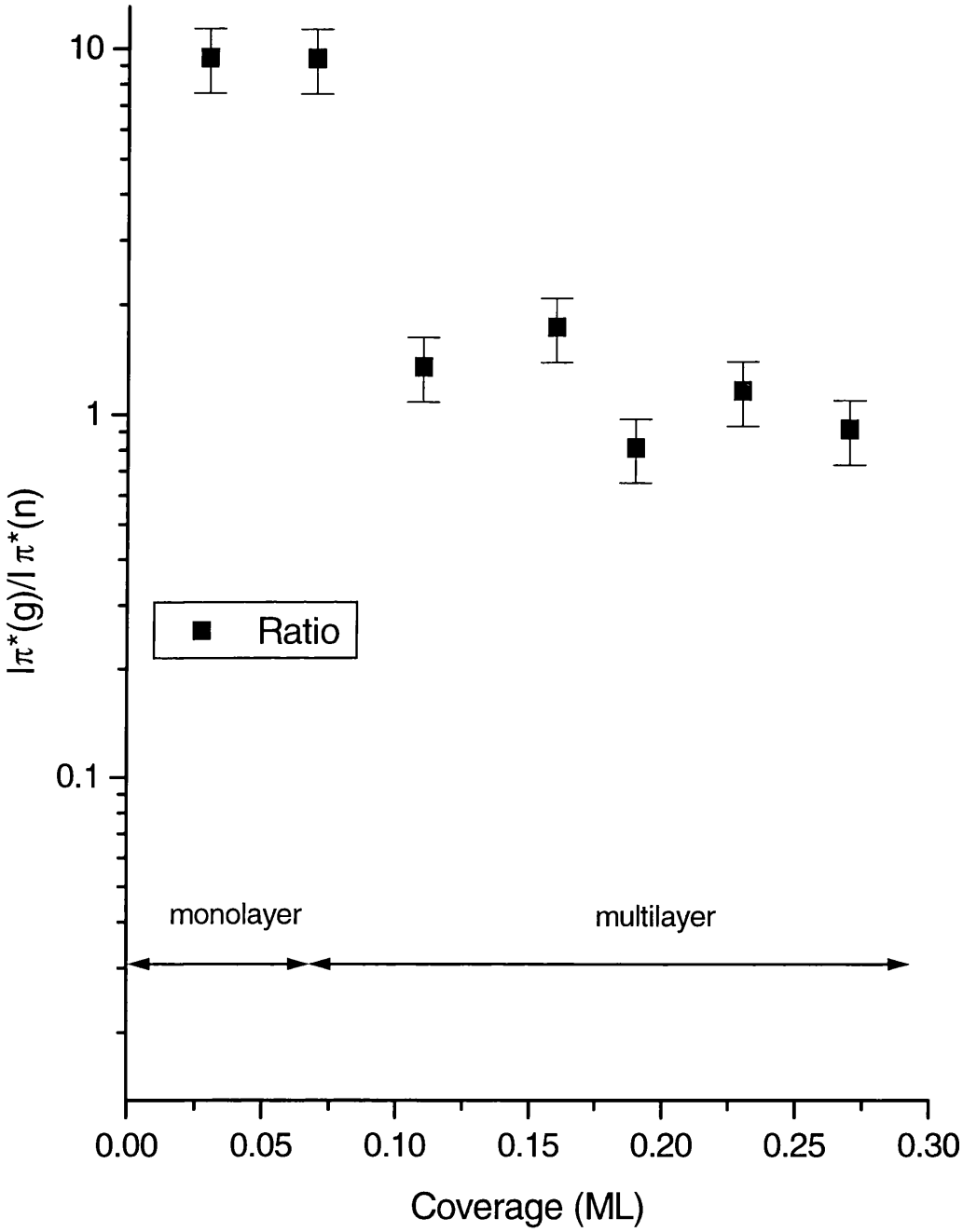

Figure 14: *Angle of molecular orientation derived from each spectra in figure 12. Also shown is the adsorption states that each coverage on the plot corresponds to.*

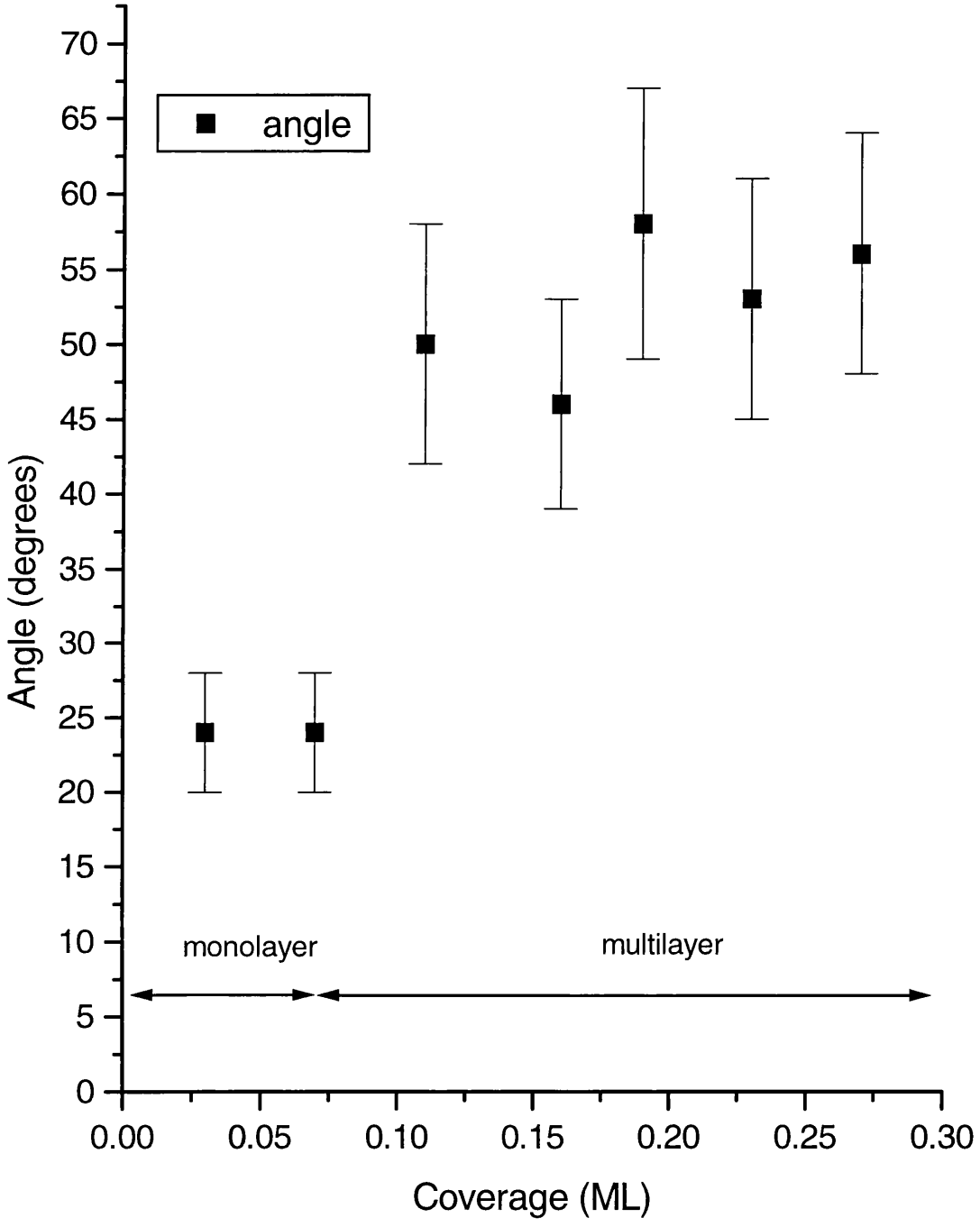

Figure 15: *Fitted NEXAFS data at three different coverages for 3-methylthiophene.*
(a) 0.03 ML fit

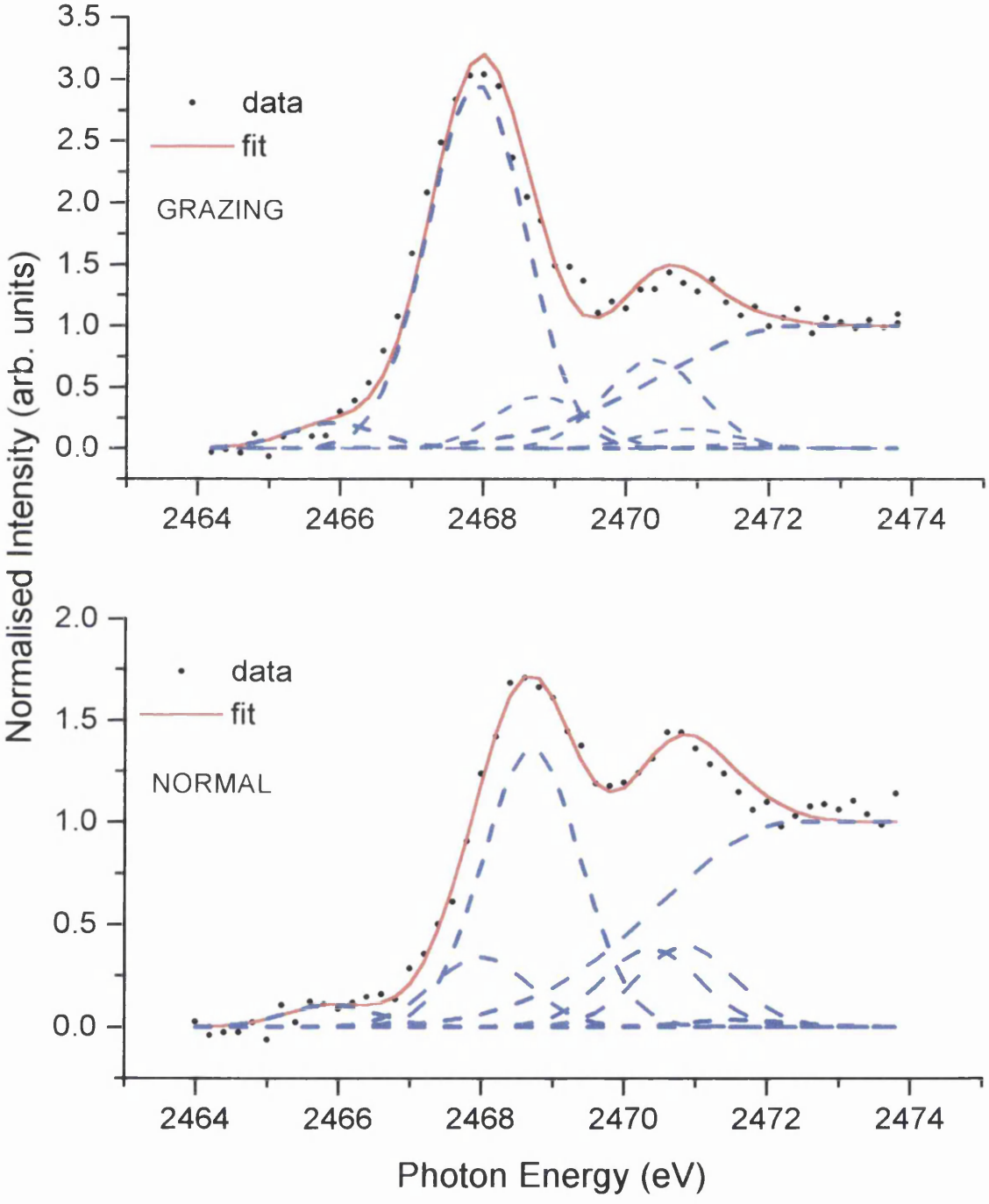

(b) 0.11 ML fit

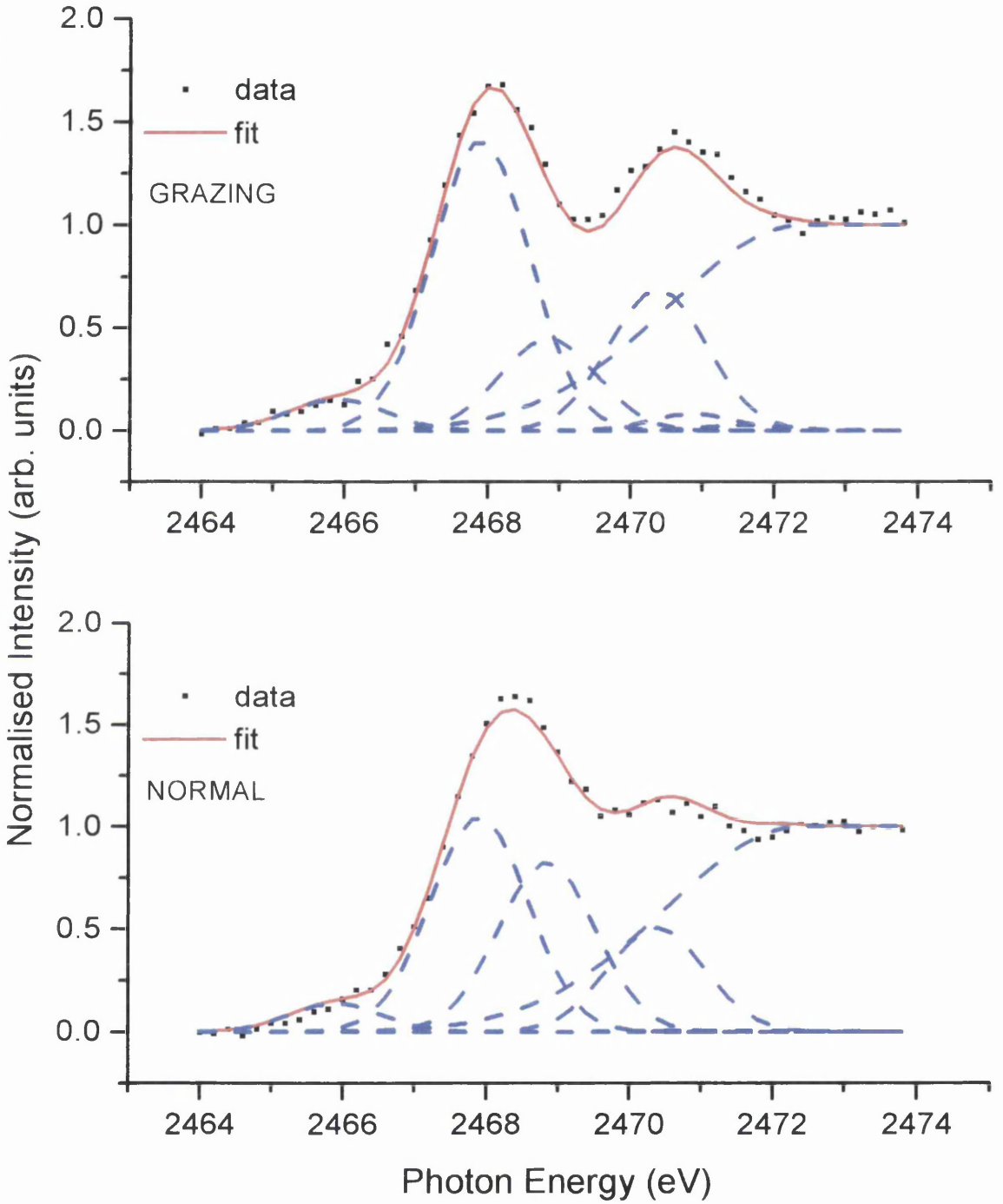
2.0
1.5
1.0
0.5
0.0
data
fit
GRAZING
2464
2466
2468
2470
2472
2474
2.0
1.5
1.0
0.5
0.0
data
fit
NORMAL
2464
2466
2468
2470
2472
2474
Normalised Intensity (arb. units)
Photon Energy (eV)

(c) 0.23 ML fit

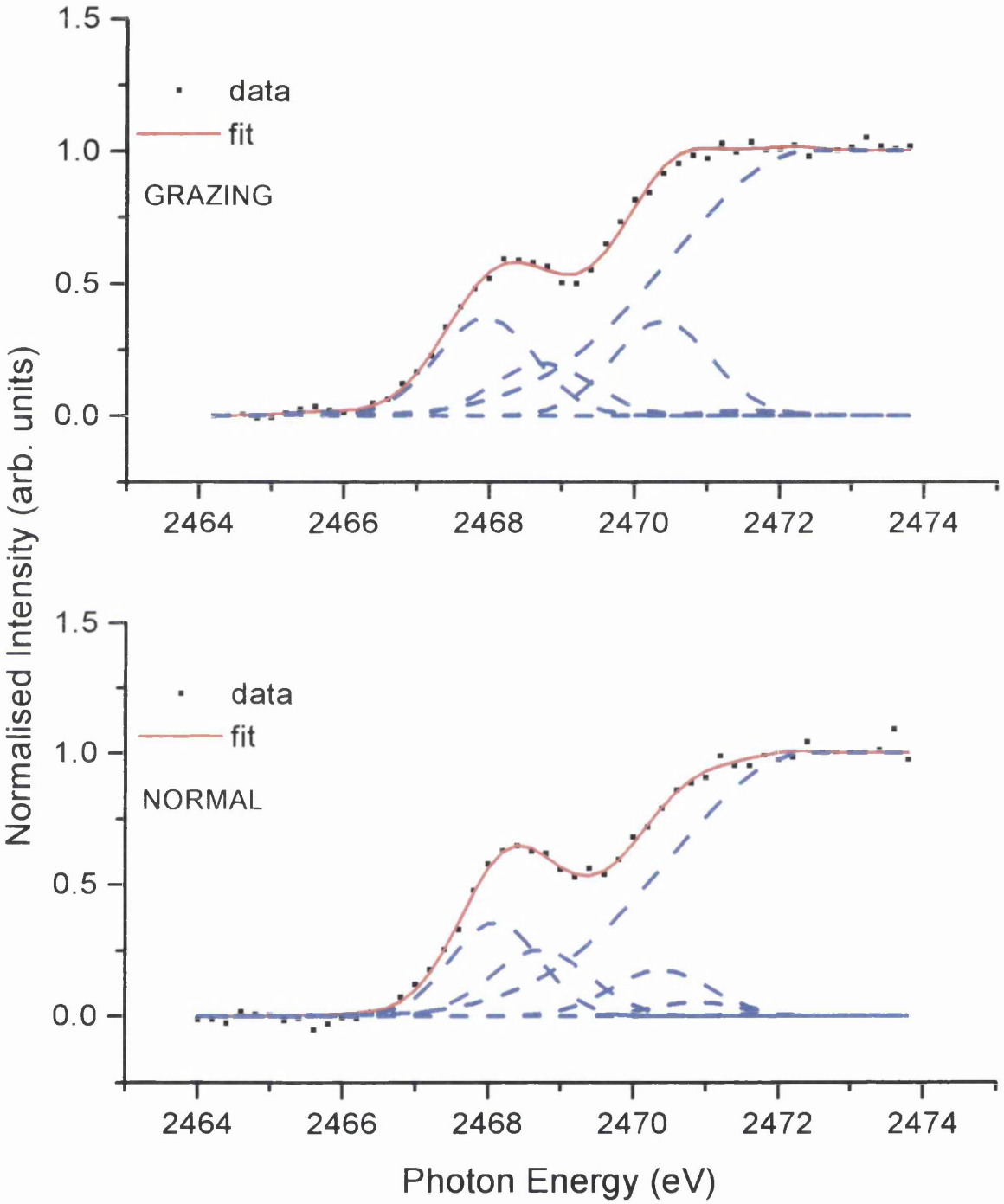
1.5
1.0
0.5
0.0
data
fit
GRAZING
2464
2466
2468
2470
2472
2474
1.5
1.0
0.5
0.0
data
fit
NORMAL
2464
2466
2468
2470
2472
2474
Normalised Intensity (arb. units)
Photon Energy (eV)

TABLE 3 *Complete list of values obtained from fitting all data shown in figure 12.*

Peak one (grazing)	Position (eV)	Area	Broadness (eV)	Peak one (normal)	Position (eV)	Area	Broadness (eV)
Peak 1 (pre-π)							
0.03	2465.9	0.26	1.48	0.03	2465.9	0.17	1.50
0.07	2465.9	0.48	1.60	0.07	2465.9	0.16	1.50
0.11	2465.9	0.24	1.48	0.11	2465.9	0.22	1.50
0.16	2465.9	0.27	1.60	0.16	2465.9	0.11	1.35
0.19	2465.9	0.04	1.60	0.19	2465.9	0.03	1.50
0.23	2465.9	0.02	1.48	0.23	2465.9	0.01	1.50
0.27	2465.9	0.01	1.28	0.27	2465.9	0.01	1.50
Peak 2 (π*)							
0.03	2467.9	5.47	1.60	0.03	2468.0	0.58	1.60
0.07	2467.9	4.41	1.60	0.07	2468.0	0.47	1.60
0.11	2467.9	2.41	1.60	0.11	2468.0	1.79	1.60
0.16	2467.9	2.91	1.60	0.16	2468.0	1.68	1.56
0.19	2467.9	0.65	1.42	0.19	2468.0	0.80	1.60
0.23	2467.9	0.64	1.60	0.23	2468.0	0.55	1.44
0.27	2467.9	0.48	1.58	0.27	2468.0	0.53	1.60
Peak 3 (σ*)							
0.03	2468.8	0.56	1.55	0.03	2468.7	2.32	1.60
0.07	2469.0	0.63	1.35	0.07	2468.7	2.20	1.60
0.11	2468.8	0.73	1.55	0.11	2468.7	1.42	1.60
0.16	2469.0	0.52	1.35	0.16	2468.7	1.19	1.60
0.19	2468.8	0.51	1.60	0.19	2468.7	0.70	1.60
0.23	2468.8	0.35	1.55	0.23	2468.7	0.43	1.60
0.27	2468.8	0.29	1.35	0.27	2468.7	0.31	1.60
Peak 4 (4s←1s)							
0.03	2470.4	0.99	1.60	0.03	2470.4	0.65	1.60

0.07	2470.4	1.37	1.60	0.07	2470.4	0.91	1.60
0.11	2470.4	1.23	1.60	0.11	2470.4	0.87	1.60
0.16	2470.4	1.04	1.60	0.16	2470.4	0.71	1.47
0.19	2470.4	0.42	1.60	0.19	2470.4	0.60	1.60
0.23	2470.4	0.61	1.60	0.23	2470.4	0.31	1.60
0.27	2470.4	0.51	1.60	0.27	2470.4	0.40	1.60
Peak 5 (4p←1s)							
0.03	2470.9	0.27	1.22	0.03	2470.9	0.67	1.60
0.07	2470.9	0.03	1.42	0.07	2470.9	0.26	1.60
0.11	2470.9	0.09	1.32	0.11	2470.9	0.01	1.50
0.16	2470.9	0.12	1.42	0.16	2470.9	0.01	1.40
0.19	2470.9	0.08	1.40	0.19	2470.9	0.01	1.60
0.23	2470.9	0.01	1.22	0.23	2470.9	0.08	1.40
0.27	2470.9	0.04	1.42	0.27	2470.9	0.01	1.60
Peak 6 (5p←1s)							
0.03	2471.6	0.08	1.60	0.03	2471.6	0.01	1.60
0.07	2471.6	0.08	1.40	0.07	2471.6	0.01	1.60
0.11	2471.6	0.04	1.50	0.11	2471.6	0.01	1.60
0.16	2471.6	0.06	1.40	0.16	2471.6	0.01	1.40
0.19	2471.6	0.01	1.60	0.19	2471.6	0.03	1.60
0.23	2471.6	0.05	1.60	0.23	2471.6	0.01	1.60
0.27	2471.6	0.02	1.40	0.27	2471.6	0.01	1.60

6.2.5 Sequentially dosed NEXAFS experiments of 3-methoxythiophene

Sequentially dosed NEXAFS spectra of 3-methoxythiophene on Cu(111) are shown in figure 16. The lowest coverage spectra (0.06 ML) in the grazing data exhibits a feature at 2467.4 eV. With increasing coverage to 0.15 ML there is a slight decrease in intensity of this feature and by 0.35 ML, this feature has collapsed entirely. The lowest coverage spectra (0.06ML) in the normal data exhibits a feature at 2468.2 eV. The first two data sets in the normal spectra look very similar and by 0.13 ML the feature at 2468.2 eV is starting to broaden and move to lower photon energies. As in the grazing case, by 0.35 ML, the feature has collapsed entirely.

As in the case of 3-methylthiophene, the features present in figure 16 were identified with reference to previous work by Stöhr *et al.*[3] The feature at 2467.4 eV in the 0.06 ML grazing incidence NEXAFS spectra in figure 16 is dominated by a π^* resonance. The feature at 2468.2 eV in the 0.06 ML normal incidence spectra in figure 16 is dominated by a σ^* resonance. Polarisation dependence of these resonances indicates that 3-methoxythiophene also adopts a roughly flat geometry on the surface at a coverage of 0.06 ML.

In all, each of the spectra in figure 16 were fitted in the same way as in the study of 3-methylthiophene and a list of the seven functions, six Gaussians and a step, that were used to fit the seven features that can be identified in the data is summarised in table 4. A complete list of the values obtained from fitting all of the data shown in figure 16 can be found in table 6.

Figure 16: *Sequentially dosed nested S K-edge NEXAFS data for 3-methoxythiophene at different coverages, as shown. The data is normalised to the S K-edge jump.*

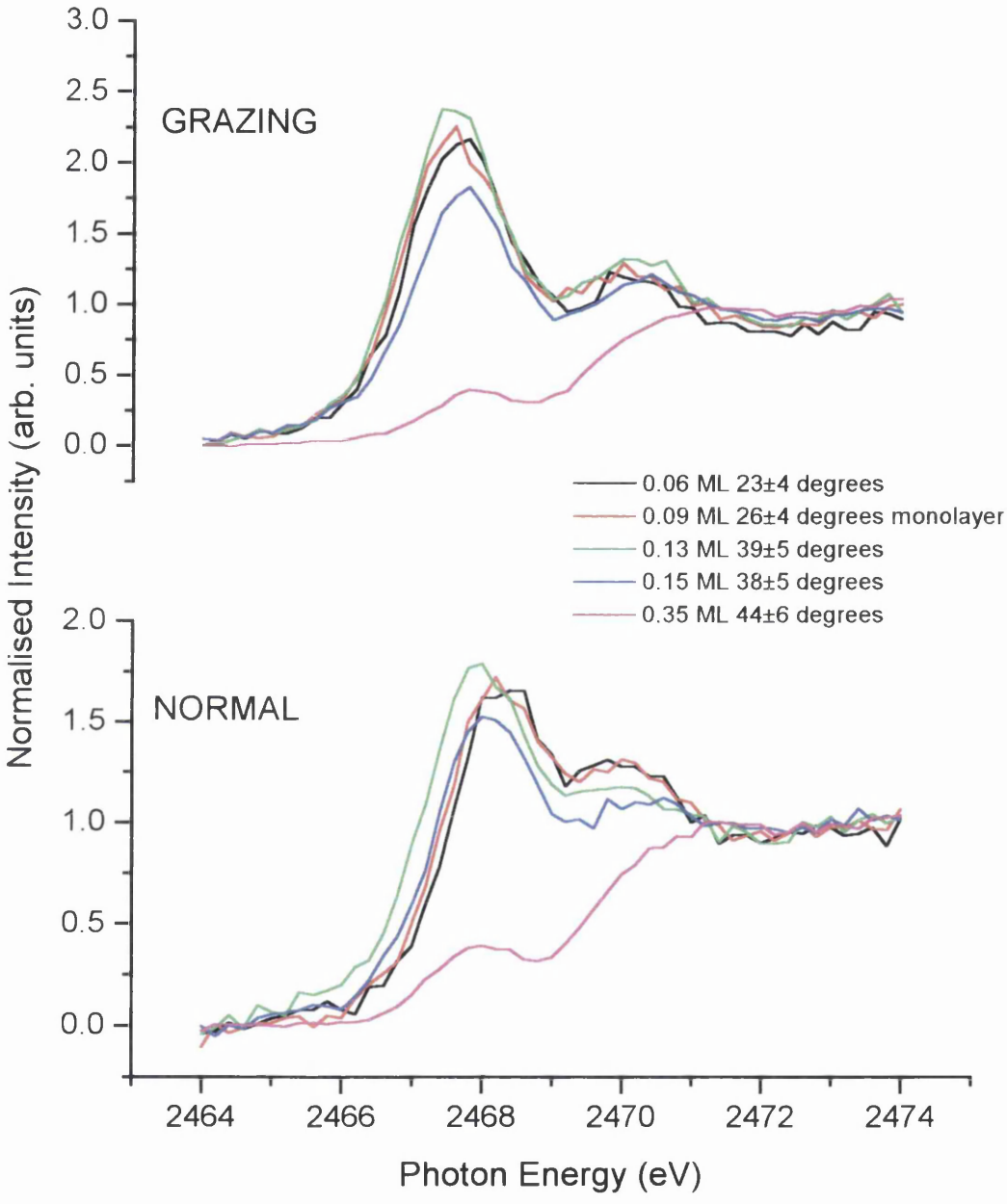

TABLE 4 *Positions of the seven features that were fitted in the data with the type of function that was used in the fitting procedure and the broadness used.*

Peak Position (eV)	Fitting Function	Assignment (ref.)	Broadness (eV)
2465.1	Gaussian	pre-π*	1.4
2467.4	Gaussian	π*	1.4
2468.1	Gaussian	σ*	1.4
2469.8	Gaussian	4s	1.4
2470.6	Gaussian	4p	1.4
2471.5	Gaussian	5p	1.4
2472.4	Step	Ionisation Threshold	4.4

TABLE 5 *Angles of inclination for NEXAFS data in figure 2 and corresponding TPD states.*

Coverage (ML)	π* area (grazing)	π* area (normal)	Ratio π*(g)/π*(n)	Angle (α) (°)	TPD state
0.06	3.15	0.30	10.50	23±4	Monolayer
0.09	3.15	0.43	7.33	26±4	Monolayer
0.13	3.46	1.25	2.77	39±5	Multilayer
0.15	2.05	0.69	2.97	38±5	Multilayer
0.35	0.36	0.18	2.00	44±6	Multilayer

AES measurements indicates that a surface with a coverage of 0.12±0.03ML represents saturation monolayer coverage. Therefore the first two data sets in table 5 (0.06 and 0.09 ML respectivley) represent surfaces with sub-monolayer and monolayer coverages. The corresponding angles of 23±4 °and 26±4 ° indicate that there is no change in angle within the monolayer within experimental error. At a coverage of 0.13 ML, the angle has risen to 39±5 ° indicating the onset of multilayer formation.

Figure 17 shows how the angle of orientation changes with increasing coverage, as summarised in table 5. Figure 18 shows that the ratio $I\pi^*(g)/\pi^*(n)$ approaches unity with increasing coverage, as expected. Fitted NEXAFS data at coverages 0.06, 0.15 and 0.35 ML respectively is shown in figures 19 (a), (b) and (c).

Figure 18: *Ratio Iπ*(g)/Iπ*(n) for each 3-methylthiophene NEXAFS spectra shown in figure 17. As expected, this ratio approaches unity with increasing coverage.*

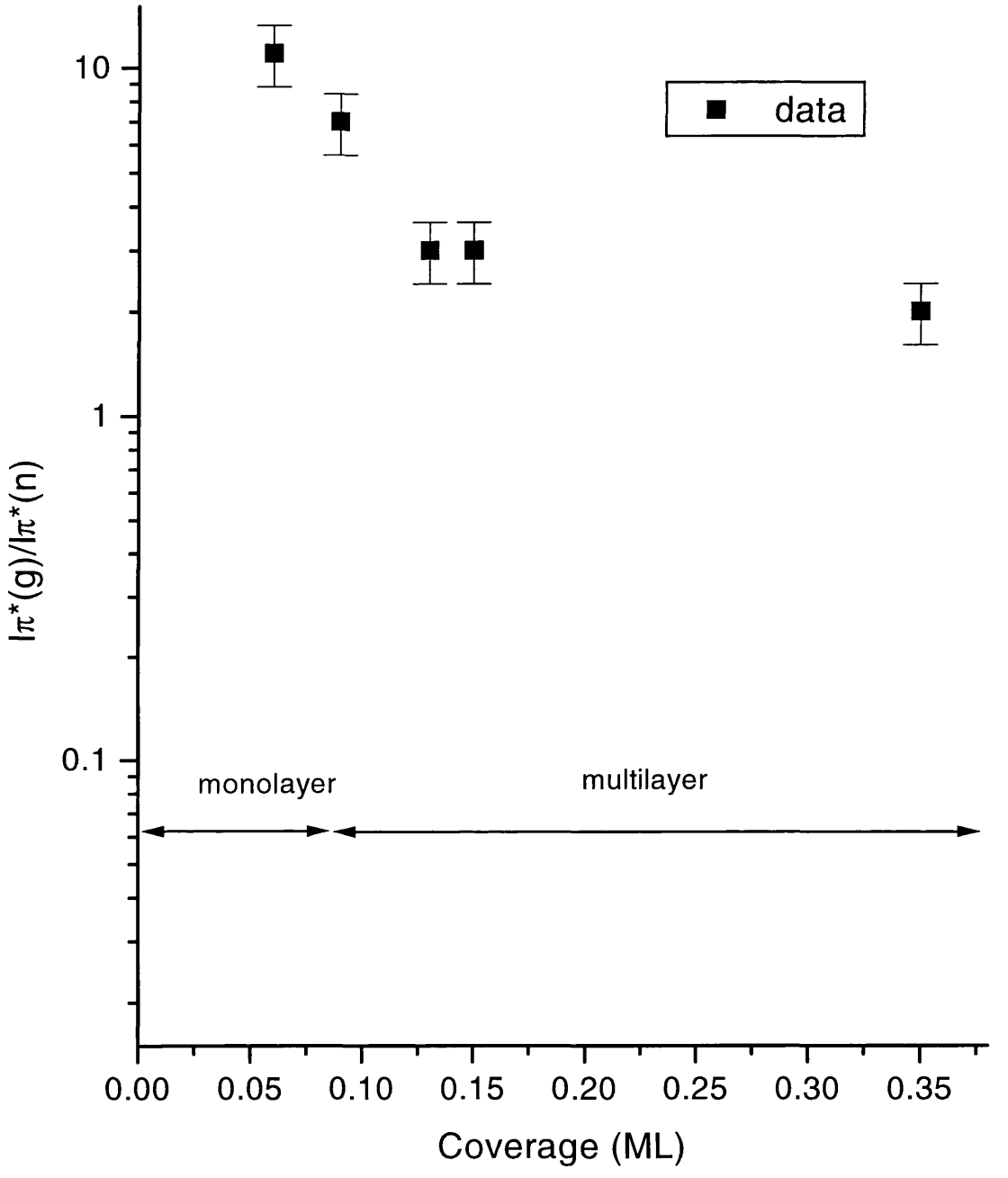

Figure 19: *Angle of molecular orientation derived from each spectra in figure 17. . Also shown is the adsorption states that each coverage on the plot corresponds to.*

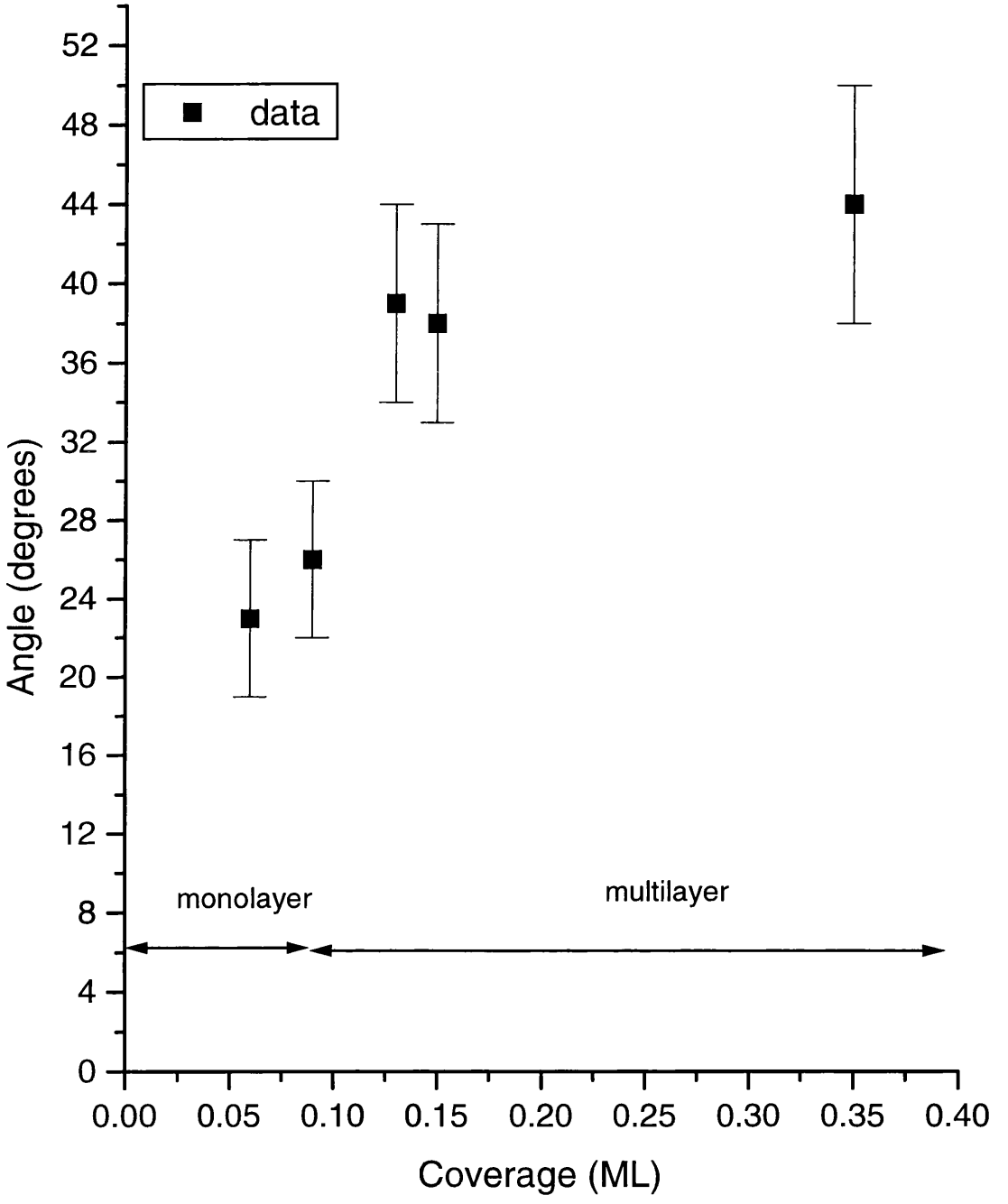

Figure 20: *Fitted NEXAFS data at three different coverages for 3-methoxythiophene (a) 0.06 ML fit.*

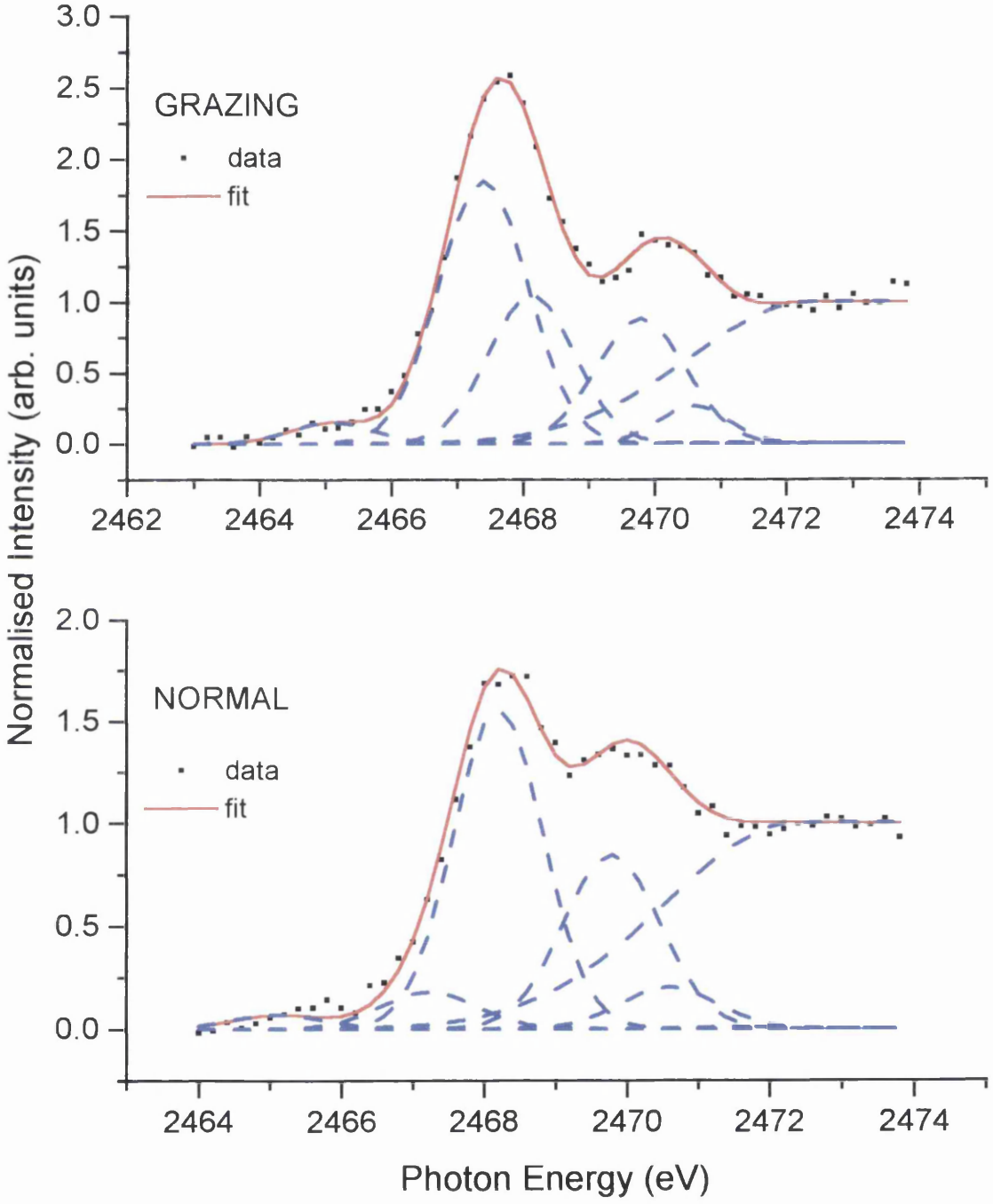

(b) 0.15 ML fit

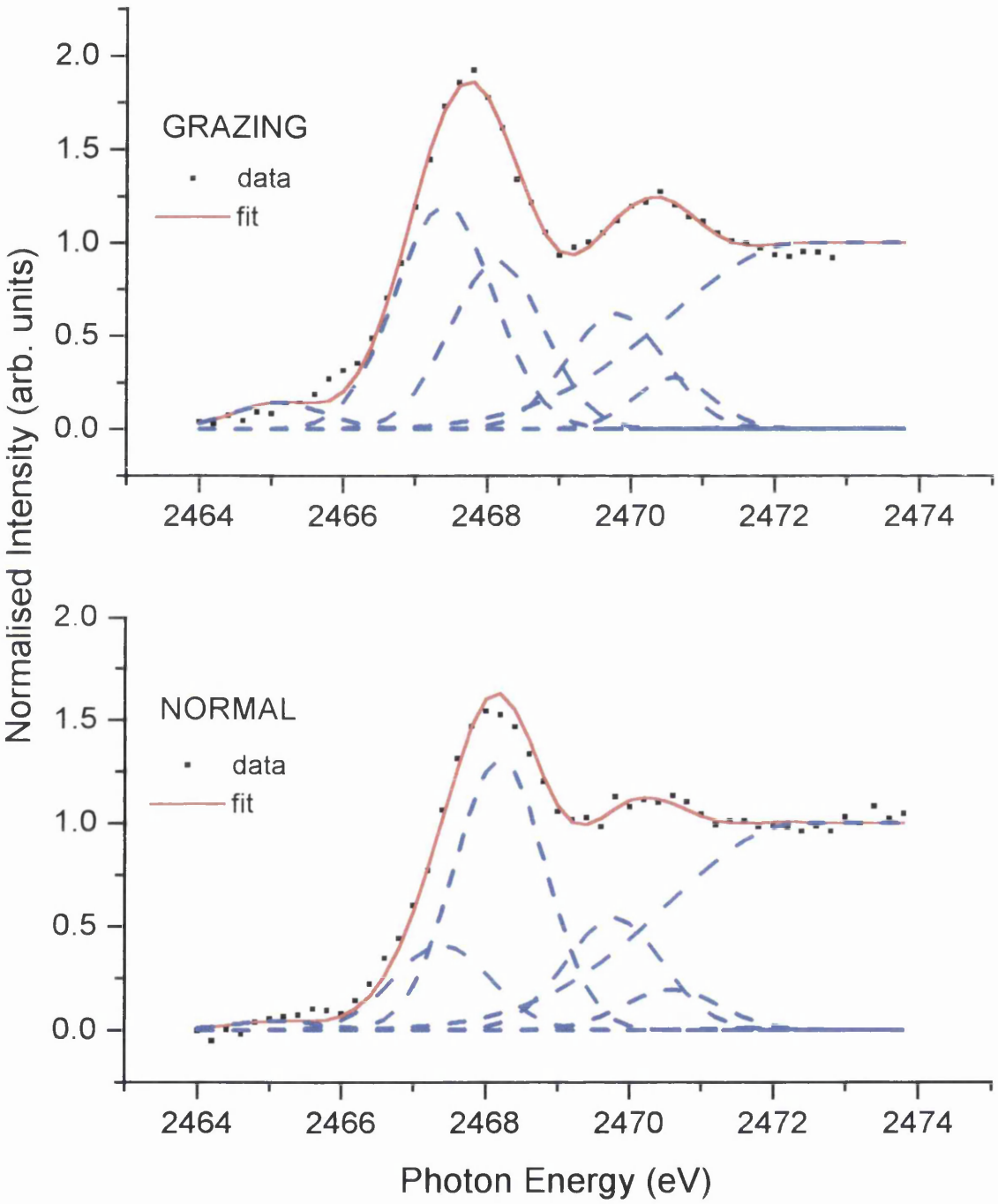
GRAZING
data
fit
NORMAL
data
fit
Normalised Intensity (arb. units)
Photon Energy (eV)
2.0
1.5
1.0
0.5
0.0
2464
2466
2468
2470
2472
2474

(c) 0.35 ML

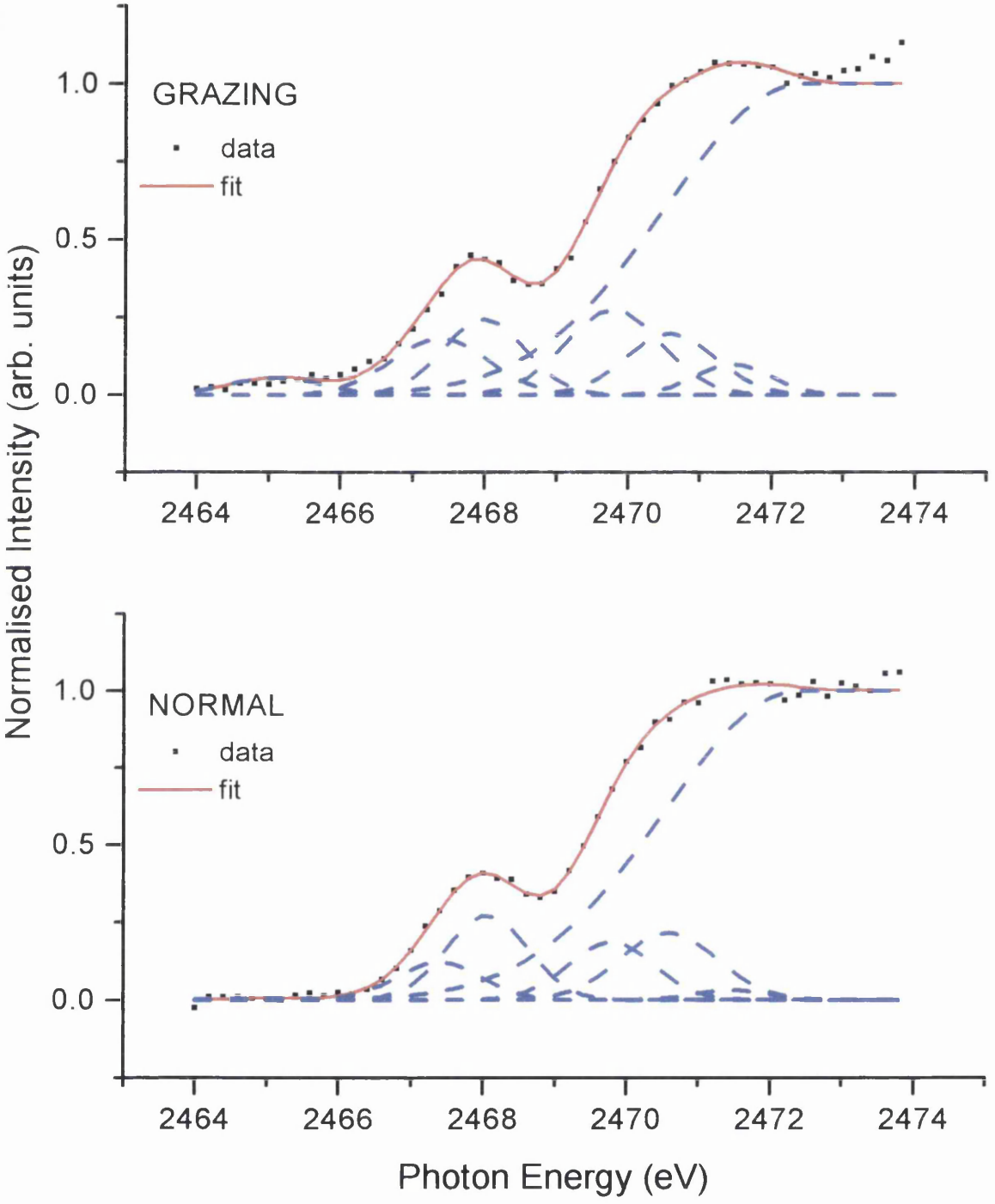
GRAZING
data
fit
NORMAL
data
fit
1.0
0.5
0.0
2464
2466
2468
2470
2472
2474
Normalised Intensity (arb. units)
Photon Energy (eV)

TABLE 6 *Complete list of values obtained from fitting all data shown in figure 16.*

Peak one (grazing)	Position (eV)	Area	Broadness (eV)	Peak one (normal)	Position (eV)	Area	Broadness (eV)
Peak 1 (pre-π)							
0.06	2465.1	0.24	1.50	0.06	2465.1	0.10	1.50
0.09	2465.1	0.18	1.50	0.09	2465.1	0.01	1.50
0.13	2465.1	0.17	1.50	0.13	2465.1	0.20	1.50
0.15	2465.1	0.23	1.50	0.15	2465.1	0.07	1.50
0.35	2465.1	0.08	1.50	0.35	2465.1	0.01	1.48
Peak 2 (π*)							
0.06	2467.4	3.15	1.60	0.06	2467.2	0.30	1.58
0.09	2467.4	3.15	1.60	0.09	2467.2	0.43	1.58
0.13	2467.4	3.46	1.60	0.13	2467.2	1.25	1.58
0.15	2467.4	2.05	1.60	0.15	2467.4	0.69	1.58
0.35	2467.4	0.36	1.60	0.35	2467.4	0.18	1.58
Peak 3 (σ*)							
0.06	2468.1	1.72	1.54	0.06	2468.2	2.46	1.48
0.09	2468.1	1.22	1.54	0.09	2468.2	2.43	1.48
0.13	2468.1	1.18	1.54	0.13	2468.2	2.19	1.48
0.15	2468.1	1.47	1.54	0.15	2468.2	2.07	1.48
0.35	2468.1	0.33	1.54	0.35	2468.1	0.39	1.34
Peak 4 (4s←1s)							
0.06	2469.8	1.50	1.60	0.06	2469.8	1.44	1.60
0.09	2469.8	1.44	1.60	0.09	2469.8	0.28	1.40
0.13	2469.8	1.44	1.60	0.13	2469.8	1.18	1.60
0.15	2469.8	1.06	1.60	0.15	2469.8	0.92	1.40
0.35	2469.8	0.45	1.60	0.35	2469.8	0.28	1.40
Peak 5 (4p←1s)							
0.06	2470.6	0.36	1.27	0.06	2470.6	0.26	1.58

0.09	2470.6	0.22	1.27	0.09	2470.6	0.36	1.58
0.13	2470.6	0.36	1.27	0.13	2470.6	0.33	1.58
0.15	2470.6	0.38	1.27	0.15	2470.6	0.37	1.60
0.35	2470.6	0.28	1.27	0.35	2470.6	0.37	1.60
Peak 6 (5p←1s)							
0.06	2471.5	0.01	1.20	0.06	2471.5	0.01	1.20
0.09	2471.5	0.14	1.20	0.09	2471.5	0.01	1.20
0.13	2471.5	0.01	1.20	0.13	2471.5	0.01	1.20
0.15	2471.5	0.01	1.20	0.15	2471.5	0.04	1.20
0.35	2471.5	0.14	1.20	0.35	2471.5	0.04	1.20

6.2.6 NIXSW

NIXSW experiments were performed in order to study the adsorption structure of both 3-methylthiophene and 3-methoxythiophene. In particular, as with thiophene, the Cu-S bond length was derived, assuming no relaxation of the substrate surface layers, from the coherent position data once the adsorption site had been determined at monolayer coverage. The Cu-S bond length was derived from the Cu surface-S distance (coherent position) obtained from fitting S 1s photoemission NIXSW profiles relative to the bulk (111) and ($\bar{1}11$) planes.

6.2.7 Substrate NIXSW experiments

NIXSW experiments for both 3-methylthiophene and 3-methoxythiophene were performed at the Daresbury laboratory in the same beam-time allocation period using the same crystal. As expected, the substrate fits for both molecules studied are identical with respect to the coherent fraction, coherent position, X-ray broadness and mosaic spread. The fitted substrate data is summarised in table 7 and a fitted Cu LVV NIXSW profile is shown in figure 20. All 3-methylthiophene and 3-methoxythiophene NIXSW data, substrate and adsorbate, was fitted in an identical procedure to that described in Chapter 4.

Table 7: *Experimental values derived from substrate NIXSW experiments.*

	Coherent fraction (f_{co})	Coherent position (D(111) (Å)	Broadness (ΔE) (eV)	Mosaic Spread (°)
Data	0.85±0.05	0	0.70	0.10

The data in table 7 is very similar to the data collected for 3-chlorothiophene and this would be expected because the experiments were performed only a few days apart using the same crystal. As with the 3-chlorothiophene data, the high fitted coherent fraction of

Figure 20: *Cu LVV NIXSW profile (black) shown with fit (red). The data shown in black fits to a coherent fraction of 0.85±0.05, a coherent position of 0 Å, a broadness of 0.7 eV and a mosaic spread of 0.1 °.*

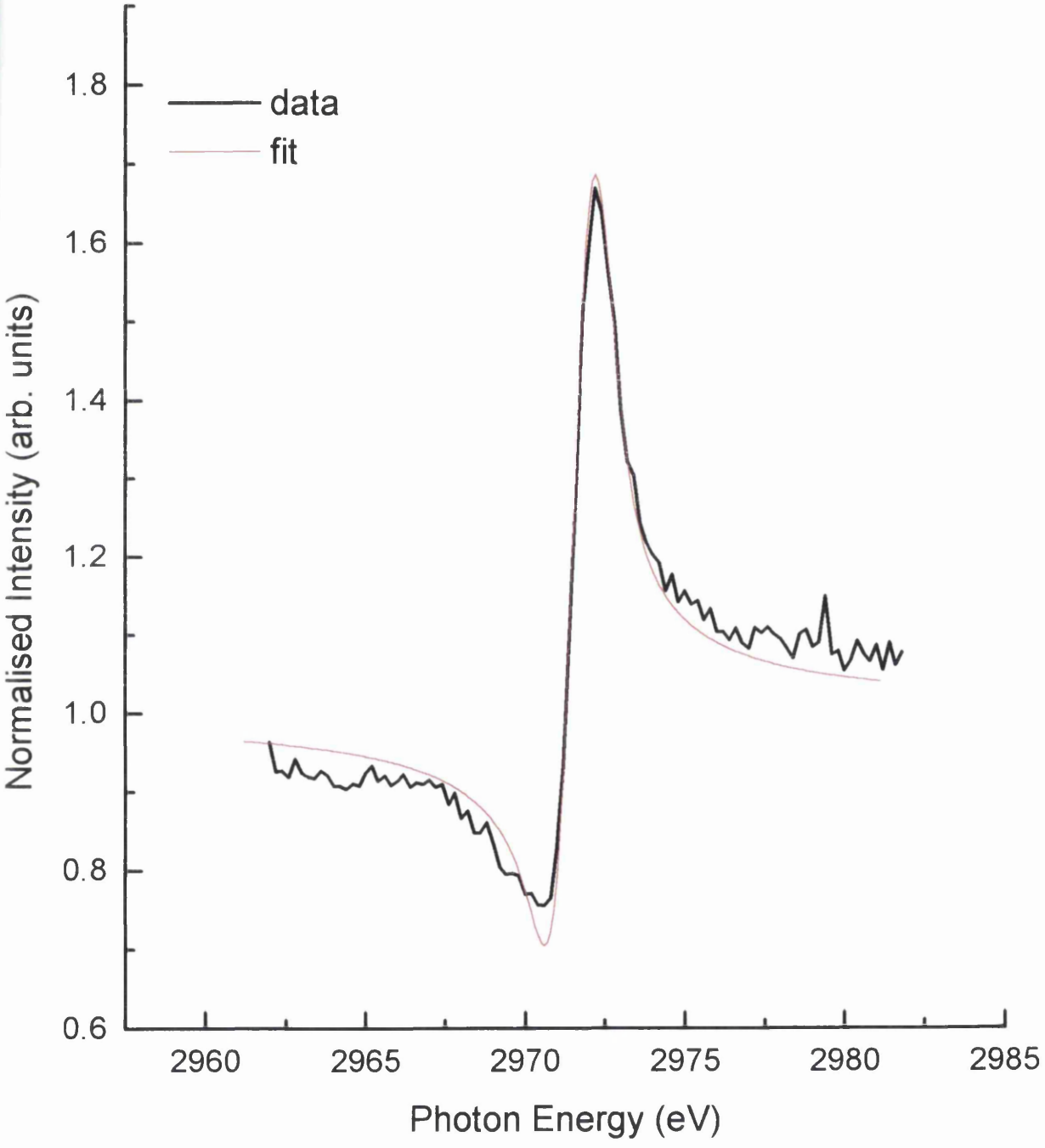

0.85±0.05 signifies that the crystal has a high degree of crystallographic order. All adsorbate profiles were subsequently fitted using a broadness of 0.70 eV and a mosaic spread of 0.10 °.

6.2.8 NIXSW experiments of 3-methylthiophene using the annealed dosing method

Annealed S 1s NIXSW experiments were performed by dosing multilayers of 3-methylthiophene and annealing to 180 K, as outlined in figure 5, in order to desorb multilayers and leave surfaces with monolayer coverages. Coverages were then calculated by analysis of XPS data from each surface as described previously. The surfaces prepared in this manner had coverages ranging from 0.07-0.09±0.02 ML. AES experiments from the initial characterisation of 3-methylthiophene show that a coverage of 0.11±0.03 ML corresponds to a saturated monolayer. Due to the errors involved, the annealed NIXSW data represents data at saturated monolayer coverage and the values obtained from analysis of the fitted data are summarised in table 8. Figures 21 and 22 show fitted NIXSW profiles with respect to (111) and ($\bar{1}$11) planes respectively at monolayer coverage, prepared by the annealed dosing method.

Table 8: *Summary of NIXSW data from S 1s NIXSW experiments at monolayer coverage for 3-methylthiophene, as prepared by the annealed dosing method.*

Monolayer Data	Plane	f_{co}	D(111) (Å)	Broadness (eV)
S 1s	(111)	0.90±0.05	0.49±0.03	0.7
S 1s	($\bar{1}$11)	0.83±0.05	0.79±0.03	0.7

A complete list of all S 1s NIXSW data, sequential and annealed, can be found in tables 9 and 10 at the end of this section.

Figure 21: *S 1s NIXSW data at monolayer coverage for 3-methylthiophene with respect to the (111) plane, as prepared by the annealed dosing method. The data is fitted to a coherent fraction of 0.90±0.05 and a coherent position of 0.49±0.03 Å.*

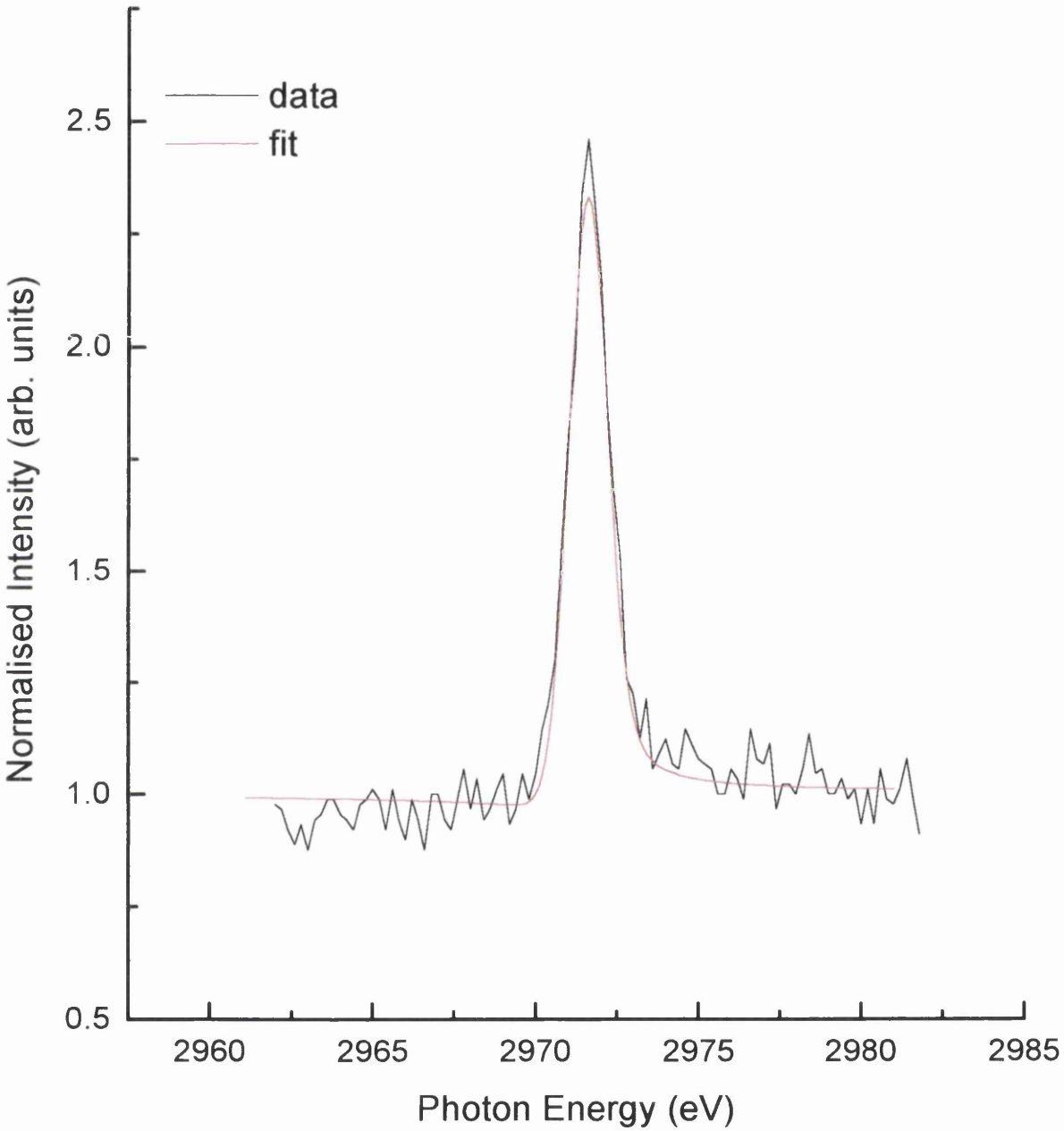

Figure 22: *S 1s NIXSW data at monolayer coverage for 3-methylthiophene with respect to the ($\bar{1}11$) plane, as prepared by the annealed dosing method. The data is fitted to a coherent fraction of 0.83±0.05 and a coherent position of 0.79±0.03 Å.*

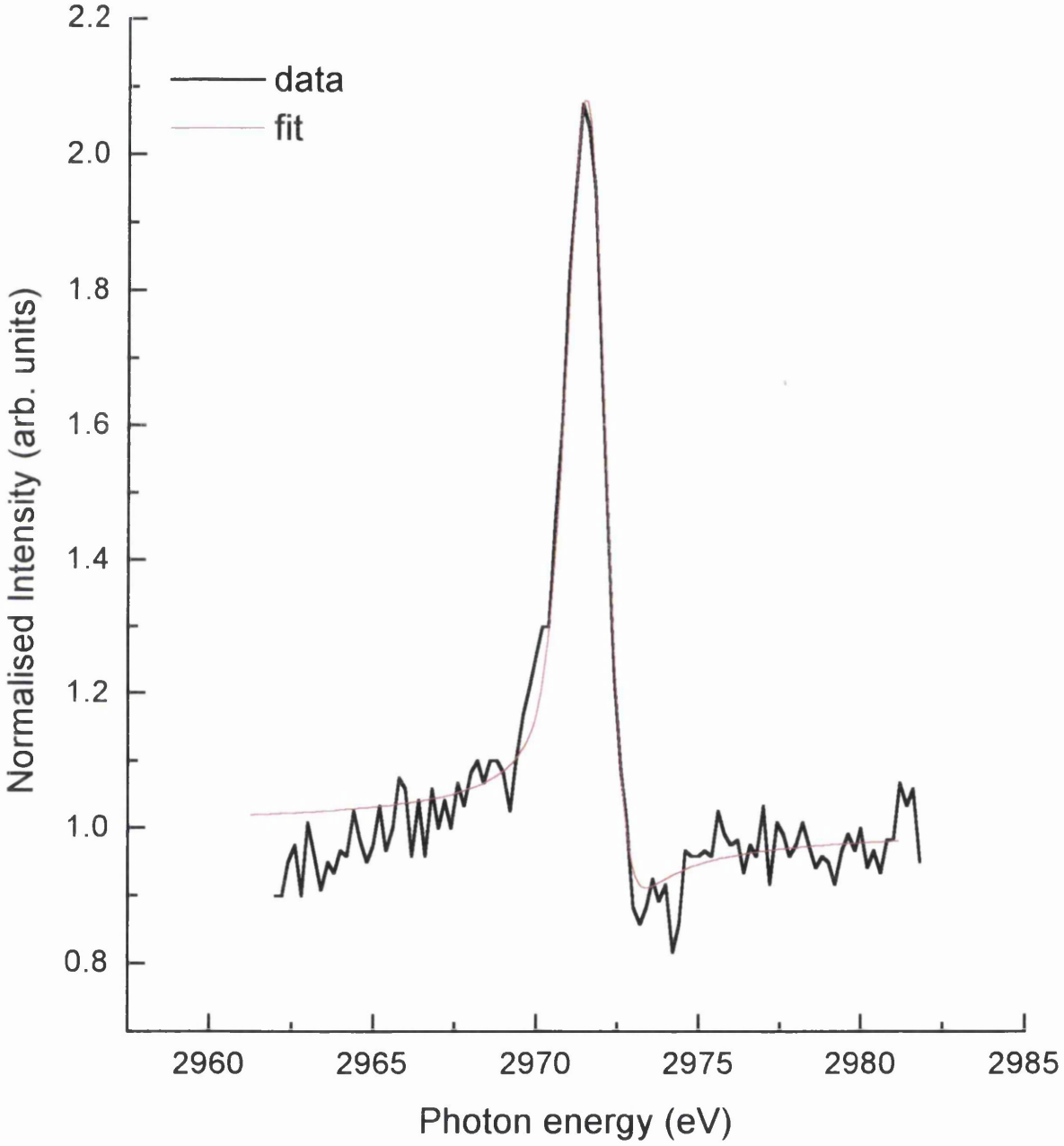

6.2.9 NIXSW experiments of 3-methylthiophene using the sequential dosing method

Sequentially dosed experiments were performed with respect to the (111) plane, as outlined in Chapter 4 and shown in figures 23, 24 and 25. Figure 23 shows how the coherent fraction varies with respect to increasing coverage and figure 24 shows how the coherent position varies with respect to increasing coverage. Figure 25 shows a fitted profile at a coverage of 0.06 ML. Figure 23 shows that the onset of multilayers is at a coverage of 0.12 ML. This coverage would be expected to be representative of a monolayer coverage because it is very close to the saturated monolayer coverage obtained by AES experiments, 0.11±0.03 ML. The highest monolayer coverage is 0.07 ML, which has a coherent fraction of 0.90±0.05. The highest monolayer coverage in the annealed experiments is 0.09 ML, which also has a coherent fraction of 0.90±0.05. It is clear that the coverages calculated from NIXSW experiments corresponding to monolayer coverage are at the lower end of the error calculated from AES experiments. Coverages of 0.12 ML in the sequentially dosed experiments also correspond to monolayer coverage with respect to the AES measurements but it must be remembered that this is because the error involved in the coverage calculation by AES is quite large. It must be concluded that in the NIXSW study, the surfaces with coverages from 0.07-0.10 ML represent monolayer coverages and the surface studied with coverages from 0.11-0.14 ML and above, represent multilayer coverages.

Figure 23 shows that the coherent fraction drops to 0.43±0.05 at a coverage of 0.12 ML and gradually drops to a value of 0.05±0.05 at a coverage of 0.36 ML. This is clearly due to the onset of randomly oriented multilayers with a distribution of heights above the surface. Figure 24 shows that the coherent position at monolayer coverage is 0.37±0.03 Å. This is quite different to the coherent position of 0.49±0.03 Å calculated in the annealed experiments and the possible reason for this is deferred to the "discussion" section. Figure 24 also shows that the coherent position rises to 0.50±0.03 Å at a coverage of 0.12 ML, from that of 0.37±0.03 Å at a coverage of 0.07 ML. This is due to the formation of randomly oriented multilayers above the monolayer, further away from

the surface, with a distribution of distances from the surface. The coherent position varies between 0.45-0.55 Å over the coverage range 0.12-0.31 ML.

Table 9: *S 1s NIXSW experiments performed for 3-methylthiophene on Cu(111) using the annealed dosing method.*

Plane	Coverage	f_{co}	D(hkl) (Å)
111	0.07	0.90	0.45
111	0.07	0.90	0.50
111	0.08	0.90	0.50
111	0.08	0.90	0.50
111	0.09	0.90	0.50
111	0.09	0.90	0.50
$\bar{1}\bar{1}1$	0.08	0.80	0.80
$\bar{1}\bar{1}1$	0.08	0.70	0.80
$\bar{1}\bar{1}1$	0.09	0.90	0.77
$\bar{1}\bar{1}1$	0.09	0.90	0.80

Table 10: *S 1s NIXSW experiments performed for 3-methylthiophene on Cu(111) using the sequential dosing method.*

Plane	Coverage	f_{co}	D(hkl) (Å)
111	0.06	0.90	0.40
111	0.07	0.90	0.37
111	0.12	0.43	0.50
111	0.17	0.40	0.57
111	0.20	0.20	0.55
111	0.25	0.20	0.45
111	0.31	0.20	0.50
111	0.36	0.05	0.05

Figure 23: *Plot of coherent fraction against coverage with respect to the (111) plane for 3-methylthiophene. Sequentially dosed.*

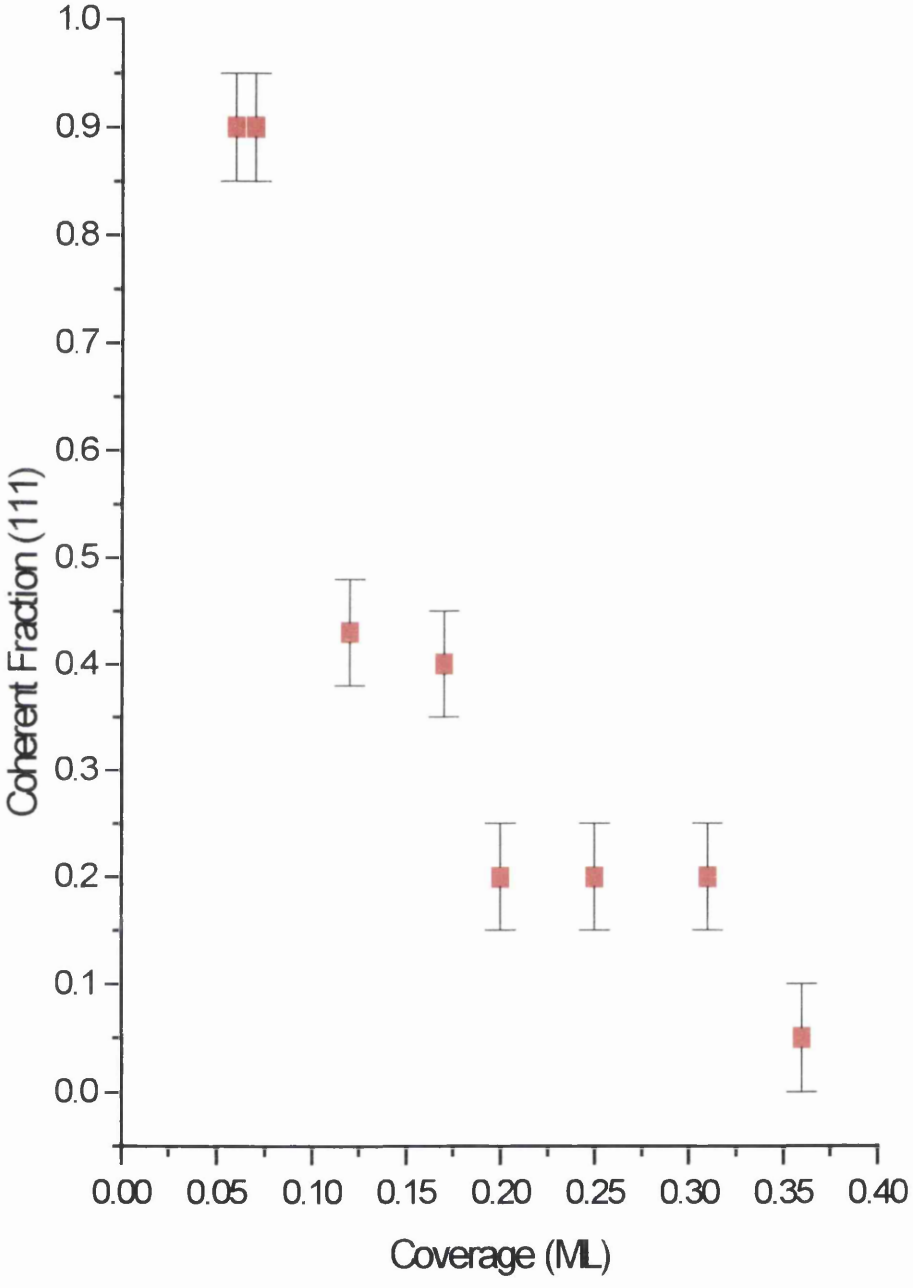

Figure 24: *Plot of coherent position against coverage with respect to the (111) plane for 3-methylthiophene. Sequentially dosed.*

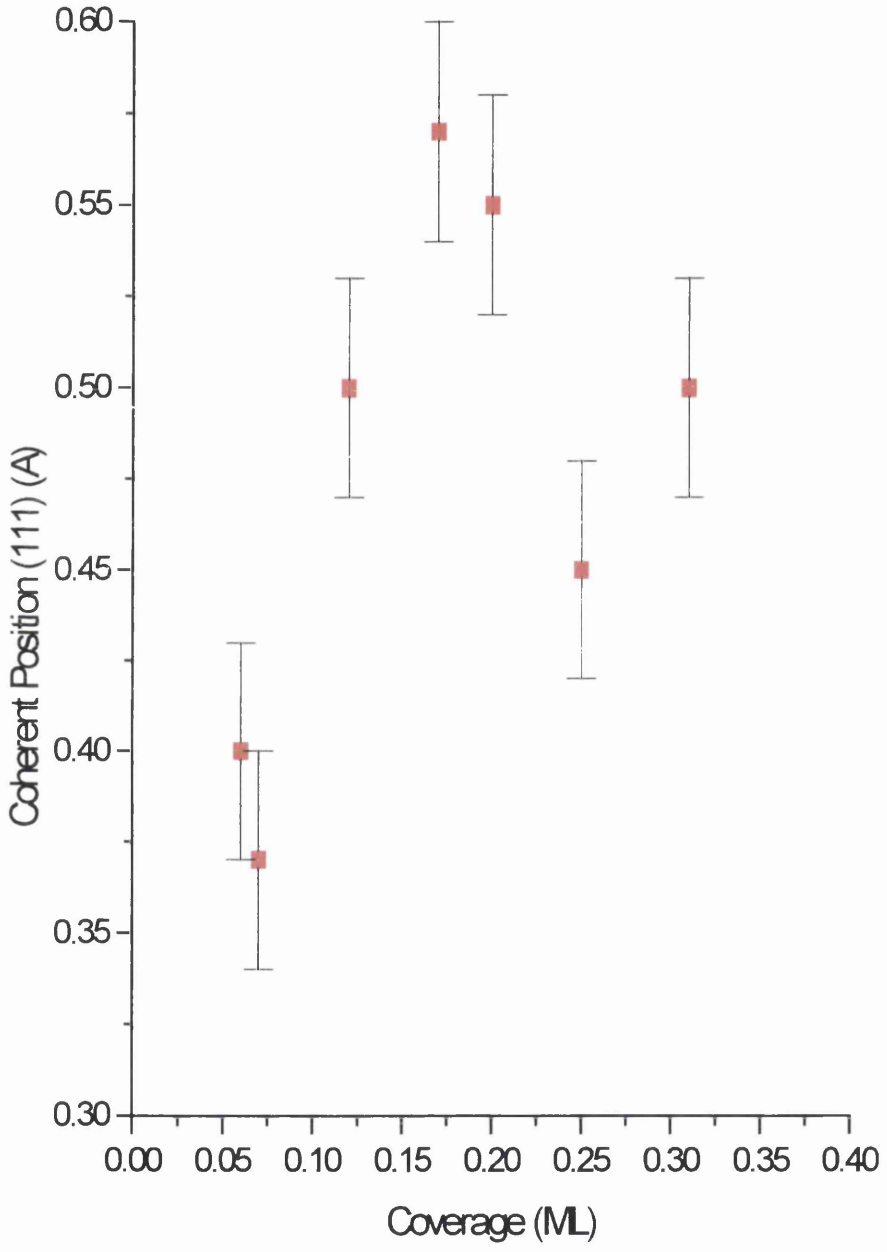

Figure 25: *Sequentially dosed 3-methylthiophene NIXSW. This data was fitted to a coherent height of 0.4 Å and a coherent fraction of 0.9.*

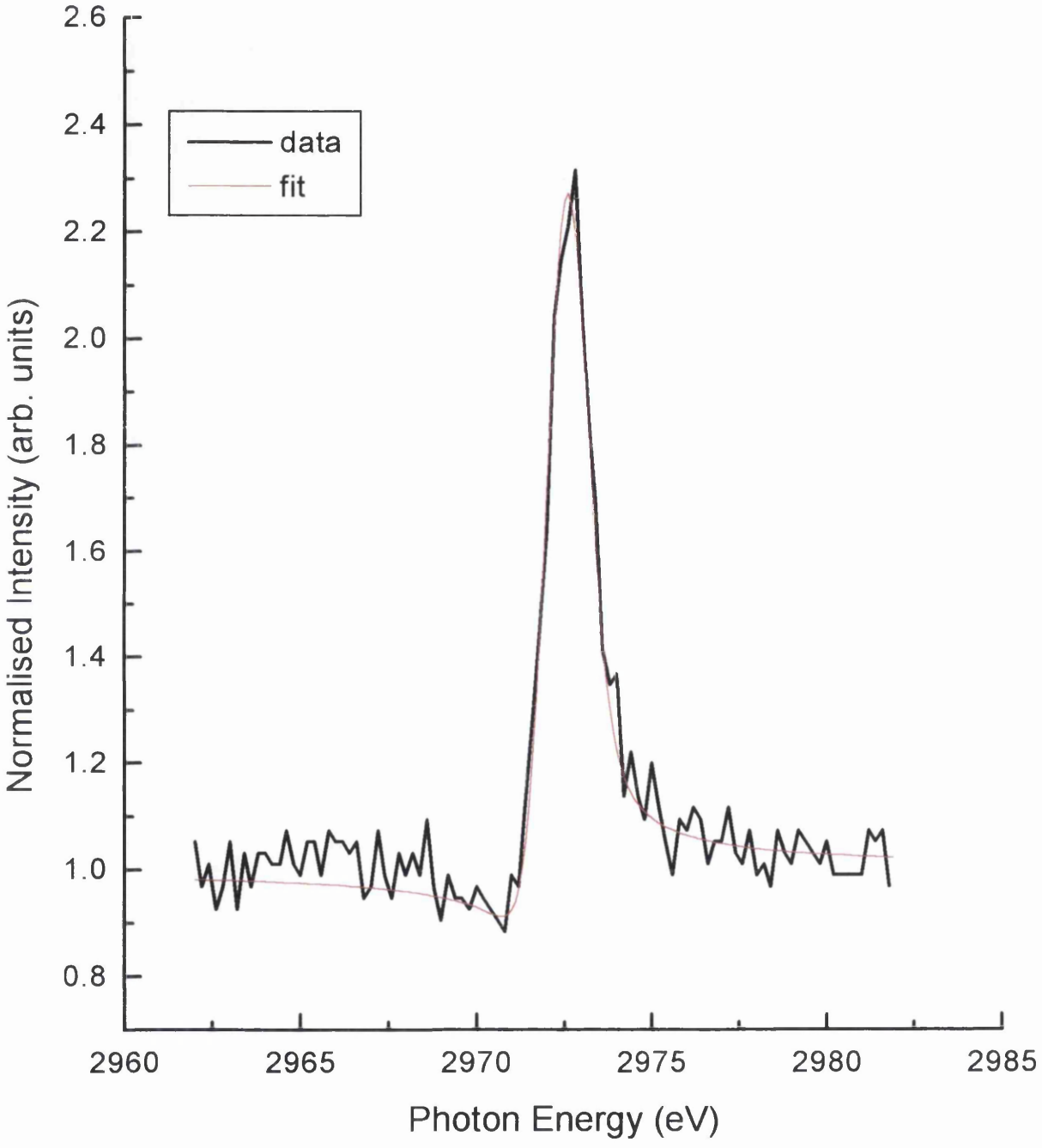

6.2.10 NIXSW experiments of 3-methoxythiophene using the annealed dosing method

Adsorbate NIXSW experiments were performed using the annealed dosing method only. Surfaces were prepared by dosing multilayers at 100 K and annealing to 220 K. In this case, annealing to the temperature suggested by figure 11 in the initial characterisation , 180 K, left surfaces with substantially more than monolayer coverage. The coverages were calculated in an identical manner as described before. Surfaces prepared by annealing to 220 K had coverages ranging from 0.04-0.08 ML. AES experiments show that a saturated monolayer of 3-methoxythiophene has a coverage of 0.12±0.3 ML.

Although the errors involved in coverage determination using both the annealed and sequential dosing methods are identical, the degree of precision that can be placed on each coverage assignment is not. In the sequential method, each surface prepared has a higher coverage than the last one because the surfaces are prepared by building up the coverage by aliquot dosing. This is therefore a very precise method of performing coverage dependent experiments. The annealed dosing method is not as good a method for performing coverage dependent experiments. Two surfaces prepared by annealing to the same temperature rarely have exactly the same coverage. Hence an error of ±0.02 ML must be considered when assigning coverages to annealed surfaces, as noted in the annealed data in Chapter 4. For this reason, the surface prepared by the annealing method with a coverage of 0.08±0.02 ML falls within the monolayer coverage range as determined by AES measurements in the initial characterisation experiments (0.12±0.03 ML). Monolayer coverage data is shown in figures 26 and 27 and is summarised in table 11. A complete list of all of the data is shown in table 12.

Table 11: *Summary of NIXSW data from S 1s NIXSW experiments at monolayer coverage for 3-methoxythiophene.*

Monolayer Data	Plane	f_{co}	D(111) (Å)	Broadness (eV)
S 1s	(111)	0.87±0.05	0.47±0.03	0.7
S 1s	($\bar{1}$11)	0.68±0.05	0.77±0.03	0.7

Table 12: *Complete list of S 1s NIXSW experiments performed for 3-methoxythiophene on Cu(111) using the annealed dosing method.*

Plane	Coverage	f_{co}	D(hkl) (Å)
111	0.04	0.90	0.45
111	0.05	0.90	0.45
111	0.07	0.90	0.47
111	0.08	0.75	0.50
111	0.10	0.65	0.50
111	0.12	0.33	0.50
111	0.14	0.45	0.50
111	0.15	0.30	0.47
111	0.19	0.27	0.53
$\bar{1}$11	0.04	0.63	0.80
$\bar{1}$11	0.05	0.57	0.73
$\bar{1}$11	0.07	0.70	0.75
$\bar{1}$11	0.08	0.80	0.77
$\bar{1}$11	0.10	0.40	0.77
$\bar{1}$11	0.12	0.27	0.73
$\bar{1}$11	0.14	0.33	0.77
$\bar{1}$11	0.15	0.27	0.83
$\bar{1}$11	0.19	0.23	0.77

Figure 26: *S 1s NIXSW data at monolayer coverage for 3-methoxythiophene with respect to the (111) plane.*

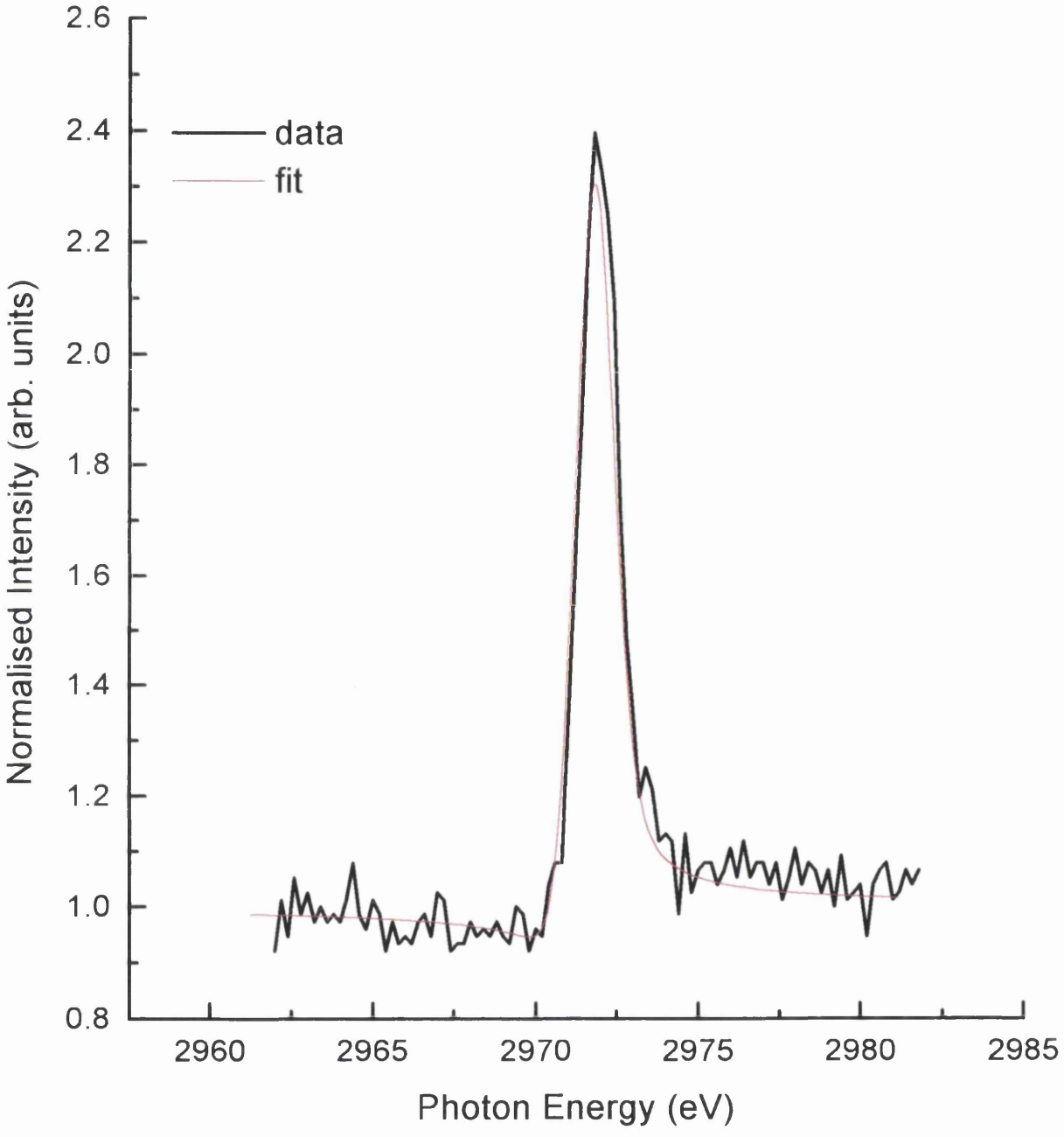

Figure 27: *S 1s NIXSW data at monolayer coverage for 3-methoxythiophene with respect to the ($\bar{1}11$) plane.*

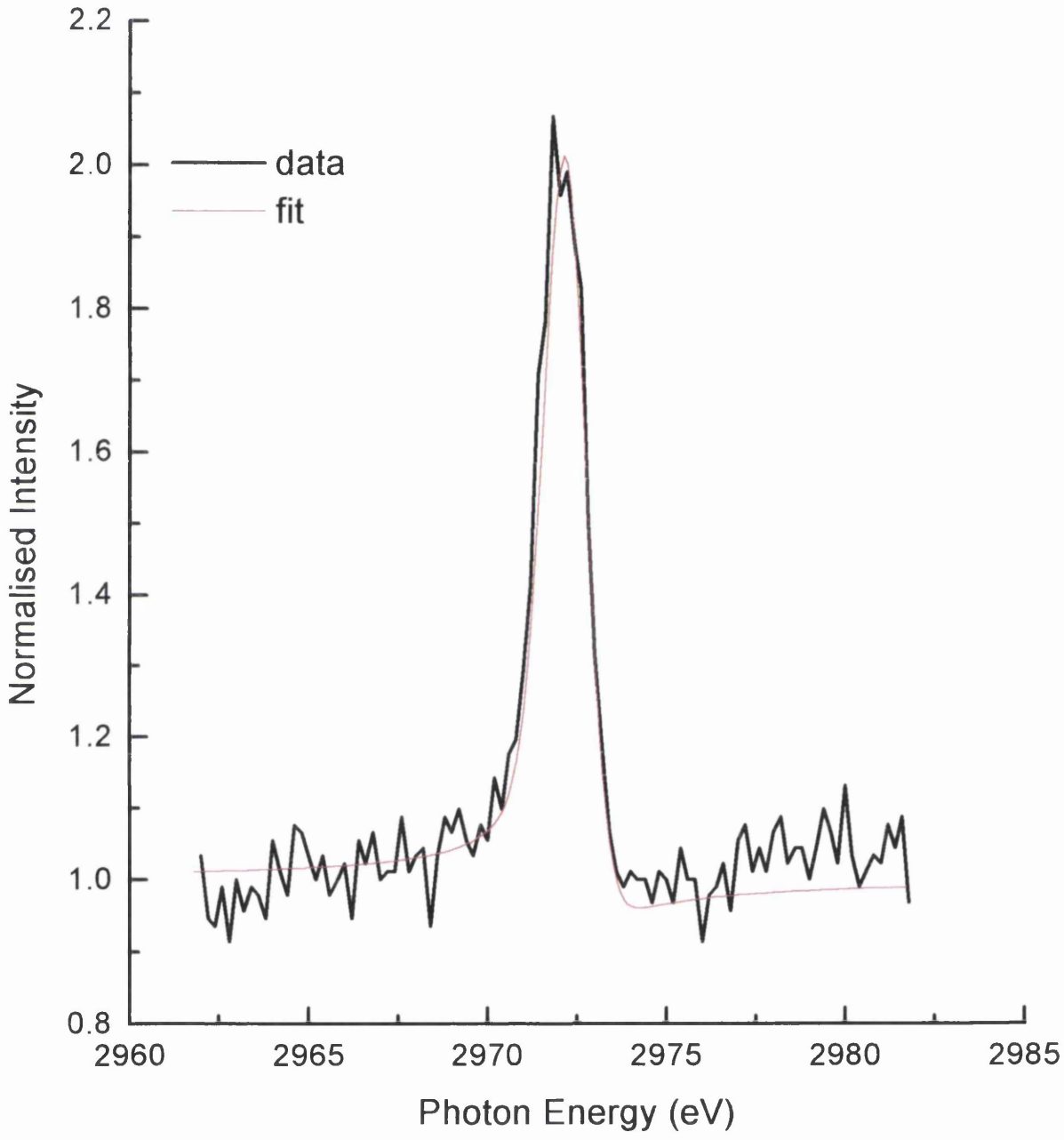

6.3 Discussion

TPD data of both 3-methylthiophene and 3-methoxythiophene show features that are present in both previous present studies, that of thiophene and 3-chlorothiophene. As in the study of thiophene, the TPD data of 3-methylthiophene, figure 2 (a), shows a broadening to lower desorption temperatures of the monolayer peak with increasing coverage up to saturation coverage. Figure 2 (a) shows that at low coverages, the monolayer peak is at 265 K and at saturation coverage has broadened significantly and moved to 235 K. As in the study of 3-chlorothiophene, the TPD data of 3-methoxythiophene shows no significant broadening to lower temperatures of the monolayer peak with increasing coverage up to monolayer coverage, figure 2(a). Also, as in the 3-chlorothiophene study, there is a small amount of dissociation of 3-methoxythiophene but like thiophene, there is no dissociation of 3-methylthiophene. As in the 3-chlorothiophene study, neither 3-methylthiophene or 3-methoxythiophene exhibit a β-like state in the corresponding TPD data.

The possible explanations for the broadening to lower temperatures of thiophene and the lack of broadening of 3-chlorothiophene were discussed in earlier chapters and are valid also in the case of 3-methylthiophene and 3-methoxythiophene. The two explanations for broadening to lower desorption temperatures in TPD data are that of islanding [4] or a gradual increase in orientational angle with increasing coverage up to the saturation of the monolayer[5]. It is interesting to note that the similarity between the thiophene and 3-methylthiophene TPD data up to α-state/monolayer coverage is mirrored in previous work concerning benzene[6] by Lambert *et al.* and toluene[7] by Bent *et al.* on Cu(110) where quite large broadening to lower desorption temperatures with increasing coverage up to saturated monolayer coverage is observed. Unfortunately, there are no surface science desorption studies of the benzene analogue of 3-methoxythiophene, anisole.

NEXAFS data for 3-methylthiophene, table 2 and figure 15, shows that the angle of orientation within the monolayer is constant at a value of 24±4 °. NEXAFS data for 3-methoxythiophene, table 5 figure 18, also shows that the angle of orientation within the monolayer varies between 23-26±4 ° and there is no broadening to lower desorption

temperatures evident in the TPD data of 3-methoxythiophene. Indeed, NEXAFS data for all four molecules studied, thiophene, 3-chlorothiophene, 3-methylthiophene and 3-methoxythiophene, show that the orientational angle does not change within experimental error within the monolayer. It could be that there is a change in orientational angle of thiophene and 3-methylthiophene but it is so small that it cannot be sufficiently probed by NEXAFS due to the inherent errors involved in calculating the angles. This means that whether there are very small changes in angle with increasing coverage (thiophene and 3-methylthiophene) or no change at all (3-chlorothiophene and 3-methoxythiophene due to pinning by the substituent group), the NEXAFS data cannot distinguish between one model or the other.

It is possible that the lone-pair on the methoxy- group interacts with the surface thereby not only pinning the molecule to a specific geometry, as described in the previous chapter (3-chlorothiophene), but also prevents the formation of islands. As this is the first surface science study of an aromatic adsorbate with a methoxy group there is no previous work with which to test this hypothesis. It does seem likely however that the lone pairs on the O of the methoxy group will interact with the surface in a similar way to the lone pairs on the Cl-group in 3-chlorothiophene. A theoretical study of the interaction of anisole with alkali metal ions by Hay *et al.*[8] whilst not directly relevant to the current study, does show that the bonding interactions from the M^+ ion to both the aromatic ring and the methoxy O are equal for small alkali metal ions and in fact for larger alkali metal ions, the interaction with the methoxy O is larger than the interaction with the aromatic ring.

The similar behaviour, within monolayer coverage, of 3-methylthiophene to that of thiophene within the α-state coverage, would suggest that the interaction of the methyl group with the surface is considerably weaker than that of both the chloro group and the methoxy group. Previous work by Hamers *et al.*[9] shows that STM images of thiophene and 2,5-dimethylthiophene are very similar and also an HREELS study of benzene and toluene on Pd(111) by Muetterties *et al.*[10] shows that the addition of a methyl group to the benzene ring has no effect on the bonding of the molecule. A PhD study of 2-Methylpyridine on Cu(110) by Woodruff *et al.*[11] shows that the molecule is tilted, rather like the 3-chlorothiophene study, but in this study with the substituent group tilted away

from the surface and not toward the surface. As this study involved a methyl group at the 2-position it is possible that there are steric reasons for this. However, a RAIRS study of toluene on Ni(111) by Raval *et al.*[12] shows that the interaction of the methyl group with the surface is quite large. Certainly, the methyl group is smaller in size to the methoxy group, but is comparable in size to the chloro group. It would appear that the presence of lone-pairs on the substituent groups is having the major effect in determining the amount of interaction between the surface and the group. This is important, as noted in the 3-chlorothiophene study, in that it can have subtle effects on the bonding of the molecule to the surface.

The presence of the methyl or methoxy group at the 3-position of the thiophene ring is preventing the gross re-organisation of the molecule in the form of a phase transition because the substituent groups are interacting with the surface thereby preventing any flipping of the molecule with increasing coverage. In the case of 3-methylthiophene, this interaction may be very weak, but there is still a sufficient effect to prevent re-organisation.

6.3.1. Adsorption site determination at monolayer coverage for both 3-methylthiophene and 3-methoxythiophene

6.3.2. Adsorption site of 3-methylthiophene as prepared by the annealed dosing method

Table 13 summarises the data obtained for 3-methylthiophene at monolayer coverage using the annealed dosing method. The values for D($\bar{1}11$) with respect to the different adsorption sites were derived from the data in table 8 with using the equations shown in the thiophene discussion section (Chapter 4) and a D(111) value of 2.57 Å (which is 0.49+2.08 Å).

Table 13: *3-methylthiophene monolayer coverage: D($\bar{1}11$) values derived from experimental D(111) (2.57 Å) values, from annealed experiments.*

Site	**D($\bar{1}11$) (Å)**	**f_{co}**
Atop	0.86	0.90
Bridging	1.90	0.30
f.c.c.	2.24	0.90
h.c.p.	1.55	0.90
experimental	***0.79***	***0.83***

From the table it is clear that the nearest fit to the experimental D($\bar{1}11$) data is the atop site, and hence the adsorption site can be described as "displaced atop". This is data is represented in Argand diagram form in figure 28.

Figure 28: *Argand Diagram showing experimental ($\bar{1}11$) value and the four derived values (green), table 1, for annealed 3-methylthiophene data. The length of the experimental vector (blue) is the coherent fraction (0.83) and the angle is given by $2\pi D(\bar{1}11)/d_H$. The nearest fit to the experimental data is the atop vector (not drawn to scale).*

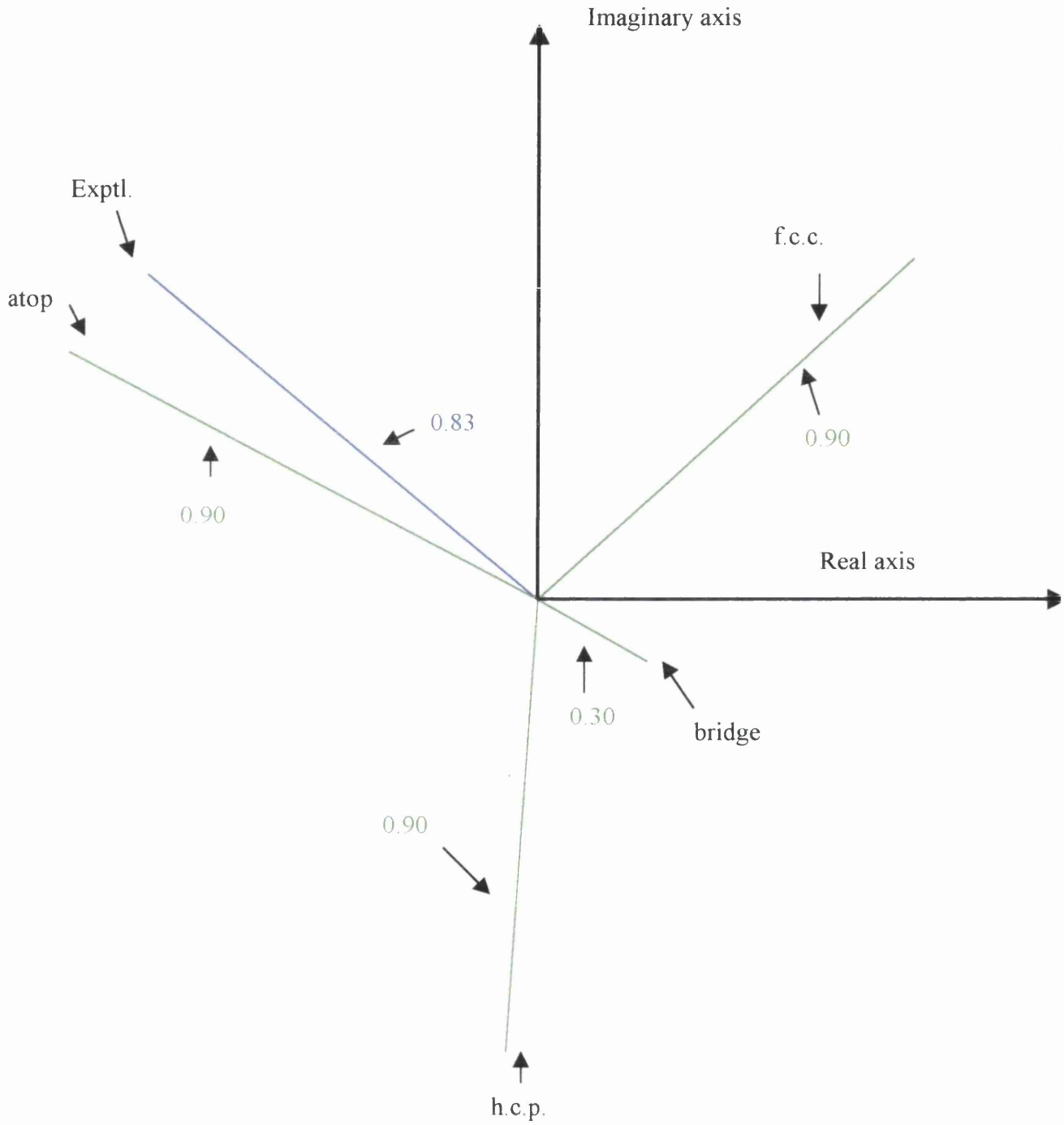

6.3.3. Adsorption site of 3-methylthiophene as prepared by the sequential dosing method

It was not possible to perform sequentially dosed NIXSW experiments with respect to the ($\bar{1}11$) plane. Figure 24 shows that the coherent position at monolayer coverage of 3-methylthiophene is 0.37±0.03 Å for the sequentially dosed data. This differs to the value obtained at monolayer coverage using the annealed dosing method, 0.49±0.03 Å. This is similar to the case with thiophene at β-state coverage where there was a significant difference in the coherent position values between the two dosing methods. In both cases, annealed and sequential dosing methods at monolayer coverage, there are coherent fractions of 0.90±0.05. This is not the case with the β-state of thiophene. In the case of Cl-NIXSW data in Chapter 4 the adsorption site could not be assigned because the coherent fraction with respect to the ($\bar{1}11$) plane was very low. As there is no ($\bar{1}11$) data at all it has to be assumed that the coherent height of 0.37±0.03 Å for the sequentially dosed data represents a well-defined height above the surface as the corresponding coherent fraction is 0.90±0.05. Using an identical procedure to the one oultined in Chapter 3, possible coherent positions for atop, bridging and 3-fold using the annealed coherent position (2.08+0.49 Å) as a bond length and a Cu-Cu bond length of 2.55 Å are summarised in table 14:

Table 14: *Coherent positions calculated with respect to the (111) plane for monolayer coverage of 3-methylthiophene prepared by sequential dosing using coherent position (2.57 Å) from annealed data as Cu-S bond length.*

Site	Coherent Position (Å)	Coherent Fraction
Atop	2.57±0.05	0.90±0.05
Bridge	2.23±0.05	0.90±0.05
3-fold	2.11±0.05	0.90±0.05

The sequentially dosed coherent position is 2.45±0.03 Å and as the coherent fraction is high, 0.90±0.05, this is a well-defined height above the surface and the nearest fit to this in the table is the atop site. As the coherent fraction is very high (0.90±0.05) there cannot be the possibility of multiple site adsorption and therefore the sequentially dosed coherent position of 2.45 Å must correspond to a single adsorption site. As in the case of thiophene, there exists the possibility of some bonding to defect sites at this coverage, which may explain why the coherent position is lower in the sequentially dosed experiments than it is in the annealed experiments. However, it is not possible to unambiguously assign the adsorption site to the atop position in the absence of ($\bar{1}11$) data.

6.3.4. Adsorption site determination of 3-methoxythiophene as prepared by the annealed dosing method

Table 15 summarises the data obtained for 3-methoxythiophene at monolayer coverage using the annealed dosing method. The values for D($\bar{1}11$) with respect to the different adsorption sites were derived from the data in table 11 using the equations shown in the thiophene discussion section (Chapter 4) and a D(111) value of 2.55 Å (which is 0.47+2.08 Å).

Table 13: *3-methoxythiophene monolayer coverage: D($\bar{1}11$) values derived from experimental D(111) (2.55 Å) values.*

Site	**D($\bar{1}11$) (Å)**	**f_{co}**
Atop	0.85	0.87
Bridging	1.89	0.29
f.c.c.	2.24	0.87
h.c.p.	1.54	0.87
experimental	***0.77***	***0.68***

From the table it is clear that the nearest fit to the experimental D($\bar{1}11$) data is the atop site, and hence the adsorption site can be described as "displaced atop". This is data is represented in Argand diagram form in figure 29.

Figure 29: *Argand Diagram showing experimental ($\bar{1}11$) value and the four derived values (green), table 1, for annealed 3-methoxythiophene data. The length of the experimental vector (blue) is the coherent fraction (0.83) and the angle is given by $2\pi D(\bar{1}11)/d_H$. The nearest fit to the experimental data is the atop vector (not drawn to scale).*

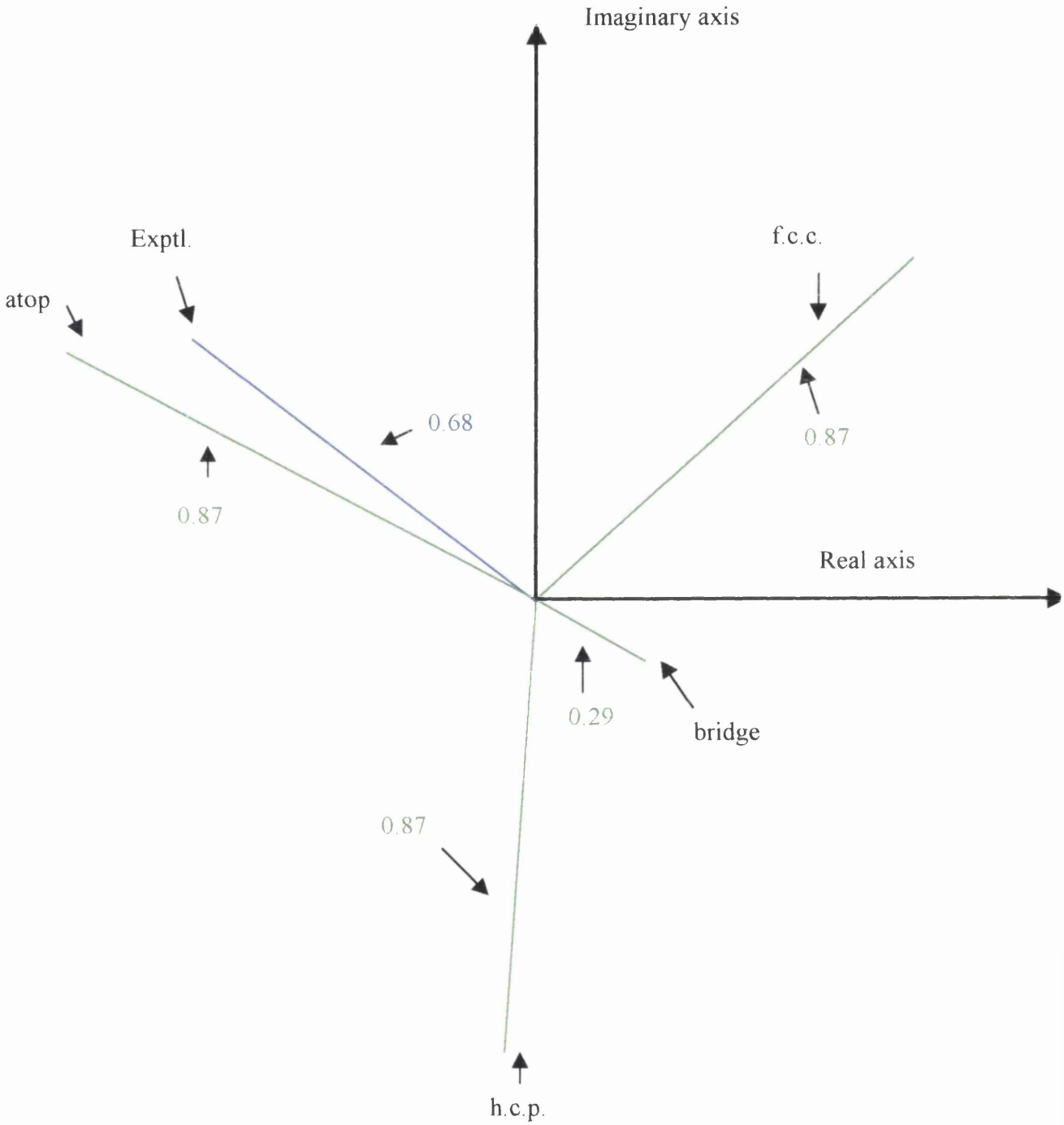

6.4. Conclusion

The major effect of adding a Me- or MeO- substituent is, as in the case of 3-chlorothiophene, the absence of a β-state like peak in the TPD data. This can be explained by the substituent group, in each case, interacting with the surface and forbidding the gross re-organisation of the molecule.

The substituent group however has no effect on the angle of orientation up to and at saturation monolayer coverage in which it was found that the angles are, within experimental error, identical for both 3-methylthiophene and 3-methoxythiophene. This means that the bonding is dominated by the π-ring in each case, as the molecules are oriented in roughly flat geometries for both molecules. Any bonding interaction between the surface and the methoxy group is re-inforcing the flat orientation of 3-methoxythiophene and not changing it. In other words, the bonding is identical to that of thiophene, which has no substituent group.

NIXSW data shows also, that the adsorption site from annealed experiments for both 3-methylthiophene and 3-methoxythiophene at monolayer coverage is displaced atop, as in the case of thiophene. For the sequentially dosed case for 3-methylthiophene, the adsorption site cannot be unambiguously defined as in the case of thiophene at β-state coverage, however the coherent fraction indicates that the significantly smaller coherent position is a well-defined distance from the surface. As the coherent fraction is 0.90±0.05 the smaller coherent fraction is indicative of a single adsorption site and there may be some bonding to defect sites, which would explain the smaller coherent position.

The only main difference between the two molecules from all of the techniques used in this study is the broadening to lower desorption temperatures of 3-methylthiophene with increasing coverage within the monolayer which is not observed in the 3-methoxythiophene study. As described before, there is no change in orientational angle within the monolayer for either molecule, but the changes in angle that cause this broadening effect may be too small to be detected, within experimental error, by the NEXAFS technique.

6.5. References

1. N.K. Singh, R.G. Jones and D.P. Woodruff, *Surface Science Letters,* 1990, **232**, L228-L231.
2. G. Distefano, M. de Palo, M. Dal Colle, A. Modelli, D. Jones and L. Favaretto, *Journal of Molecular Structure (Theochem),* 1997, **418**, 99-111.
3. A.P. Hitchcock, J.A. Horsley and J Stöhr, *Journal of Chemical Physics,* 1986, **85** (9), 4835-4848.
4. S.J. Stranick, M.M. Kamna and P.S. Weiss, *Surface Science*, 1995, **338**, 41-59.
5. M. Xi, M.X. Yang, S.K. Jo and B.E. Bent, *Journal of Chemical Physics*, 1994, **101**, 9122-9131.
6. J.R. Lomas, C.J. Baddeley, M.S. Tikhov and R.M. Lambert, *Langmuir*, 1995, **11**, 3048-3053.
7. P.W. Kash, D.-H. Sun, M. Xi, G.W. Flynn and B.E. Bent, *Journal of Physical Chemistry,* 1996, **100**, 16621-16628.
8. J.B. Nicholas and B.P. Hay, *Journal of Physical Chemistry A,* 1999, **103**, 9815-9820.
9. X. Chen, E.R. Frank and R.J. Hamers, *Journal of Vacuum Science and Technology B*, 1996, **14** (2), 1136-1140.
10. V.H. Grassian and E.L. Muetterties, *Journal of Physical Chemistry,* 1987, **91**, 389-396.
11. R. Terborg, M. Polcik, J.-T. Hoeft, M. Kittel, M. Pascal, J.H. Kang, C.L.A. Lamont, A.M. Bradshaw and D.P. Woodruff, *Surface Science,* 2000, **457**, 1-10.
12. A.M. Coats, E. Cooper and R. Raval, *Surface Science,* 1994, **307-309**, 89-94.

Chapter 7. Summary

7.1. Summary

The most drastic effect of adding a substituent group at the 3-position of thiophene in terms of the bonding of the molecule to Cu(111), is that it forbids the gross re-organisation of the molecule by way of a phase transition.

Table 1: *Summary of the results from the characterisation experiments.*

Molecule	T_{max} (K)	Coverage (ML)
Thiophene (saturated α-state)	211	0.08±0.03 ML
Thiophene (saturated β-state)	173	0.14±0.03 ML
3-chlorothiophene (saturated monolayer)	225	0.11±0.03 ML
3-methylthiophene (saturated monolayer)	235	0.11±0.03 ML
3-methoxythiophene (saturated monolayer	250	0.12±0.03 ML

As table 1 shows, the coverage of α-state thiophene and a monolayer of 3-chlorothiophene, 3-methylthiophene and 3-methoxythiophene are identical within experimental error. This means that the substituent group is not affecting the packing density of the molecule over this coverage range.

Table 2 shows that, for the same coverage range as shown in table 1, the substituent group does not affect the orientation of the molecule. For 3-chlorothiophene, analysis of the angle of orientation determined from both NEXAFS and NIXSW shows

that the chloro-group exerts a subtle twist on the molecule. Evidence for this interaction comes from the physisorption Cu-Cl distance calculated in section 5.3.3.

Table 3 shows that for all of the molecules studied, again over the same coverage range as in table 1, the Cu-S bond lengths are identical within experimental error. For both thiophene, at β-state coverage, and 3-methylthiophene, at monolayer coverage, the Cu-S bond lengths are shorter for the sequentially dosed experiments compared to the annealed experiments. In the case of thiophene, this is due to the fact that the sequential dosing method produces surfaces in which there is a distribution of adsorption sites. In the case of 3-methylthiophene, at the lower monolayer coverage, because the related coherent fraction is 0.90±0.05, there cannot be a large distribution of heights above the surface, so there cannot be a distribution of adsorption sites. However, there could be a slight contribution from defect sites, in which case the Cu-S bond length would shorten. On annealing, the 3-methylthiophene molecules would order and adsorb on atop sites with a Cu-S bond length identical within experimental error to that of thiophene at α-state coverage.

Table 2: *Summary of NEXAFS results.*

Molecule	π* position (eV)	σ* position (eV)	Iπ*(g)/Iπ*(n)	Angle (degrees)
Thiophene (saturated α-state coverage)	2467.8	2468.7	8.00	25±4
3-chlorothiophene (saturated monolayer coverage)	2467.3	2468.2	16.92	18±3
3-methylthiophene (saturated monolayer coverage)	2467.9	2468.7	9.38	24±4
3-methoxythiophene (saturated monolayer coverage)	2467.4	2468.2	7.33	26±4

Table 3: *Summary of NIXSW results.*

Molecule	Preparation method	D(111) (Å)
Thiophene (saturated α-state coverage)	Annealed	2.62±0.03
Thiophene (saturated β-state coverage)	Annealed	2.88±0.05
3-chlorothiophene (saturated monolayer coverage)	Annealed	2.62±0.03
3-methylthiophene (saturated monolayer coverage)	Annealed	2.57±0.03
3-methoxythiophene (saturated monolayer coverage)	Annealed	2.55±0.03
Thiophene (saturated α-state coverage)	Sequential	2.54±0.03
Thiophene (saturated β-state coverage)	Sequential	2.58±0.05
3-methylthiophene (saturated monolayer coverage)	Sequential	2.45±0.03